Univ.-Prof. Dr.-Ing. A. Schlenkhoff (Hrsg.)
LuFG Wasserwirtschaft und Wasserbau
FB D – Abteilung Bauingenieurwesen
Bergische Universität Wuppertal

Hany Ahmed

Wave Interaction with Vertical Slotted Walls as a Permeable Breakwater

Bericht Nr. 19, 2011

Vorwort (Hrsg.)

Die Küstengebiete der Erde sind die bevorzugten Siedlungsräume der Menschheit. Die Siedlungsdichte ist hier besonders hoch, aber auch die Infrastruktur und die landwirtschaftliche Nutzung konzentrieren sich besonders in den flachen Niederungszonen der Küstengebiete. Gleichzeitig unterliegen fast alle Lockergesteinsküsten einer zunehmenden Erosion, die zum großen Teil ursächlich auf den steigenden Meeresspiegel zurückzuführen ist. Aber auch bauliche Eingriffe in den Flussregionen und Küstenschutzmaßnahmen stellen häufig eine Ursache für eine regionale Veränderung der Sedimentverfrachtung dar. Was an einer Stelle dem Küstenschutz dient kann an anderer Stelle negative Folgen mit sich bringen, so dass Küstenschutzmaßnahmen wissenschaftlich und ingenieurtechnisch mit besonderer Weitsicht begründet sein müssen.

Die Bevölkerungszunahme, die Verstädterung und die Konzentration von Werten in diesen Regionen rücken in Kombination mit einem wahrscheinlich weiter beschleunigt ansteigenden Meeresspiegel die konkurrierenden Nutzungsansprüche stärker in das Bewusstsein und wecken ein steigendes Bedürfnis nach Schutzeinrichtungen. Die Deltas der großen Flüsse stellen dabei die am meisten vom Meeresspiegelanstieg betroffenen Regionen dar. Dies gilt insbesondere auch für das Nildelta. Aus dieser Sicht heraus sind möglichst einfache, kostengünstige und umweltverträgliche Schutzmaßnahmen gefragt, die bei der Verteidigung der Küstenlinie helfen können. Langfristig sind solche Maßnahmen in ein integriertes KüstenZonenManagement einzubinden. Ägypten ist gerade dabei sich auch von der wissenschaftlichen Seite her mit diesen Problemen und möglichen Lösungsansätzen zu beschäftigen. Die vorliegende Dissertation soll hierzu einen Beitrag leisten.

Wuppertal, Dezember 2011 *Andreas Schlenkhoff*

BERGISCHE
UNIVERSITÄT
WUPPERTAL

Wave Interaction with Vertical Slotted Walls as a Permeable Breakwater

Vom Fachbereich D (Abteilung Bauingenieurwesen)
der Bergischen Universität Wuppertal

genehmigte

Dissertation

zur Erlangung des akademischen Grades
Doktor-Ingenieur (Dr.-Ing.)

von
M. Sc. Hany Gomaa Ibrahim Ahmed
aus Kairo – Ägypten

© 2011 LuFG Wasserwirtschaft und Wasserbau, Bergische Universität Wuppertal
Vervielfältigung nur mit ausdrücklicher Genehmigung des Herausgebers

Prüfung am:	07. Dezember 2011
Erster Gutachter:	Univ.-Prof. Dr.-Ing. Andreas Schlenkhoff LuFG Wasserwirtschaft und Wasserbau Bergische Universität Wuppertal
Zweiter Gutachter:	Univ.-Prof. Dr.-Ing. habil. Torsten Schlurmann Franzius-Institut für Wasserbau und Küsteningenieurwesen Leibniz Universität Hannover
Vorsitzender:	Univ.-Prof. Dr.-Ing. Matthias Pulsfort LuFG Geotechnik Bergische Universität Wuppertal
Weitere Mitglieder:	Univ.-Prof. Dr.-Ing. habil. Wolfhard Zahlten LuG Baumechanik und numerische Methoden Bergische Universität Wuppertal Obering. Dr.-Ing. Mario Oertel LuFG Wasserwirtschaft und Wasserbau Bergische Universität Wuppertal

Acknowledgments

I owe my deepest gratitude to those people who helped me to complete this thesis. My sincere thanks go to the Ministry of Higher Education (Egypt) for sponsoring 4 years scholarship in Germany to do this research work. I would like to thank the University of Wuppertal for having me here.I would like to express my profound thanks to my supervisor and first reviewer Univ.-Prof. Dr.-Ing. A. Schlenkhoff (University of Wuppertal) for all the necessary help, encouragement, guidance and support from the initial to the final level. He enabled me to overcome many difficulties during four-year research. Also many thanks to my second reviewer, Univ.-Prof. Dr.-Ing. habil. Torsten Schlurmann.

I am also grateful to my colleagues, Dr.-Ing. Mario Oertel, Dipl.-Ing. Georg Heinz (University of Wuppertal) and Dr.-Ing. Daniel Bung (University of Hannover). Thanks for their advice and for helping me in the lab to carry out the experiments of this study. My sincere thanks to Ms. Melanie Sichelschmidt, administrative officer, for all the necessary help whom taken care of all the administrative work, so that I could concentrate on my research.

I am deeply grateful to Prof. Dr-Ing. Anas M. A. El-mulla for his very helpful advice and support.

I would like to take the opportunity to express my gratitude to all the members of the hydraulic & irrigation Dep. at Al-Azhr University, Cairo Egypt, where I did my undergraduate and master studies.

A special thanks to all my friends who have helped and supported me throughout my time at university. Last but not least, I dedicate this thesis to my family (my parents, my wife, M. El-kholy, my children Basmala & Sidra, and my brothers) for their constant love and support, without which the completion of this thesis would not were possible.

Abstract

The development of coastal areas depends on shore protection against waves and currents. Solid breakwaters are commonly used along shorelines, but they are often unsuitable due to environmental impacts. Permeable breakwaters like rows of piles have been suggested as a more environmentally friendly alternative, but the performance of piles alone has been proven as too weak. Breakwaters with impermeable skirts in combination with piles are assumed to perform better. However, wave-structure-interaction and flow behavior of this type are more complicated, but have to be analyzed before designing.

The objective of the present dissertation thesis is to describe the flow behavior and the hydraulic performance of this kind of permeable breakwaters. A numerical model has been developed based on an Eigen function expansion method for wave interaction with a single and a double vertical slotted wall. Experimental tests have been conducted on a model scale of 1 to 25 to validate the numerical model and to assess the performance characteristics of the reflection (*CR),* transmission *(CT)* and energy losses (*CE).* Additional, experimental tests have been conducted to measure and analyze the velocity distribution in front and behind of the vertical slotted wall and to understand the pattern that dissipates wave energy.

To fulfill the above-mentioned objectives, this thesis is divided into the following Chapters: Chapter 1 gives an introduction into the problem. Chapter 2 is dealing with the state of the art and an extensive literature review. A numerical model based on Eigen fuction expansion is described in Chapter 3. The numerical model is suitable to determine the wave interaction with single or double vertical slotted wall breakwaters. Furthermore, Stokes second-order wave theory has been compared to the linear wave theory assumption. In Chapter 4, a series of experimental tests are shown, which have been conducted in the wave flume of the University of Wuppertal. The set-up and the measurement devices are explained. Additional, attention has been given to the measurement of the velocities via PIV. The results have been discussed and analyzed with emphasis on the interaction of waves with the

vertical slotted walls. In Chapter 5, the results of the numerical model are compared with previous studies and the experimental work of this study. Chapter 6 closes with a summary, concluding remarks, recommendations and suggestions for future studies. The major results from this study are the following:

- The numerical model has been validated by comparisons with previous studies and experimental results of this study. The agreement is generally satisfying.
- The degree of target protection can be achieved through a combination of permeability area and its location.
- The coefficient of friction f and the coefficient of porosity ε have significant influence on *CR, CT* and *CE* of the permeable breakwaters, while the influence of added mass coefficient *cm* is low and can be neglected for this configuration.
- For the case of double walls, the second wall should be constructed at a distance of an uneven multiple of a quarter of the wavelength (0.25 L, 0.75 L and 1.25 L). This position can increase the dissipation of the energy up to 40 % than a single wall.
- PIV measurements can be used in the laboratory for measuring the co-existing and transmitted waves and to visualize the wave interaction with a permeable breakwater. The achievable accuracy of PIV measurement within this set-up is a function of the relative time increment $\delta t/T$.

Finally, it is recommended to use vertical slotted walls as breakwaters for the protection against waves, whenever it is possible. The progressively decreasing depth of the permeability part of the wall can be used to minimize the transmission of wave energy. For double rows of vertical slotted walls, the spacing between rows should be an uneven multiple of a quarter of the wavelength.

Deutsche Zusammenfassung

Die weitere Entwicklung von Küstenregionen steht in engem Zusammenhang mit den Möglichkeiten, geeignete Schutzmaßnahmen gegen Wellen und Strömung zu schaffen. Üblicherweise werden für diesen Zweck massive, undurchlässige Bauwerksstrukturen gebaut, die aber wegen gerade dieser Eigenschaften erhebliche negative Nebeneffekte für die Umwelt mit sich bringen. Durchlässige Wellenbrecher, wie zum Beispiel auf Lücke gesetzte Pfahlreihen, werden zwar als umweltfreundlicher eingestuft, erreichen aber häufig nicht die gewünschte Schutzwirkung. Solche Wellenbrecher können allerdings in Kombination mit undurchlässigen Schürzen eine wesentlich bessere Wirkung entfalten. Die hydrodynamischen Verhältnisse der Um- und Durchströmung sowie die Energieumwandlung durch die Interaktion zwischen Wellen und Bauwerk werden sehr komplex, müssen aber für die angemessene Dimensionierung des Bauwerks bekannt sein.

Ein Ziel der vorgelegten Dissertation ist die Beschreibung der Strömungseigenschaften und der Wellen-Bauwerk-Interaktion. Dafür wird ein numerisches Modell genutzt, welches die Methode der Entwicklung nach Eigenfunktionen verwendet. Als eine typische Bauwerkskonfiguration wird eine bzw. mehrere hintereinander liegende, geschlitzte Wände mit Schürzen gewählt. Die Validierung des Modellansatzes wird mithilfe von Literaturdaten und physikalischen Modellversuchen geführt. Die eigenen Versuche werden in einem Maßstab 1 zu 25 in der Wellenrinne der Bergischen Universität Wuppertal gefahren. Ziel der Versuche ist die Bestimmung der hydrodynamischen Parameter wie Reflektion, Transmission und Energiedissipation. Weiterhin wird das Geschwindigkeitsfeld vor und hinter dem Bauwerk mittels PIV untersucht und anhand der Wirbelstrukturen beschrieben.

Die Dissertation gliedert sich wie folgt: Kapitel 1 gibt eine Einführung in die allgemeine Problematik. Kapitel 2 spiegelt den Stand des Wissens wider und gibt eine ausführliche Literaturübersicht. Das numerische Modell, basierend auf der Entwicklung von Eigenfunktionen, wird in Kapitel 3 beschrieben. Ziele des

numerischen Modells sind die Bestimmung der hydrodynamischen Parameter und die Beschreibung der Welleninteraktion mit dem Bauwerk. Weiterhin wird das zunächst entwickelte Modell, welches sich auf die lineare Wellentheorie stützt, nach der Stoke'schen Second Order Theorie erweitert, um auch im Grenzbereich längerer Wellen noch Aussagen treffen zu können. In Kapitel 4 werden die Versuchsreihen, die in der Wellenrinne der Bergischen Universität Wuppertal durchgeführt wurden, beschrieben. Dabei werden der gewählte Versuchsaufbau und die eingesetzte Messtechnik erläutert. Zusätzlich werden die Geschwindigkeitsmessungen, die mit einem PIV System durchgeführt worden sind, hinsichtlich der Messgenauigkeit optimiert. Die Messtechnik und die daraus ableitbaren Ergebnisse werden diskutiert. In Kapitel 5 werden die Ergebnisse der numerischen Simulation den Ergebnissen der Versuchsreihen und zusätzlich den Ergebnissen von verfügbaren Untersuchungen aus der Literatur gegenübergestellt, diskutiert und bewertet. Die wichtigsten Ergebnisse der Dissertation werden in Kapitel 6 noch einmal zusammengefasst und zusammen mit Empfehlungen und einem Ausblick bewertet.

Die wichtigsten Ergebnisse dieser Dissertation sind:

- Das entwickelte numerische Modell ist gut geeignet, die hydrodynamische Wirkungsweise des untersuchten Bauwerkstyps zu beschreiben.
- Das untersuchte Bauwerk, bestehend aus einer Kombination von einer oder mehreren Pfahlreihen und undurchlässigen Schürzen, kann die gewünschte Wirkung durch eine geeignete Wahl und Anordnung der durchlässigen Bauwerksteile erreichen.
- Bei der numerischen Simulation haben der Reibungskoeffizient und die Porosität den bestimmenden Einfluss auf die Bauwerkswirkung und damit auf die Reflektion, die Transmission und die Energiedissipation. Die sogenannte zusätzlich zu beschleunigende Masse (added mass), die im numerischen Modell ebenfalls berücksichtigt wird, hat hingegen nur einen unbedeutenden Einfluss.
- Für die Bauwerkskonfiguration mit zwei hintereinander liegenden geschlitzten Wänden zeigt sich, dass der Abstand der Wände im Verhältnis zur Wellenlänge einen erheblichen Einfluss auf die Gesamtwirkung ausübt.

Eine maximale Energiedissipation kann erwartet werden, wenn der Abstand zwischen den beiden Wänden ein ungerades Vielfaches einer viertel Wellenlänge beträgt (0.25 L, 0.75 L, 1.25 L). Diese Anordnung erhöht die Energiedissipation um biszu 40 %.

- PIV Messungen können im Labor den Erkenntnisgewinn über die Strömungsphänomene erheblich steigern. Die Unsicherheit bei der Bestimmung der Geschwindigkeit in einem stark instationären Strömungsfeld kann durch die geeignete Wahl des relativen Zeitschrittes $\delta t / T$ minimiert werden.

Abschließend kann der untersuchte Bauwerkstyp als gut geeignet für Schutzmaßnahmen gegen Wellen eingegestuft werden. Wegen der gut abstimmbaren Wirkungsweise und den geringeren Umweltbeeinträchtigungen sollten daher vorzugsweise geschlitzte Wände aus einer Kombination von Pfählen und Schürzen gewählt werden, wenn die Örtlichkeiten oder die Ansprüche an die Schutzwirkung es erlauben. Es sind allerdings weitere Untersuchungen für die Optimierung des Bauwerkstyps erforderlich.

TABLE OF CONTENTS

Title		Page
Acknowledgment …….……..		I
Abstract……		III
Deutsche Zusammenfassung…….……...		V
TABLE OF CONTENTS…….……		IX
LIST OF FIGURES …….…….……..		XII
LIST OF PHOTOS.…….……		XX
LIST OF TABLES……..…….…….....		XXI
NOTATIONS…..……...……..……		XXII
CHAPTER 1 INTRODUCTION		
1.1	GENERAL……...	1
1.2	STATEMENT OF THE PROBLEM……...	3
1.3	RESEARCH METHODOLOGY……...…….	5
CHAPTER 2 LITERATURE REVIEW		
2.1	INTRODUCTION …….....	7
2.2	TYPES OF BREAKWATERS ……...…….	8
2.3	PREVIOUS STUDIES IN PERMEABLE BREAKWATERS……...	13
2.4	SUMMARY……...……...……...	40
2.5	OBJECTIVES OF THE STUDY……..……...	41

CHAPTER 3
THEORETICAL INVESTIGATION

3.1 INTRODUCTION……..……..... 43

3.2 NUMERICAL MODEL BASED ON LINEAR WAVE THEORY……. 44

3.3 NUMERICAL MODEL BASED ON NONLINEAR WAVE THEORY…….…… 51

3.4 NUMERICAL MODEL FOR LINEAR WAVE WITH DOUBLE VERTICAL SLOTTED WALL……..…….... 55

CHAPTER 4
EXPERIMENTAL INVESTIGATION AND VELOCITY MEASUERMENTS

4.1 INTRODUCTION 63

4.2 TEST FACILITY……...……..... 63

4.3 PHYSICAL MODEL…….……...…...…….. 66

4.4 INSTRUMENTATION……....…… 69

4.5 PARTICLE IMAGE VELOCIMETRY (PIV) …… 75

4.6 TEST SETUP……...……..... 82

4.7 WAVE CHARACTERISTICS……...…….. 82

4.8 TEST PROCEDURE……..……. 83

4.9 ANALYSIS OF DATA……..…….…… 83

4.10 VELOCITY MEASUREMENT……... 86

4.11 MESUREMENT OF REFLECTION AND TRANSMISSION COEFFICIENTS USING PIV..... 94

CHAPTER 5
RESULTS AND DISCUSSIONS

5.1 INTRODUCTION……..……..…… 107

5.2 DATA ANALYSIS ……..…… 108

5.3 WAVE INTERACTION WITH A SINGLE VERTICAL SLOTTED WALL ……..…… 109

5.4 NON LINEAR WAVE (STOKES SECOND-ORDER WAVE) INTERACTION WITH SINGLE VERTICAL SLOTTED WALL……...……. 136

5.5 LINEAR WAVE INTERACTION WITH DOUBLE VERTICAL SLOTTED WALLS BREAKWATER…… 140

CHAPTER 6
SUMMARY, CONCLUSIONS AND RECOMMENDATION

6.1 SUMMARY …… 190

6.2 CONCLUSIONS ……..…… 191

6.3 RECOMMENDATIONS……..……...……..… 196

6.4 SCOPE FOR FUTURE STUDY…….……. 197

REFERENCES ……...…… 198

LIST OF FIGURES

Figure No.	Title	Page
1.1	Cross section of the Yeoho port breakwater	2
1.2	Definition sketch for a vertical slotted wall breakwater	5
2.1	Vertical flexible breakwaters	8
2.2	Some types of partial protection breakwaters	12
2.3	Breakwater with pervious vertical walls at both seaward and landward sides	15
2.4	Details of suspended pipe breakwater	20
2.5	Rows of cylinders without a back wall	22
2.6	Vertical slotted barriers	23
2.7	Vertical double slotted barriers	26
2.8	Vertical cylinders breakwater	27
2.9	Schematic showing horizontal and vertical orientations and screen spacing	28
2.10	Pile supported vertical wall breakwater side view and front view	33
2.11	Circular piles supported vertical wall breakwater	36
2.12	Schematic diagram for the breakwater model	38
3.1	Definition sketch for a vertical slotted wall breakwater	45
3.2	Definition sketch of double vertical slotted wall breakwater	56
4.1	MATLAB GUI a wave flume (IGAW software)	66
4.2	The measured wave heights	71
4.3	Illustration of how velocity information is extracted from two images	76

4.4	The relation between the specific velocity and the relative time $\delta t / T$	81
4.5	Sketch of experimental setup	82
4.6	Velocity magnitude (cm/s) of incident waves when the wave crest is within the VOF	89
4.7	The maximum horizontal velocity along the x axis when the wave crest is within the VOF	90
4.8	The velocity magnitude (cm/sec) in front of and behind the barrier for F = 0.75 Hz and h_i = 4 cm	91
4.9	The vorticity magnitude (1/sec) in front of and behind the barrier for F = 0.75 Hz and h_i = 4 cm.	92
4.10	The velocity vector in front of and behind the barrier for F = 0.75 Hz and h_i = 4 cm.	93
4.11	Analysis of co-existing, incident and reflected wave at the crest and trough	96
4.12	The maximum velocity magnitude of co-existing waves along x direction when the wave crest is within the VOF.	101
4.13	Velocity magnitude of co-existing waves when the wave crest is within the VOF.	102
4.14	Velocity magnitude of transmitted waves when the wave crest is within the VOF	103
4.15	The maximum velocity magnitude of transmitted waves along x direction when the wave crest is within the VOF.	104
4.16	The distribution of the horizontal velocity of incident, co-existing and transmitted waves at the wave crest for the frequency of wave F = 2 Hz	104
4.17	The distribution of the horizontal velocity of incident, co-existing and transmitted waves at the wave crest for the frequency of wave F = 0.75 Hz	105
5.1	Influence of porosity ε, f and cm on permeability parameter G	116
5.2	Influence of ε on hydrodynamic coefficients for a single vertical slotted wall breakwater as function of kd for	117

	dm = 0.6 d, f = 2 and cm = 0.	
5.3	Influence of f on hydrodynamic coefficients for a single vertical slotted wall breakwater as function of kd for dm = 0.6 d, ε = 50 % and cm = 0.	118
5.4	Influence of cm on hydrodynamic coefficient for a single vertical slotted wall breakwater as function of kd for dm = 0.6 d, ε = 50 %, and f = 2.	119
5.5	Comparison between the present results and numerical results of Isaacson et al. (1998) as a function of ($k.du$) for various ε , du = 0.5d, h_i/L = 0.07, f = 2 and cm = 0	120
5.6	Comparison of the present results with prediction results of Abul_Azm (1993) as a function of (kd) for h_i/L = 0.025	121
5.7	Comparison of the present results with prediction and experimental results of Suh. et al. (2006) for a pile-supported vertical wall as a function of (kd) for various du with ε = 0.5, f = 0.50 and cm = 0	122
5.8	Comparison of experimental of PIV with experimental of Ultrasonic measurements and prediction results for dm=0.2 d, porosity = 0.5, f = 2 and cm = 0	123
5.9	Comparison of experimental and predicted results as a function of (kd) for various middle permeable part with constant ε = 0.5, f = 2 and cm = 0	128
5.10	Comparison of experimental and predicted results as function of (kd) for various middle permeable part with constant ε = 0.5, f = 2 and cm = 0	129
5.11	Comparison of measured and predicted reflection and transmission coefficients as a function of relative permeable middle part dm/d and ε = 0.5, f = 2 and cm = 0	130
5.12	Comparison of experimental and predicted results as a function of (kd) for fixed upper skirt at du = 0.4 d and various draft of lower skirt with constant ε = 0.5, f = 2 and cm = 0	131
5.13	Comparison of experimental and predicted results as a function of (kd) for fixed upper skirt at du = 0.4 d and various draft of lower skirt with constant ε = 0.5, f = 2 and cm = 0	132

5.14	Comparison of experimental and predicted results as a function of (kd) for fixed lower skirt at dw = 0.4 d and various draft of upper skirt with constant $\varepsilon = 0.5, f = 2$ and cm = 0.	133
5.15	Comparison of experimental and prediction results as a function of (*kd*) for fixed lower skirt at *dw* = 0.4 *d* and various draft of upper skirt with constant $\varepsilon = 0.5, f = 2$ and *cm* = 0	134
5.16	Comparison of experimental and prediction results as a function of (*kd*) for fixed middle permeable part *dm* = 0.2 *d* and different location from water surface with constant porosity ε = 0.5, $f = 2$ and *cm* = 0.	135
5.17	Comparison between the waves profile of linear and Stokes second-order waves at $T = 1$ s and $h_i = 0.025\ L$….	137
5.18	Comparison of predicted results of nonlinear waves (Stokes second-order theory) with measured and predicted results of linear waves as a function *kd* for various *dm*, $\varepsilon = 0.5, f = 2$ and *cm* = 0	138
5.19	Comparison of predicted results of nonlinear waves (Stokes second-order theory) with measured and predicted results of linear waves as a function *kd* for various *dm*, $\varepsilon = 0.5, f = 2$ and *cm* = 0	139
5.20	Comparison of the present results with prediction and experimental results of Isaacson et al. (1999) as a function of (*k du*) for $\varepsilon = 5$ % , *du* = 0.5d, $h_i / L = 0.07$ $\lambda/du = 1.1$, $f = 2$ and *cm* = 0	144
5.21	Comparison of experimental and prediction results as function of (*kd*) for various middle permeable part with constant $\varepsilon = 0.5$, $\lambda/d = 0.25, f = 2$ and *cm* = 0	145
5.22	Comparison of experimental and prediction results as function of (*kd*) for various middle permeable part with constant $\varepsilon = 0.5$, $\lambda/d = 0.25, f = 2$ and *cm* = 0	146
5.23	Comparison of experimental and prediction results as function of (*kd*) for various middle permeable part with constant $\varepsilon = 0.5$, $\lambda/d = 0.5, f = 2$ and *cm* = 0	147
5.24	Comparison of experimental and prediction results as function of (*kd*) for various middle permeable part with constant $\varepsilon = 0.5$, $\lambda/d = 0.5, f = 2$ and *cm* = 0	148

5.25 Comparison of experimental and prediction results as function of (kd) for various middle permeable part with constant $\varepsilon = 0.5$, $\lambda/d = 0.75$, $f = 2$ and $cm = 0$ 149

5.26 Comparison of experimental and prediction results as function of (kd) for various middle permeable part with constant $\varepsilon = 0.5$, $\lambda/d = 0.75$, $f = 2$ and $cm = 0$ 150

5.27 Comparison of experimental and prediction results as function of (kd) for various middle permeable part with constant $\varepsilon = 0.5$, $\lambda/d = 1$, $f = 2$ and $cm = 0$ 151

5.28 Comparison of experimental and prediction results as function of (kd) for various middle permeable part with constant $\varepsilon = 0.5$, $\lambda/d = 1$, $f = 2$ and $cm = 0$ 152

5.29 Comparison of experimental and prediction results as function of (kd) for various middle permeable part with constant $\varepsilon = 0.5$, $\lambda/L = 0.125$, $f = 2$ and $cm = 0$ 153

5.30 Comparison of experimental and prediction results as function of (kd) for various middle permeable part with constant $\varepsilon = 0.5$, $\lambda/L = 0.125$, $f = 2$ and $cm = 0$ 154

5.31 Comparison of experimental and prediction results as function of (kd) for various middle permeable part with constant $\varepsilon = 0.5$, $\lambda/L = 0.25$, $f = 2$ and $cm = 0$ 155

5.32 Comparison of experimental and prediction results as function of (kd) for various middle permeable part with constant $\varepsilon = 0.5$, $\lambda/L = 0.25$, $f = 2$ and $cm = 0$ 156

5.33 Comparison of experimental and prediction results as function of (kd) for various middle permeable part with constant $\varepsilon = 0.5$, $\lambda/L = 0.375$, $f = 2$ and $cm = 0$ 157

5.34 Comparison of experimental and prediction results as function of (kd) for various middle permeable part with constant $\varepsilon = 0.5$, $\lambda/L = 0.375$, $f = 2$ and $cm = 0$ 158

5.35 Comparison of experimental and prediction results as function of (kd) for various middle permeable part with constant $\varepsilon = 0.5$, $\lambda/L = 0.5$, $f = 2$ and $cm = 0$ 159

5.36 Comparison of experimental and prediction results as function of (kd) for various middle permeable part with 160

constant $\varepsilon = 0.5$, $\lambda/L = 0.5$, $f = 2$ and $cm = 0$

5.37 Comparison between measured and predicted reflection and transmission coefficients as a function of relative permeable middle part dm/d and $\varepsilon = 0.5$, $\lambda/d = 0.25$, $f = 2$ and $cm = 0$ 161

5.38 Comparison between measured and predicted reflection and transmission coefficients as a function of relative permeable middle part dm/d and $\varepsilon = 0.5$, $\lambda/\mathrm{d} = 0.5$, $f = 2$ and $cm = 0$ 162

5.39 Comparison between measured and predicted reflection and transmission coefficients as a function of relative permeable middle part dm/d and $\varepsilon = 0.5$, $\lambda/d = 0.75$, $f = 2$ and $cm = 0$ 163

5.40 Comparison between measured and predicted reflection and transmission coefficients as a function of relative permeable middle part dm/d and $\varepsilon = 0.5$, $\lambda/d = 1$, $f = 2$ and $cm = 0$ 164

5.41 Comparison between measured and predicted reflection and transmission coefficients as a function of relative permeable middle part dm/d, and $\varepsilon = 0.5$, λ/L=0.125, $f = 2$ and $cm = 0$ 165

5.42 Comparison between measured and predicted reflection and transmission coefficients as a function of relative permeable middle part dm/d and $\varepsilon = 0.5$, $\lambda/L = 0.25$, $f = 2$ and $cm = 0$ 166

5.43 Comparison between measured and predicted reflection and transmission coefficients as a function of relative permeable middle part dm/d and $\varepsilon = 0.5$, $\lambda/L = 0.375$, $f = 2$ and $cm = 0$ 167

5.44 Comparison between measured and predicted reflection and transmission coefficients as a function of relative permeable middle part dm/d and $\varepsilon = 0.5$, $\lambda/L = 0.5$, $f = 2$ and $cm = 0$ 168

5.45 Effect of chamber width on reflection, transmission and energy dissipation coefficients for various λ/d , $\varepsilon = 0.5$, $kd = 4.772$, $f = 2$ and $cm = 0$ 170

5.46 Effect of chamber width on reflection, transmission and 171

	energy dissipation coefficients for various λ/d, ε = 0.5, kd = 0.2689, f = 2 and cm = 0	
5.47	Effect of chamber width on reflection, transmission and energy dissipation coefficients for various λ/d , ε = 0.5, kd = 1.363, f = 2 and cm = 0	172
5.48	Effect of chamber width on reflection, transmission and energy dissipation coefficients for various λ/d, ε = 0.5, kd = 0.577, f = 2 and cm = 0	173
5.49	Effect of chamber width on reflection, transmission and energy dissipation coefficients for various λ/L, ε = 0.5, kd = 4.772, f = 2 and cm = 0	174
5.50	Effect of chamber width on reflection, transmission and energy dissipation coefficients for various λ/L, ε = 0.5, kd = 2.689, f = 2 and cm = 0	175
5.51	Effect of chamber width on reflection, transmission and energy dissipation coefficients for various λ/L, ε = 0.5, kd = 1.363, f = 2 and cm = 0	176
5.52	Effect of chamber width on reflection, transmission and energy dissipation coefficients for various λ/L, ε = 0.5, kd = 0.577, f = 2 and cm = 0	177
5.53	Comparison between prediction results for single and double vertical slotted wall as function of (kd) for various λ/d, ε = 0.5, dm = 0.2 d, f = 2 and cm = 0	182
5.54	Comparison between prediction results for single and double vertical slotted wall as function of (kd) for various λ/d, ε = 0.5, dm = 0.4 d, f = 2 and cm = 0	183
5.55	Comparison between prediction results for single and double vertical slotted wall as function of (kd) for various λ/d, ε = 0.5, dm = 0.6 d, f = 2 and cm = 0	184
5.56	Comparison between prediction results for single and double vertical slotted wall as function of (kd) for various λ/d, ε = 0.5, dm = 0.8 d, f = 2 and cm = 0	185
5.57	Comparison between prediction results for single and double vertical slotted wall as function of (kd) for various λ/L, ε = 0.5, dm = 0.2 d, f = 2 and cm = 0	186

5.58	Comparison between prediction results for single and double vertical slotted wall as function of (*kd*) for various λ/L, ε = 0.5, *dm* = 0.4 *d*, *f* = 2 and *cm* = 0	187
5.59	Comparison between prediction results for single and double vertical slotted wall as function of (*kd*) for various λ/L, ε = 0.5, dm = 0.6 *d*, *f* = 2 and *cm* = 0	188
5.60	Comparison between prediction results for single and double vertical slotted wall as function of (*kd*) for various λ/L, ε = 0.5, *dm* = 0.8 *d*, *f* = 2 and *cm* = 0	189

LIST OF PHOTOS

Photo No.	Title	Page
1.1	Hanstholm breakwater (Denmark)……..….	2
4.1	General view of the wave flume…….....	64
4.2	View of the flume end…….....	64
4.3	View of the wave generating system……..	65
4.4	View of the physical model ……...	67
4.5	View of the single vertical slotted wall model……...	68
4.6	View of double vertical slotted wall model……	68
4.7	View of measuring devices for wave profile and wave velocity……	70
4.8	View of sensors and Ultralab…….…….	71
4.9	View of sensor in front of the model……..	72
4.10	View of sensor in the rear side……...	72
4.11	View of measuring devices for wave velocity……	79
4.12	View of particles at the measuring area…….	79
5.1	Water profile at the first wall at λ / L = 0.125 at θ = 90 and h_i = 3 cm, T = 1 s, ε = 0.5 and dm = 0.2 d.	180
5.2	Water profile at the first wall at λ / L = 0.125 at θ = 270 and h_i = 3 cm, T = 1 s, ε = 0.5 and dm = 0.2 d.	180
5.3	Water profile at the first wall at λ / L = 0.25 at θ = 90 and h_i = 3 cm, T = 1 s, ε = 0.5 and dm = 0.2 d…	181
5.4	Water profile at the first wall at λ / L = 0.25 at θ = 270 and h_i = 3 cm, T = 1 s, ε = 0.5 and dm = 0.2 d……..……	181

LIST OF TABLES

Table No.	Title	Page
4.1	Chamber width 2λ of the double vertical slotted wall model	69
4.2	Experimental Program	69
4.3	Distance between wave sensors	74
4.4	Details of the waves, camera and field of view	81
4.5	Sample of measured and calculated data for the single vertical slotted wall model with $dm = 0.2\ d$	83
4.6	Comparison between the theoretical and measured horizontal water-particle velocities	88
4.7	Calculation of the reflection coefficient	100
4.8	Calculation of the transmission coefficient	100

NOTATIONS

Symbol	Definition	Dimension
$2A$	Distance between the centers of two adjacent piles	L
A_m , A_{im} , A_{1m} , A_{2m} , A_{3m} and A_{4m}	Initially unknown coefficients	-
B	Total chamber width	L
C_C	Empirical contraction coefficient	
Cd	Coefficient of discharge	-
CE	Energy losses coefficient	-
CR	Reflection coefficient	-
CT	Transmission coefficient	-
D	Diameter of pile, $du+dm$	L
F	Frequency	Hz
F_o	Hydrodynamic forces	F
KC	Keulegan-Carpenter Number	_
L	Wave length	L
M	Maximum overturning moment	F.L
N	Finite number of terms	-
Re	Real part of a complex value	-
Rn	Reynolds Number	_
R_u	Run-up	L
T	Wave period	T
X, Y, Z	Three dimensional axis	L
x_{12} , x_{13}	Distance between wave probes	L
a	Gap between piles	L
a_1, a_2, a_3	Wave amplitude of co-existing wave which is measured by Sensor 1, 2, 3 respectively.	L
a_t	Wave amplitude of transmitted wave which is measured by Sensor 4.	L

b	Breakwater width	L
cm	Added mass coefficient	-
cdm	Distance from the water surface to the center of the permeability part	L
d	Water depth	L
dm	Draft of permeable intermediate part	L
du	Draft of upper impermeable part	L
dw	Draft of lower impermeable part	L
e, exp	Exponential number (2.72)	-
f	Friction coefficient	-
g	Acceleration of gravity	LT^{-2}
h_i	Incident wave height	L
h_r	Reflected wave height	L
h_t	Transmitted wave height	L
i	Imaginary number ($\sqrt{-1}$)	-
k	Incident wave number	L^{-1}
l	Length of the jet flowing through the gap between piles	L
n, m	Numbers	-
p, q	Limits of integration	-
s	Inertia coefficient	-
t	Time	T
z	Distance from the water surface to the set point	L
ϕ_i	Incident wave potential	-
ϕ_{i1}	First-Order wave potential	-
ϕ_{i2}	Second-Order wave potential	-
$\phi, \phi_1, \phi_2, \phi_3$	Velocity potential	-
θ	Phase of wave	π

α	Head loss coefficient	-
β	Energy dissipation coefficient	-
$\delta^{-}, \delta_{o}^{-}, \delta_{1}^{-}{}_{mn}$	Integration formula	-
$\delta_{2}^{-}{}_{mn}, \delta_{01}^{-}{}_{mn},$		
$\delta_{02}^{-}{}_{mn}$		
η, η_1, η_2	Wave elevation	L
ε	Porosity	-
λ	Half distance of the chamber width	L
μ_m	Evanescent wave numbers	L^{-1}
μ_0	Propagating wave numbers	
υ	Kinematics viscosity	$L^2 T^{-1}$
π	3.14	-
π_1, π_2, π_3	Name of region	-
ρ	Water density	$FL^{-4}T^2$
ω	Angular wave frequency	T^{-1}

CHAPTER 1
INTRODUCTION

1.1 GENERAL

The development and use of coastal regions plays an important role in the national income for many countries around the world. It is a source of attraction for human activities. Therefore, it has enjoyed significantly structures like residential, commercial, industrial buildings, public infrastructure projects and harbors projects, which link between the country's internal and external world. Additionally, it is a significant source for food through fishing activities, commercial cooperation and has been recently provided with large areas for recreation and tourism facilities. A major problem which face the development in these regions is how we can protect the coastal area, harbors and marines by using the best methods, which have less side effects on the adjacent and neighbor shores moreover could be environmental-friendly as well as, it should be less expensive as possible. It is evidenced that most sites for craft harbors, marinas, some parts of the coastal line and coastal aquaculture facilities need some forms of perimeter protection.

In fact, there are many types of coastal protection structures such as artificial beaches, nourishment, breakwaters, jetties, seawalls, artificial headlands and groins. Many types of breakwaters can be used such as the main breakwater (Rubble mound breakwater), massive vertical face breakwaters (block type, caisson type, and cellular type), composite breakwaters (vertical super structure of plain concrete blocks or caissons resting on a large foundation of rubble mound), and flexible breakwaters (row of contact piles or sheet piles). The previous types are fully protection breakwaters and the others are partial protection breakwaters such as (floating types, submerged types, detached wall types and permeable breakwaters like screen types, slotted vertical barriers, perforated caissons, array closely pipe breakwaters, pile-

supported vertical wall breakwater or skirt breakwater. These types will be further explained in detail in the forthcoming chapters.

Permeable breakwaters have already been implemented in form of pile breakwaters, which are formed from a series of piles, placed in rows. Such breakwaters exist at Hanstholm (Denmark) Photo 1.1, Marsa el Brega (Libya), Osaka (Japan) and Pass Christian Mississippi (USA), (Sundar, 2003) and implemented in form of curtain wall-pile breakwaters at Yeoho port (Korea), (Suh et al., 2007) Figure 1.1.

Photo 1.1: Hanstholm breakwater (Denmark). [8 - panoramio]

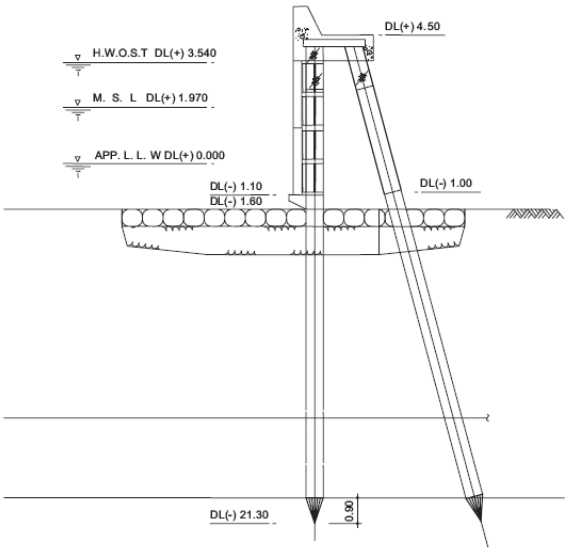

Figure1.1: Cross section of the Yeoho port breakwater. [72 - Suh, 2007]

1.2 STATEMENT OF THE PROBLEM

Breakwaters, either fully protection or partially protection, are structures constructed to protect the shoreline, other coastal structures, marinas, etc. by reflecting and/or dissipating the incident wave energy and thus reduce wave action in the leeside of the breakwater system. The fully protection breakwaters provide a higher degree of protection than partially protection breakwaters. However, a fully protection breakwater may not be of a competitive cost and time of construction wise with a permeable breakwater in relatively deeper water depths. Often they block littoral drift and cause severe erosion and accretion in neighboring beaches and siltation of navigation channel. In addition, they prevent the circulation of water and deteriorate the water quality within the harbor. In some places, they obstruct the passage of fish and bottom dwelling organisms and a solid soil foundation is also needed to support such heavy structures. The most common type of fully protection breakwater is the rubble mound, which consists of layers of graded stone with large concrete blocks as armor layer, which increases the width for deeper water, leaving a large footprint and requiring a great amount of construction. In addition, in offshore locations with severe wave climate, the construction of rubble mound breakwater is not practical as the stones are easily carried away by the waves. An alternative is concrete caissons, which have inherent problems like scour and instability, because of excessive reflections from its vertical solid face. The vertical composite breakwater is a better option in which a rubble mound dissipates the wave under normal conditions and a caisson wall provide additional protection at high tide. However, if the tidal current is large, construction of a composite breakwater will create a disturbance to the natural flow of water.

It is clear that the increasing construction cost and environmental constraints encourage alternative considerations to the traditional fully protection breakwaters for coastal shelter and shore protection. In order to overcome the above-mentioned problems, permeable barriers were suggested. In order to reduce the wave reflection on the up-wave side, to reduce the wave transmission to an acceptable level and to make the incident turbulence and vortexes in the intermediate area depth, it is proposed to use vertical barriers with impermeable parts in lower and upper of

barriers and permeable part in the middle as shown in Figure 1.2. This type of breakwater is complex, where the lower part is considered as a submerged breakwater, the middle part is considered as a slot barrier and the upper part is considered as a semi-submerged barrier. The flow behavior through this type is complicated and needs further studies to find out the hydrodynamic characteristics and performance efficiency of this type in response to waves.

When an array of slotted walls that has more than one row is used, the phenomenon becomes much more complicated and the second row of the slotted walls reflects a portion of the energy. The reflected portion is partially transmitted back through the first row and partially re-reflected by it. In addition, a portion of the energy is scattered, the scattered wave having a frequency that depends upon the slots dimensions, and a portion of the energy is dissipated by skin drag and form drag.

The flow behavior through a number of slotted walls is quite complicated. The wave interaction with such structures is quite difficult and hence researchers focus on experimental and theoretical investigations to understand the flow behavior through a group of slotted walls. For the last several decades, considerable research has focused on examining the efficiency of permeable structures as a breakwater by evaluating its transmission, reflection characteristics and energy loss. This topic needs further studies to find out the engineering solutions by encouraging the provision of scientific technically, environmentally, economically sound and sustainable perimeter protection measures, a move towards schemes designed to work with nature rather than against, and this solution could enjoy high efficiency. In addition, the proposal breakwater here has several important advantages, as follows:

- It allows free passage of sediments, thereby reducing the potential erosion on the down-drift side and reducing accretion on the north-drift side, they are normally a result of the construction of a conventional fully protection breakwater.
- It allows for continuous refreshing the shore area water masses, which in turn minimizes the pollution aspects and environmentally friendly giving great advantage.

- The time of construction is short compared with some conventional fully protection breakwater.
- The construction of a permeable breakwater will allow the free passage of tidal currents with the least disturbance to the environment.
- The two slotted wall breakwater can be used as platform for small ships, where they can approach them closer, and berth on its lee side for loading and unloading operations.
- It is practical, especially when the soil has a low bearing capacity.
- Occupy small zone, in order not to affect the seabed creatures.
- It is relatively inexpensive and considered as cost-effective in deeper waters substitutes for the conventional type of breakwaters.

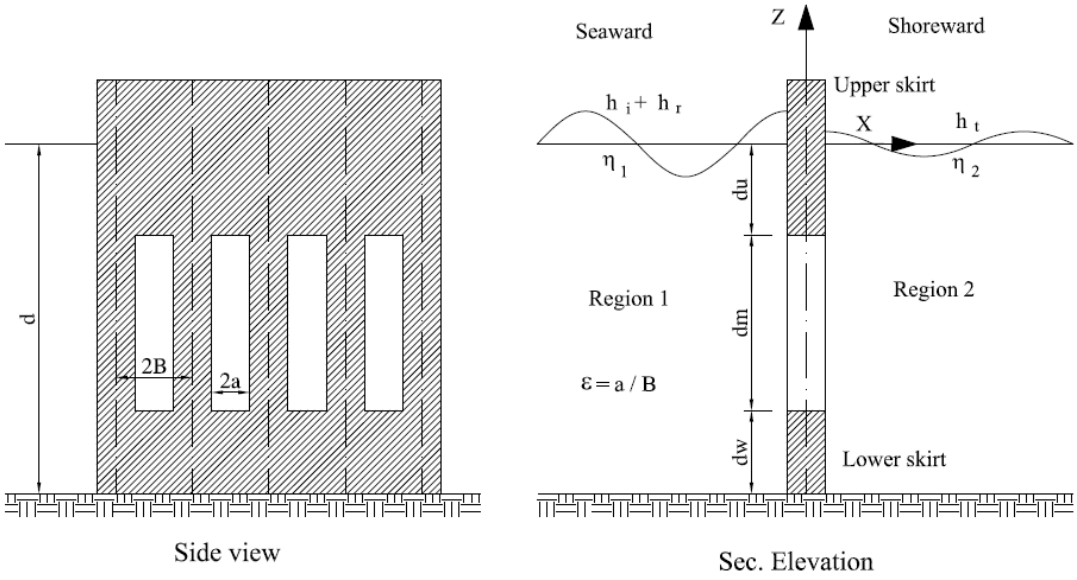

Figure 1.2: Definition sketch for a vertical slotted wall breakwater.

1.3 RESEARCH METHODOLOGY

To fulfill the above-mentioned objectives, the following approaches are adopted:

1. Literature review based on various sources of references such as theses, technical papers, technical reports, books, patents, articles, etc., has been conducted to provide sufficient knowledge about the different types of

breakwaters and understanding wave attenuation concepts, wave protection systems, laboratory and field studies for the design and investigations for the similar types of permeable breakwaters.

2. Numerical models, applying the Eigen function expansion method, have been developed to get the linear waves interaction with single and double vertical slotted walls breakwaters and another numerical model has been established to get the Stokes second-order wave interaction with a single vertical slotted wall breakwater.
3. A series of the experimental tests were conducted for physical models with different parameters under effect of linear waves for both single and double vertical slotted wall. In addition to that, a series of the experimental tests have been conducted to measure the velocity field by PIV and to plot the velocity vector and vortex in front and behind the breakwater to understand the pattern of flow and to interpret the energy dissipation. The measurements were discussed and analyzed to detect interaction of waves with the vertical slotted wall where the effect of permeability on wave interaction with a barrier and the hydrodynamic characteristics of this model were investigated via PIV.
4. Analysis, discussions and comparisons of the numerical models with previous studies and with the experimental works of this study are conducted to validate the numerical models. Curves and important relationships between the different parameters are plotted and described.
5. Finally, summaries, conclusion remarks, recommendations and suggestions for future studies are presented.

CHAPTER 2
LITERATURE REVIEW

2.1 INTRODUCTION

The development in coastal areas generally depends on protecting of the projects against the water waves and currents. Breakwaters are commonly used along shorelines, channel entrances, beaches, harbors, or marinas. There are no universal standards or guidelines to define the maximum acceptable wave height within the proposed project sites. The degree of wave protection and engineering design of them depends on the owner's or engineer's perception of acceptable costs, the characteristics of the location, environmental conditions, economics, types of the available materials in the site, damage risks and the nature of use.

The main function of a breakwater is to provide shore protection by controlling the wave height and current velocity allowed to be transmitted along the coast and inside the harbors. In shore erosion control, breakwaters can be used to promote accretion of a protective beach. Harbors may broadly be classified as natural and artificial. In the later type, breakwaters are the main structures and classified according to the degree of protection into fully protection breakwaters and partially protection breakwaters. The fully protection breakwaters are commonly used and known as the conventional breakwaters, although they have inherent drawbacks like being massive, non-environmental, causing excessive reflections, uneconomical in deeper water etc. while the partially protection breakwaters are recent-use and known as nonconventional breakwaters and investigated to overcome the defects of the conventional breakwaters.

Several studies were done in the past by many investigators to propose new configurations of breakwaters, to improve their performance, and to study their hydrodynamic behavior in attenuating the incident waves. Great attention was given

in particular to the development of different geometric configurations. Attempts were also made to understand the physical behavior of breakwaters action by various numerical model studies.

In this chapter, a review of literature has been carried out based on the types of breakwaters. Some of the available publications on the investigation of these types have been reviewed to understand the recent developments in these types.

2.2 TYPES OF BREAKWATERS

2.2.1 Full protection breakwaters

There are many types of breakwaters; some of them are full protection breakwaters like rubble mound breakwaters, solid vertical massive breakwaters, composite breakwaters and flexible breakwaters.

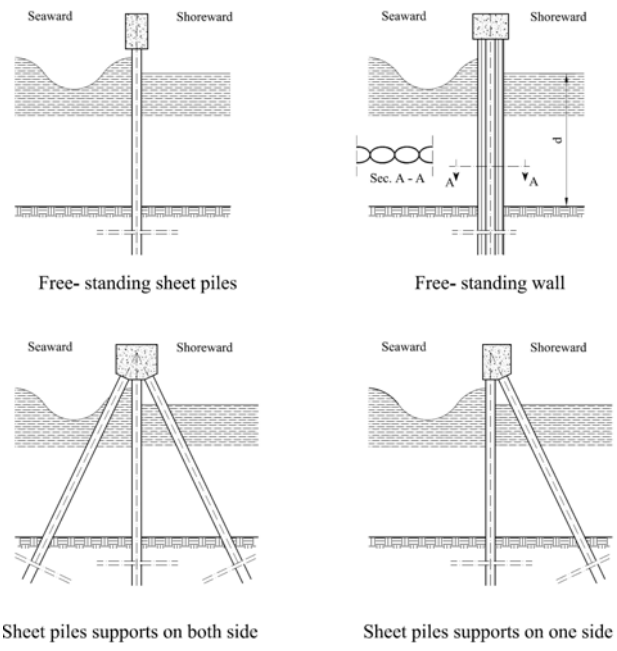

Figure 2.1: Vertical flexible breakwaters. [77 - Truit, 1987]

These types form free-standing walls, or walls supported by battered piles, are shown in Figure 2.1. Some of the full protection breakwaters were described in detail by U. S. Army (1984). Flexible breakwaters are usually consisting of sheet-pile or

reinforced concrete tubular piles of miscellaneous constructions (steel sheet piling included), are propped either on one side or on both by piles (usually by concrete piles).

2.2.1 Partial protection breakwaters

The objectives of these structures are basically to represent a balance between environmental requirements for water quality inside the marine basin, and providing partial wave protection for the sheltered site. As the water depth increases, a breakwater that extends through the full water depth may be uneconomic, and the partial protection breakwaters may be used instead. There are many types of the partial protection breakwaters such as pneumatic and hydraulic breakwaters, submerged breakwaters, floating breakwaters, flexible floating breakwaters, detached breakwaters, perforated breakwaters, piles breakwaters, pipe breakwaters and slotted breakwaters. Some of the partial protection breakwaters are shown in Figure 2.2:

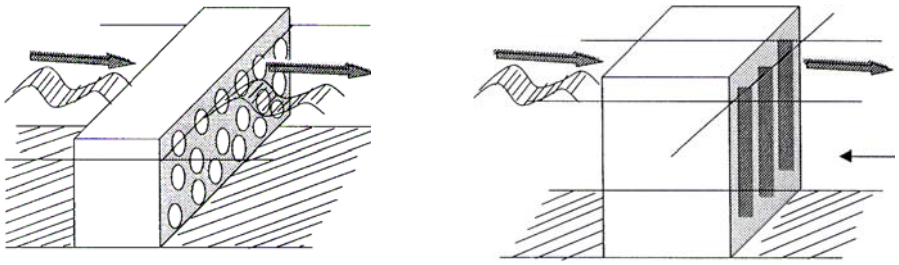

(a) Perforated breakwater. (b) Slotted breakwater. [39 - Koraim, 2005]

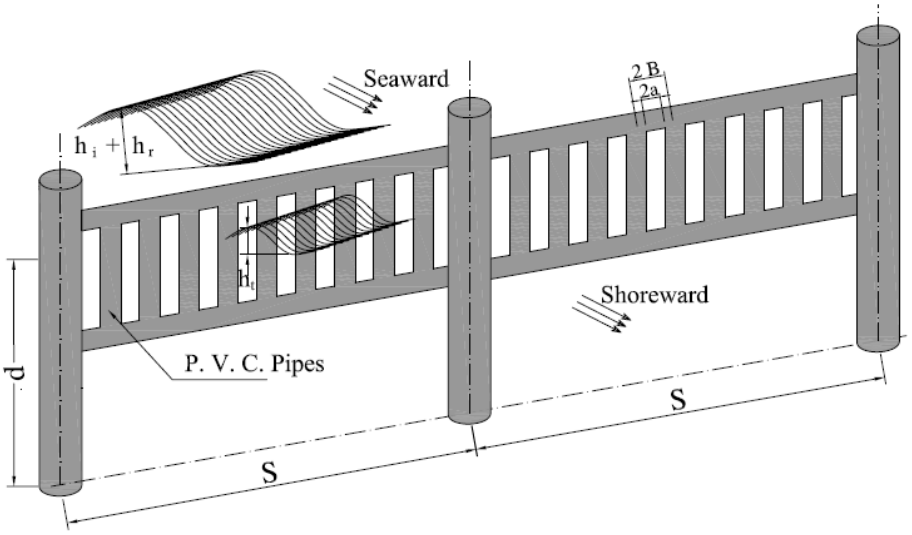

(c) Pipe breakwater. [17 - Galal, 2002]

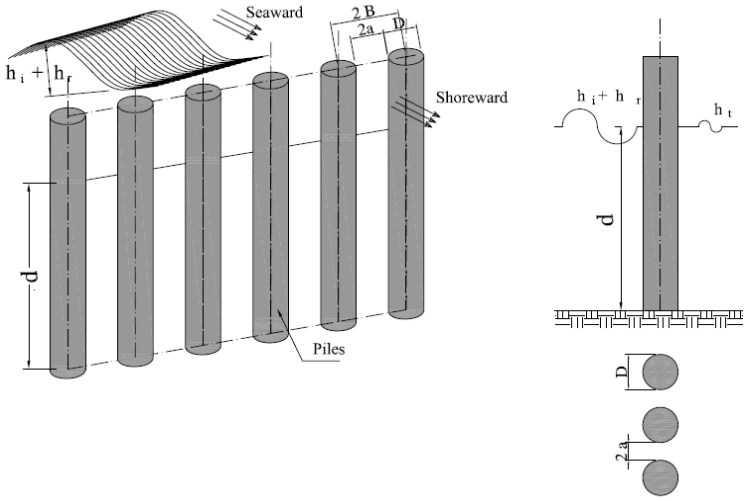

(d) Closely spaced circular pile breakwater. [17 - Galal, 2002]

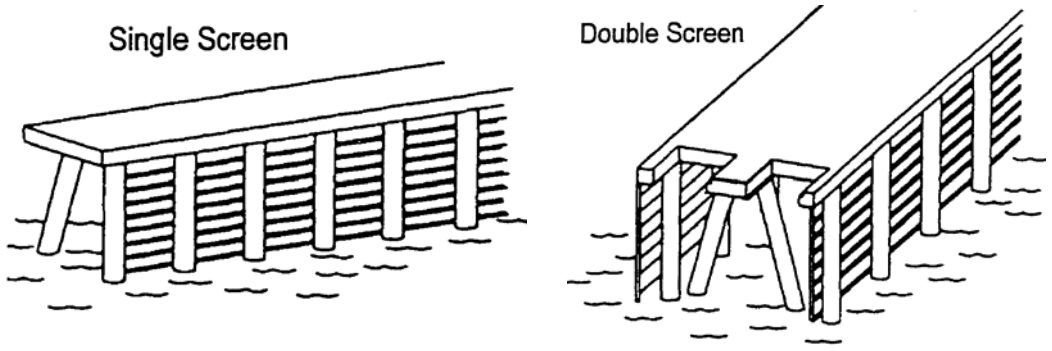

(e) A single and a double wave screen breakwater. [3 - Allsop, 1994]

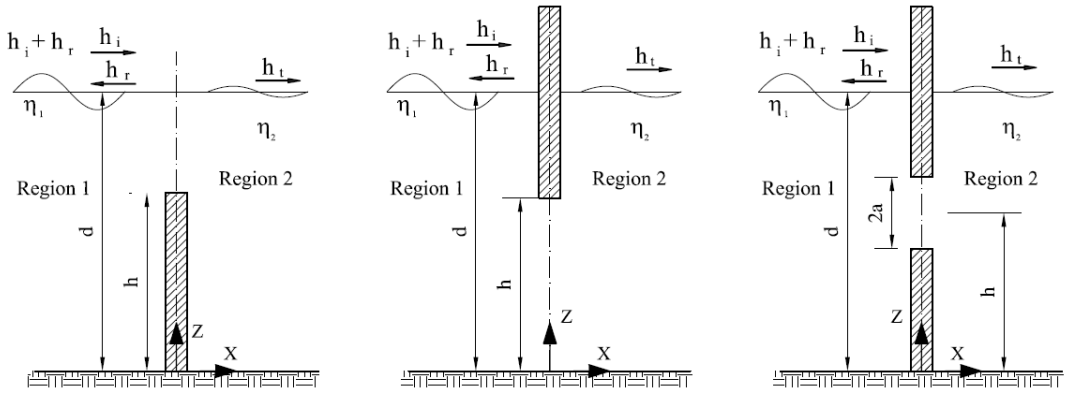

(f) Rigid thin barrier breakwater. [2 - Abul-Azm, 1993]

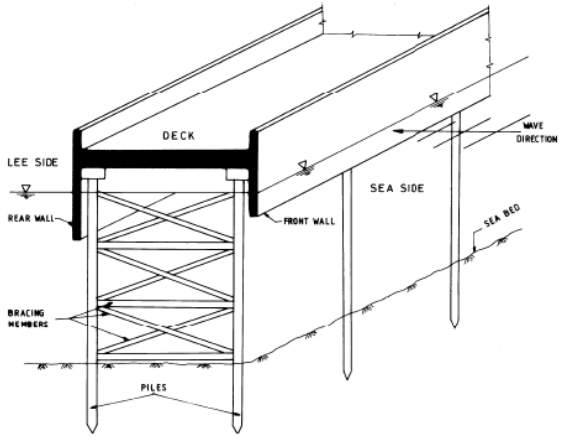

(g) Partially immersed twin wall breakwater. [58 - Neelamani, 2002]

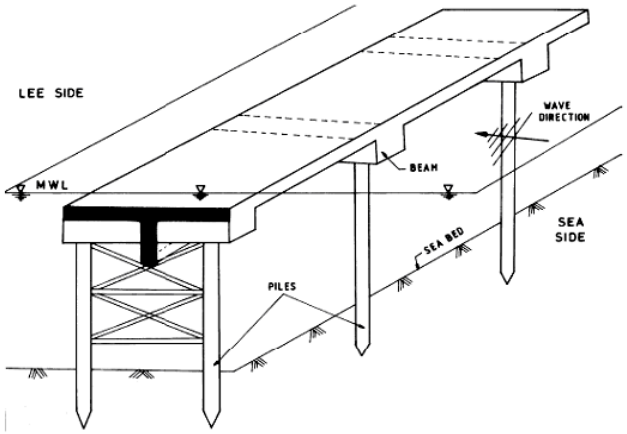

(h) T-type breakwater. [56 - Neelamani, 2002]

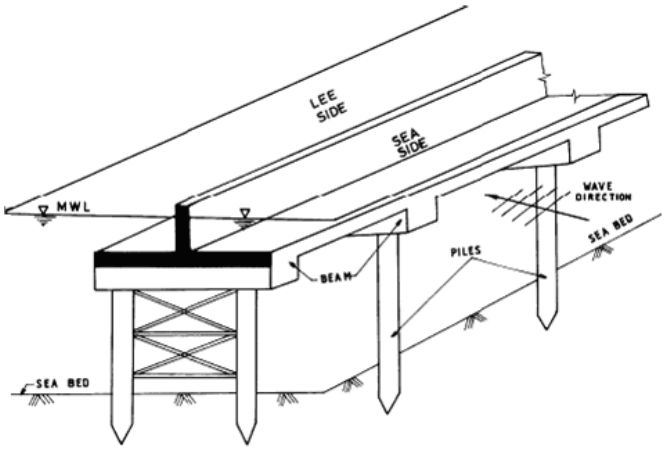

(i) ⊥ - type breakwater. [57 - Neelamani, 2002]

Figure 2.2: Some types of partial protection breakwaters.

The advantages of these breakwaters will be mentioned later. From the partial protection breakwater types, the permeable wave barriers types are commonly used as a good shore or marina protection system, so we will mention it in more detail.

2.3 PREVIOUS STUDIES IN PERMEABLE BREAKWATERS

Wiegel (1960) presented some experimental results for intermediate water depths and an approximate equation for calculating the wave transmission coefficient behind a rigid, thin vertical floating barrier. The approximate solution assumed that the transmitted wave power (average wave energy per unit time) is equal to the wave power below the vertical breakwater. The author reported an equation for the transmission coefficient depending on the small amplitude power wave theory. This theory is found to satisfactorily predict the wave transmission for wave steepness up to 0.05, especially when the depth of immersion of the plate is more than 20% of the water depth.

Sollitt and Cross (1972) derived a theory to predict the wave reflection and transmission characteristics of a permeable breakwater of rectangular cross section. The theory solved for a damped wave component within the breakwater and matches boundary condition at the windward and leeward breakwater faces to predict the reflected and transmitted wave components. An approximate solution to the conventional rubble mound breakwater designs was formulated with an additional consideration for wave breaking. The small amplitude wave motion in the porous medium was considered to be governed by the continuity equation. In the theoretical formulation, it was assumed that, the force exerted by the porous medium in fluid includes two components: (1) a resistance force, which is proportional to fluid velocity, (2) an inertial force, which is linearly proportional to the fluid acceleration. The resistance was expressed in terms of a friction coefficient. The friction coefficient f was calculated implicitly using the Lorentz principle of equivalent work. This principle states that the energy dissipation during one wave period should be the same whether evaluated from the true nonlinear formula or from its equivalent linearized form. In their linear approximation, the fluid velocity inside the medium was assumed to be linearly proportional to the pressure difference between the two sides of the porous medium.

Grüne et al. (1974) reported the transmission coefficient for vertical slotted walls as a function of porosity, shape of wall element and wave approach direction through an experimental study. It was concluded that the transmission coefficient reduces with an increase in the wall thickness and wave steepness. The shape of the elements had less influence for normally incident waves.

Abdul Khader et al. (1981) studied the hydraulic aspects of closely spaced circular cylinders as a breakwater, with respect to parameters like cylinder spacing, cylinder diameter, wave steepness and relative water depth and experimental results were compared with the available theories. Case study of the closely spaced pile breakwater, consisting of single row of octagonal piles, constructed in Singapore was examined. The tests were done with pipes of diameters 37.8 mm and 25.1 mm with different gap ratios resulting in porosity in the range of 5 % to 30 %. It was observed that increase in transmission with porosity was rapid up to 20 % porosity and was gradual beyond 20 %. The diameter of the cylinders did not significantly affect transmission. For a given porosity, transmission was found to decrease slightly with an increase in wave steepness and relative depth.

Hagiwara (1984) outlined a theoretical analysis using an integral equation derived for the unknown horizontal velocity component in a previous wall. The integral equation was proposed for estimating the reflection and transmission coefficients of upright structures for wave dissipation, and various factors related to wave and structural condition having influences on the wave dissipating characteristics. He examined two-dimensional experiments in a wave channel 20 m long, 0.6 m wide and 1.0 m deep. The breakwater model consists of two slotted walls as shown in Figure 2.3. He concluded that the head loss coefficient and apparent orifice length related to the drag coefficient *Cd*, the inertia coefficient s and the geometric dimensions of the slotted wall. He found that the wave dissipating characteristics of the upright structure with the pervious wall is explained well by the integral equation theory and the theoretical results are in good agreement with experimental data with respect to reflection, transmission and the wave dissipation coefficients.

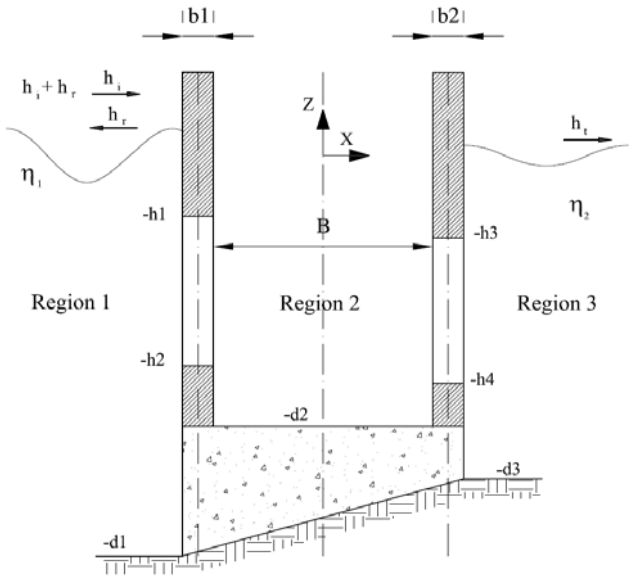

Figure 2.3: Breakwater with pervious vertical walls at both seaward and landward sides. [22 - Hagiwara, 1984]

Hutchinson et al. (1984) conducted tests on a 1:12 model of the then proposed pile breakwater for the Half Moon Bay Marina, Auckland, New Zealand and reported that 50 % reduction in wave transmission could be obtained using 300 mm timber vertical piles at 37mm spacing. The forces were found to be 22 *kN* per meter compared to 53 *kN* per meter on a solid breakwater. It was further found that a barrier 2 m deep, 1.5 m behind the pile breakwater reduced the wave transmission to 30 %.

Patarapanich et al. (1985) reported model tests on the 1:25 model of the breakwater for the boat harbor at Jervoise Bay, in Western Australia at 10m water depths. The submergence of the skirt was varied from 0.2 to 0.9 and the porosity was varied up to 20 %. The relative water depth was varied from 0.2 to 0.6 to model intermediate to deep-water conditions. The skirt breakwater was recommended for short wave or for deep-water conditions. Wave transmission was found to decrease with a decrease in porosity and an increase in submergence of the skirt. The experimental results showed higher transmission than the expected value of 0.3, which was estimated based on power transmission theory beneath the rigid barrier of Wiegel (1960) and expression of Hayashi et al., (1968) for transmission through closely spaced piles.

The force acting on the skirt was found to be higher than theoretical value predicted by potential flow theory and was much lower than the design wave force calculated from the curves of Miche-Rundgren in shore protection manual (1984) .

Truit et al. (1987) conducted experimental studies on wave transmission through a breakwater consisting of a single row of piles for both regular and random waves and reported that experimental results on transmission coefficient followed closely with the theoretical solution of Hayashi et al. (1966).

Gardner and Townsend (1988) reported their studies on model tests of a 250 m long slotted vertical screen breakwater for a marina at Plymouth, England. The site conditions prevented the construction of breakwater using rubble mound or caissons or floating breakwaters. The requirements of the breakwater were to have minimum size and least reflections along with required protection from waves. Hence a vertical screen structure supported on piles was proposed. Reflection and transmission coefficients were measured for single and double screens for which porosity was varied between 8 % and 35 %. It is reported that a porosity of 8 % for a single and 16 % for double screen gave acceptable values of reflection *CR* and transmission *CT* coefficients, and that the performance of screens with horizontal slots was similar to screens with vertical slots.

Herbich (1989) studied the wave transmission through a breakwater consisting of closely spaced piles experimentally (either one or two rows of circular piles with row distance, center to center, equals to twice the pile diameter). Results showed that the pile diameter has a minimal effect on wave transmission and the gap ratio (*G/D*) is the most effective variable. The reduction in gap spacing from 20 % to 10 % reduced the values of wave transmission coefficient by approximately 30 %. However, for a 10 % gap ratio (*G/D*), adding a second row of piles reduces the wave transmission coefficient (*CT*) by about 5 to 10 %. Finally, the wave transmission coefficient decreases as the wave steepness (h_i/L) increases.

Mani (1989) investigated experimentally transmission and reflection of single row and double rows of vertical piles and suggested that a transmission coefficient of the order of 0.5 can be achieved by providing double rows of piles at a *G/D* ratio of 0.22.

Double rows of piles were found to be 30 % more efficient than a single row of piles with the same *G/D*.

Dalrymple et al. (1991) investigated the reflection and transmission coefficients on a porous breakwater for normal and oblique wave incidence. The problem was solved by Eigen function expansions theory. For oblique wave incidence, the reflection and transmission coefficients were significantly altered and they were calculated. Using a plane-wave assumption, which involves neglecting the evanescent Eigen modes that exist near the structure boundaries (to satisfy matching conditions), the problem were reduced from a matrix problem to one, which was analytic.

Bennett et al. (1992) studied a mathematical model of a slotted wave screen breakwater. A theory was given to describe the interaction of an incident plane wave with a slotted wave screen breakwater. The effects of energy dissipation in the flow through the screen were accounted for by a semi-empirical nonlinear term involving a head-loss coefficient, expressed in terms of the screen porosity avoiding the need to determine the coefficient experimentally. Calculations of the reflection coefficient were presented for both an isolated screen and a screen with a solid backing wall and compared with experimental data. The experimental results agreed well with theoretical results. It was also observed that the results for both horizontal and vertical orientation of slots were extremely close.

Fugazza et al. (1992) studied the hydraulic design of perforated breakwaters. The authors analyzed the wave attenuation produced by the permeable structure and propose design formulas that can be used for the optimized hydraulic design of Jarlan-type breakwaters. A closed form solution for wave reflection from a multi chamber perforated wall caisson was proposed. The proposed model, based on the linear wave theory, was validated by comparison of the theoretical results with the experimental measurements of other authors. It was shown that the reflection is minimized when the wave chamber width is about one quarter of the wavelength. The results showed that the Jarlan-type breakwater with a single chamber gives the most effective wave reduction in the range of practical applications and that no particular configuration of the porous wall can be suggested as the best one. The

energy losses at the wall were computed using the plate orifice formula when the diameter of the pores is relatively larger than 0.5 times the thickness of the wall; otherwise the pipe formula was used. The size of the breakwater cannot be standardized, since the optimum hydraulic design of the structure is linked to the parameters of the design wave. Moreover, the proposed design formulas were used to approximately predict the response of the structure to incident irregular waves.

Kriebel (1992) investigated wave transmission and wave forces for vertical wave barriers. This type may be called wave screen or slit-type breakwater. A theoretical analysis was reported based on application of continuity, momentum and energy equations to flow through the slots in the breakwater, accounting for head losses associated with flow constriction and re-expansion. Experimental test using regular waves with four different frequencies were conducted. The author concluded, wave transmission decreased as the wave steepness increased and as the porosity decreased. However, wave forces increased under these same previous conditions. The wave transmission decreased only at the expense of a large increased in the wave force on the wall. The maximum wave energy dissipation occurred when $CT = 0.5$.

Kakuno et al. (1993) investigated the scattering of small amplitude water waves by an array of vertical cylinders theoretically and experimentally. The authors developed a method of matched asymptotic expansions to estimate the reflection and the transmission coefficients without considering real fluid effects.

Losada et al. (1993) investigated obliquely impinging waves on dissipative multilayered media, consisting of alternating layers of upright porous walls and water, of equal or different thickness using linear wave theory. The tests confirmed that the performance of upright absorbers with constant porosity can be improved by decreasing the porosity of the porous screens towards the rear of the absorber for $\omega^2 d/g > 0.4$ and that constant porosity absorbers produce minimum reflection when $\omega^2 d/g < 0.3$.

Allsop et al. (1994) described typical problems of harbor design and influence of wave reflections from harbor structures. Modifications to existing vertical walls and

alternative forms of construction were described with emphasis on porous structures and slotted barriers. Use of multiple screens was recommended for increased performance. Laboratory tests revealed that porosity in the range of 10 % to 25 % and a spacing of the impermeable rear skirt at *B/L* in the range of 0.15 to 0.25 could result in acceptable reflections.

Yu (1994) studied wave-induced oscillation in a semicircular harbor with porous breakwaters based on the linear potential wave theory and a newly derived boundary condition for the breakwaters. By separation of variables, general expressions of the velocity potential in terms of unknown constants were obtained in the harbor region and in the open sea. These expressions were matched so that the porous boundary condition and the continuity of mass flux and free surface at the harbor entrance are satisfied. The velocity potential and, consequently, the free surface oscillation in the whole domain concerned were thus determined. The frequency response of a harbor with breakwaters of various porous properties was investigated. It was noted that the inertial effect of the porous structure is mainly to increase the resonant wave number and it does not reduce the amplitude of the resonant oscillation significantly. On the other hand, the porous resistance gave rise to little change of the resonant wave number but it reduced the amplitude of the resonant oscillation effectively. A small but finite permeability of the breakwater was found to be optimal to diminish the resonant oscillation.

Lengricht (1995) studied experimentally attenuation of regular waves by different semi submerged vertical seawalls. It was proved that dissipation of initial wave energy can be extended when the semi submerged breakwater is designed as a pervious wall, to induce additional turbulent motion in the flow. The most noticeable result was that the rate of energy dissipation is not significantly influenced by the type of construction (perforated or slotted) when relative void ratios and porosity of the structure are equal.

Mani et al. (1995) investigated a suspended pipe breakwater for small harbors where moderate wave agitations are admissible. The structure (Figure 2.4) consisted of a row closely spaced pipes mounted onto a frame and suspended from support piles

spaced far apart. This can be considered as variation of the skirt breakwater. It was concluded that suspended pipe breakwater is economical, efficient and a promising substitute for pile breakwater. A gap to diameter ratio of 0.22 and draft to water depth ratio of 0.46 were recommended to achieve wave transmission coefficient less than 0.5. They noticed that, for $h_i/gT^2 > 0.008$, the suspended pipe breakwater can attenuate incident waves by 50 %. However, for $0.005 < h_i/gT^2 < 0.008$, the incident wave can attenuate by 40 %. The suspended pipe breakwater can reduce the investment cost by about 40 % and attenuate waves with the same efficiency as that of a row of closely spaced piles.

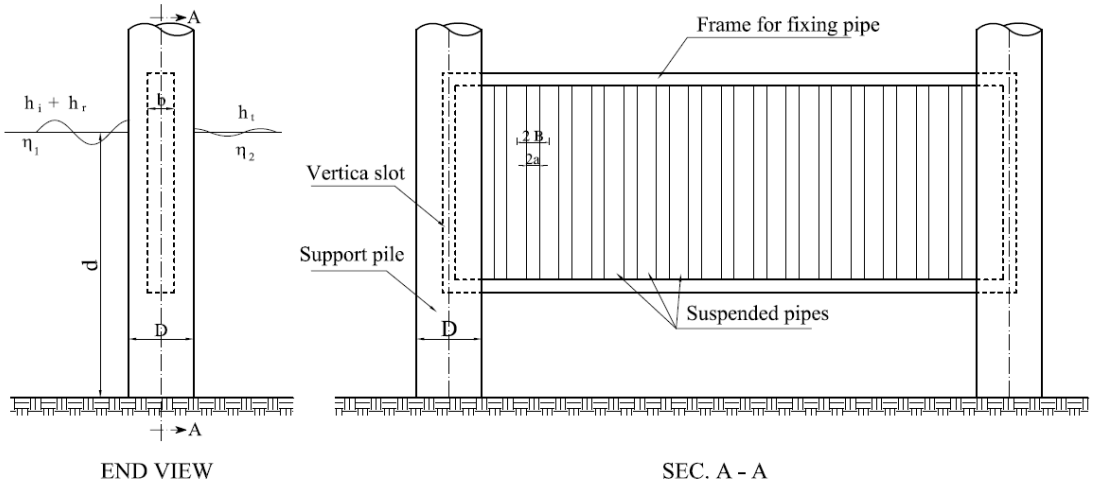

Figure 2.4: Details of suspended pipe breakwater. [47 - Mani, 1998]

Suh et al. (1995) studied the wave reflection from perforated-wall caisson breakwaters. Using the Galerkin Eigen function method, an analytical model was developed that can predict the reflection coefficient of a perforated-wall caisson mounted on a rubble foundation when the waves are obliquely incident to the breakwater at an arbitrary angle. The waves were normally incident to a perforated-wall caisson lying on a flat sea bottom, the result of the proposed model was shown to exactly agree with the solution by Fugazza and Natale (1992).

Yu (1995) investigated the diffraction of water waves by porous breakwaters based on the linear potential wave theory. The formulation of the problem included a newly derived relation for the fluid motion through thin porous structures in addition to the

conventional governing equation and boundary conditions for small-amplitude waves in ideal fluids. The porous boundary condition, indirectly verified by collected experimental data, was obtained by assuming that the flow within the porous medium was governed by a convection-neglected and porous-effect-modeled Euler equation. A vertically two-dimensional problem with long-crested waves propagating in the normal direction of an infinite porous wall was solved and the solution was compared with available experimental data. The wave diffraction by a semi-infinite porous wall was studied by the boundary-layer method, in which the outer approximation was formulated by virtue of the reduced two-dimensional solution. It was demonstrated that neglecting of the inertial effect of the porous medium lead to an under-estimate of the functional performance of the porous breakwaters.

McConnel et al. (1996) reported model studies of the seawall for the Victoria harbor in Hong Kong, for which the Government of Hong Kong fixed the desired level of reflection as less than 50 %. Different types of structures were considered and detailed tests were done on chambered seawalls with porous walls by changing chamber width, number of chambers, and the porosity. It was concluded that the performance of more number of narrow slits were better than wider slits of the same porosity. The *B/L* ratio of the chamber for least reflection was found to vary between 0.11 and 0.15 as against 0.2 to 0.25 as reported by earlier investigators.

Kakuno et al. (1997) investigated theoretically and experimentally the scattering of small amplitude water waves impinging on several rows of vertical cylinders of arbitrary cross section with or without a back-wall as shown in Figure 2.5. A theoretical method of matched asymptotic expansions was developed without considering real fluid effects. The energy loss caused by flow separation near cylinders was modeled by introducing a complex blockage coefficient. The theory with the empirical coefficients determined for an array of cylinders agrees well with experimental results obtained using different scales of models with or without a back wall.

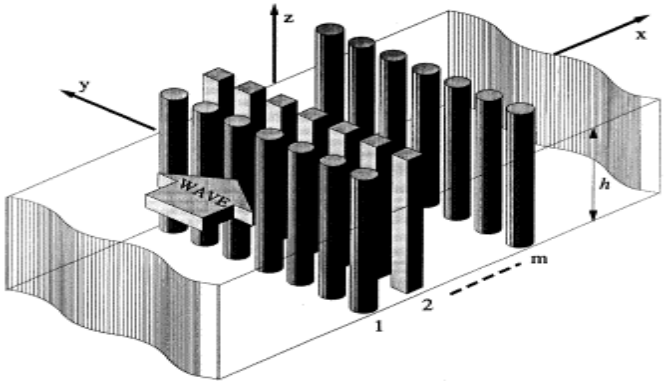

Figure 2.5: Rows of cylinders without a backwall. [38 - Kakuno, 1997]

Cox et al. (1998) presented an improved model of a curtain wall breakwater consisting of a perforated front wall installed at some distance in front of the impermeable rear curtain wall. Tests were carried out for understanding the impact of water depth, wave length, incident wave height, barrier submergence, barrier separation and porosity on transmission and reflection coefficients. The experiments confirmed that reflections were minimized for an optimum front wall porosity of about 20 %. The wave steepness was found to have little effect on transmission and reflection coefficients. This concept was selected as the best suitable one for the Royal Prince Alfred Yacht Club (RPAYC) on Pittwater in Sydney based on its features like low reflection, visual impact, and low impact on current and sediment flow.

Isaacson et al. (1998) outlined a numerical calculation of wave interactions with a thin vertical slotted barrier extending from the water surface to some distance above the seabed as shown in Figure 2.6. The numerical model is based on an Eigen function expansion method and utilizes a boundary condition at the barrier surface that accounts for energy dissipation within the barrier. The authors also described laboratory tests to assess the proposed numerical method. The permeable wave barrier was constructed of vertical panels of width 2.0 cm and thickness of 1.30 cm, such that the porosity of the barrier can be varied by changing the dimensions of the slots between the panel members. Half and fully immersed barriers with porosities of 0.05, 0.1, 0.2, 0.3, 0.4 and 0.5 were tested.

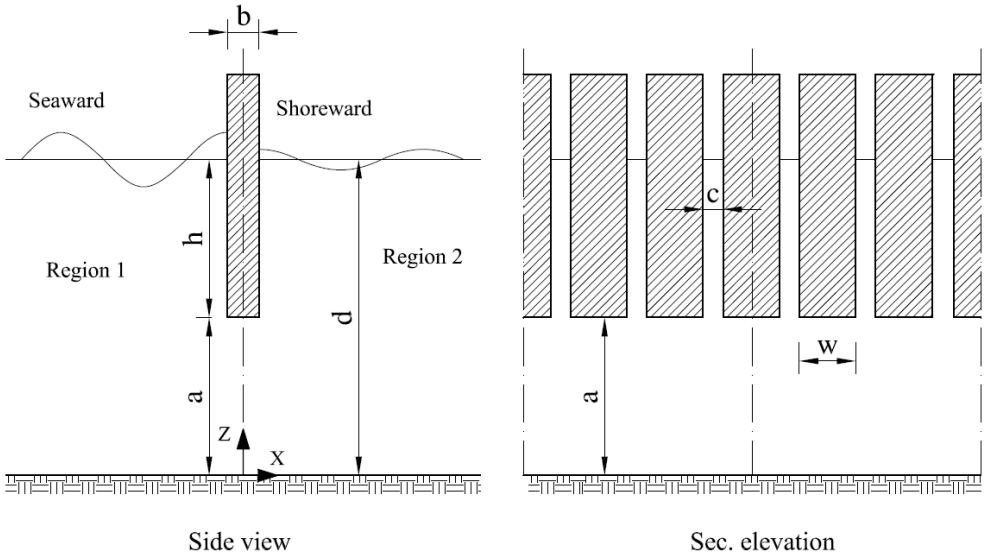

Figure 2.6: Vertical slotted barriers. [34 - Isaacson, 1998]

The numerical solution explained that, the reflection, transmission and head loss coefficients depend on the permeability parameter G that is generally complex and depend on the friction coefficient f and inertia coefficient s where the inertia coefficient depend on the added mass coefficient cm and given by

$$G = \frac{\varepsilon}{f - is} \tag{2-1}$$

$$s = 1 + cm\left(\frac{1-\varepsilon}{\varepsilon}\right) \tag{2-2}$$

where "ε" is the porosity of the model ($\varepsilon = c / w$).

The numerical results compared well with the theoretical predictions for the limiting cases of an impermeable barrier and a permeable barrier extending down to the seabed, and close agreement was found in all cases. Comparisons with experimental measurements of the transmission, reflection, and energy dissipation coefficients for a partially submerged slotted barrier were carried out and it was found that a good agreement between numerical and experimental results, using constant values of *cm* and *f* for varying porosities, implied that, f and cm do not vary with porosity. The

method was found to over predict slightly the wave transmission through the barrier at high wave steepness. Based on comparison with experimental results, empirical coefficients *cm* and *f* to be used in the numerical model were suggested as 0 and 2 respectively. Further, the authors compared the effect of porosity on both partially submerged and fully submerged slotted barriers using experimental and numerical results. Constant values of added mass coefficient cm and friction parameter f were used in both cases for all porosities and the numerical results.

Mani (1998) studied experimentally the wave transmission through partially submerged pipe breakwater. The author developed a formula for estimating the wave transmission coefficient and the wave acting forces. The author found that, the transmission coefficient decreased as the wave parameter (h_i/gT^2) increased and the gap between piles (G) decreased. The dimensionless force also decreased exponentially with increasing the wave steepness parameter. In addition, the force acting on the structure depended largely on wave steepness, depth of submergence, and gap to diameter ratio. Finally, results indicated that the submerged pipe breakwater resulted in reduction of forces by about 20 to 40 % relative to the forces acting on an equivalent solid plate.

Bergmann and Oumeraci (1999) conducted tests on a single and multiple chamber system with porosity varying between 11 % and 40.5 % and proposed analytical expressions for transmission *CT* and reflection *CR* coefficients. The multi-chamber system with progressively decreasing porosity of the screens was reported to be efficient in wave damping. Multi-chamber systems were found to be effective over a wider range of B/L beyond 0.3.

Chakrabarti (1999) investigated the interaction of waves with a breakwater consisting of three rows of spaced panels separated by a chamber. The seaside panel consisted of a single row with 40 % porosity while the port side panel consisted of two closely spaced rows with 33 % porosity. This type of breakwater was found to be most efficient for the ratio of gT^2/L in the range of 6-18. The differential pressures experienced at the panels were only a fraction of the corresponding pressure

expected at a solid vertical wall. At most frequencies of the waves, the loads on the sea side panels were substantially lower than those in the port side panels.

Hsu and Wu (1999) studied the Second-order wave interaction with porous structures numerically. In this study the mathematical formulation of water-wave interaction of the fluid field with a porous structure as a two-dimensional, non-linear boundary value problem (bvp) in terms of a generalized velocity potential was reported. The non-linear bvp was reformulated into an infinite set of linear bvps of ascending order by Stokes perturbation technique, with wave steepness as the perturbation parameter. Only the first- and second-order linear bvps were retained in this study. Each linear bvp was transformed into a boundary integral equation. In addition, the boundary element method (BEM) with linear elements was developed and applied to solve the first- and second-order integral equations. The first- and second-order wave profiles, reflection and transmission coefficients, and the amplitude ratio of the second-order components were computed as well. The numerical results demonstrated that the second-order component can be neglected for a deep water-wave and may become significant for an intermediate depth wave.

Isaacson et al. (1999) outlined a numerical calculation of wave interactions with a pair of thin vertical slotted barriers extending from the water surface to some distance above the seabed as shown in Figure 2.7. The authors also described laboratory tests undertaken to assess the numerical model. The numerical model is based on an Eigen function expansion method and utilizes a boundary condition at the surface of each barrier which accounts for energy dissipation within the barrier. Experiments were carried out by used pair of thin vertical slotted barriers with porosities of 0, 5 and 10 % and spacing between them were 0.22, 0.55 and 1.1 of λ/d. Comparisons were carried out with previous numerical studies for a permeable barrier extending down to the seabed, and close agreement was found in all cases. Laboratory tests were carried out to provide an assessment of the numerical model.

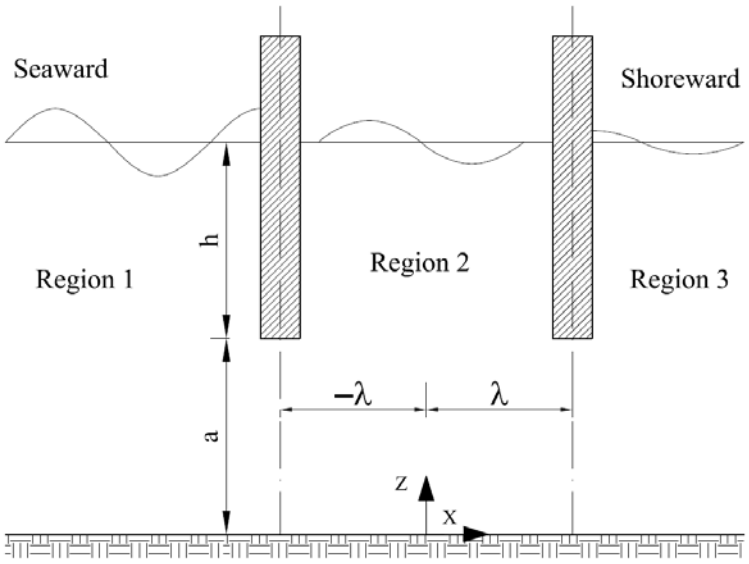

Figure 2.7: Vertical double slotted barriers. [35 - Isaacson, 1999]

A comparison of corresponding numerical predictions of the transmission, reflection and energy dissipation coefficients with experimental results was given. The agreement was generally satisfactory and indicated that the numerical method was able to adequately account for the energy dissipation by the slotted breakwaters, provided that the relevant empirical coefficients were chosen. The energy dissipation within the slotted barrier was related to friction and added mass coefficients which were estimated by fitting with experimental results.

Nakamura et al. (1999) proposed double skirt breakwater with different drafts to reduce both transmission and reflection based on numerical and experimental studies. The draft of the front skirt was recommended as half of the rear skirt for minimum reflection. The energy dissipation of the double skirt was found to be much more than single skirt and a maximum of about 95 % was observed. Flow visualization of the experimental study revealed the presence of vortex flow beneath the skirts, with the one beneath the front skirt being more pronounced. Larger vortices were observed corresponding to minimum reflection coefficient.

Subba et al. (1999) investigated the transmission of waves through two rows of perforated piles for the influence of water depth, wave steepness, spacing between piles and spacing of pile rows along with effect of staggering of piles. The studies revealed that perforated piles attenuate more wave energy than non-perforated piles and the staggering of piles had little effect on the wave transmission. The transmission was found to be least when spacing between the pile rows equals pile diameter for both perforated and non-perforated piles.

Park et al. (2000) developed an analytical model by using Eigen function expansion method that can predict the scattering of irregular waves, in case of a breakwater consisting of an array of vertical cylinders as shown in Figure 2.8. The authors presented simple formulas for calculating the reflection and transmission coefficients. The authors examined the prediction ability of the developed model by comparing the theoretical results with the experimental ones. The experiments were carried out in the wave flume at the Coastal and Harbour Engineering Research Center of the Korea Ocean Research and Development Institute. The wave flume was 53 m long, 1.25 m high, and 1.0 m wide, and all experiments were carried out in water of 0.50 m depth.

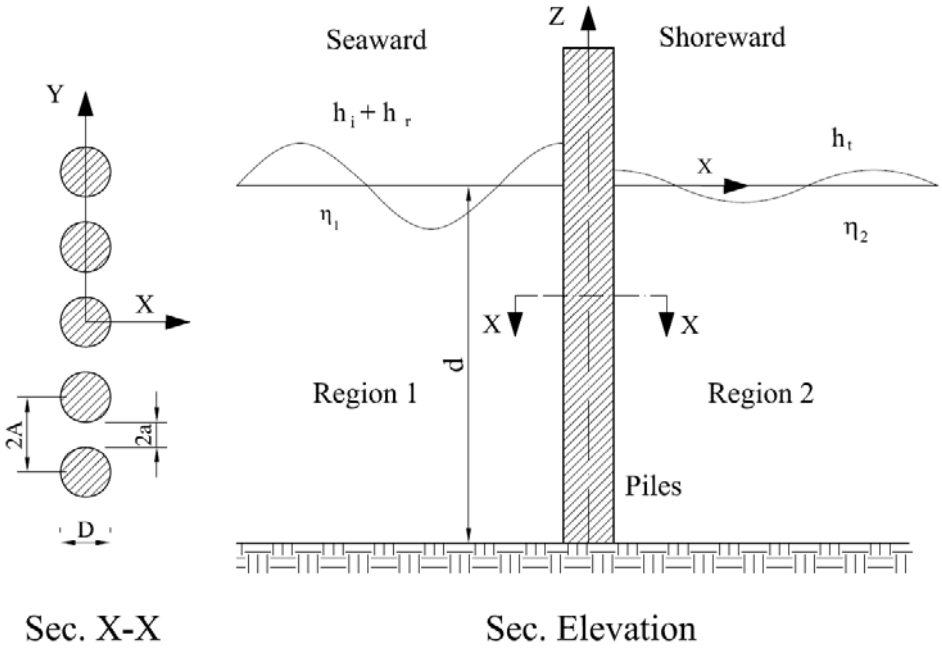

Figure 2.8: Vertical cylinders breakwater. [61 - Park, 2000]

Hall et al. (2000) studied the wave transmission through multi-layered wave screens. The model was a wave screen with a porous vertical wall, usually constructed using rectangular slots oriented in either a horizontal or vertical direction and attached to vertical piles or support structures as shown in Figure 2.9. A wave screen breakwater was composed of a series of screens attached to the support system. Hydraulic mode1 tests were undertaken in a two-dimensional wave flume. The tests investigated the impact of slot orientation, screen porosity and screen spacing on the transmission coefficient for single, double and triple screen systems. The screens were subjected to irregular wave conditions of varying wave height, wave period and water depth. The results showed that wave screens could reduce wave transmission by up to 60 % for a single screen and 80 % for a double screen. The wave transmission was found to be a function of the number of screens used, screen porosity and orientation, wave steepness, relative depth, d/gT^2 and dimensionless gap space. Empirical equations were developed for single and double screen systems and were able to predict the performance of the wave screens within 3 % of the actual value for a single screen system and 9 % for a double screen system.

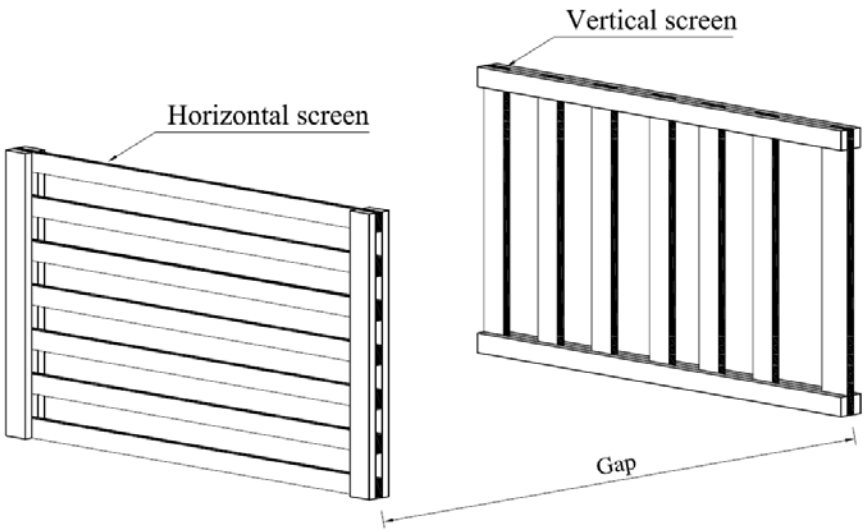

Figure 2.9: Schematic showing horizontal and vertical orientations and screen spacing. [23 - Hall, 2000]

Sahoo et al. (2000) investigated the trapping and generation of surface waves by submerged vertical permeable barriers or plates kept at one end of a semi-infinitely

long channel of finite depth for various barrier and plate configurations. The various fixed barrier configurations were (1) a surface-piercing barrier; (2) a bottom-touching barrier; (3) a barrier with a gap; and (4) a fully submerged barrier. The theoretical solution was based on an Eigen function expansion method. In this study the boundary condition on the porous obstacle was the one developed by Yu and Chwang (1994), which is a generalization of the porous boundary condition developed by Chwang (1983). It was observed that the porous effect parameter plays a very important role in modeling the dissipation of the wave energy, and wave trapping depends on the position of the barrier. The wave amplitudes at large distances were obtained and analyzed for different values of the porous-effect parameter and the distance between the wave maker and the channel end-wall.

Williams et al. (2000) investigated the interaction of linear waves with absorbing-type caisson breakwaters, which possess one, or two, perforated or slotted front faces which result in one, or two, interior fluid regions (chambers). A theoretical method by Eigen function expansion technique was developed to calculate the reflection and transmission and the energy dissipation (wave damping) under the assumption of potential flow and linear wave theory a boundary-value problem within the interior region(s) of a caisson breakwater. The perforated or slotted surfaces were idealized as thin porous plates. Energy dissipation in the interior fluid region(s) inside the breakwater was modeled through a damping function, which was taken to be proportional to the chamber width and inversely proportional to the cube of the incident wavelength. The theoretical predictions of the reflection coefficients for the two-chamber structures using the present model were compared with those obtained from laboratory experiments by other authors and a good agreement was found. From this study, it was found that the inclusion of the damping in the interior fluid region gives rise to improved agreement between theory and experiment.

Nakamura et al. (2001) investigated a new type of breakwater consisting of two different walls to mitigate secondary effects which caused by high reflection waves from conventional curtain-walled breakwater. The structure had a rear impermeable curtain wall extending up to the seabed and located on the shore side of the breakwater and the other was consisted of an array of inclined plates with the same

gap and located on the offshore side. Draft depths of these walls are presumed to be deep enough to overcome the tidal difference. The mechanism of effective dissipation of wave energy was enhanced the generation of vortex flows from the plate-array front wall. The experiments revealed that reflection is a minimum for a definite value of *B/L* for each of the configurations tested. The minimum *B/L* for down fin configuration is 0.13 whereas *B/L* for up fin configuration is 0.18 for minimum reflection. For longer waves, the wave height inside the chamber was higher than the incident wave, and no definite peak was observed corresponding to the minimum reflection configuration. Comparison with impermeable curtain wall for same draft and chamber width revealed that *B/L* for minimum transmission for the present model was independent of tidal fluctuations; whereas, *B/L* of the impermeable curtain wall for minimum reflection is dependent on tidal fluctuation.

Hall et al. (2001) investigated the transmission of waves through single and multiple wave screens. The model was a porous vertical wall constructed by rectangular slats oriented in either a horizontal or vertical direction and attached to vertical piles or support structures. The experimental study were undertaken for the screens, where they were subjected to irregular waves with varying wave height, wave period and water depth. The authors concluded that the wave transmission can be reduced by 60 % for a single screen and 80 % for double screens. The transmission coefficient was found to be a function of number of screens, porosity, orientation, wave steepness, relative depth and gap between screens. Empirical equations were developed for single and double screen systems for vertical and horizontal arrangement of slats.

Zhu et al. (2001) investigated the interaction between waves and a slotted seawall analytically as well as experimentally. The analytical investigations based on the linear wave theory concluded that the porosity and the wave height influence reflection, which is reported to be least when B/L of the chamber is around 0.25. The reflection behavior becomes optimal when the porosity is moderate about 0.2. The immersed depth had some effect on the reflection coefficient of the seawall structure, but the improvement was small when the immersed depth was larger than the half of the water depth. A series of physical model tests were carried out to examine the

analytical results and the comparisons showed a good agreement, provided, certain parameters of the model were suitably chosen. This demonstrated that the analytical model is able to account adequately for the energy dissipation by the slotted plate and can provide information for the design of such seawalls.

Requejo et al. (2002) derived a theoretical method by using an Eigen function expansion method for the potential flow around and inside vertical porous breakwaters for regular waves. He also investigated the extension to irregular waves. Analytical expressions were derived for functional performance variables (reflection, transmission and dissipation) and for stability (horizontal and vertical forces, including the corresponding overturning moments). These expressions were numerically exploited to demonstrate the capability of the model for design purposes. The parameters required in the porous flow model were expressed in terms of the porous material characteristics and were investigated experimentally. Some additional experiments using a vertical permeable structure with an impermeable back wall were carried out to validate the model. These experiments allowed the calibration of the porous flow parameters (permeability coefficient, turbulent friction coefficient and added mass coefficient). Calibration has been carried out minimizing the errors between the numerical model and the experiments for dissipation inside the porous rubble. The general agreement between model and experimental data was found excellent. For the permeable structure with a back wall, it can be said that the reflection and the dissipation depend strongly on the wave steepness and the relative width, since these two parameters determine the location of the reflection. Once the model was validated, its capability was exploited to analyze the influence of non-dimensional parameters (structure width, stone size, porosity, wave height, period, water depth, etc.) on the functional and stability behavior.

Sundar et al. (2003) investigated the hydrodynamic performance characteristics of a quadrant front face, pile supported breakwater. The breakwater model consists of a quadrant front face resting on piles. The authors reported the variation of the reflection and transmission coefficients due to both regular and random waves as a function of a scattering parameter and the effect of the gap ratio (spacing between the piles/pile diameters) and relative water depth (water depth/pile height) on the above

coefficients. In addition, the variation of dynamic pressures exerted on the quadrant front face as well as the total forces exerted on the entire model were measured and presented in a dimensionless form.

Koraim (2005) investigated the efficiency of three different partial protection breakwater types theoretically and experimentally. The three breakwater models were; a caisson partially immersed in the seawater and supported on a large spaced pile system, a closely spaced vertical square or circular piles, and a caisson partially immersed in the seawater and supported on closely spaced pile system. Different wave, seabed, and structural characteristics affecting the breakwater efficiency were taken into considerations. Eigen function expansion method was used to determine the efficiency of this breakwater. The author concluded that, the caisson breakwater is efficient in controlling the transmitted waves especially when the breakwater draft is greater than 0.4 of the water depth and the breakwater width equal to the water depth. The efficiency of the caisson breakwater increases when constructed on nearly flat beaches and the supporting pile system increases the efficiency of the breakwater as the number of piles per unit length of the breakwater increases. The embedded length of the supporting piles must be increased to avoid the effect of the local scour. The proposed theoretical model for estimating the transmitted wave heights using the caisson breakwater gives good agreement with the experimental results. The efficiency of the pile breakwaters increases as the waves become short and the gap-width or diameter ratio decreases. The efficiency of the double row model is higher than the single row model, and the efficiency of the double rows model increases as the distance between the rows of piles increases. The square pile breakwater is more efficient than the circular pile breakwater by an amount of 20 to 25 %.

Huang (2006) studied the interactions between narrow-banded random waves and multi-chamber perforated structures. A time-domain method, based on linear velocity potential theory, was presented to study the interaction between narrow-banded random waves and perforated structures. A simple relation was derived to estimate the jet length of flows through the perforated wall. The reflection coefficient of narrow banded random waves from perforated structures was calculated by assuming a Rayleigh distribution of the heights of incident random waves. A comparison of the

predicted and measured reflection coefficients showed that the method could provide a prediction better than that of regular waves.

Suh et al. (2006) described the hydrodynamic characteristics of a pile-supported vertical wall breakwater, the upper part of which consisted of an impermeable vertical wall and lower part consisted of an array of vertical piles as shown in Figure 2.10. An Eigen function expansion method was used for the analysis and estimated reflection, transmission, run-up and wave forces acting on the breakwater. The method was further extended to random waves. The method adopted was similar to Isaacson et al. (1998) except for the formulation of permeability parameter *G*, for which the method of Mei et al. (1974) was adopted.

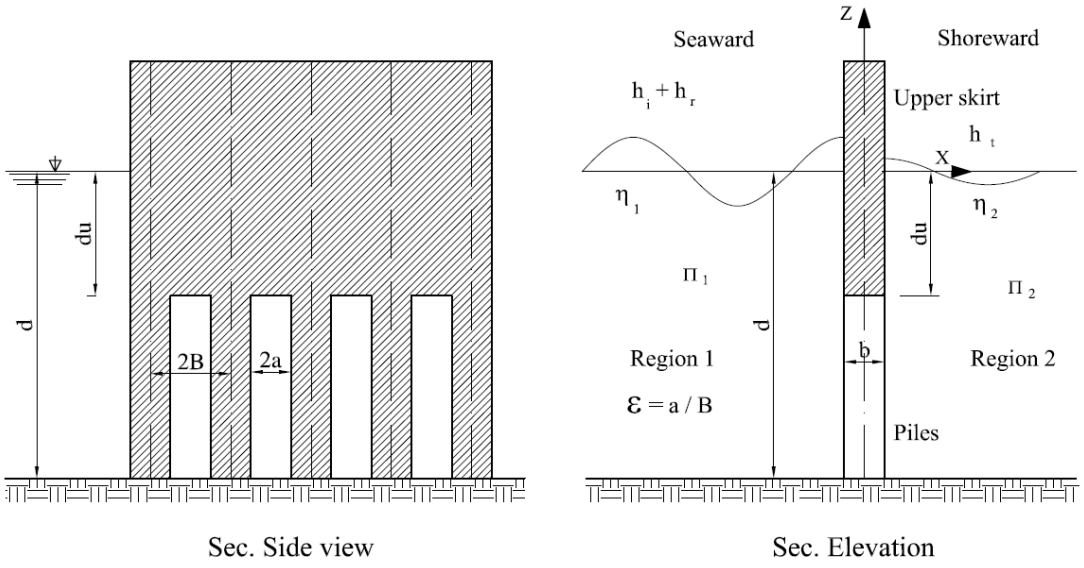

Figure 2.10: Pile supported vertical wall breakwater. [71 - Suh, 2006]

The wave period was determined according to the frequency of the component wave, while the root-mean-squared wave height was used for all the component waves to compute the energy dissipation between piles. Large-scale laboratory experiments were conducted for pile-supported vertical wall breakwaters with a constant spacing between piles but various drafts of the upper vertical wall. Comparisons between measurement and prediction showed that the numerical model adequately reproduces most of the important features of the experimental results for both regular and irregular waves. The pile-supported vertical wall breakwater always gave smaller transmission and larger reflection than a curtain wall breakwater with the same draft

as that of the upper wall, or a pile breakwater with the same porosity as that of the lower part, of the pile-supported vertical wall breakwater.

Huang et al. (2007) investigated the scattering of long waves by slotted breakwaters in the presence of currents by using a simple model. The theory was based on the long wave equations without friction, and it was an extension of the theory which has been described by Mei et al. (1974) for pure waves. The dissipation of wave energy caused by the barrier was modeled by a linearized dissipation coefficient determined by the *Lorentz's principle* of equivalent work. For a moderate current strength, a reasonable agreement was found between the predicted reflection and transmission coefficients with the experimental results, showed that the model was promising in modeling the wave scattering by slotted barriers in the presence of a current. Model results showed that both the wave-following and wave-opposing currents can increase the reflection coefficient and reduce the transmission coefficient. The model can be used to study the interaction between long waves and similar models in coastal waters.

Huang (2007) investigated the wave interaction with one or two rows of closely spaced rectangular cylinders. Experimental results were reported on the wave reflection and transmission through one row or two rows of closely spaced rectangular cylinders. An empirical expression was proposed for the friction factor which models the head loss due to closely spaced rectangular cylinders. Algebraic expressions were presented to calculate the reflection and transmission coefficients of regular waves for a single slotted wall or double slotted walls. Comparisons between the experiments and calculations showed that the simplified model can enable a quick calculation of the reflection and transmission coefficients to be made with reasonable accuracy.

Laju et al. (2007) suggested using the piles supported double skirt as breakwater for large draft modern container ships. The basic concept of a pile supported breakwater was to serve as an impervious barrier near the free surface where there is more water particle movement while leaving the lower region unobstructed. The barriers were supported on closely spaced concrete or steel piles. The authors developed the

numerical model of Isaacson et al. (1999) to be compatible with them search which, based on Eigen function expansion theory for linear waves. The experimental studies were described in detail to investigate the hydrodynamic characteristics of piles supported double skirt. The numerical results were compared with the experimental results and a good agreement in general was found.

Liu et al. (2007) investigated wave interaction with a new type of perforated breakwater, consisting of a perforated front wall, a solid back wall and a wave absorbing chamber between them with a two-layer rock-filled core. The fluid domain was divided into three sub-domains according to the components of the breakwater. Then by means of the matched Eigen function expansion method, an analytical solution was obtained to assess the hydrodynamic performance of the new structure. An approach based on a step approach method is introduced to solve the complex dispersion equations for water wave motions within two-layer porous media. Numerical results were compared with previous results of other researchers, and very good agreement was found. It was found that the performances of perforated breakwaters with two-layer or single-layer surface piercing rock fill are similar. In addition, the perforated breakwater with a submerged rock-filled core of a suitable thickness (a/h = 0.5 to 0.8) should be a better choice, when the reductions of the wave force and the reflection coefficient are both required.

Suh et al. (2007) studied wave reflection and transmission by curtain wall-pile breakwaters using circular piles. The mathematical model was used to compute the hydrodynamic characteristics of a curtain wall–pile breakwater (CPB) using circular piles as shown in Figure 2.11, by modifying the model developed for rectangular piles by Suh et al. (2006).

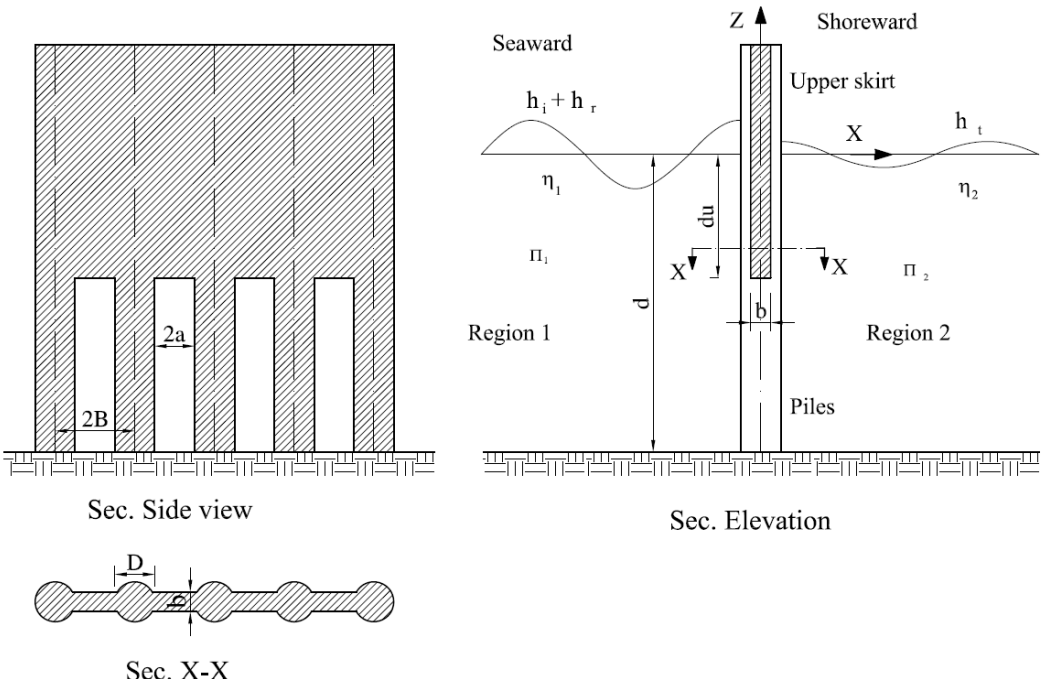

Figure 2.11 Circular piles supported vertical wall breakwater. [72 - Suh, 2007]

Laboratory experiments were conducted for CPB with various values of draft of curtain wall, spacing between piles, wave height and period. The permeability parameter in this study expressed by

$$G = \frac{1}{\frac{\beta}{\omega} - il} \tag{2.3}$$

where β = energy dissipation coefficient which were given by Kim (Suh et al., 2006).

$$\beta = \frac{8\alpha}{9\pi} h_i \omega \frac{1}{\sqrt{(R+2)^2 + P^2}} \frac{5 + \cosh(2kd)}{2kd + \sinh(2kd)} \tag{2.4}$$

where $P = lk$; $R = \beta k / \omega$, α = head loss coefficient and given by the plate orifice formula (Mei,1983)

$$\alpha = \left(\frac{1}{\varepsilon \bar{C}_c} - 1 \right)^2 \tag{2.5}$$

where C_c = empirical contraction coefficient for which Mei et al. (1974) suggested to use the formula

$$C_c = 0.6 + 0.4\varepsilon_o^2 \tag{2.6}$$

and l = length of the jet flowing through the gap between piles and related to the blockage coefficient as

$$l = 2C \tag{2.7}$$

$$C = \frac{\pi}{4} a (1 - \varepsilon_o)^2 \frac{1}{1 - \xi}, \qquad \xi = \frac{\pi^2}{12}(1 - \varepsilon_o)^2 \tag{2.8}$$

where $\bar{\varepsilon}$

$$\frac{1}{\bar{\varepsilon}^2} = \frac{1}{D} \int_{-\frac{D}{2}}^{\frac{D}{2}} \frac{dx}{\varepsilon(x)^2} \tag{2.9}$$

with the spatially varying porosity

$$\varepsilon(x) = 1 - \frac{\sqrt{(D/2)^2 - x^2}}{(D/2) + a} \tag{2.10}$$

They concluded that, as the draft of the curtain wall increases and the porosity between piles decreases, the reflection and transmission coefficient increases and decreases, respectively. As the relative water depth increases, however, the effect of porosity disappears because the wave motion is minimal in the lower part of a water column for short waves.

Rageh et al. (2009) investigated the hydrodynamic efficiency of vertical walls with horizontal slots. The model consisted of one row of vertical wall suspended on supporting piles. The wall was divided into two parts; the upper part extending above the water level to some distance below sea level was impermeable.

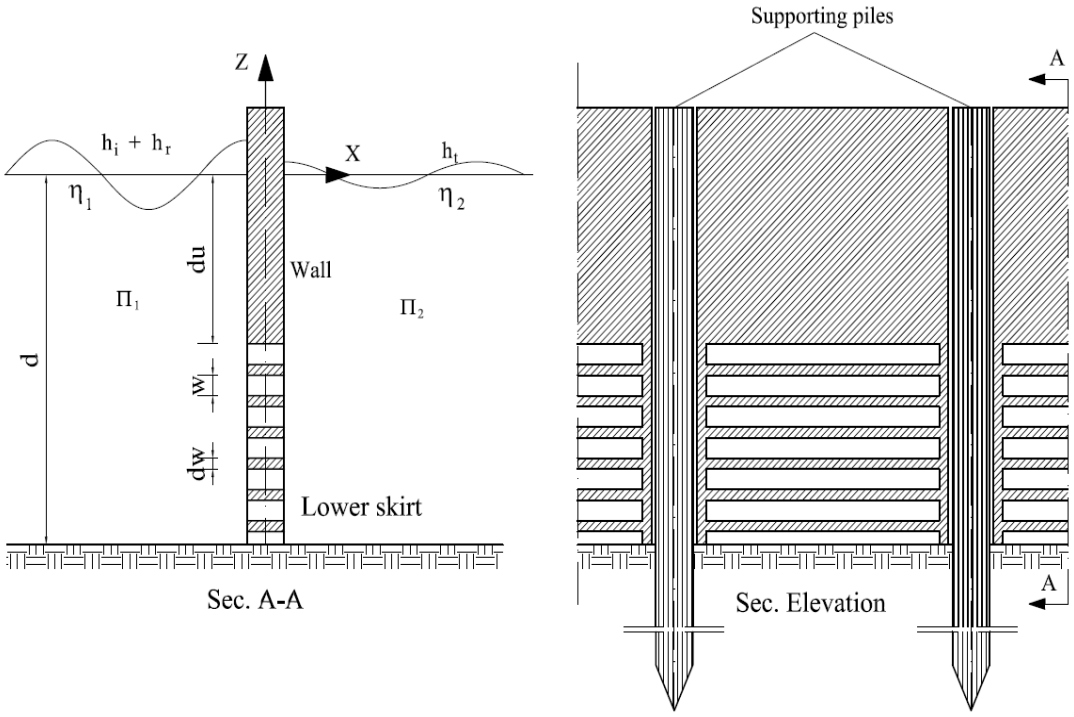

Figure 2.12 Schematic diagram for the breakwater model [62 - Rageh, 2009]

The other part of the wall was permeable which is consisted of closely spaced horizontal slots as shown in Figure 2.12. The model was investigated experimentally and theoretically. The theoretical model was based on the linear wave theory and an Eigen function expansion method. The efficiency of the breakwater was presented experimentally and theoretically as a function of the transmission, the reflection and the wave energy loss coefficients for different wave and structure parameters. The theoretical results were compared with the experimental results and results of other studies. The results indicated that the proposed theoretical model can be accepted for predicting the different hydrodynamic coefficients when the friction factor ranged from 5 to 6.

Mani (2009) investigated the experimental and numerical efficiency of zigzag porous screen breakwater. The model was comprised of two rows of staggered piles with

zigzag porous screen suspended in between and submerged up various depths. The numerical model was studied to determine wave transmission and reflection coefficients were carried out based on the method of Yu (1995) for wave motion near the porous boundary. The studies clearly indicated that the transmission coefficient of the order of 0.5 can be achieved for $h_i/gT^2 > 0.008$ for 50 % submergence, whereas the reflection coefficient can be effectively reduced to 0.2. The reduction in wave force was of the order of 50 %, which was primarily due to reduction in reflection coefficient. Substantial reduction in wave force contributes directly to reduction in the cost of construction of the breakwater, a definite advantage over other similar breakwaters.

Tao et al. (2009) studied wave interaction with a perforated cylindrical breakwater analytically by linear potential wave theory. The breakwater was assumed a thin skin, bottom-mounted and surface-piercing. The porosity of the breakwater was uniform vertically but various in the circumferential direction. This allowed the choice of a partially impermeable wall or a vertical slot in the breakwater. Three different basic configurations of the breakwater were investigated, namely, (1) uniformly porous cylinder; (2) porous cylinder with partial impermeable wall; and (3) porous cylinder with an opening. The performance of these types of breakwaters was studied. Wave parameters and breakwater configurations including angle and position of opening or partial impermeable wall as well as porosity. Parametric studies with regard to the wave-amplification factor, wave forces, and elevation contours were made. The results were found useful in the design of coastal and offshore structures. It was found that by making the porosity non uniform, the amplification factor, wave forces, and elevation contours become more complex than its counterpart of uniform porosity. Incident waves with smaller short-crestedness along with solid walls generally result in larger wave forces, whilst an opening on the breakwater and limiting incident waves, i.e., plane or standing waves clearly lead to larger amplification factors within the breakwater. The effect of the location of the solid or opening center appears to be insignificant on the inline wave force, but rather significant on the transverse wave force. They concluded that the wave force is insensitive to the location of the solid or opening center. Due to asymmetrical geometry, wave forces induced by standing incident waves are no longer zero. Here

the component in the direction perpendicular to the incident wave may come forth, although the magnitude is normally small.

2.4 SUMMARY

From the review of the literature, the objectives of this study clearly arise in the following important points.

- Permeable breakwaters are increasingly perceived as an environmentally friendly design and many types of structures has already been examined.
- It has been observed shortening in the systematic analysis of the influence of the porosity or the location and distribution of the barrier porosities.
- The proposed structure is a combination of several geometries, which already were investigated, and it should combine the respective advantages in terms of reflection, transmission and energy dissipation.
- The proposed structure in this study has not yet been studied.
- The main hydrodynamic characteristics that are relevant in the interaction of waves with permeable structures can be described by the Eigen function expansion method. This approach is expected to provide good results.
- The energy dissipation and the overall performance are depending on the porosity of the structure as well as their arrangement. The friction and the added mass coefficients are usually determined empirically by experimentation.

2.5 OBJECTIVES OF THE STUDY

The aims of the present study are to understand the hydrodynamic characteristics of single and double vertical slotted walls through experimental studies and to formulate a numerical model from a detailed parametric study with the various parameters that are important in dictating its design. The objectives of this study can be summarized as follows:

1. To develop a numerical model for regular linear wave interaction with a single and double vertical slotted wall and to develop a numerical model for nonlinear (Stokes second-order) wave interaction with a single vertical slotted wall.

2. To validate and assess the performance characteristics of these breakwaters by estimating *CR, CT* and *CE*, experimental tests were conducted.

3. To understand the flow behavior and hydrodynamic performance characteristic of this proposed breakwaters under linear and nonlinear waves (Stokes second-order theory).

4. To measure and analyze the velocity in front of and behind the breakwaters and to understand the pattern that dissipates wave energy as well as to investigate the wave interaction with the model via PIV.

The Eigen function expansion method is the suitable tool to explore the hydraulic characteristics for such permeable breakwaters and the laboratory studies are to confirm and assess the theoretical assumptions. Therefore, the phases of the study can be implemented as follows:

Theoretical investigations

- A theoretical study will be done to investigate the linear wave interaction with single and double vertical slotted walls.

- A theoretical study will be done to investigate nonlinear wave interaction with a single vertical slotted wall taking Stoke second-order wave theory as an example.

Parametric study varying like wave characteristic, the draft of permeable and impermeable parts and the spacing between two walls.

Experimental investigations

- Experimental studies could be done with a constant water depth and a constant porosity of the permeable part.

- Further on, the impermeable upper and lower parts should be varied. This is to investigate the influence of the proportion of the permeable part $dm = 0.2\,d$, $0.4\,d$, $0.6\,d$ and $0.8\,d$ on the performance.

- Additional, the effect of a second wall should be experimentally analyzed. Especially, the width of the gap between the two walls should be optimized in order to maximize the energy dissipation.

CHAPTER 3
THEORETICAL INVESTIGATION

3.1 INTRODUCTION

Permeable breakwaters are employed to protect the harbor and the marina and to attenuate the wave action wherever full protection breakwaters are not costly effective and led to deterioration for water mass within the harbor. This type of breakwaters provides shelter from waves and currents by dissipating the wave energy and by permitting some wave action and water mass exchange through the sheltered area, which in turn reduces the pollution inside the harbor.

Many authors investigated the performance of partially immersed bodies and pile breakwaters numerically by using the Eigen function technique. Lamb (1932), Martin and Dalrymple (1988), Kakuno and Liu (1993), Isaacson et al. (1998) and Park et al. (2000) provided numerical solution for pile breakwaters. Abul-Azm (1993) provided numerical solutions for thin semi-immersed breakwaters.

In this chapter, numerical solutions have been presented for wave interaction with a permeable breakwater (vertical slotted wall). This solution depends mainly on the exact numerical solution using Eigen function technique. This study has been used to develop three numerical models

- The first model is applied for a structure of one row of a vertical slotted wall with lower and upper impermeable parts and a permeable part in the middle as shown in Figure 3.1. The numerical model can be used to count the hydrodynamic characteristic (*CR*, *CT* and *CE*) for linear waves.
- The second model is similar to the first model but it can be used to count the hydrodynamic characteristic (*CR*, *CT* and *CE*) for nonlinear wave (Stokes second-order wave).

- The third model is applied to a structure of two rows of identical vertical slotted walls with lower and upper impermeable parts and a permeable part in the middle as shown Figure 3.2. This numerical model can be used to count the same hydrodynamic characteristic based on the linear wave theory.

The first and second structure can be used to protect beaches and small or medium harbors. The third structure serves multipurpose and it is useful for the big harbors. The vessels can be berthed on the lee side and the top surface can be used for loading/unloading as well as for movement of men and material. The numerical solutions are based on Eigen function technique which has also been employed earlier by Kakuno and Liu (1993), Isaacson et al. (1996, 1998), Park et al. (2000), Koraim (2005), Suh et al. (2006), Laju et al. (2007) and Suh et al. (2007).

3.2 NUMERICAL MODEL BASED ON LINEAR WAVE THEORY

3.2.1 General

The wave interaction with a vertical slotted wall breakwater has been modeled for linear, monochromatic waves. In general, the draft of lower and upper impermeable parts is *du* and *dw* respectively as shown in Figure 3.1. The seabed is horizontal and located at $z = -d$. The analysis assumptions are; waves are assumed to be regular, small amplitude, normally incident on the structure. The wave height is h_i and the angular frequency is ω. The model is assumed as rigid with negligible deformations. The fluid is incompressible, inviscid, and the motion is non-rotational. The breakwater is continuous and located at $x = 0$. The distance between the centers of two adjacent legs is denoted by *2B* and the width of the opening between the legs is denoted by 2a, and the thickness of the wall in the direction of *x* is denoted by *b*. The porosity is denoted by $\varepsilon = a/B$. The region where $x \leq 0$ is referred to as region π_1 and the region at $x \geq 0$ is referred to as region π_2.

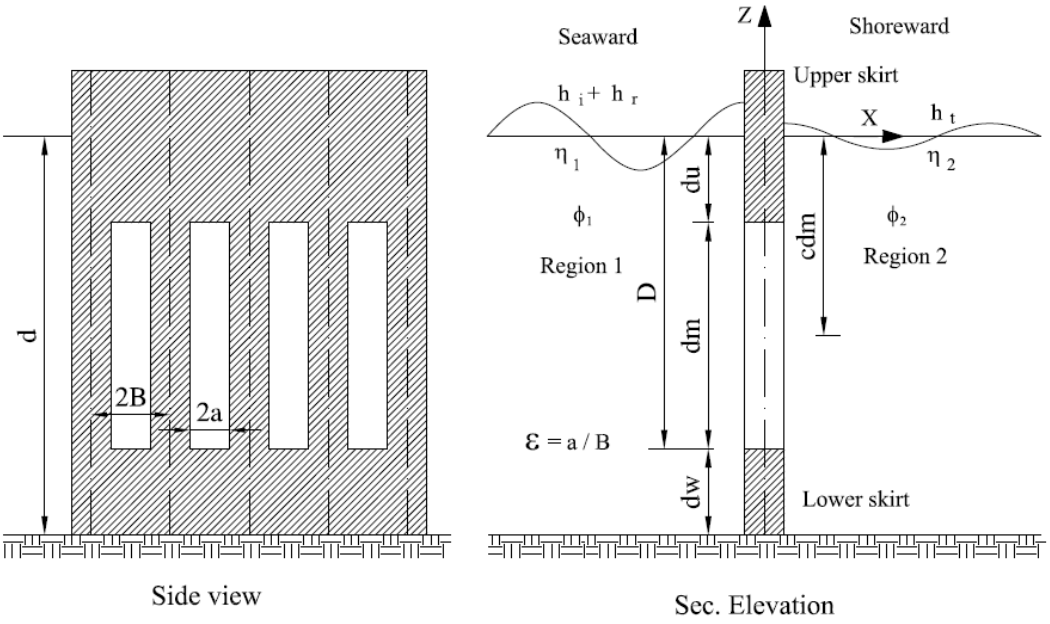

Figure 3.1: Definition sketch for a vertical slotted wall breakwater.

The velocity potential Φ is assumed as periodic motion in time T and it can be expressed as follows:

$$\Phi(x,z,t) = \mathrm{Re}\,\frac{-igh_i}{2\omega}\phi(x,z)\frac{1}{\cosh\ kd}e^{-i\omega t} \tag{3-1}$$

where the symbol Re represents the real part of a complex value, ω is the wave angular frequency, g =gravitational acceleration. $i = \sqrt{-1}$; k = wave number and must be satisfying the dispersion relationship $\omega^2 = gk\tanh(kd)$. The horizontal and vertical spatial variation $\phi_n(x,z)$ should be determined in each region.

3.2.2 Governing equations

The governing equations for the potential function $\Phi(x,z,t)$ are the modified Laplace's equation, which are defined as follows:

$$\frac{\partial^2 \Phi}{\partial x^2} + \frac{\partial^2 \Phi}{\partial z^2} = 0 \tag{3-2}$$

The free surface boundary and the bed boundary conditions are:

$$\frac{\partial \Phi}{\partial z} - \frac{\omega^2}{g}\Phi = 0 \qquad \text{at} \quad z = 0 \tag{3-3}$$

$$\frac{\partial \Phi}{\partial z} = 0 \qquad \text{at} \quad z = -d \tag{3-4}$$

We assume that the length scale of the flow near the breakwater is of the order of the pile dimensions, which is much smaller than the wave length, so that the wall has no thickness mathematically and the three-dimensional feature near the breakwater does not significantly affect the two-dimensional solution. Then $\phi_1(x,z)$ and $\phi_2(x,z)$ must satisfy the following matching condition at $x = 0$.

$$\frac{\partial \phi_1(x)}{\partial x} = \frac{\partial \phi_2(x)}{\partial x} = 0$$

$$\text{for} \quad -du \le z \le 0 \quad \text{and} \quad -d \le z \le -D \tag{3-5}$$

3.2.3 Permeable boundary condition

The permeable boundary condition along the slotted wall may be developed based on the formulation of Sollitt and Cross (1972) and as adopted by Yu (1995) and Isaacson et al. (1998) for a thin vertical barrier. This may give:

$$\frac{\partial \phi_1(x)}{\partial x} = \frac{\partial \phi_2(x)}{\partial x} = iG^{-}(\phi_1(x) - \phi_2(x))$$

$$\text{at} \quad x = 0, \quad -D \le z \le -du \tag{3-6}$$

where the subscripts indicate the regions of the fluid domain and the horizontal mass fluxes in the two regions must be the same at the breakwater and the horizontal

velocity at the opening is proportional to the difference of velocity potentials, or the pressure difference, across the breakwater. The proportional constant $G = G/b$, G is called the permeability parameter, which is generally complex. Equation (3-6) corresponds to the fluid velocity normal to the piles being proportional to the velocity potential across the slotted wall with a complex constant of proportionality. The real part of G corresponds to the resistance of the piles. The imaginary part of G corresponds to a phase differences between the velocity and the pressure due to inertial effects. There are several ways to express the constant G that related the permeability to the physics of the flow within the barrier. For example, the resistance may be expressed in terms of a friction coefficient (e.g. Sollitt and Cross 1972), a drag coefficient (e.g. Hagiwara 1984) and a head loss coefficient (e.g. Mei et al. 1974). The inertial effects are generally expressed in terms of an added mass coefficient (e.g. Sollitt and Cross 1972) or an effective orifice length (e.g. Mei et al. 1974). We adopt the method of Isaacson et al. (1998), which depends on the method, of Sollitt and Cross (1972) and G is then expressed as:

$$G = \frac{\varepsilon}{f - is} \tag{3-7}$$

where ε is the porosity of the piles, f is the friction coefficient and s is an inertia coefficient given by:

$$s = 1 + cm\left(\frac{1-\varepsilon}{\varepsilon}\right) \tag{3-8}$$

where "*cm"* is an added mass coefficient. The friction coefficient f can be calculated from a linearization of the velocity squared term associated with the head loss across the barrier. In the original formulation of Sollitt and Cross (1972), f is calculated implicitly using the *Lorentz principle* of equivalent work so that the nonlinear effects of wave steepness are retained. This requires an iterative procedure, and in the present work we follow the formulation of Yu (1995) such that f is treated simply as a constant which is assumed to be known.

3.2.4 Eigen function expansion

To obtain the solution for ϕ_1 and ϕ_2, which satisfy the seabed, free surface, and radiation conditions, we use the Eigen function expansion method. We closely follow the approach of Isaacson et al. (1998) and Suh et al. (2006). The velocity potential is expressed as a series of infinite number of solutions:

$$\phi_1(x) = \phi_i - \sum_{m=0}^{\infty} A_m \cos[\,\mu_m(d+z)]\exp(\,\mu_m x) \tag{3-9}$$

$$\phi_2(x) = \phi_i + \sum_{m=0}^{\infty} A_m \cos[\,\mu_m(d+z)]\exp(-\mu_m x) \tag{3-10}$$

where,

$$\phi_i = \cosh[\,k(d+z)]\exp(\,ikx) \tag{3-11}$$

where ϕ_i is the incident wave potential, A_m are initially unknown, the wave numbers μ_m are the solutions of the dispersion relation, $\omega^2 = -g\mu_m \tan(\mu_m d)$, which have an infinite discrete set of real roots $\pm\,\mu_m\,(m \geq 1)$ for non-propagating evanescent waves and a pair of imaginary roots $\mu_o = \pm ik$ for propagating waves. We take $\mu_o = -ik$ so that the propagating waves in Eqs. (3-9 and 3-10) correspond to reflected and transmitted waves, respectively. We also take the positive roots for $(m \geq 1)$ so that the non-propagating waves die out exponentially with the distance from the breakwater. Eqs. (3-9 and 3-10) satisfy all relevant boundaries, they automatically satisfy the requirement that the horizontal velocities must be matched at the breakwater. In order to solve for the unknown coefficients, the matching conditions are used at the breakwater.

First, Eqs. (3-9 and 3-10) are substituted into Eqs. (3-5) and (3-6), respectively. Then, we obtain the following equations:

$$\mu_m \sum_{m=o}^{\infty} A_m \cos[\ \mu_m (d\ +\ z)] = -\mu_o \cos[\ \mu_o (d\ +\ z)]$$

$$\text{at} \quad -\ du\ \le\ z\ \le\ 0 \tag{3-12}$$

$$\mu_m \sum_{m=o}^{\infty} A_m \cos\ \left[\mu_m (d\ +\ z)\right] = -\mu_o \cos[\ \mu_o (d\ +\ z)]$$

$$\text{at} \quad -\ d\ \le\ z\ \le\ -\ D \tag{3-13}$$

$$(\mu_m\ -\ 2\,iG^{-})\sum_{m=o}^{\infty} A_{1m} \cos[\ \mu_m (d\ +\ z)] = -\mu_o \cos[\ \mu_o (d\ +\ z)]$$

$$\text{at} \quad -\ D\ \le\ z\ \le\ -\ du \tag{3-14}$$

Now, Eqs. (3-12), (3-13) and (3-14) can be multiplied by $\cos[\ \mu_n (d\ +\ z)]$, and integrated with respect to z over the appropriate domain of z (i.e. for piles without skirt z = -d to 0.0, for piles with upper skirt z = -du to 0.0, and z = -d to –du, for the present study z = -du to 0.0, z = -D to -du and z = -d to -D). This gives rise of a matrix equation for A_m :

$$\sum_{m=0}^{\infty} C_{mn} A_m\ =\ b_n\ . \qquad \text{for} \quad n\ =1, 2, \ldots \infty \tag{3-15}$$

where:

$$C_{mn} = \mu_m \delta^{-}{}_{mn}[(-du,0) + (-d,-D)] + (\mu_m - 2iG^{-})\delta^{-}{}_{mn}(-D,-du) \tag{3-16}$$

$$b_n = -\mu_o \delta^{-}_{o\,mn}[(-du,0) + (-D,-du) + (-d,-D)] \tag{3-17}$$

$$\delta^{-}{}_{mn}(p,q) = \int_p^q \cos[\,\mu_m (d+z)]\cos[\,\mu_n (d+z)]dz \tag{3-18}$$

$$= \begin{cases} \dfrac{1}{2}\left\{\dfrac{\sin[(\ \mu_m + \mu_n)(d+z)]}{\mu_m + \mu_n} + \dfrac{\sin[(\ \mu_m - \mu_n)(d+z)]}{\mu_m - \mu_n}\right\}_p^q & \text{for} \quad m \neq n \\ \dfrac{1}{4\,\mu_m}\{2\,\mu_m (d+z) + \sin[\ 2\,\mu_m (d+z)]\}_p^q & \text{for} \quad m = n \end{cases}$$

(3-19)

$$\bar{\delta}_{o_{mn}}(p,q) = \int_{p}^{q} \cos[\mu_o(d+z)]\cos[\mu_n(d+z)]dz \tag{3-20}$$

The numerical solution to equation (3-15) is truncated to a finite number of terms *N*, and thus becomes a complex matrix equation of rank *N*, which can be solved for the first *N* unknown coefficient A_m . Once these were calculated, the various engineering wave properties can be determined. The real reflection and transmission coefficients, denoted (*CR, CT*) respectively, are defined as the appropriate ratios of wave heights: $CR = h_r / h_i$ and $CT = h_t / h_i$, where h_r, h_t are the reflected and transmitted wave heights respectively. These are given in terms of A_m by

$$CR = |A_0| \tag{3-21}$$

$$CT = |A_0 + 1| \tag{3-22}$$

The energy losses coefficient (*CE*), which is the portion of the incident wave energy that is dissipated by the breakwater, is given by

$$CE = 1 - CR^2 - CT^2 \tag{3-23}$$

3.3 NUMERICAL MODEL BASED ON NONLINEAR WAVE THEORY

3.3.1 General

In this section, the previous model for the vertical slotted wall has been developed for the nonlinear waves (Stokes second-order wave theory).

The model has been developed for the same assumption and condition as for the linear wave. The second-order velocity potential Φ is assumed as periodic motion in time T and can be expressed as follows:

$$\Phi(x,z,t) = -i\,\mathrm{Re}\left[\frac{gh_i}{2\omega}\phi(x,z)\frac{1}{\cosh\ kd}e^{\ i\omega t} + \frac{3\pi h_i}{8kT}\left(\frac{\pi h_i}{L}\right)\phi_{ns}(x,z)\frac{1}{\sinh^{\ 4}(kd)}e^{-2i\omega t}\right] \quad (3\text{-}24)$$

where the symbol Re represents the real part of a complex value. The first term denoted for the first-order velocity potential. ω is wave angular frequency, g is gravitational acceleration. $i = \sqrt{-1}$; k = wave number and must be satisfying the dispersion relationship $\omega^2 = gk\tanh(kd)$, where the dispersion relation is the same as that for of the linear wave [Chakrabarti (1987); Sarpkaya and Isaacson (1981)]. The horizontal and vertical spatial variation $\phi_n(x,z)$ should be determined in each region.

3.3.2 Governing equations

The governing equations of this study are the same as for the previous model that are mentioned in section 3.2.2.

3.3.3 Permeable boundary condition

The permeable boundary condition of this study is the same as for the previous model that is mentioned in section 3.2.3.

3.3.4 Eigen function expansion

To obtain the solution for ϕ_1 and ϕ_2, which satisfy the seabed, free surface, and radiation conditions, it is used the Eigen function expansion method. We closely follow the method of Isaacson et al. (1998) and Suh et al. (2006). The velocity potential is expressed in a series of infinite number of solutions

$$\phi_1(x) = c_1\phi_{i1} + c_2\phi_{i2} - \sum_{m=0}^{\infty} A_m \left[c_1 \cos[\ \mu_m(d + z)]\ \exp(\ \mu_m x) + c_1 \cos[\ 2\mu_m(d + z)]\ \exp(\ 2\mu_m x)\right] \quad (3\text{-}25)$$

$$\phi_2(x) = c_1\phi_{i1} + c_2\phi_{i2} + \sum_{m=0}^{\infty} A_m \left\{c_1 \cos[\ \mu_m(d + z)]\ \exp(\ -\mu_m x) + c_1 \cos[\ 2\mu_m(d + z)]\ \exp(\ -2\mu_m x)\right\} \quad (3\text{-}26)$$

where,

$$\phi_{i1} = \cosh[\ k(d + z)]\ \exp(\ ikx\ ) \quad (3\text{-}27)$$

$$\phi_{i2} = \cosh[\ 2k(d + z)]\ \exp(\ 2ikx\ ) \quad (3\text{-}28)$$

$$c_1 = \frac{gh_i}{2\omega}\frac{e^{-i\omega t}}{\cosh(\ kd\ )} \quad (3\text{-}29)$$

$$c_2 = \frac{3\pi h_i}{8T}\left(\frac{\pi h_i}{L}\right)\frac{e^{-2i\omega t}}{\sinh^4(kd\ )} \quad (3\text{-}30)$$

where ϕ_{i1} is the first-order incident wave potential, ϕ_{i2} is the second-order incident wave potential, A_m is initially unknown, the wave numbers μ_m is the solution of the dispersion relation as also has been discussed in section 3.2.4.

In order to solve for the unknown coefficients, the matching conditions are used at the breakwater. First, Eqs. (3-25) and (3-26) are substituted into Eqs. (3-5) and (3-6), respectively. Then, we obtain the following equation:

$$\sum_{m=o}^{\infty} A_m \{c_1 \cos[\ \mu_m (d\ +\ z)]\mu_m\ +\ 2\mu_m c_2 \cos[\ 2\mu_m (d\ +\ z)]\} =$$

$$-\ c_1 \mu_o \cos[\ \mu_o (d + z)] - 2c_2 \mu_o \cos[\ 2\mu_o (d + z)]$$

$$\text{at} \quad -\ du\ \le\ z\ \le\ 0 \tag{3-31}$$

$$\sum_{m=o}^{\infty} A_m \{c_1 \cos[\ \mu_m (d\ +\ z)]\mu_m\ +\ 2\mu_m c_2 \cos[\ 2\mu_m (d\ +\ z)]\} =$$

$$-\ c_1 \mu_o \cos[\ \mu_o (d + z)] - 2c_2 \mu_o \cos[\ 2\mu_o (d + z)]$$

$$\text{at} \quad -\ d\ \le\ z\ \le\ -D \tag{3-32}$$

$$\sum_{m=o}^{\infty} A_m \{(\mu_m\ -\ 2iG^{-})c_1 \cos[\ \mu_m (d\ +\ z)]\ +$$
$$(2\mu_m\ -\ 2iG^{-})c_2 \cos[\ 2\mu_m (d\ +\ z)]\} = -c_1 \mu_o \cos[\ \mu_o (d\ +\ z)]\ -$$
$$2c_2 \mu_o \cos[\ 2\mu_o (d + z)]$$

$$\text{at} \quad -\ D\ \le\ z\ \le\ -du \tag{3-33}$$

Now, Eqs. (3-31), (3-32) and (3-33) can be multiplied by $\cos[\ \mu_n (d\ +\ z)]$, and integrated with respect to z over the appropriate domain of z (i.e. for piles without skirt z = -d to 0.0, for piles with upper skirt z = -du to 0.0, and z = -d to –du, for the present study z = -du to 0.0, z = -D to -du and z = -d to -D). This gives rise of a matrix equation for A_m :

$$\sum_{m=0}^{\infty} C_{mns}\ A_{ms}\ =\ b_{ns}\ . \qquad \text{for} \quad n = 1, 2, \ldots \infty \tag{3-34}$$

where:

$$C_{mns} = [(\mu_m - 2iG^{-})c_1\delta^{-}_{1\,mn} + (2\mu_m - 2iG^{-})c_2\delta^{-}_{2\,mn}](-D,-du) +$$

$$[\mu_m c_1\delta^{-}_{1\,mn} + 2\mu_m c_2\delta^{-}_{2\,mn}](-du,0) + [\mu_m c_1\delta^{-}_{1\,mn} + 2\mu_m c_2\delta^{-}_{2\,mn}](-d,-D) \tag{3-35}$$

$$b_{ns} = (-\mu_o c_1\delta^{-}_{01\,mn} - 2\mu_o c_2\delta^{-}_{02\,mn})[(-du,0) + (-D,-du) + (-d,-D)] \tag{3-36}$$

$$\delta_{1\,mn}^{-}(p,q) = \int_{p}^{q} \cos[\ \mu_m(d+z)]\cos[\ \mu_n(d+z)]\,dz \tag{3-37}$$

$$= \begin{cases} \dfrac{1}{2}\left\{\dfrac{\sin[(\ \mu_m+\mu_n)(d+z)]}{\mu_m+\mu_n} + \dfrac{\sin[(\ \mu_m-\mu_n)(d+z)]}{\mu_m\quad\mu_n}\right\}_p^q & \text{for } m \neq n \\ \dfrac{1}{4\mu_m}\left\{2\mu_m(d+z)+\sin[\ 2\mu_m(d+z)]\right\}_p^q & \text{for } m=n \end{cases} \tag{3-38}$$

$$\delta_{2\,mn}^{-}(p,q) = \int_{p}^{q} \cos[\ \ 2\mu_m z\,]\cos[\ \ \mu_n z\,]\,dz \tag{3-39}$$

$$= \begin{cases} \dfrac{1}{2}\left\{\dfrac{\sin[(\,2\mu_m+\mu_n)(d+z)]}{2\mu_m+\mu_n} + \dfrac{\sin[(\,2\mu_m-\mu_n)(d+z)]}{2\mu_m\quad\mu_n}\right\}_p^q & \text{for } m \neq n \\ \left\{\dfrac{1}{6\mu_m}\sin[\,3\mu_m(d+z)] + \dfrac{1}{2\mu_m}\sin[\,\mu_m(d+z)\right\}_p^q & \text{for } m=n \end{cases} \tag{3-40}$$

$$\delta_{01\,mn}^{-}(p,q) = \int_{p}^{q} \cos[\ \mu_o(d+z)]\cos[\ \mu_n(d+z)]\,dz \tag{3-41}$$

$$\delta_{02\,mn}^{-}(p,q) = \int_{p}^{q} \cos[\ 2\mu_o z\,]\cos[\ \mu_n z\,]\,dz \tag{3-42}$$

The numerical solution to equation (3-34) is similar to the solving equation (3-15). Finally, the hydrodynamic characteristic *CR, CT* and *CE* are given in terms of A_m by:

$$CR = |A_0| \tag{3-43}$$

$$CT = |1 + A_0| \tag{3-44}$$

The energy losses coefficient (*CE*), which is the portion of the incident wave energy that is dissipated by the breakwater, is given by:

$$CE = 1 - CR^2 - CT^2 \tag{3-45}$$

3.4 NUMERICAL MODEL FOR LINEAR WAVE WITH DOUBLE VERTICAL SLOTTED WALL

3.4.1 General

In this section, a numerical model has been developed for the linear wave interaction with double identical vertical slotted walls breakwaters. The model has been developed for the same assumptions and conditions of the linear wave interaction with single vertical slotted wall breakwaters. The first wall is located in the seaward at a distance ($-\lambda$) and the second unit is located in the shoreward at a distant (λ) from the origin point with a horizontal slab as platform as shown in Figure (3-2). The velocity potential $\Phi(x,z,t)$ was mentioned earlier in equation (3-1).

3.4.2 Governing equations

The governing equations for the potential function, $\Phi(x,z,t)$ is the modified Laplace equation which is defined in equation (3-2), The free surface boundary and the bed boundary conditions were defined in equation (3-3) and (3-4) respectively. The fluid domain is subdivided in to three regions by the breakwater and the two-dimensional potential ϕ in Eq. (3-1) is denoted ϕ_1, ϕ_2 and ϕ_3 in regions 1, 2 and 3 respectively. The pressure and horizontal velocity are equated along the matching boundaries within the fluid, and are applied to suitable boundaries within the fluid along the surface of each unit. The conditions along the matching boundaries are thus:

$$\frac{\partial \phi_1(x)}{\partial x} = \frac{\partial \phi_2(x)}{\partial x} = 0 \qquad \text{at} \quad x = -\lambda$$

$$\text{for } -du \le z \le 0 \text{ and } -d \le z \le -D \tag{3-46}$$

$$\frac{\partial \phi_2(x)}{\partial x} = \frac{\partial \phi_3(x)}{\partial x} = 0 \qquad \text{at} \quad x = \lambda$$

$$\text{for } -du \le z \le 0 \text{ and } -d \le z \le -D \tag{3-47}$$

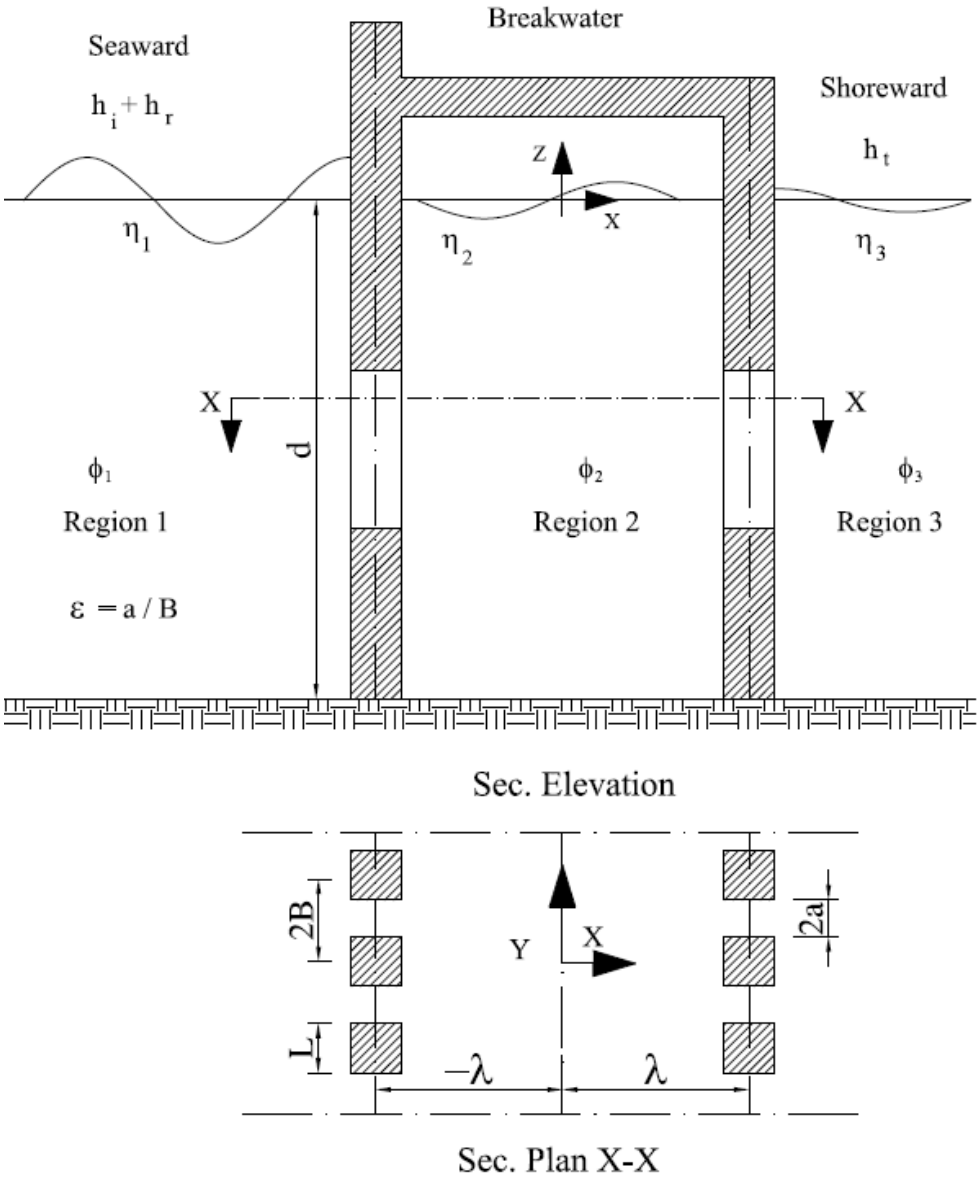

Figure 3.2: Definition sketch of double vertical slotted wall breakwater.

3.4.3 Permeable boundary condition

The permeable boundary condition along the permeable pile may be developed on the basis of the formulation of Sollitt and Cross (1972) and as adopted by Yu (1995) for a thin vertical barrier. This may give

$$\frac{\partial \phi_1(x)}{\partial x} = \frac{\partial \phi_2(x)}{\partial x} = iG^{-}(\phi_1(x) - \phi_2(x))$$

$$\text{at } x = -\lambda \text{ for } -D \le z \le -du \tag{3-48}$$

$$\frac{\partial \phi_2(x)}{\partial x} = \frac{\partial \phi_3(x)}{\partial x} = iG^{-}(\phi_2(x) - \phi_3(x))$$

$$\text{at } x = \lambda \text{ for } -D \le z \le -du \tag{3-49}$$

where the subscripts indicate the regions of the fluid domain and the horizontal mass fluxes in the two regions must be the same at the breakwater and that the horizontal velocity at the opening is proportional to the difference of velocity potentials, or the pressure difference, across the breakwater. The proportional constant $G^{-} = G/b$, G is called the permeability parameter and it was defined previously in Eq. (2-3).

3.4.4 Eigen function expansion

To obtain the solution for ϕ_1, ϕ_2 and ϕ_3 which are satisfying the seabed free surface and radiation conditions. The velocity potential is expressed in a series of infinite number of solutions as follow:

$$\phi_1(x) = \phi_i + \sum_{m=0}^{\infty} A_{1m} \cos[\ \mu_m (d + z)] \exp(\ \mu_m (x + \lambda))$$

$$\text{at } x \le -\lambda \tag{3-50}$$

$$\phi_2(x) = \sum_{m=0}^{\infty} A_{2m} \cos[\ \mu_m (d + z)] \exp(\ -\mu_m (x + \lambda)) + \sum_{m=0}^{\infty} A_{3m} \cos[\ \mu_m (d + z)] \exp(\ \mu_m (x - \lambda))$$

$$\text{at } -\lambda \le x \le \lambda \tag{3-51}$$

and

$$\phi_3(x) = \sum_{m=0}^{\infty} A_{4m} \cos[\ \mu_m (d + z)] \exp(\ -\mu_m (x - \lambda))$$

$$\text{at } -\lambda \le x \le \lambda \tag{3-52}$$

where ϕ_i and μ_m were defined earlier in Eq. (3-11), (3-12) respectively. Applying the matching conditions at the breakwater; the coefficients A_{1m}, A_{2m}, A_{3m} and A_{4m} can be determined. First, Eqs (3-50), (3-51) and (3-52) are substituted into Eqs. (3-46), (3-47), (3-48) and (3-49) we obtain the following equation:

$$\mu_m \sum_{m=o}^{\infty} A_{1m} \cos[\ \mu_m (d + z)] = \mu_o \cos[\ \mu_o (d + z)] \exp(\ \mu_o \lambda)$$

$$\text{at } x \le -\lambda \quad \text{for} \quad -du \le z \le 0 \tag{3-53}$$

$$\mu_m \sum_{m=o}^{\infty} A_{1m} \cos[\ \mu_m (d + z)] = \mu_o \cos[\ \mu_o (d + z)] \exp(\ \mu_o \lambda)$$

$$\text{at } x \le -\lambda \quad \text{for} \quad -d \le z \le -D \tag{3-54}$$

$$\mu_m \sum_{m=o}^{\infty} A_{2m} \cos[\ \mu_m (d + z)] - \mu_m \sum_{m=o}^{\infty} A_{3m} \cos[\ \mu_m (d + z)] \exp(\ -2\mu_m \lambda) = 0$$

$$\text{at } x \le -\lambda \quad \text{for} \quad -du \le z \le 0 \tag{3-55}$$

$$\mu_m \sum_{m=o}^{\infty} A_{2m} \cos[\ \mu_m (d + z)] - \mu_m \sum_{m=o}^{\infty} A_{3m} \cos[\ \mu_m (d + z)] \exp(\ -2\mu_m \lambda) = 0$$

$$\text{at } x \le -\lambda \quad \text{for} \quad -d \le z \le -D \tag{3-56}$$

$$\mu_m \sum_{m=o}^{\infty} A_{2m} \cos[\mu_m (d+z)] \exp(-2\mu_m \lambda) - \mu_m \sum_{m=o}^{\infty} A_{3m} \cos[\mu_m (d+z)] = 0$$

$$\text{at } x \le \lambda \qquad \text{for} \qquad -du \le z \le 0 \tag{3-57}$$

$$\mu_m \sum_{m=o}^{\infty} A_{2m} \cos[\mu_m (d+z)] \exp(-2\mu_m \lambda) - \mu_m \sum_{m=o}^{\infty} A_{3m} \cos[\mu_m (d+z)] = 0$$

$$\text{at } x \le \lambda \qquad \text{for} \qquad -d \le z \le -D \tag{3-58}$$

$$\mu_m \sum_{m=o}^{\infty} A_{4m} \cos[\mu_m (d+z)] = 0 \qquad \text{at } x \le \lambda \text{ for } -du \le z \le 0 \tag{3-59}$$

$$\mu_m \sum_{m=o}^{\infty} A_{4m} \cos[\mu_m (d+z)] = 0 \qquad \text{at } x \le \lambda \text{ for } -d \le z \le -D \tag{3-60}$$

Also:

$$(\mu_m - iG^-) \sum_{m=o}^{\infty} A_{1m} \cos[\mu_m (d+z)] + iG^- \sum_{m=0}^{\infty} A_{2m} \cos[\mu_m (d+z)] +$$
$$iG^- \sum_{m=0}^{\infty} A_{3m} \cos[\mu_m (d+z)] \exp(-2\lambda\mu_m) =$$
$$(iG^- + \mu_o) \exp(\mu_o \lambda) \cos[\mu_o (d+z)]$$

$$\text{at } x \le -\lambda \qquad \text{for} \qquad -D \le z \le -du \tag{3-61}$$

$$(iG^-) \sum_{m=o}^{\infty} A_{1m} \cos[\mu_m (d+z)] + (\mu_m - iG^-) \sum_{m=0}^{\infty} A_{2m} \cos[\mu_m (d+z)] -$$
$$(iG^- + \mu_m) \sum_{m=0}^{\infty} A_{3m} \cos[\mu_m (d+z)] \exp(-2\lambda\mu_m) =$$
$$-(iG^-) \exp(\mu_o \lambda) \cos[\mu_o (d+z)]$$

$$\text{at } x \le -\lambda \qquad \text{for} \qquad -D \le z \le -du \tag{3-62}$$

$$(\mu_m + iG^-) \sum_{m=0}^{\infty} A_{2m} \cos[\mu_m (d+z)] \exp(-2\lambda\mu_m) -$$
$$(\mu_m - iG^-) \sum_{m=0}^{\infty} A_{3m} \cos[\mu_m (d+z)] -$$
$$-iG^- \sum_{m=0}^{\infty} A_{4m} \cos[\mu_m (d+z)] = 0$$

$$\text{at } x \le \lambda \qquad \text{for} \qquad -D \le z \le -du \tag{3-63}$$

$$(iG^{-})\sum_{m=0}^{\infty} A_{2m}\cos[\ \mu_m(d\ +\ z)]\exp(\ -2\lambda\mu_{\ m})+$$

$$iG^{-}\sum_{m=0}^{\infty} A_{3m}\cos[\mu_m(d+z)]+(\mu_m-iG^{-})\sum_{m=0}^{\infty} A_{4m}\cos[\mu_m(d+z)]=0$$

$$\text{at } x \le \lambda \qquad \text{for} \qquad -D \le z \le -du \tag{3-64}$$

Now Eqs. (3-53):(3-64) are integrated with respect to *z* over the appropriate domain of z (i.e. for piles without skirt *z* = -*d* to 0.0, for piles with upper skirt *z* = -*du* to 0.0 and z = -*d* to -*du*). For the present study z = -*du* to 0.0, z = -*D* to -du and z = -*d* to -*D* and multiplying each resulting equation by $\cos[\ \mu_n(d\ +\ z)]$, and each pair of resulting equations is then added to obtain two sets of equation for A_{im}. This gives rise to a matrix equation for A_{1m}, A_{2m}, A_{3m} and A_{4m}:

$$\begin{bmatrix} \sum_{m=0}^{\infty} C_{11}^{(mn)} & \sum_{m=0}^{\infty} C_{12}^{(mn)} & \sum_{m=0}^{\infty} C_{13}^{(mn)} & \sum_{m=0}^{\infty} C_{14}^{(mn)} \\ \sum_{m=0}^{\infty} C_{21}^{(mn)} & \sum_{m=0}^{\infty} C_{22}^{(mn)} & \sum_{m=0}^{\infty} C_{23}^{(mn)} & \sum_{m=0}^{\infty} C_{24}^{(mn)} \\ \sum_{m=0}^{\infty} C_{31}^{(mn)} & \sum_{m=0}^{\infty} C_{32}^{(mn)} & \sum_{m=0}^{\infty} C_{33}^{(mn)} & \sum_{m=0}^{\infty} C_{34}^{(mn)} \\ \sum_{m=0}^{\infty} C_{41}^{(mn)} & \sum_{m=0}^{\infty} C_{42}^{(mn)} & \sum_{m=0}^{\infty} C_{43}^{(mn)} & \sum_{m=0}^{\infty} C_{44}^{(mn)} \end{bmatrix} \begin{bmatrix} A_{1m} \\ A_{2m} \\ A_{3m} \\ A_{4m} \end{bmatrix} = \begin{bmatrix} b_{1n} \\ b_{2n} \\ b_{3n} \\ b_{4n} \end{bmatrix}$$

for n =1, 2, 3, … ∞ (3-65)

where:

$$C_{11} = \mu_m[\delta_{mn}^{-}(-du,0)+\delta_{mn}^{-}(-d,-D)]+(\mu_m - iG^{-})\delta_{mn}^{-}(-D,-du) \tag{3-66}$$

$$C_{12} = (iG^{-})\delta_{mn}^{-}(-D,-du) \tag{3-67}$$

$$C_{13} = (iG^{-})\exp(-2\lambda\mu_m)\delta_{mn}^{-}(-D,-du) \tag{3-68}$$

$$C_{14} = 0 \tag{3-69}$$

$$C_{21} = (iG^{-})\delta^{-}_{mn}(-D,-du) \tag{3-70}$$

$$C_{22} = \mu_m[\delta^{-}_{mn}(-du,0) + \delta^{-}_{mn}(-d,-D)] + (\mu_m - iG^{-})\delta^{-}_{mn}(-D,-du) \tag{3-71}$$

$$C_{23} = \mu_m \exp(-2\lambda\mu_m)\left[\delta^{-}_{mn}(-du,0) + \delta^{-}_{mn}(-d,-D)\right] + (iG + \mu_m)\exp(-2\lambda\mu_m)\delta^{-}_{mn}(-D,-du) \tag{3-72}$$

$$C_{24} = 0 \tag{3-73}$$

$$C_{31} = 0 \tag{3-74}$$

$$C_{32} = \mu_m \exp(-2\lambda\mu_m)[\delta^{-}_{mn}(-du,0) + f_{mn}(-d,-D)] + (iG + \mu_m)\exp(-2\lambda\mu_m)\delta^{-}_{mn}(-D,-du) \tag{3-75}$$

$$C_{33} = -\mu_m[\delta^{-}_{mn}(-du,0) + \delta^{-}_{mn}(-d,-D)] + (iG^{-} - \mu_m)\delta^{-}_{mn}(-D,-du) \tag{3-76}$$

$$C_{34} = (-iG^{-})\delta^{-}_{mn}(-D,-du) \tag{3-77}$$

$$C_{41} = 0 \tag{3-78}$$

$$C_{42} = (iG^{-})\exp(-2\lambda\mu_m)\delta^{-}_{mn}(-D,-du) \tag{3-79}$$

$$C_{43} = (iG^{-})\delta^{-}_{mn}(-D,-du) \tag{3-80}$$

$$C_{44} = \mu_m[\delta^{-}_{mn}(-du,0) + \delta^{-}_{mn}(-d,-Dw)] + (\mu_m - iG^{-})\delta^{-}_{mn}(-D,-du) \tag{3-81}$$

$$b_{1n} = \mu_o \exp(\lambda\mu_o)\delta^{-}_{on}[(-du,0) + \delta^{-}_{on}(-D,-du)] + (iG^{-} + \mu_o)\exp(\lambda\mu_o)\delta^{-}_{on}(-d,-D) \tag{3-82}$$

$$b_{2n} = (-iG^{-})\exp(\lambda\mu_o)\delta^{-}_{on}(-d,-D) \tag{3-83}$$

$$b_{3n} = b_{4n} = 0 \tag{3-84}$$

$$\bar{\delta}_{mn}(p,q) = \int_p^q \cos[\mu_m(d+z)]\cos[\mu_n(d+z)]\,dz \tag{3-85}$$

$$= \begin{cases} \dfrac{1}{2}\left\{\dfrac{\sin[(\mu_m+\mu_n)(d+z)]}{\mu_m+\mu_n} + \dfrac{\sin[(\mu_m-\mu_n)(d+z)]}{\mu_m-\mu_n}\right\}_p^q & \text{for } m \neq n \\ \dfrac{1}{4\mu_m}\left\{2\mu_m(d+z)+\sin[2\mu_m(d+z)]\right\}_p^q & \text{for } m = n \end{cases} \tag{3-86}$$

The numerical solution to equation (3-65) is truncated to a finite number of terms (N), and thus becomes a complex matrix equation of rank $4N$, which can be solved for the first N unknown values of each set coefficient A_{1m}, A_{2m}, A_{3m} and A_{4m} after calculation for them. The real reflection and transmission coefficients, denoted (CR, CT) respectively, are given in terms of A_{1m} and A_{4m} by

$$CR = |A_{10}| \tag{3-87}$$

$$CT = |A_{40}| \tag{3-88}$$

The energy losses coefficient (CE), is given by

$$CE = 1 - (CR^2 + CT^2) \tag{3-89}$$

CHAPTER 4
EXPERIMENTAL INVESTIGATION AND VELOCITY MEASUERMENTS (PIV)

4.1 INTRODUCTION

A comprehensive experimental program on the performance characteristics of single and double vertical slotted walls was taken up to validate the results evaluated through the numerical model developed during the course of this study. The study involved the fabrication of the model, erecting it the wave flume, subjecting it to waves of predefined characteristics. The composite wave elevation measured on the sea side of the model with three wave gauges formed the basis for decomposing it to as reflected and incident waves. A wave gauge housed on the lee side of the model measured the transmitted wave elevation. In addition, the wave velocity, velocity distribution before and after the barrier, velocity vector, locations of vortices were measured and depicted by photos.

4.2 TEST FACILITY

4.2.1 Wave flume

Experiments were carried out in the wave flume of the hydraulics laboratory of the Department of Civil Engineering at University of Wuppertal, Germany (IGAW). The flume is 24 m long, 0.30 m wide and 0.5 m deep as shown in Photo 4.1. Waves were generated by a single paddle wave actuator located at the up wave end that can be piston or flap type and connected with a computer to generate regular waves of different heights and frequencies. An artificial parabolic beach is located at the downstream end of the flume in order to minimize wave reflection as shown in Photo 4.2. Tests were carried out with a constant water depth of 0.3 m and with generator motions corresponding to regular wave trains with different wave periods (T = 0.5 to 2 s). The tests were conducted with a wave height of 1cm to 4 cm. The vertical barriers to be tested were placed in the test section 12.20 m from the wave generator.

Photo 4.1: General view of the wave flume.

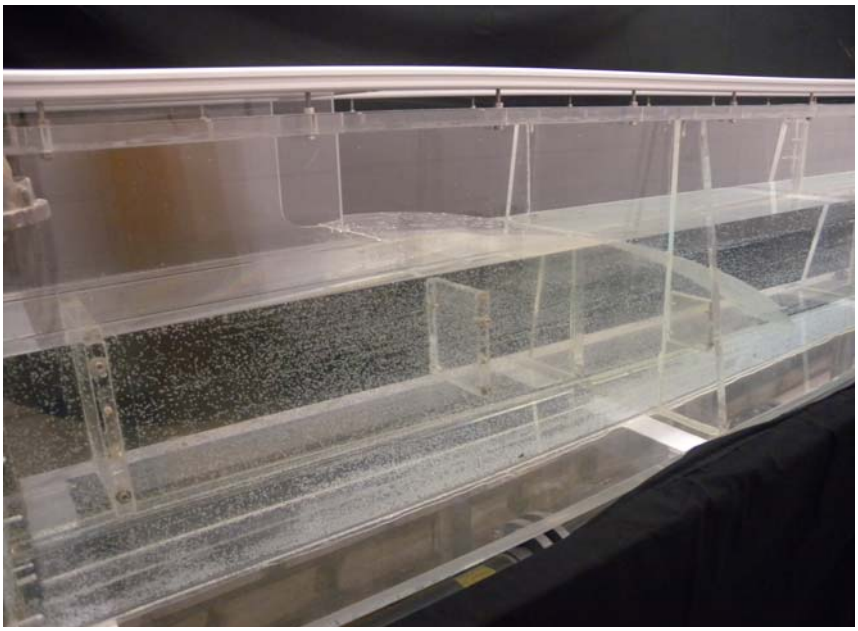

Photo 4.2: View of the flume end.

4.2.2 Wave generation system

Within the mechanical, geometric and hydrodynamic limitations of the system, the wave generating system is capable of generating different kinds of two dimensional regular wave sequences. The wave maker can operate in two different modes: (a) in piston mode for generation of shallow water waves, or (b) in flap mode for generation of deep water waves. As well as the wave generating system is cable of generating random and breaking waves. The wave generator is shown in Photo 4.3

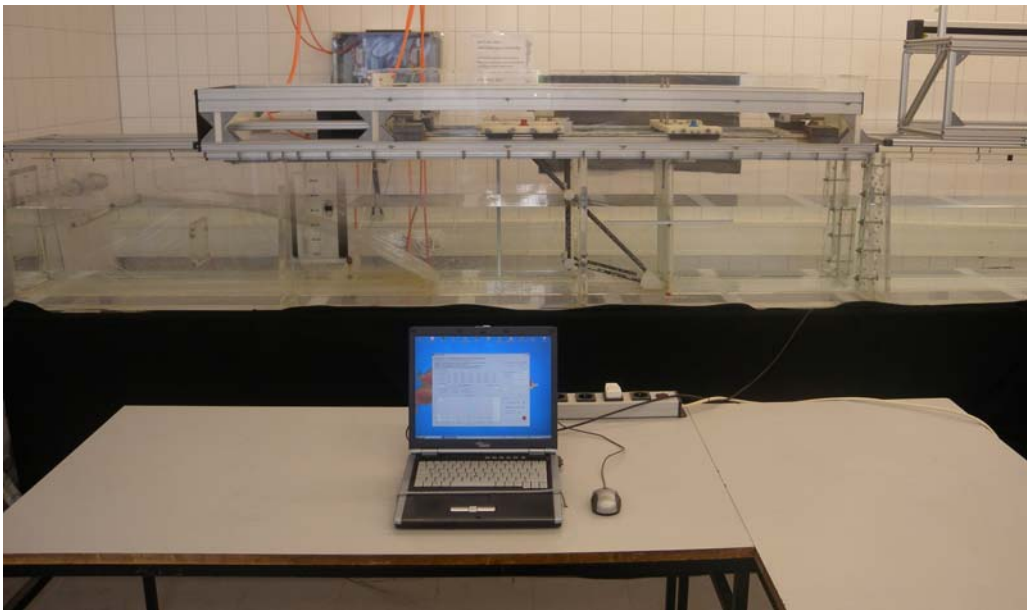

Photo 4.3: View of the wave generating system.

4.2.3 Servo actuator and wave controller

The actuator consists of paddle, two rigid arms with articulation, two spiral shafts and two motors. The motors are connected with two driver high voltage. The drivers receive the signal from two PC-RS232 with USB adapter. The existing software code was written by Oertel (2008/2009) under MATLAB GUI program that deliver the finite wave with certain frequency, number of waves and the wave height as shown in Figure 4.1.

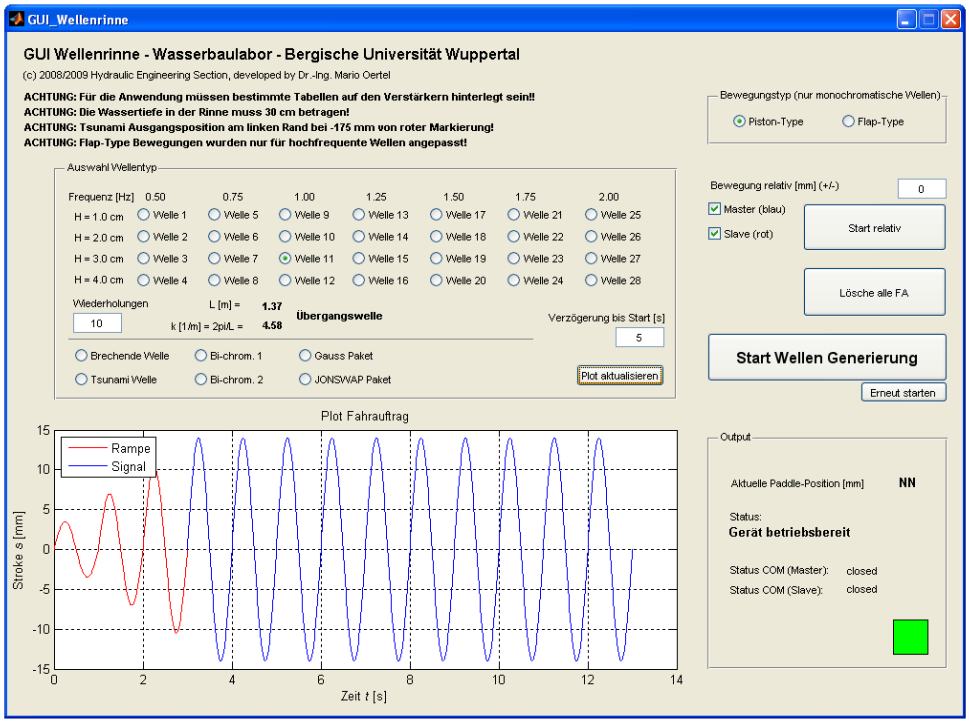

Figure 4.1: MATLAB GUI a wave flume (IGAW software).

4.3 PHYSICAL MODEL

The proposed breakwater models were constructed of vertical panels of width of 2.5 cm, and thickness of 2.5 cm where the porosity of the barriers is 50 % in the middle section. The upper and lower parts are impermeable parts with different depth as a ratio from the water depth. The models were fabricated from aluminum components as shown in Photo 4.4. The experimental works are divided into two stages.

1. The first stage was carried out for a single vertical wall model as shown in Photo 4.5. The model was located at 12.2 m from the paddle. The model was tested under regular waves. This work was carried out for four different categories:
   - Various *dm* as a proportion of the total depth *dm* = 0.8*d*, 0.6*d*, 0.4*d* and 0.2*d*.
   - Constant *du* at *du* = 0.4*d* and various *dw* = 0.1*d*, 0.2*d*, 0.3*d*, 0.4*d* and 0.5*d*.
   - Constant *dw* at *dw* = 0.4*d* and various *du* = 0.1*d*, 0.2*d*, 0.3*d*, 0.4*d* and 0.5*d*.
   - Constant *dm* at *dm* = 0.2*d* at various location of *cdm*.

Photo 4.4: View of the physical model.

2. The second stage was carried out for double identical vertical slotted walls as shown in Photo 4.6. The model was tested under regular waves. The first wall was located at a fixed distance of 12.2 m from the paddle. The second wall was located at various distances from the first one, where the chamber width 2λ are various as shown in table 4.1.

The experimental program for single and double walls model is reported as shown in table 4.2.

Photo 4.5: View of the single vertical slotted wall model.

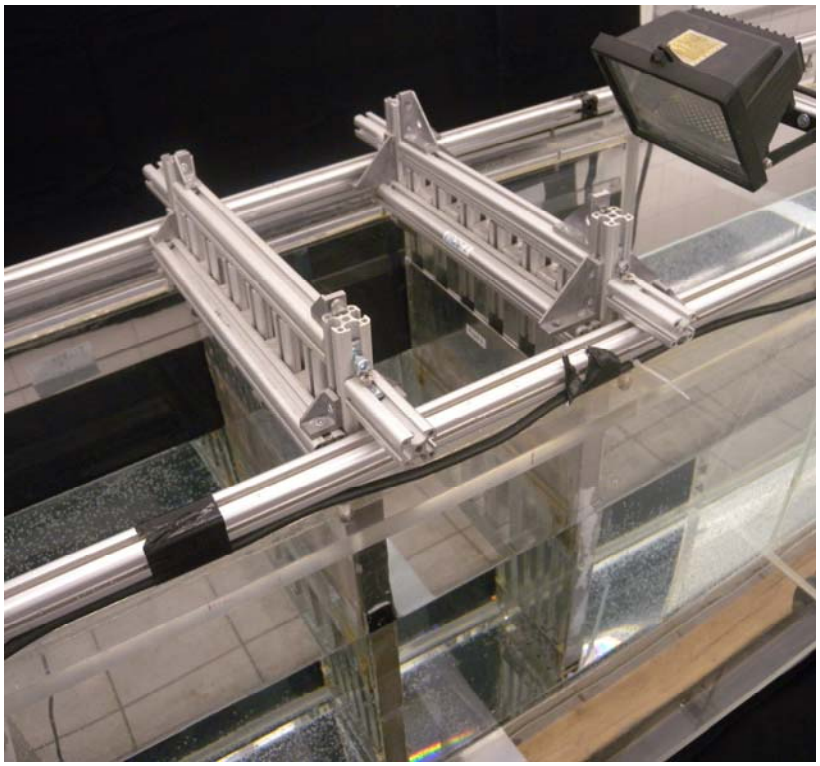

Photo 4.6: View of double vertical slotted wall model.

Table 4.1: The chamber width 2λ of the double vertical slotted wall model.

	depth (*d*)	wave length (*L*)
2 λ	0.5 *d*	0.25 *L*
	1.0 d	0.50 *L*
	1.5 *d*	0.75 *L*
	2.0 *d*	*1.00 L*

Table 4.2: Experimental Program.

Model	Investigation	*dm*	*du*	*dw*	*cdm*	*kd*	*λ*
Single Wall	Inf. of Permeable depth	0 to *d*	according to *dm*		0.5 *d*	various	
	Inf. of *dm/d*					fixed	
	Inf. of lower part	various	0.4 *d*	0.1 *d* :0.5 *d*	various	various	
	Inf. of upper part		0.1 *d*: 0.5 *d*	0.4 *d*	various	various	
	Inf. of Location *dm*	0.2 *d*	various		0.1 *d*: 0.7 *d*	various	
Double Wall	Inf. of permeable depth	0 to *d*	according to *dm*		0.5 *d*	various	*0.125 L* *0.250 L* 0.375 L
	Inf. of *dm/d*					fixed	0.500 L 0.25 *d* 0.50 *d* 0.75 *d* 1.00 *d*

4.4 INSTRUMENTATION

4.4.1 General

For the present physical model study, the wave velocities were measured by PIV via high speed camera which will be discussed in detail later. The wave profiles were measured by Ultrasonic sensors USS635 (range of 635 mm). A view of the instrumentation set-up is shown in Photo 4.7.

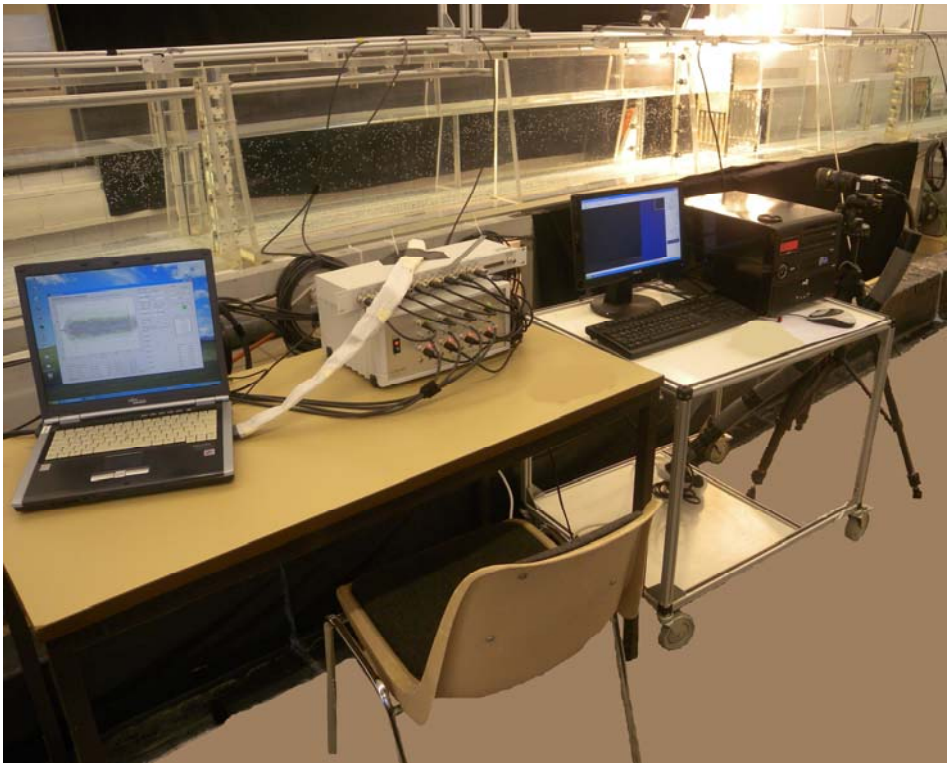

Photo 4.7: View of measuring devices for wave profile and wave velocity.

4.4.2 Ultrasonic sensors

The water surfaces were measured by four Ultrasonic sensors type USS 635. The blind area and the maximum working range is 60 mm and 350 mm respectively which are corresponding to voltage 0 to 10 V. The output frequency is 75 Hz. The reproduce ability is $\pm$0.15 %. The wave sensors were connected with Ultralab ULS 80D that 8 channels and its out-put are analogue 0 to 10 V and RS232. The sensors and Ultralab are shown in Photo 4.8. The digital signals of the wave history were read by PC card and were plotted for four locations as shown in Figure 4.2.

Photo 4.8: View of sensors and Ultralab. [87]

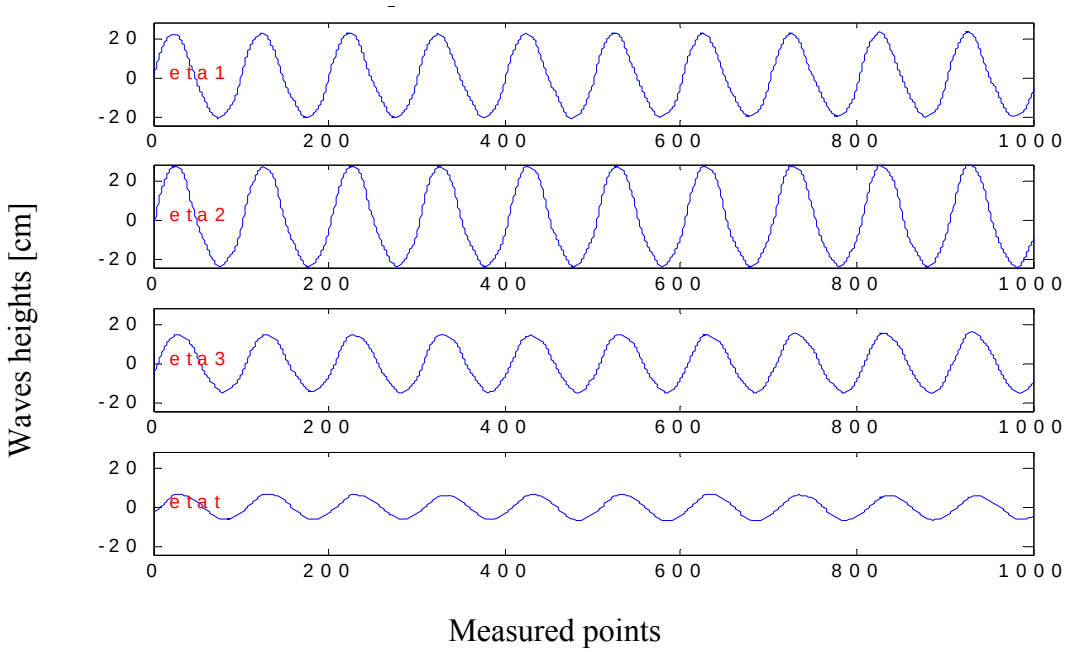

Figure 4.2: Measured wave heights.

First, three probes were kept at a distance of 2.2 m in front of the model. The spacing between the first three probes was adjusted for each of the wave period so as to calculate the reflection coefficient by the three-probe method of Mansard and Funke (1980) as shown in Photo 4.9. The wave transmission was measured by a sensor kept

at the rear side of the model at a distance of about the longest wave length considered for testing purpose as shown in Photo 4.10.

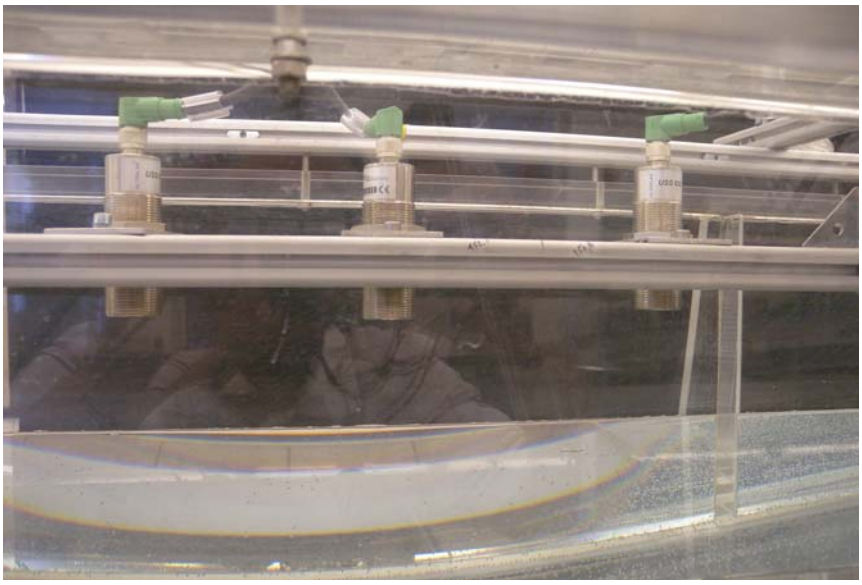

Photo 4.9: View of sensor in front of the model.

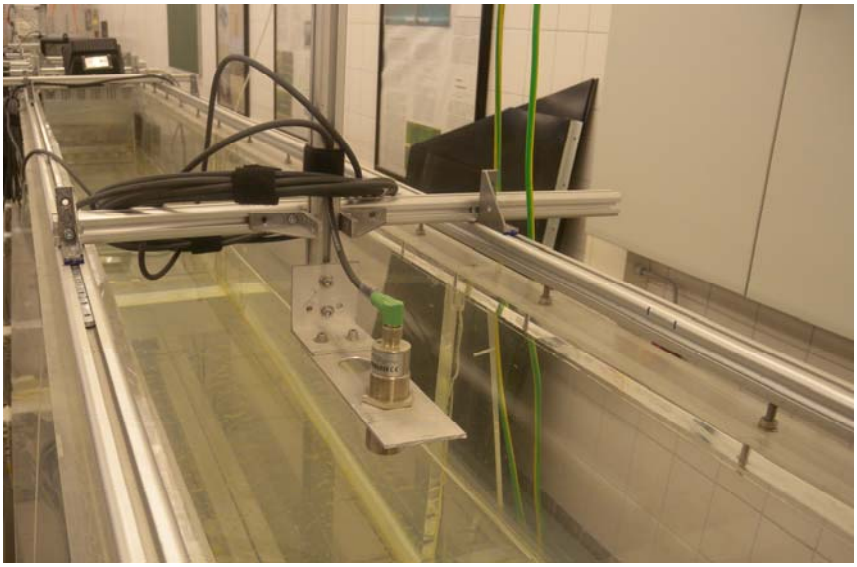

Photo 4.10: View of sensor in the rear side.

4.4.3 Calibration of Ultrasonic sensors

To be more precise, the calibration of a sensor is required to convert the voltage output to physical quantities under investigation. The calibration was done for each set of experiments to minimize the calibration errors in the experiments. The calibration procedure was carried out by finding the output of the sensor, in terms of voltage associated to the minimum and maximum voltage, for a known value of input physical parameter (distance). The results of calibration were taken into account and the outputs were corrected in the settings of sensor for Ultrasonic Sensors Acquisition (Software of IGAW 2010 version 3.1).

4.4.4 Position of wave sensors in front of the breakwater model

Three wave sensors were located in front of the structure at a distance of 2.2 m from the breakwater model to measure the incident and reflected wave heights. The optimal distance between the wave sensors is a function of the wave length and has been adopted as recommended by Mansard and Funke (1980). The minimum distances between wave sensors are tabled in table 4.3 for different wave periods. For the fixed three waves sensor method, the distance between the wave sensors can be obtained as follows: The distance between the first two wave probes (x_{12}) in the line of wave propagation is one tenth of wave length.

$$(x_{12}) = L / 10 \tag{4.1}$$

The distance between the first and third wave probes (x_{13}) in the line of wave propagation should satisfy the following conditions

$$\mathrm{L} / 6 < x_{13} < L / 3 \tag{4.2}$$

$$x_{13} \neq L / 5 \tag{4.3}$$

$$x_{13} \neq 3\, L / 10 \tag{4.4}$$

The positions of the wave gauges were changed accordingly to the recommendation of Mansard and Funke (1980). One wave probe was placed on the lee side of the breakwater to measure the transmitted wave height. It is assumed that the beach on the lee side of the breakwater is a perfect absorber and the wave heights which were recorded by the wave probes at the lee side are due to the transmitted waves only. Moreover, all experimental readings were taken before any reflection from the absorber of the flume end or the wave paddle by examining the plotted wave's records and using the approximate arrival time of the first reflected wave.

Table 4.3: Distance between wave sensors.

Frequency F (sec^{-1})	Wave length L (m)	$x_{12} = L/10$ (m)	$x_{13} = L/4$ (m)
2.00	0.395	0.0395	0.099
1.75	0.517	0.0517	0.129
1.50	0.701	0.0701	0.175
1.25	0.973	0.0973	0.973
1.00	1.383	0.1383	0.346
0.75	2.037	0.2040	0.509
0.50	3.268	0.3300	0.817

4.5 PARTICLE IMAGE VELOCIMETRY (PIV)

4.5.1 General

In this section, sufficient knowledge about PIV and its applications in velocity measurements has been presented. In addition to that new application of PIV in wave structure interaction has been investigated. In the recent years, Particle Image Velocimetry (PIV) is one of the optical methods, which were increasingly applied to velocity measurements of fluid. The working principle is quite simple; the fluid is seeded with light reflecting particle, a light sheet illuminates the particle in the measurement plane and a high speed camera is used to take two exposures of the illuminated plane. The two exposures should be taken within a short interval, so that the same particles are caught in both exposures. The two exposures can be taken either as a double exposure of one image or as two different images. The method with two images is more commonly used and based on a cross-correlation.

The aim of the cross-correlation is to find the distance that particle pattern has moved during the inter image time and translate this into a velocity measure. The relation between velocities v and particle displacements Δx is

$$v = \frac{\Delta x}{M \Delta t}$$

where M is the magnification and Δt is the inter image time.

The cross-correlation function is not calculated on the whole image but on smaller parts of these called interrogation areas, see Figure 4.3. The cross-correlation functions can be calculated in a number of different ways. The finite Fourier transforms is the direct method to compute the cross-correlation but it is quickly becomes very heavy to apply when larger data-sets are to be analyzed. A more efficient way to estimate cross-correlation functions is to use fast Fourier transforms (FFTs). Additional advanced correlation algorithms are selectable for improved performance such as local adaptive window shift and deformation and correlation averaging.

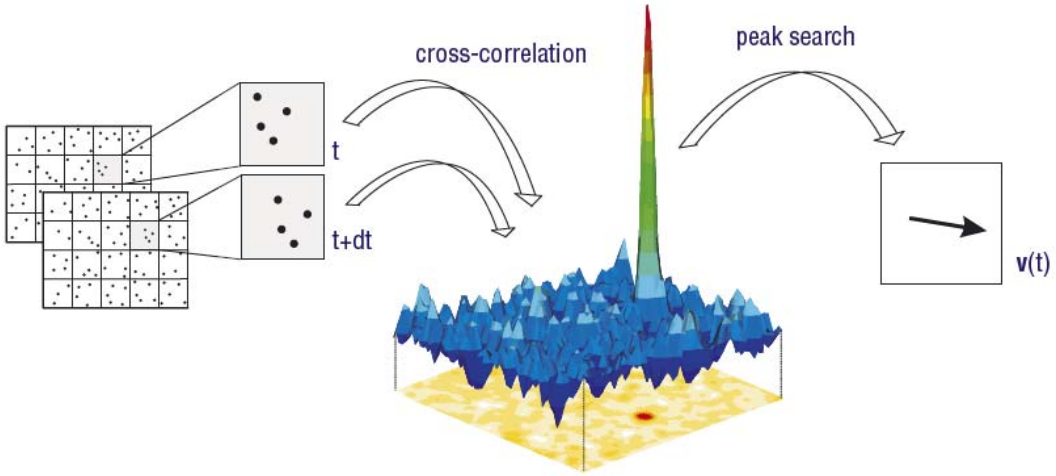

Figure 4.3: Illustration of PIV method. [source: LaVision]

Since 1980, the Particle Image Velocimetry (PIV) technique was developed as non-intrusive method in the field of hydrodynamics to measure the velocity field, acceleration and vortices as well as to report the water surface displacement and also PIV was used to investigate the wave interaction with structures. Up to date PIV has become a standard method, where it is based on a digital near-field photogrammetry and has its main field of application in wave theories, burning analysis, aerodynamics, and geo-technics. The PIV is capable of providing the velocity vector over a selected two-dimensional region of the flow, with sufficient accuracy and spatial resolution. The velocities are often reported to be measured within 1 to 2 % error. In addition the PIV is the most settable method to analyze and plot vortices. The velocity measurement must be made simultaneously over several closely spaced locations from which spatial derivatives can be evaluated using finite difference schemes. The efficiency of this technique was proved in measuring the velocity field in both 2D and 3D.

The convention for two-dimensional PIV is to illuminate a single plane of the flow with a light sheet whose thickness is less than the depth of field of the image recording system. In this situation, the depth of the measurement plane is determined by the thickness of the light sheet. Volume illumination is an alternative approach, whereby the test section is illuminated by a volume of light. This mode of

illumination was used to measure three dimensional velocity vectors using a single camera (Willert and Gharib 1992), multiple cameras (Okamoto et al. 1995) and a holographic camera (Gray and Greated 1993; Hinsch 1995).

Some applications are the investigation of the interaction of wave induced flow fields with wave damping structures and semi-submerged breakwaters (Belorgey et al. 1986). Greated et al. (1992) and She et al. (1997) showed that PIV is applicable to a flow field within a breaking wave in three-dimensional. Gray and Greated (1988) applied the Particle Image Velocimetry (PIV) to measure the velocity distributions in two dimensions under water waves.

Lengricht and Graw (1995) investigated the flow field beneath gravity waves by two particle tracking methods. The first particle tracking methods was frame-by-frame and the second enhanced system allowed storing a time series up to 63 video images in the hardware of a PC frame grabber board. Both of them were adequate tools to visualize the flow to get information about particle motion beneath gravity waves. They were used to detect regions of particular eddy activities, e.g. caused by interaction of the incoming waves with coastal structures. Meinhart et al. (2000) investigated particle image velocimetry experiments where optical access is limited or in micro scale geometries. The depth of the measurement plane must be defined by the focusing characteristics of the recording optics. A theoretical expression for the depth of the two-dimensional measurement plane was derived and it was shown to agree well with experimental observations. The results showed that the particle concentration must be chosen judiciously in order to balance the desired spatial resolution and signal-to-noise ratio of the particle-image field.

Lengricht et al. (2000) presented PIV for wave-structure interactions of monochromatic waves and a semi-submerged vertical wall, wave-structure interactions of regular waves propagating oblique towards a submerged horizontal plate and a breaking wave occurring due to the superposition of numerous wave components of a real sea state. After the adaptation of the stereoscopic PIV-system to the specific conditions in a wave flume, the flow conditions beneath gravity waves were mapped very sufficiently. The wave structure interactions were recorded very

easily and rapidly by physical modeling. Time history velocity field was recorded and presented as three-dimensional velocity maps. The PIV system investigated wave-induced motion in the vicinity of coastal structures in order to get information about turbulence parameters and wave energy dissipation as well as their distributions both locally and in time. Furthermore, complex wave motion investigated by observing and capturing the particular flow phenomena in a wave flume, e.g. real sea states consisting of numerous components superposing or decaying.

Chang et al (2001, 2005) investigated both experimentally and numerically a solitary and cnoidal waves interaction with a submerged rectangular obstacle. Cowen et al (2003) used PIV to make vertically resolved two-dimensional measurements in swash zone flows, which are notoriously recalcitrant to quantitative measurement by PIV. The spatially and temporally resolved velocity fields measured in a plunging and spilling wave-driven swash zone are used to investigate the boundary layer structure of the mean and turbulent quantities as well as the phase evolution of the bed shear stress, near-bed turbulent kinetic energy, and the dissipation.

4.5.2 PIV setup

Measurements of the velocity field, vortices and the surface elevation were performed at a distance of 12.2 m from the wave maker using the high-speed camera of IGAW (Motion Scope M3), where the model of a single slotted wall and measurement devices were constructed as shown in Photo 4.11.

The camera was placed at 1.5 m (focus) from the center of the flume, it should be noted, that the minimum focusing distance should be 1.00 m for this camera. The light settings and particles are shown in Photo 4.12. There should be a black plate at the back of the flume to avoid the visibility of the wall through the glass. The detail of the single slotted wall model was previously mentioned in detail in Section 4.3. The water depth was fixed during the experiments at 30 cm. It is essential that, the

measurements must be terminated before any (small) reflected wave has returned to the measurement position from both the flume end and the wave maker.

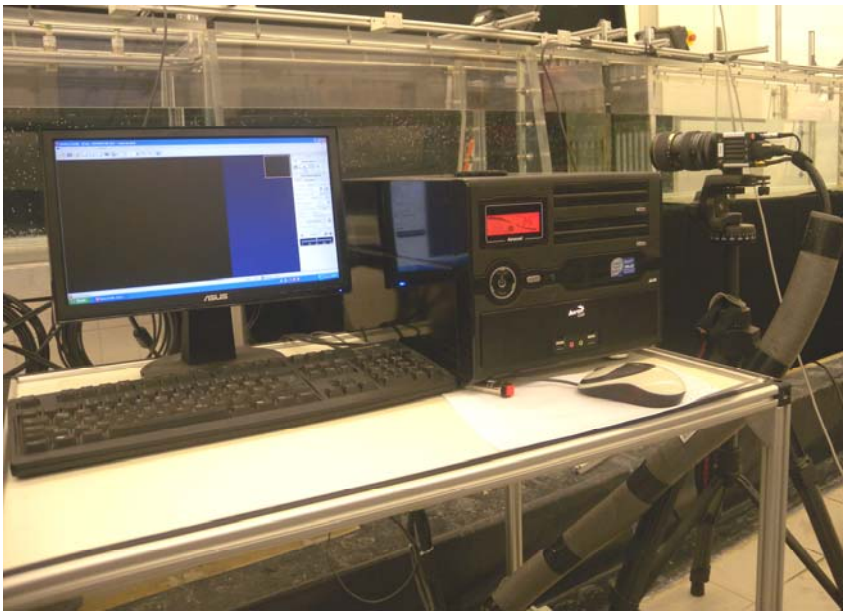

Photo 4.11: View of measuring devices for wave velocity.

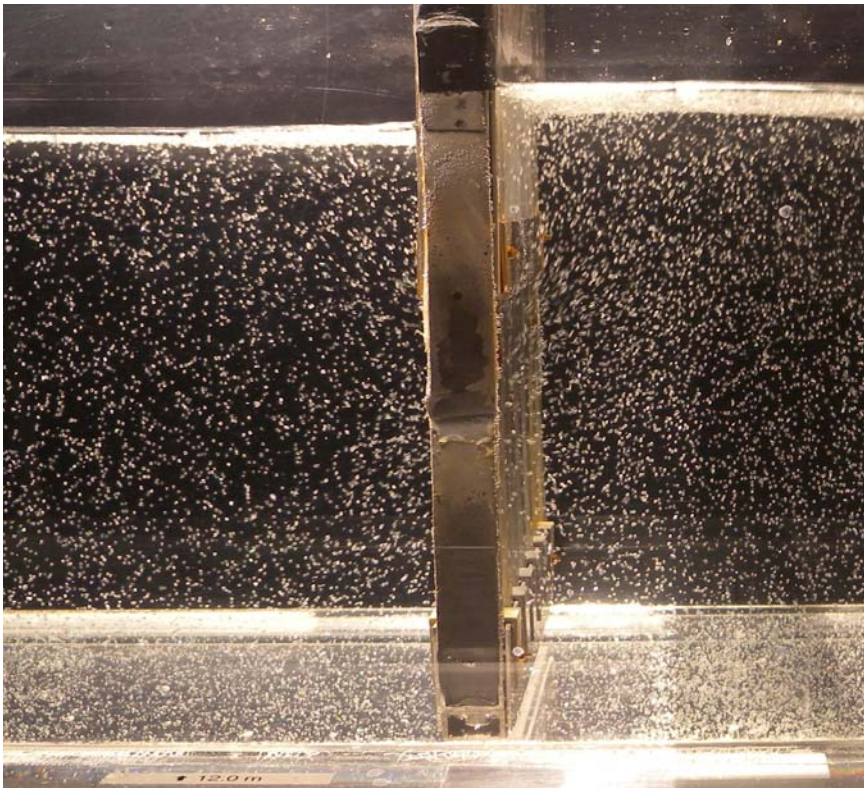

Photo 4.12: View of particles at the measuring area.

4.5.3 PIV accuracy

The accuracy of PIV on the velocity wave measurement due to the time increment δt was optimized. It is found that the time increment should be taken in a range of 0.01T < δt < 0.015 T, such that the error of measurements will be less than $\pm$ 5 % for all used waves where T is the wave period.

Figure 4.4 shows the relation between the relative time $\delta t / T$ and the relative horizontal particle velocity U_{-ex} / U_{-th} where U_{-ex} is the measured horizontal particle velocity by PIV, U_{-th} is the calculated horizontal particle velocity by linear airy wave theory and T is the wave period. It is clear from the Figure that, the accuracy of the measured wave-particle velocity is affected by the relative time increment $\delta t / T$. It is noted that, the error is major for small analysis time where the error is more than 30 % at $\delta t / T < 0.005$ for short waves and the error is more than 20 % for intermediate waves at $\delta t / T < 0.0025$. The error of intermediate waves is improved quickly while the error of short waves is improved gradually.

The time increment should be taken in a range of 0.01 T < δt < 0.015 T, such that the error of measurements will be less than $\pm$ 5 % within this study. The achievable accuracy of PIV measurement within this set-up is shown to be limited by the influence of the relative time $\delta t / T$.

The sampling interval, time between two selected frames, Field Of View (FOV), resolution of the camera and the characteristics of waves are tabled in details in table 4.4.

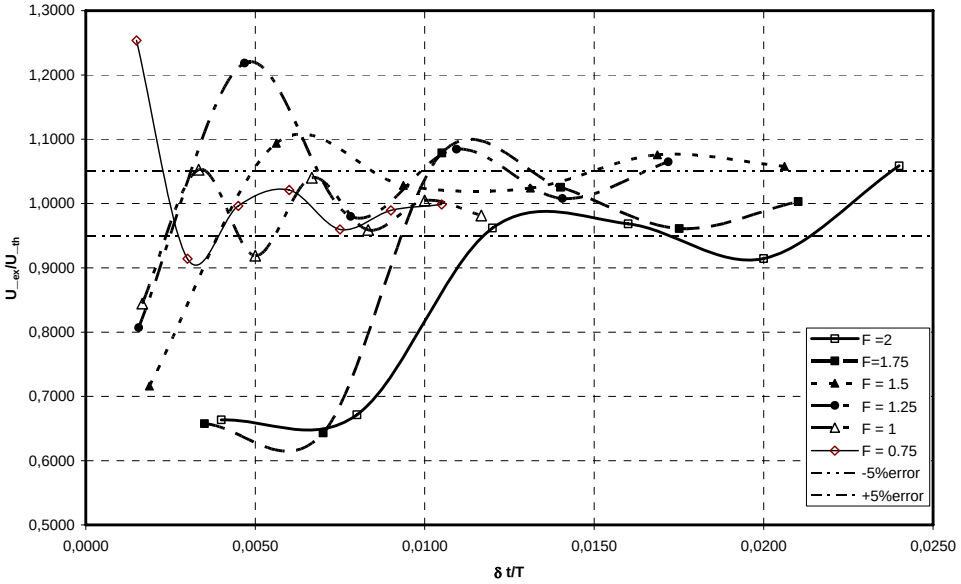

Figure 4.4: The relation between the specific velocity and the relative time.

Table 4.4: Details of the waves, camera and field of view.

Frequency of waves F (Hz)	Wave height h_i (m)	Frequency of Camera (fps)	Time between two selected frames (sec)	Resolution (Square pixels)	FOV (cm^2)
2.00	0.01	1000	0.008	624*512	22.5*18.5
1.75	0.01	1000	0.008	624*512	22.5*18.5
1.50	0.02	800	0.009	800*576	28.5*20.5
1.25	0.02	800	0.011	800*576	28.5*20.5
1.00	0.03	600	0.010	1024*768	36.5*26.5
0.75	0.04	500	0.014	1200*704	42.5*24.5

4.6 TEST SETUP

The complete experimental setup showing details of the flume, position of the model and locations of wave probes are shown in Figure 4.5. The test section in a water depth, *d* of 30 cm was located at a distance of 12.2 m from the wave maker. The tests were conducted for regular wave and a height of waves in range of 1 to 4 cm. The heights of waves were measured with four wave sensors. The first three sensors were kept in front of the model at a distance of 2.2 m from the model. The transmitted wave was measured by a sensor, which was kept at the rear side of the model at distance of 2.2 m from the model. For the double walls model, the first wall and the three sensors in front of the model was fixed, the second wall was located at various distances from the first wall and the fourth sensor was kept at a fixed distance of 2.2 m from the second wall.

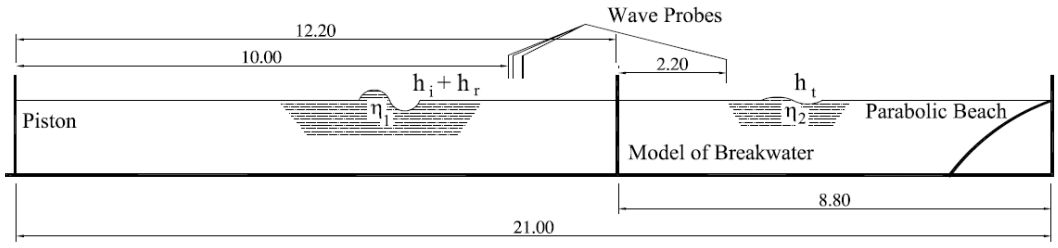

Figure 4.5: Sketch of experimental setup.

4.7 WAVE CHARACTERISTICS

4.7.1 Regular wave tests

The regular waves are waves with a single frequency and are described by a distinct wave height and an associated time period. The breakwater models were described earlier and subjected to the action of regular waves, for a period ranging from $T = 0.5$ to 2 s. For a particular wave period, monochromatic waves with four different wave heights of 0.01, 0.02, 0.03 and 0.04 m. The *kd* values were between 0.5 and 4.772. Sample data of regular waves acquired by the wave sensors for a typical test with *dm* = 0.2 *d* are shown in table 4.5.

Table 4.5: Sample of measured and calculated data for the single vertical slotted wall model with $dm = 0.2d$:

Run	F	a_1	a_2	a_3	a_t	Calculated date		
	s^{-1}	mm	mm	mm	mm	*CR*	*CT*	*kd*
1		6.880	9.204	5.767	0.085			
2		6.835	9.277	5.936	0.092			
3	2.000	6.835	9.277	5.936	0.092	0.971	0.022	4.772
4		4.836	15.907	16.223	0.422			
5		5.008	16.002	16.282	0.435			
6	1.500	5.018	16.119	16.462	0.438	0.937	0.116	2.689
7		5.716	9.161	19.275	2.750			
8		5.732	9.204	19.346	2.725			
9	1.125	5.901	9.239	19.298	2.698	0.874	0.248	1.937
10		21.289	25.634	14.816	6.471			
11		21.365	25.685	14.831	6.440			
12	1.000	21.310	25.730	14.903	6.382	0.670	0.420	1.363
13		26.078	30.860	17.331	9.201			
14		26.169	31.105	17.357	9.274			
15	0.750	26.169	31.105	17.357	9.274	0.621	0.450	0.925

4.8 TEST PROCEDURE

Each of the models was subjected to the action of regular waves as discussed above. Once the wave maker was started, the time histories of the wave elevations from the wave sensors were recorded simultaneously and, the acquired data were viewed on the computer screen as a preliminary check of the quality of the measured data. The sampling frequency adopted for data acquisition is 300 Hz and the total duration of the record was 60 s. Sufficient time gaps were allowed between successive runs to restore calm water condition in the wave flume. The data were stored in the hard disk of the PC and were used to calculate some parameter to analysis. The arrival time of the wave at the model depends on the wave frequency, and hence the time series of waves were analyzed separately. The time series corresponding to the clear repetition of the regular occurrences of the events before any reflected wave influences the wave field was selected for analysis and the rest of the time record was discarded. Totally, 90 runs were conducted for the single vertical slotted wall model and 176 runs were conducted for the double vertical slotted wall model.

4.9 ANALYSIS OF DATA

A detailed analysis of the data collected by wave's probes in the experimental study is essential to obtain all desired information for further investigations. The method of analysis of the data in the present study were carried out by IGAW software, that calculate the reflection coefficient depending on Mansard and Funke (1980) for the three wave probe method, which based on the least squares analysis. The input data are the wave history as a time domain file. A window of 10 sec from the record data after the reflection was selected. The selected data was converted to frequency domain by Fast Fourier Transformation. Finally, the spectrum of the incident, transmitted and reflected wave height were calculated. Accordingly, the reflection and transmission coefficients were found directly.

A detailed analysis of the data collected by PIV in the experimental study is essential to obtain all desired information for further investigations. The analysis of the data

carried out by MatPIV (Sveen 2004) which is adopted in this study. This software can calculate velocity and vorticity magnitude, plot the velocity vector and decompose the particle velocity into horizontal and vertical components.

4.9.1 Software

There are several PIV programs available. Some of them are freeware, like e. g. MATPIV (Sveen 2004) which was adopted in this study. MATPIV can be used as a toolbox within MATLAB and was developed in several m-files performing the necessary PIV calculations.

The process is started by specifying the coordinate system to calculate the transformation from the local camera coordinates to the physical world coordinates in the experimental work. Thereafter, a mask to the images is applied to where there are no particles to save calculation time. The images are interrogated to estimate the velocity field by calculating the displacement, where the time is known. After the velocity field is found, the velocity fields are filtered using three different filters. The first is a Signal-to-Noise ratio filter, where the Signal-to- Noise ratio is taken as the ratio of the highest peak in the correlation plane to the second highest peak. Filtering is followed with a global filter, that excludes vectors based on the mean of the ensemble plus a factor times the standard deviation and remove vectors that are significantly larger or smaller than a majority of the vectors. Finally, local median and mean filters based on the squared difference between individual velocity vector and the median or the mean of their surrounding neighbors are applied, followed by interpolation of outliers.

4.10 VELOCITY MEASUREMENT

4.10.1 Measurements of incident velocity

PIV is able to measure the velocities with high accuracy. MatPIV (Sveen, 2004) was employed to decompose the particle velocity into horizontal and vertical components.

Figure 4.6 (a to f) shows the velocities magnitude for the incident waves, which were investigated during the experimental work. The characteristics of the waves and the field had been mentioned earlier in table 4.4. The measurements illustrate the extent of compatibility between PIV and the linear airy theory, where the high particle velocities are located at the surface of the water and the particle velocity of intermediate wave diminish in amplitude with depth, while the particle velocity of the short-wave vanishes after the mid-depth as shown in sub-Figures 4.6 a and 4.6 b.

The Figure 4.7 (a to f) is plotted for the maximum horizontal particle velocity along the x-direction. The maximum of the horizontal velocity corresponding to the coordinate at the wave crest can be determined through the fitting curve. It is noted that the maximum horizontal water particle velocity must be associated with the crest of the wave and must be located near the water surface far away from the bottom of the flume to avoid the effect of the bottom. Therefore, the high horizontal velocities, which were recorded near from the bottom, must be neglected.

Note that u is similar in phase with the wave profile, which shows the compatibility between the measured particle velocity via PIV and the calculated velocity by linear airy wave theory. Finally, PIV is easy to use in measuring the velocity of waves with high accuracy.

4.10.2 Comparison PIV with the theoretical velocity of incident waves

The comparison between the water-particle velocity measurements via PIV and the linear theory of incident waves can be carried out through comparison of the velocity

or one of its components (u or v). The comparison by one of the velocity components is the better way to reduce the error percentage. The maximum horizontal velocity at the crest of the waves is adopted as a comparison point for example. The comparison of velocities is reported in table 4.6, which clarifies, that the error percentage is higher for high frequencies where the error is more than $\pm$ 3 % and lesser for lower frequencies where the error is less than $\pm$ 0.2 %. This may be due to that the velocities of higher frequencies are small, where the error increases with decreasing the velocity and also may be related to the energy position resulting from the dumping of particle which leads to lack of complete stability of the water, the size of used particle and the accuracy of used devices. Anyway, the results of PIV are perfectly acceptable for high velocities and satisfying to some extent in the low velocities.

4.10.3 Particle velocity measurement (PIV) behind and in front of the barrier

In overview, to indicate the way of energy dissipation by the structure, PIV was used to measure the velocities behind and in front of the barrier. The velocity magnitude, the velocity vectors and the vortices of the wave are reported in Figure 4.8, Figure 4.9 and Figure 4.10 respectively, where the wave frequency is 0.75 Hz, $dm = 0.2d$, $\varepsilon = 50$ % , $h_i = 4$ cm and the phase = (π / 2) for Figures a and the phase = (3 π / 2) for Figures b. The phase observed in the front of the barrier. The sampling interval is 0.002 s and for analysis of velocity is $\delta t = 0.014\ T$. The resolution of the camera is 1264 x 864 (square pixels). The model was situated at 12.2 m from the wave maker.

It is clear that, the higher velocities are observed near the slots far away from the water surface and the bottom. This is because part of the wave energy is obstructed by the impermeable parts and the horizontal velocities are equal to zero. The other part is dissipated as vortices by the slots. The vortices are observed in the area which is associated to the higher velocities. The vortices areas concentrate in the middle depth due to the permeable part. The remaining part of the wave energy passages through the permeable part like a jet with high velocity as shown in Figure 4.8. The

velocity vector is plotted in Figure 4.9. The large vectors denoted to higher velocity. The passage of wave energy through the constriction is redistributed over the depth. The energy of the transmitted wave is less than the energy of the incident wave because the large part of the wave energy is reflected and dissipated by the impermeable parts and the slots.

Table 4.6: Comparison between the theoretical and measured horizontal water-particle velocities.

Frequency F (Hz)	Water depth d (m)	Wave height h_i (m)	Maximum u (m/sec) Linear theory	Maximum u (m/sec) measurements	Error percent
2.00	0.3	0.01	0.063	0.0610	+3.17 %
1.75	0.3	0.01	0.055	0.0564	-2.53 %
1.50	0.3	0.02	0.095	0.0973	-2.41 %
1.25	0.3	0.02	0.082	0.0826	-0.77 %
1.00	0.3	0.03	0.107	0.1075	-0.47 %
0.75	0.3	0.04	0.129	0.1288	+0.16 %

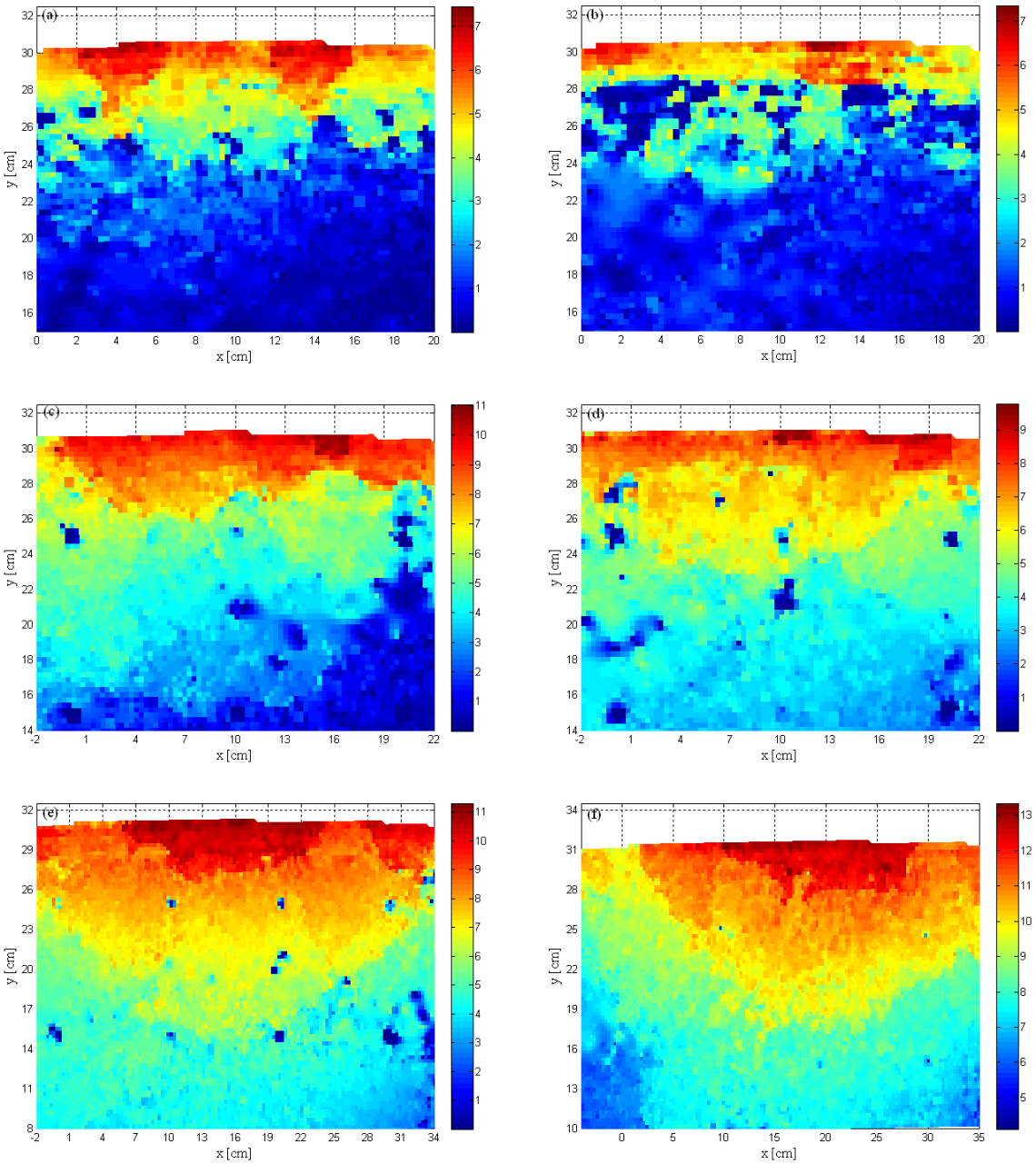

Figure 4.6: Velocity magnitude (cm/sec) of incident waves when the wave crest is within the VOF.

a) for $F = 2.00$ Hz and $h_i = 1$ cm,

b) for $F = 1.75$ Hz and $h_i = 1$ cm,

c) for $F = 1.50$ Hz and $h_i = 2$ cm,

d) for $F = 1.25$ Hz and $h_i = 2$ cm,

e) for $F = 1.00$ Hz and $h_i = 3$ cm, and

f) for $F = 0.75$ Hz and $h_i = 4$ cm.

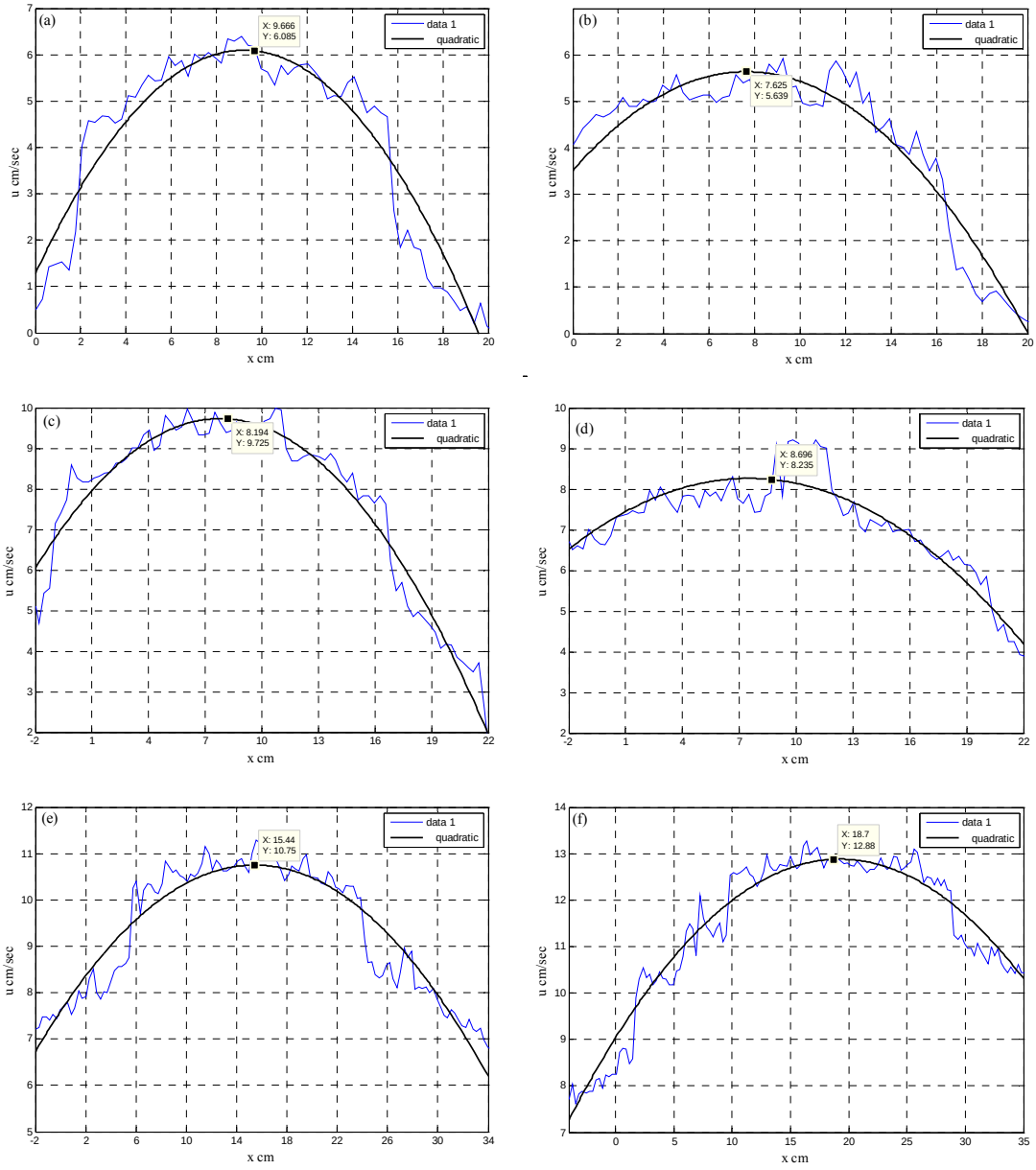

Figure 4.7: Maximum horizontal velocity along the x axis when the wave crest is within the VOF.

a) for F = 2.00 Hz and h_i = 1 cm,

b) for F = 1.75 Hz and h_i = 1 cm,

c) for F = 1.50 Hz and h_i = 2 cm,

d) for F = 1.25 Hz and h_i = 2 cm,

e) for F = 1.00 Hz and h_i = 3 cm and

f) for F = 0.75 Hz and h_i = 4 cm.

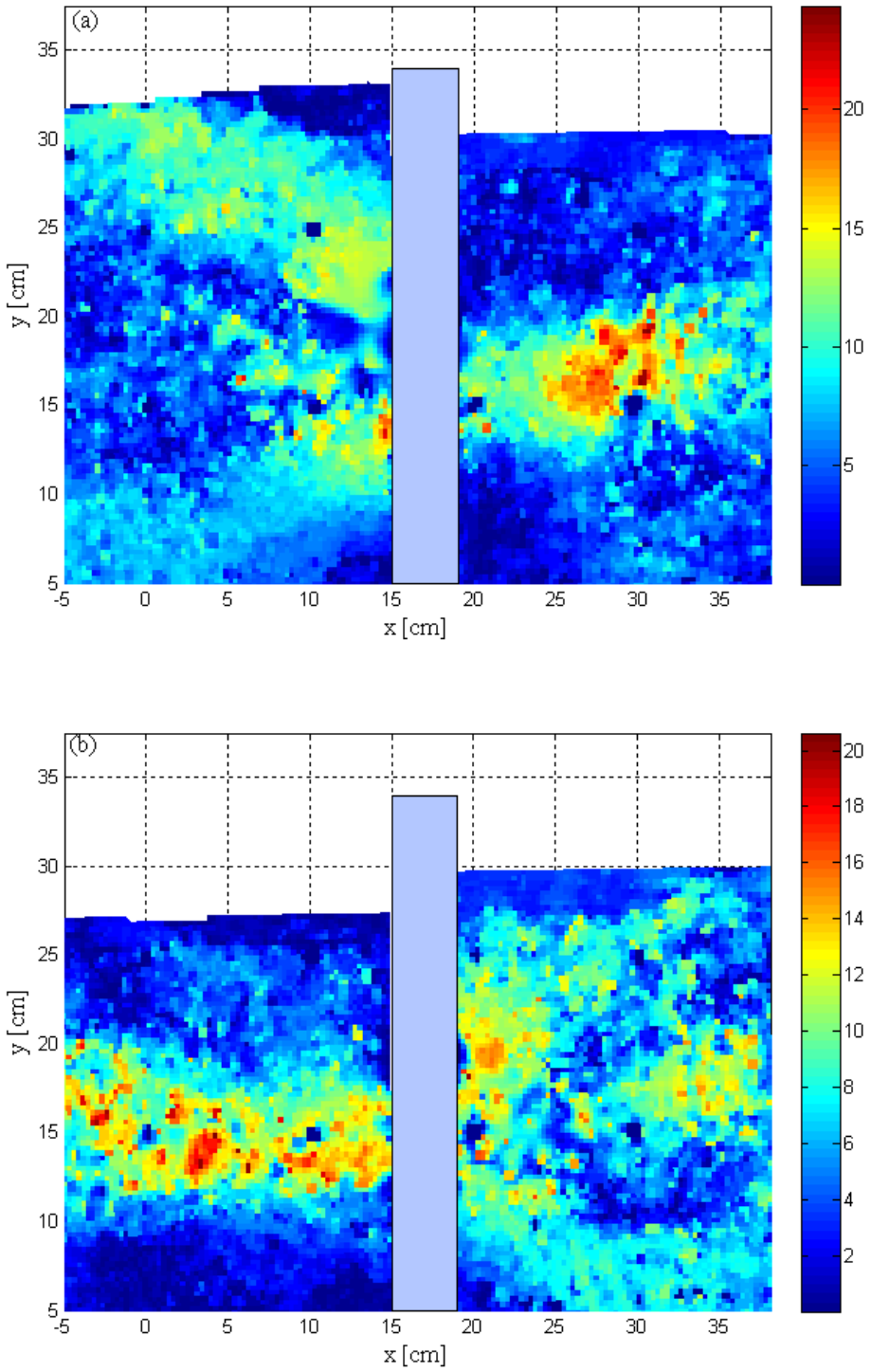

Figure 4.8: Velocity magnitude (cm/sec) in front of and behind the barrier for F = 0.75 Hz and h_i = 4 cm.
a) for the phase = (π /2) and
b) for the phase = (3 π /2).

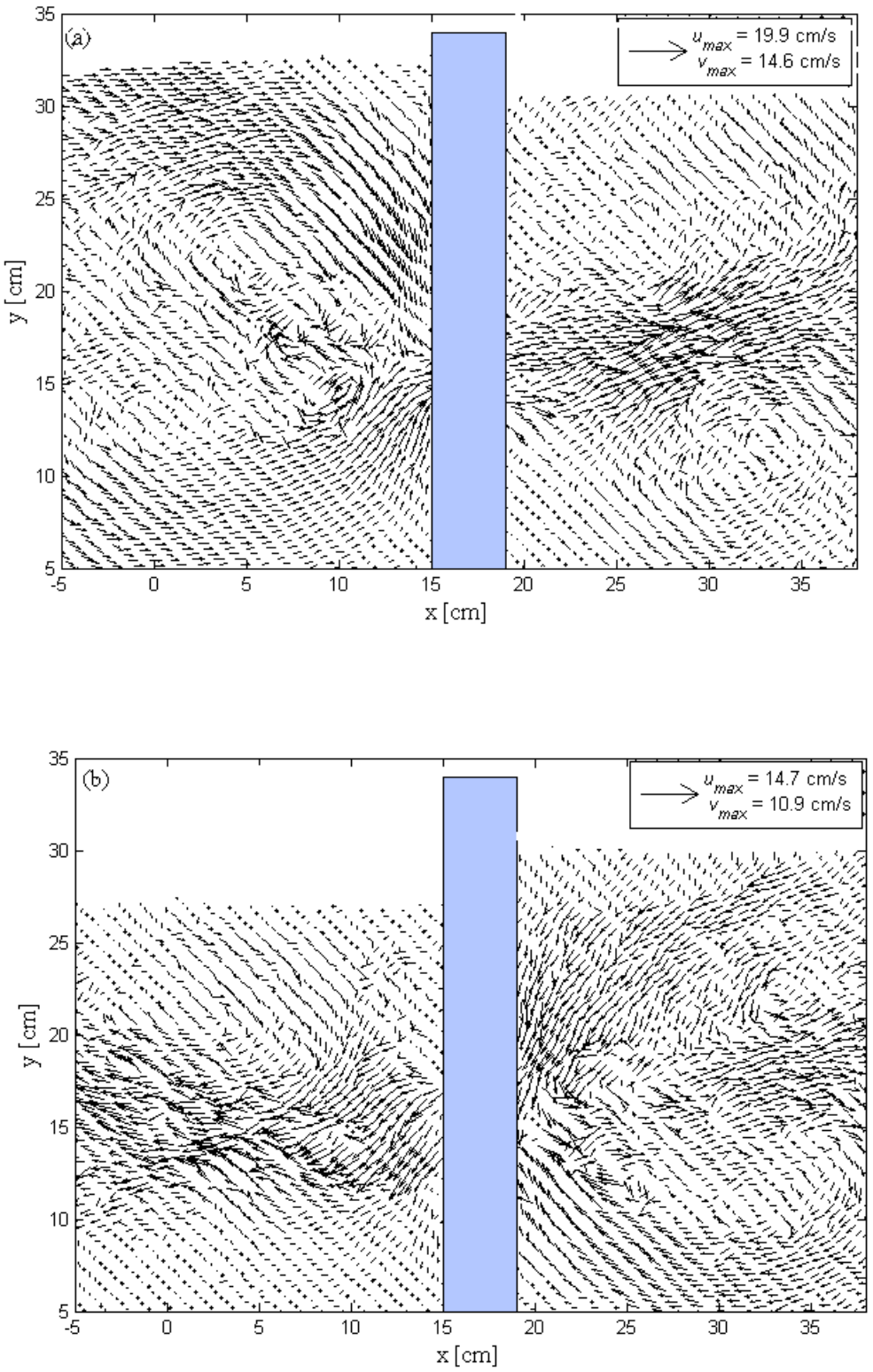

Figure 4.9: Velocity vector in front of and behind the barrier for F = 0.75 Hz and h_i = 4 cm.
a) for the phase = (π /2) and
b) for the phase = (3 π /2).

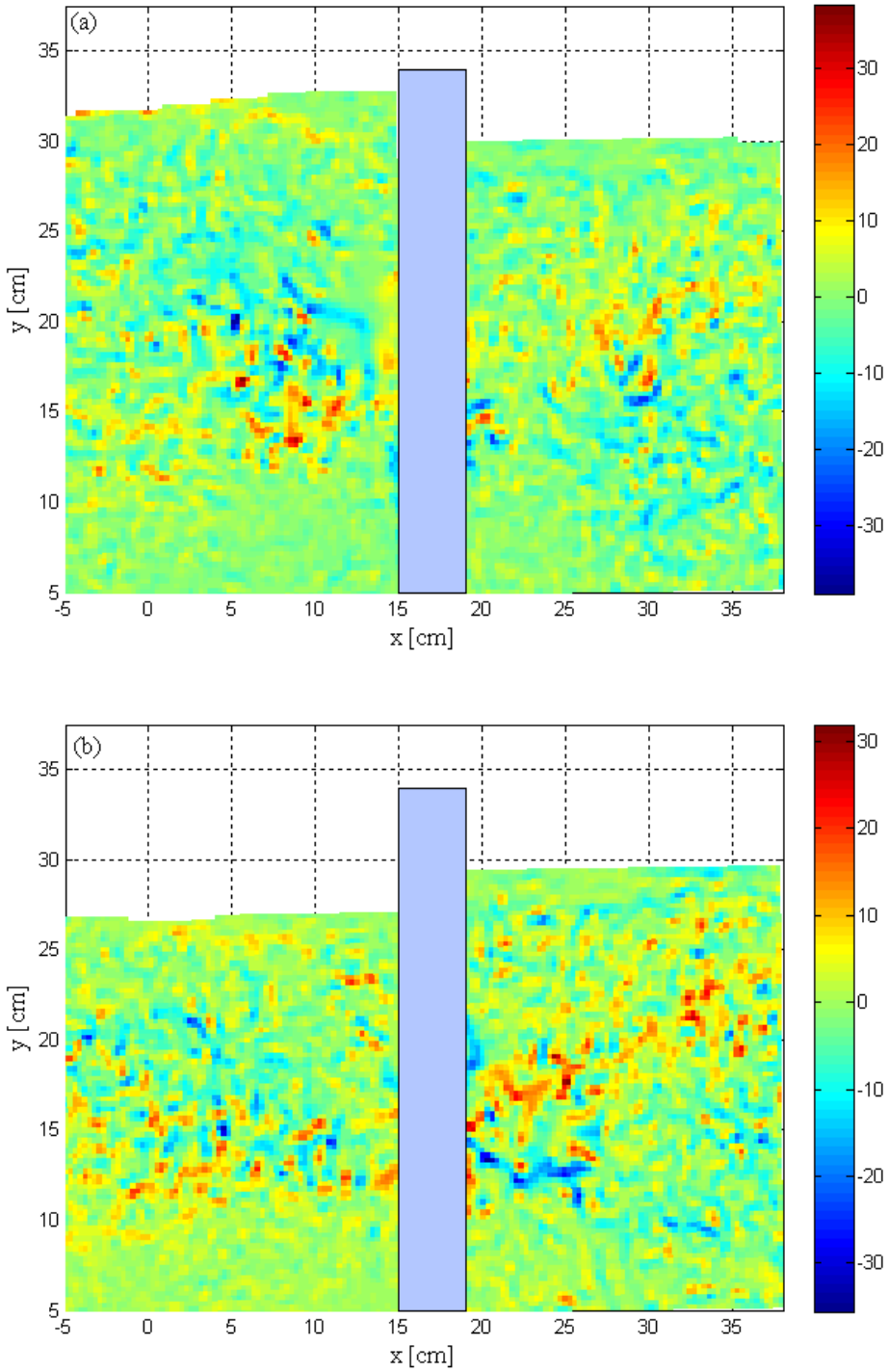

Figure 4.10: Vorticity magnitude (1/sec) in front of and behind the barrier for F = 0.75 Hz and h_i = 4 cm.
a) for the phase = (π /2) and
b) for the phase = (3 π /2).

4.11 THE MESUREMENT OF REFLECTION AND TRANSMISSION COEFFICIENTS USING PIV

4.11.1 General

In this section the velocity of co-existing and transmitted wave are measured and analyzed via PIV and also the reflection and transmission coefficients of the single vertical slotted wall are detected via PIV. In addition, the hydrodynamic performance (*CR*, *CT* and *CE*) of a vertical slotted wall are detected by PIV.

4.11.2 Measurement methods of reflection coefficient

1. A two-point method which consists of measuring simultaneously the co-existing wave (two progressive wave trains moving in opposite direction) at two known positions on a line parallel to the direction of wave propagation. Fourier analysis of these two signals will then produce the amplitudes and phases of the wave components at these two positions, by means of which the standing wave can be resolved into incident and reflected waves. This method has, however, certain limitation.
    - Limited frequency range,
    - critical probe spacing,
    - high sensitivity to errors in the measurement of waves.

    This method was described in details by Thornton and Calhoun (1972) and was developed by Goda and Suzuki (1976) through applying linear wave theory to monochromatic waves.
2. A three- point method which depends on a least square analysis for decomposing the measured spectra into incident and reflected spectra with greater accuracy and range. It is assumed that the waves are travelling in a channel in a longitudinal direction and reflecting from some arbitrary structure or beach and travelling in the opposite direction. It runs through simultaneously measurement of the linear superposition of waves at three points, which are in reasonable proximity to each other and are on a line parallel to the direction of

wave propagation. A least squares method separates the incident and reflected spectra from the measured co-existing spectra. This method advanced for periodic and irregular waves by Mansard and Funke (1980).

3. PIV method, which was employed to find the reflection coefficient of co-existing wave by measuring the velocity at the set point and compares it with the velocity of incident wave at the same point. The characteristics of incident wave must be known in advance. The method is summarized as follows.

4.11.3 PIV method

Let us assume that a wave is travelling in a flume in longitudinal direction and reflecting from some arbitrary structure or beach. The standing wave can be considered as the superposition of two progressive waves of the same amplitude and period, but travelling at the same speed in opposite direction so that the net travel is zero leaving only the vertical oscillation. The co-existing wave can be considered as a partially standing wave and consists of a superposition of incident wave (progressive wave) and reflected wave (non-progressive wave) as shown in Figure 4.11. The progressive wave travels along the x axis at a given velocity (v_i) and wave height hi which are known in advance. The co-existing wave travels along the x axis at a given velocity (v_{co}) and wave height hco, which are measured. On the other hand, assume the reflected wave travels in opposite directions with the incident wave at unknown velocity (v_r) and wave height h_r. The characteristics of reflected wave can be calculated by a given date both incident and co-existing waves. The co-existing wave is considered as a standing wave when the reflection coefficient is 100 %, and is considered as a linear wave when the reflection coefficient is 0 %.

The crest of a wave that associated to the maximum horizontal velocity of an incident wave according to the linear wave theory is taken as a comparison point. The horizontal velocity of a standing wave at this location is denoted by us and is equal zero. The horizontal velocity of the incident wave is maximum and denoted by ui-max. As well as, the horizontal velocity of the reflected wave is maximum and denoted by u_{r_max}. The net travel will be in the direction of the incident wave.

The horizontal velocity of the co-existing wave at this point is uco-max (the maximum relative horizontal velocity) and decomposes into $u_{i\text{-}max}$ and $u_{r\text{-}max}$. Then

$$u_{r-\max} = u_{i-\max} - u_{co-\max} \tag{4-1}$$

Where u is a function of h (wave height) and $u_{co\text{-}\max}$ is measured and $u_{i\text{-}max}$ is known in advance, then the reflection coefficient can be calculated as follows.

$$CR = \frac{u_{r-\max}}{u_{i-\max}} = \frac{h_r}{h_i} \tag{4-2}$$

Notes: the small relative horizontal velocity for the field before a breakwater means the higher reflection and vice versa (i.e. the horizontal velocity of standing wave at the crest u_s = 0.00 means the reflection coefficient = 100 %). The reflection coefficient can be calculated by the comparison of the horizontal velocity of the crest or the trough (taking into account the direction of movement).

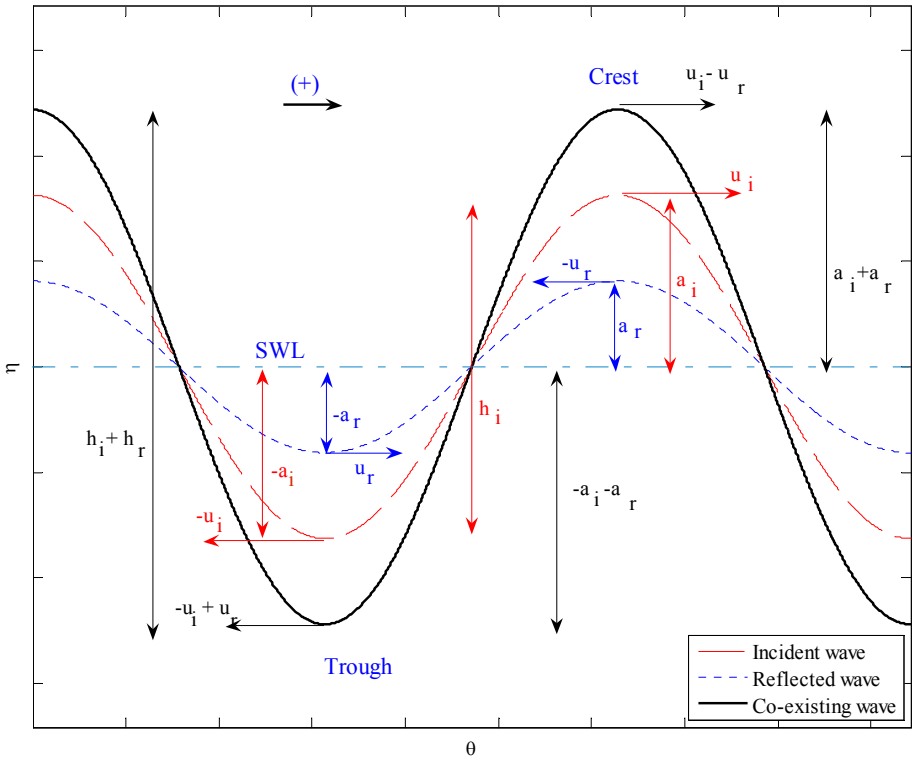

Figure 4.11: Analysis of co-existing, incident and reflected wave.

4.11.4 Measurement method of co-existing velocity

This method is adopted to find out the orbit velocity at a certain point such as the crest of the wave. The crest of a wave is detected by observation at one position, which must be located inside the FOV of the high speed camera. In this study, the measuring area is fixed and the measurements are performed at 12.2 m from the wave maker. The model is situated in a distance of one wave length behind of FOV to make the comparison point (the crest of wave) within the FOV of the high speed camera. It is noted that, the crest of waves occurs at 0.5 *L*, *L* , 1.5 *L* ,….n *L* from the model. The camera records at least a complete cycle of the wave. At the comparison point, the particle velocities were recorded. The recorded velocities were decomposed into the horizontal and the vertical components u and v in x and z direction respectively by applying MatPIV. This velocity is supposed as relative velocity, which consists of the superposition of the incident and reflected wave.

Figure 4.12 shows the velocities of co-existing waves along the x direction in front of the barriers. The characteristics of the wave and the field of this Figure are the same characteristics of the wave and the field which mentioned earlier in table 4.4. The measuring areas are located at approximate one wave length before the model. The x coordinate of the wave crest can be marked from the Figure. It is clear that, the horizontal particle velocity is minor at the crest of wave but not reaches zero, this means the wave is partially a standing wave.

Figure 4.13 shows the maximum horizontal water particle velocities for co-existing waves along the x direction. The maximum of the horizontal velocity corresponding to the coordinate of the crest wave can be determined through the fitting curve. It is noticed that, the maximum horizontal velocity at the crest of wave is associated with a trough point between two consecutive peaks points.

4.11.5 Measurement method of transmission coefficient

In the same way the transmission coefficient can be determined by measuring the maximum horizontal velocity of the transmitted wave u_t and comparing it with u_i, which is known in advance, then

$$CT = \frac{u_{t-\max}}{u_{i-\max}} = \frac{h_t}{h_i} \tag{4-3}$$

4.11.6 Measurement of transmitted wave velocity

The velocity of a transmitted wave can be measured by a simple method like the way which is used to measure the velocities of incident waves because the transmitted waves are considered as propagating waves. In this study the measuring area is fixed and the measurements are performed at 12.2 m from the wave maker. The model is situated in a distance of one wave length in front of FOV. The velocity was calculated and decomposed into the horizontal and the vertical water particle velocities (u and v) in the x and z direction by MatPIV.

Figure 4.14 shows the velocity magnitude of the transmitted waves in the field which include the crest of the wave. The Figure 4.14 (a to f) is plotted for the same characteristics of waves and field as mentioned earlier in table 4.4. It is clear that, the characteristics of a transmitted wave are similar to the characteristics of an incident wave (linear wave) but the velocity magnitude of the transmitted waves is less than the velocity magnitude of the incident waves as a result of reflection and dissipation of a large part from the waves.

Figure 4.15 shows the maximum of the horizontal particle velocities for transmitted waves along x direction. The Figure 4.15 (a to f) is plotted for the same characteristics of the wave and the field which mentioned earlier in Figure 4.14. By the same way of analysis, the velocity of the transmitted wave can be determined at the crest of the wave (phase = π /2). The maximum of the horizontal velocity

corresponding to the coordinate of the crest wave can be determined by the fitting curve. Note that the trend of *u* curve is similar to the trend of the wave profile, which shows the compatibility between the measured particle velocity via PIV and the calculated velocity by linear airy wave theory.

4.11.7 Horizontal velocity distribution

It is noted that the maximum horizontal particle velocity should be located near the water surface far away from the bottom of the flume to avoid the effect of the bottom. Therefore, the high horizontal velocities, which were recorded near the bottom, must be neglected.

Figures 4.16 and 4.17 illustrate the horizontal velocity distribution at the crest of an incident, co-existing and transmitted wave for both high frequency F = 2 Hz (short wave and lower frequency F = 0.75 Hz (high intermediate waves) respectively. Generally, the amplitude of horizontal velocity decreases with depth. Note that for intermediate waves, the orbits diminish in amplitude with depth and also become flatter but the orbit vanishes after 0.5 d for short waves in both incident and transmitted waves. The orbits of incident and transmitted waves agree with the linear airy theory but the co-existing wave are different somewhat. It is noted that, the maximum horizontal velocity from these Figures is closed with that detected from Figures 4.7, 4.13 and 4.15, which is used to calculate the reflection and transmission coefficients. Therefore, the hydrodynamic performance of this structure can be investigated through the horizontal velocity distribution of the incident and transmitted wave where the velocity is a measure of wave energy.

4.11.8 Reflection and transmission coefficients

The reflection and transmission coefficients can be calculated in terms of velocities, which were measured previously. The results are tabled in tables 4.7 and 4.8. The reflection and transmission coefficients can be calculated directly but the energy

dissipation coefficient can be calculated from the measured transmission and reflection coefficients according to the Equation 3-23 in the previous section 3.2.4..

Table 4.7: Calculation of the reflection coefficient.

Frequency F (Hz)	Water depth d (m)	Wave height h_i (m)	Maximum $u_{i\text{-}max}$ (m/sec)	Maximum u_{ex_max} (m/sec)	CR
2.00	0.3	0.01	0.0610	0.0035	0.94
1.75	0.3	0.01	0.0564	0.0018	0.96
1.50	0.3	0.02	0.0973	0.0084	0.91
1.25	0.3	0.02	0.0826	0.0110	0.87
1.00	0.3	0.03	0.1075	0.0320	0.70
0.75	0.3	0.04	0.1288	0.0540	0.58

Table 4.8: Calculation of the transmission coefficient.

Frequency F (Hz)	Water depth d (m)	Wave height h_i (m)	Maximum $u_{i\text{-}max}$ (m/sec)	Maximum u_{t_max} (m/sec)	CT
2.00	0.3	0.01	0.0610	0.002	0.03
1.75	0.3	0.01	0.0564	0.003	0.05
1.50	0.3	0.02	0.0973	0.012	0.12
1.25	0.3	0.02	0.0826	0.022	0.27
1.00	0.3	0.03	0.1075	0.043	0.40
0.75	0.3	0.04	0.1288	0.062	0.48

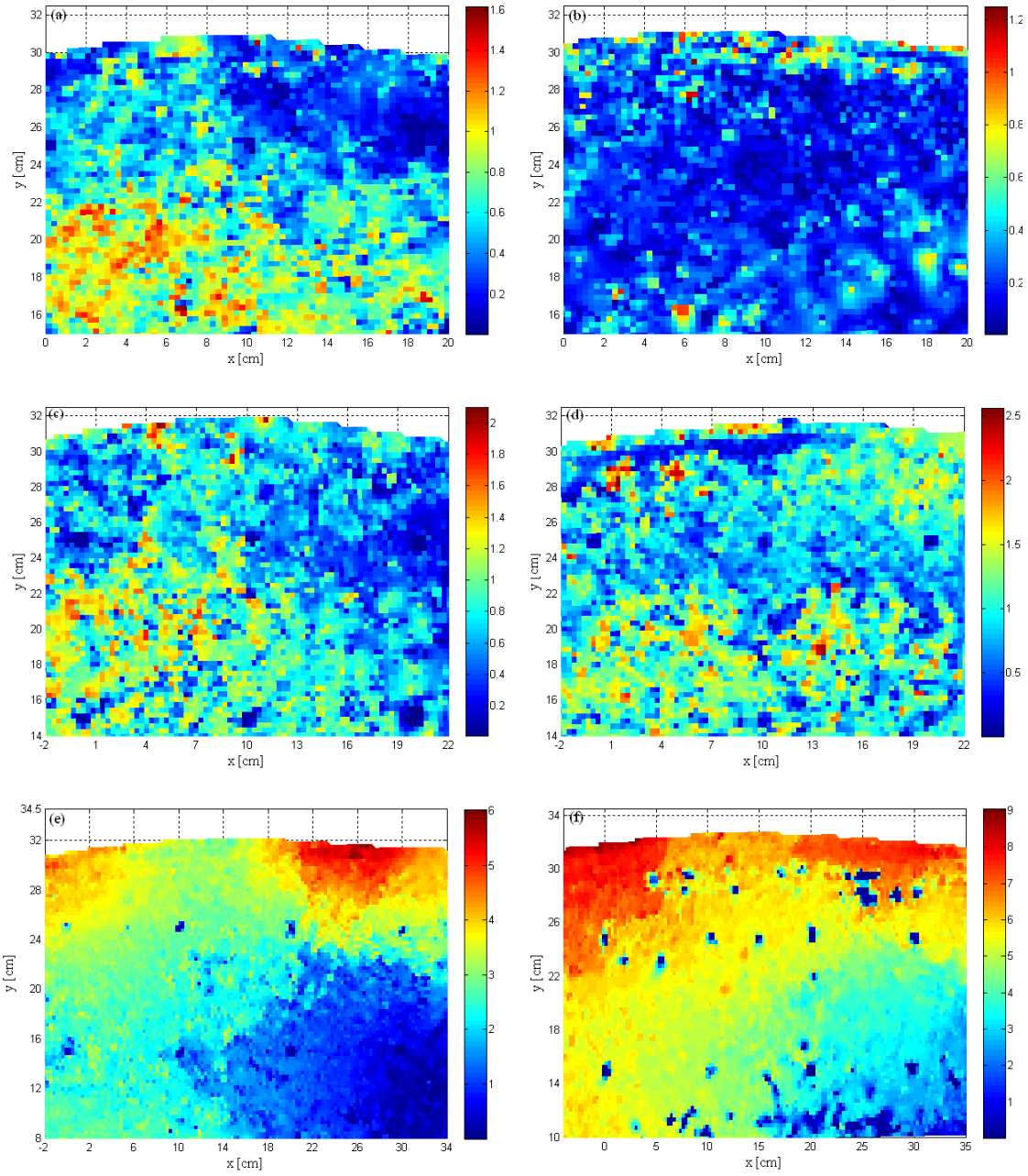

Figure 4.12: Velocity magnitude (cm/sec) of co-existing waves when the wave crest is within the VOF.

a) for F = 2.00 Hz and h_i = 1 cm,

b) for F = 1.75 Hz and h_i = 1 cm,

c) for F = 1.50 Hz and h_i = 2 cm,

d) for F = 1.25 Hz and h_i = 2 cm,

e) for F = 1.00 Hz and h_i = 3 cm, and

f) for F = 0.75 Hz and h_i = 4 cm.

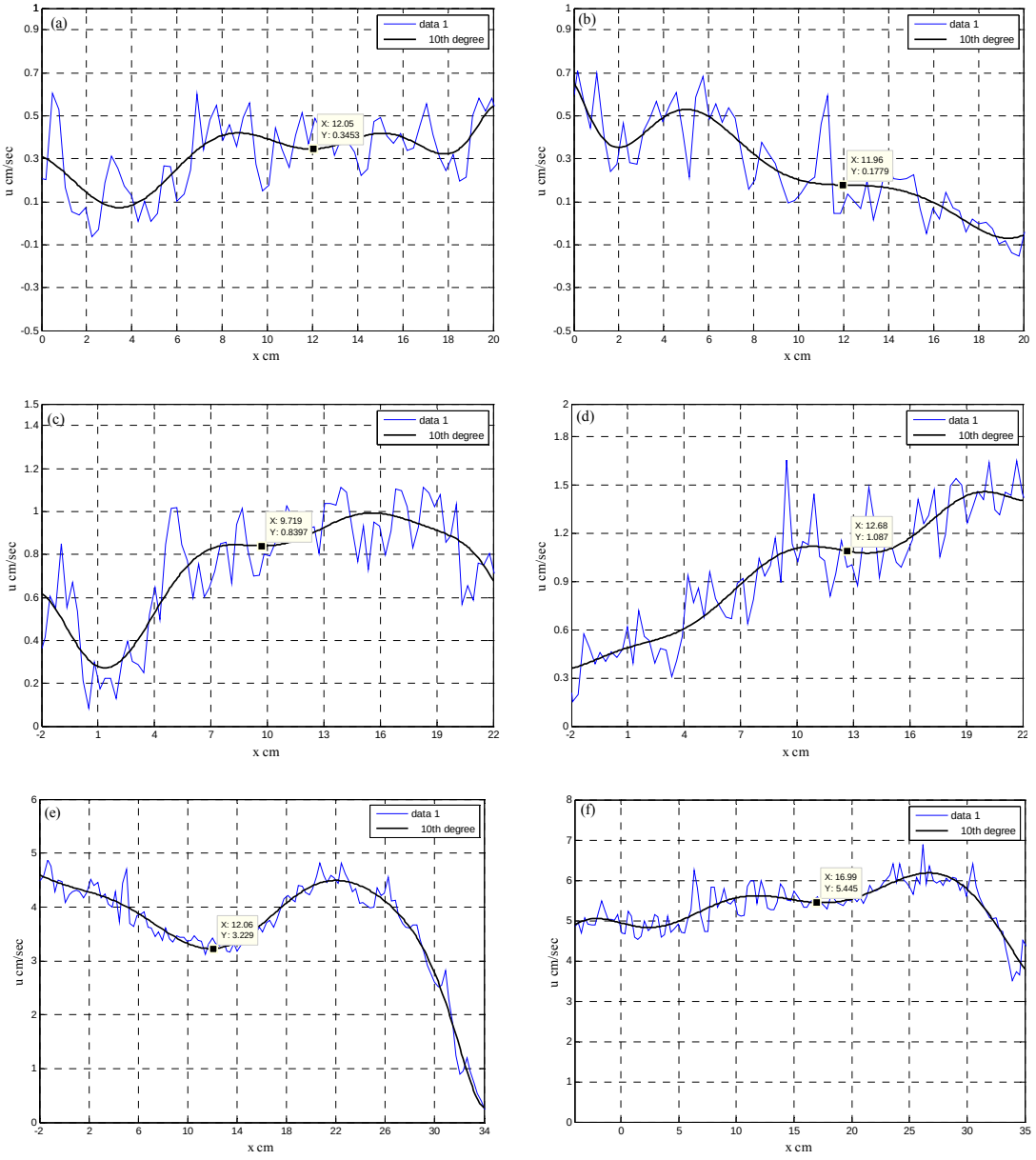

Figure 4.13: Maximum horizontal velocity of co-existing waves along x direction when the wave crest is within the VOF.

a) F = 2.00 Hz and h_i = 1 cm,

b) F = 1.75 Hz and h_i = 1 cm,

c) F = 1.50 Hz and h_i = 2 cm,

d) F = 1.25 Hz and h_i = 2 cm,

e) F = 1.00 Hz and h_i = 3 cm, and

f) F = 0.75 Hz and h_i = 4 cm.

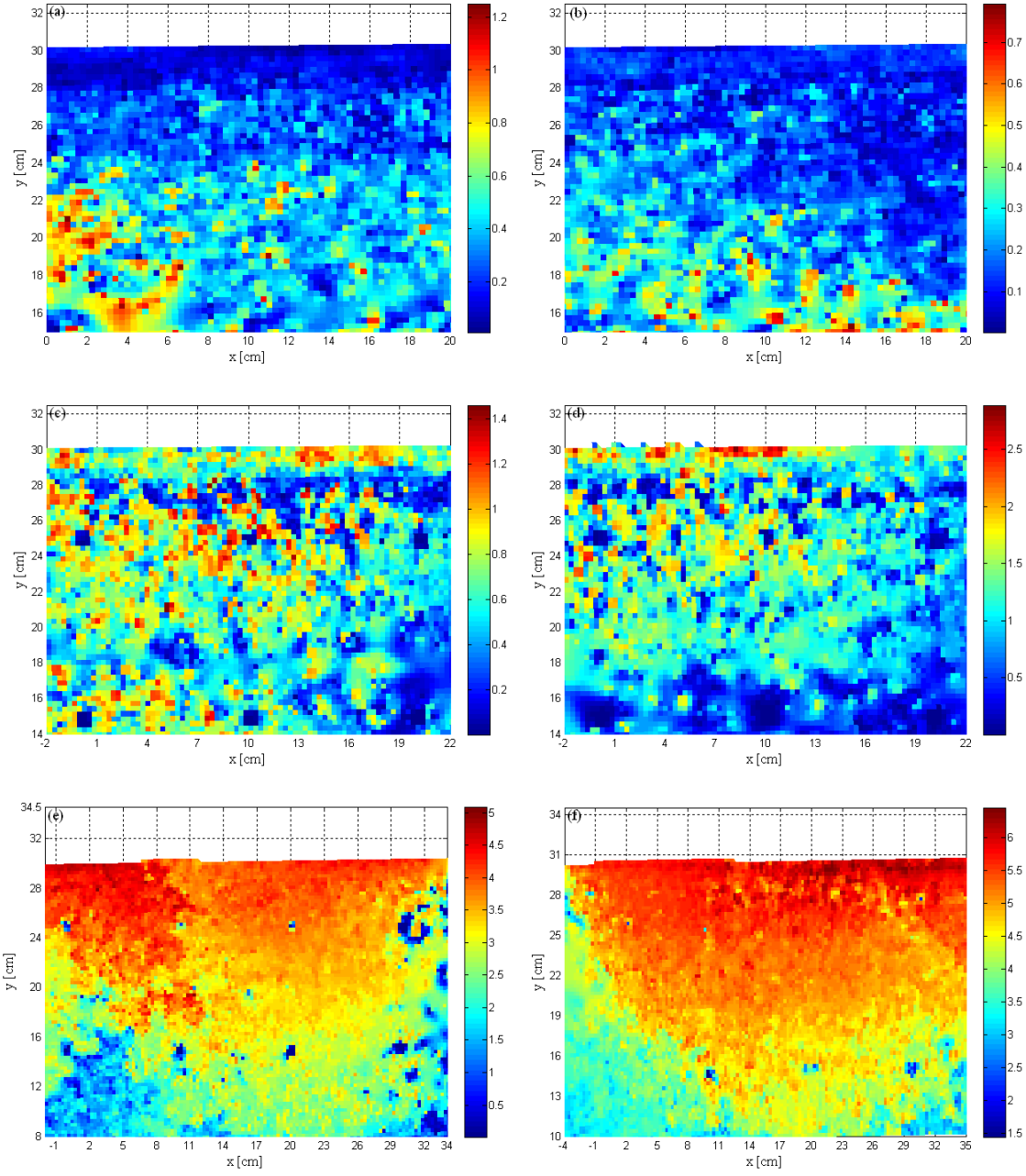

Figure 4.14: Velocity magnitude (cm/sec) of transmitted waves when the wave crest is within the VOF.

a) for $F = 2.00$ Hz and $h_i = 1$ cm,

b) for $F = 1.75$ Hz and $h_i = 1$ cm,

c) for $F = 1.50$ Hz and $h_i = 2$ cm,

d) for $F = 1.25$ Hz and $h_i = 2$ cm,

e) for $F = 1.00$ Hz and $h_i = 3$ cm, and

f) for $F = 0.75$ Hz and $h_i = 4$ cm.

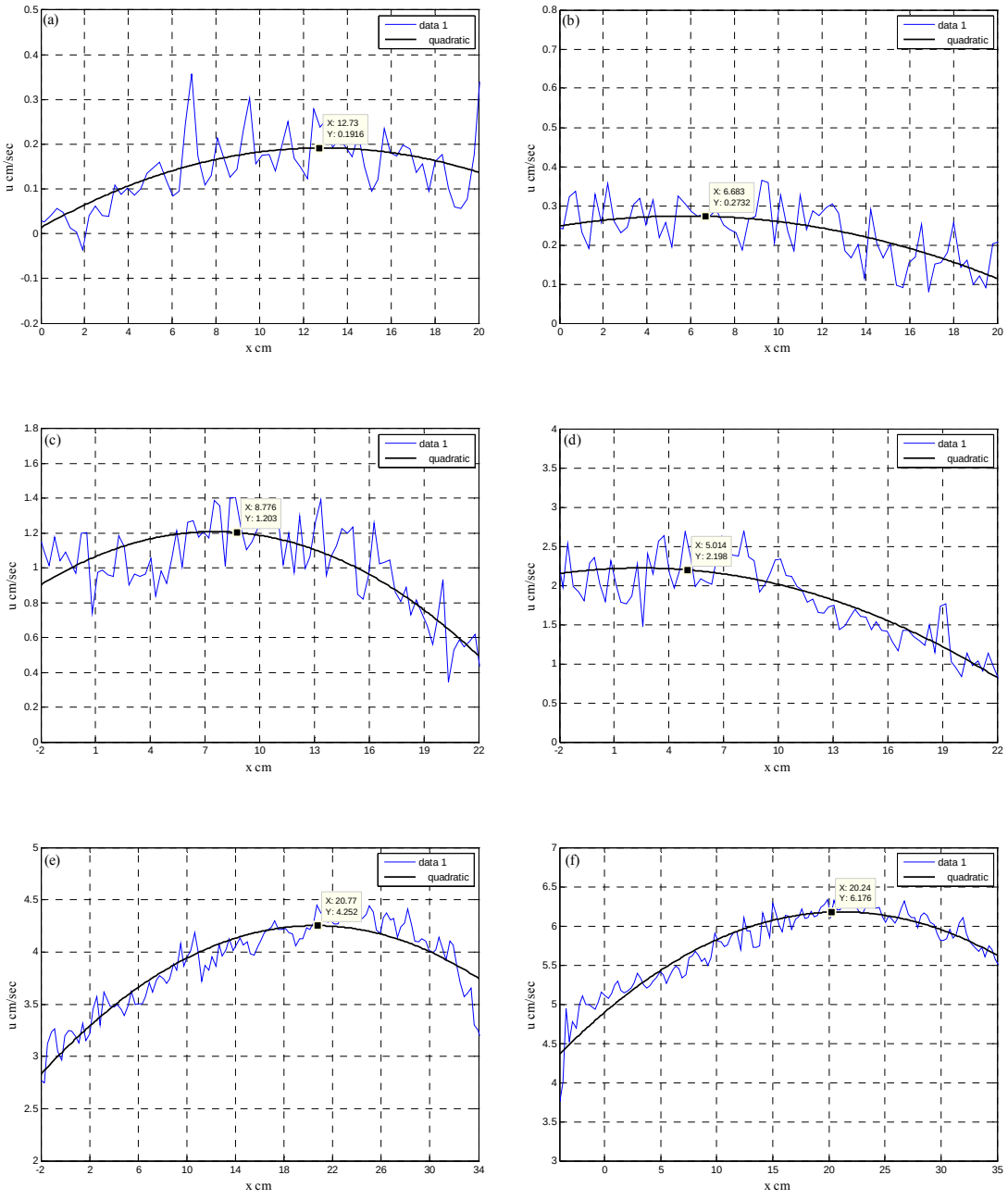

Figure 4.15: Maximum horizontal velocity of transmitted waves along x direction when the wave crest is within the VOF.

a) F = 2.00 Hz and h_i = 1 cm,

b) F = 1.75 Hz and h_i = 1 cm,

c) F = 1.50 Hz and h_i = 2 cm,

d) F = 1.25 Hz and h_i = 2 cm,

e) F = 1.00 Hz and h_i =3 cm, and

f) F = 0.75 Hz and h_i =4 cm.

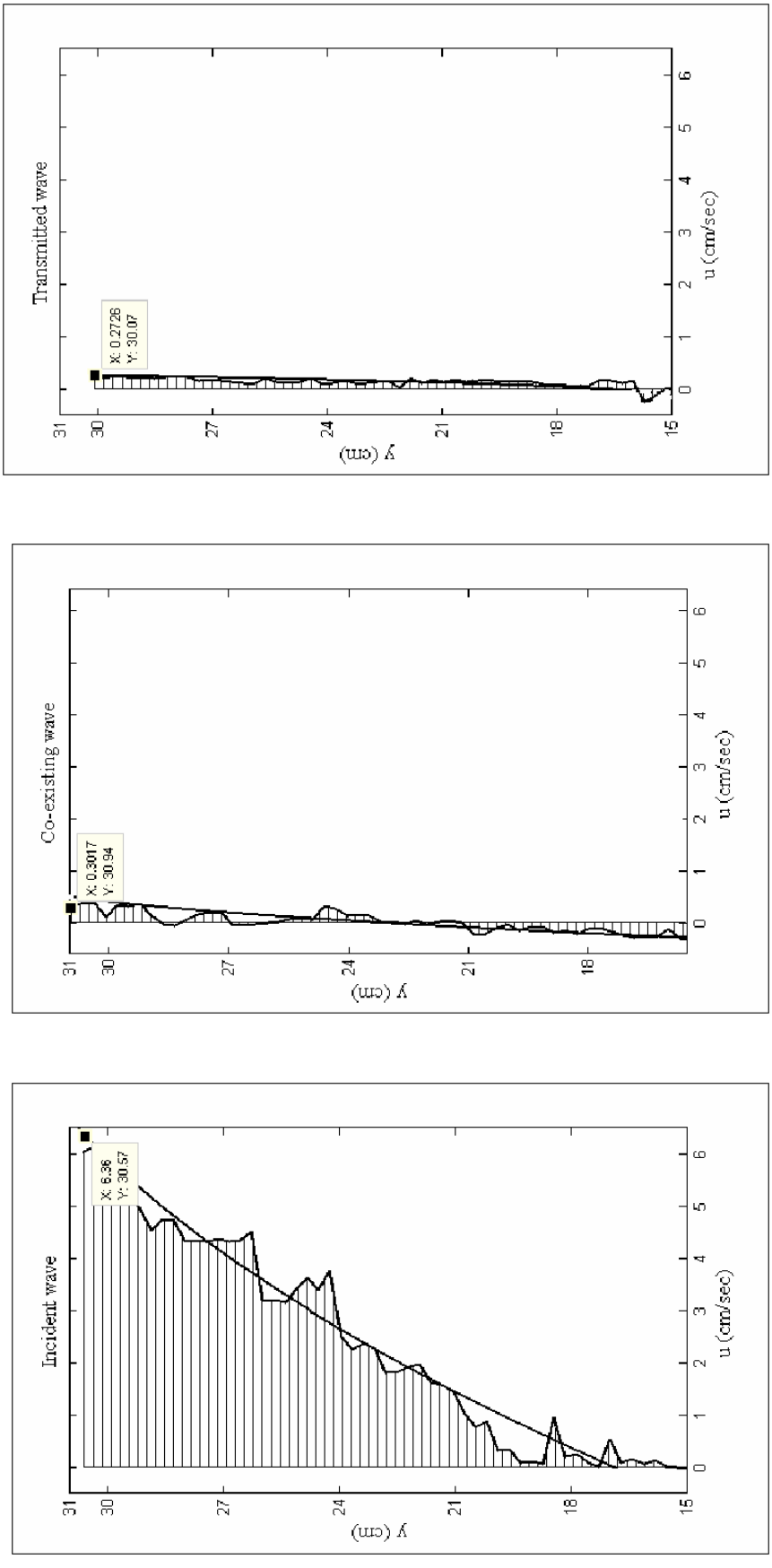

Figure 4.16: Distribution of the horizontal velocity of incident, co-existing and transmitted waves at the wave crest for the frequency of wave F= 2 Hz.

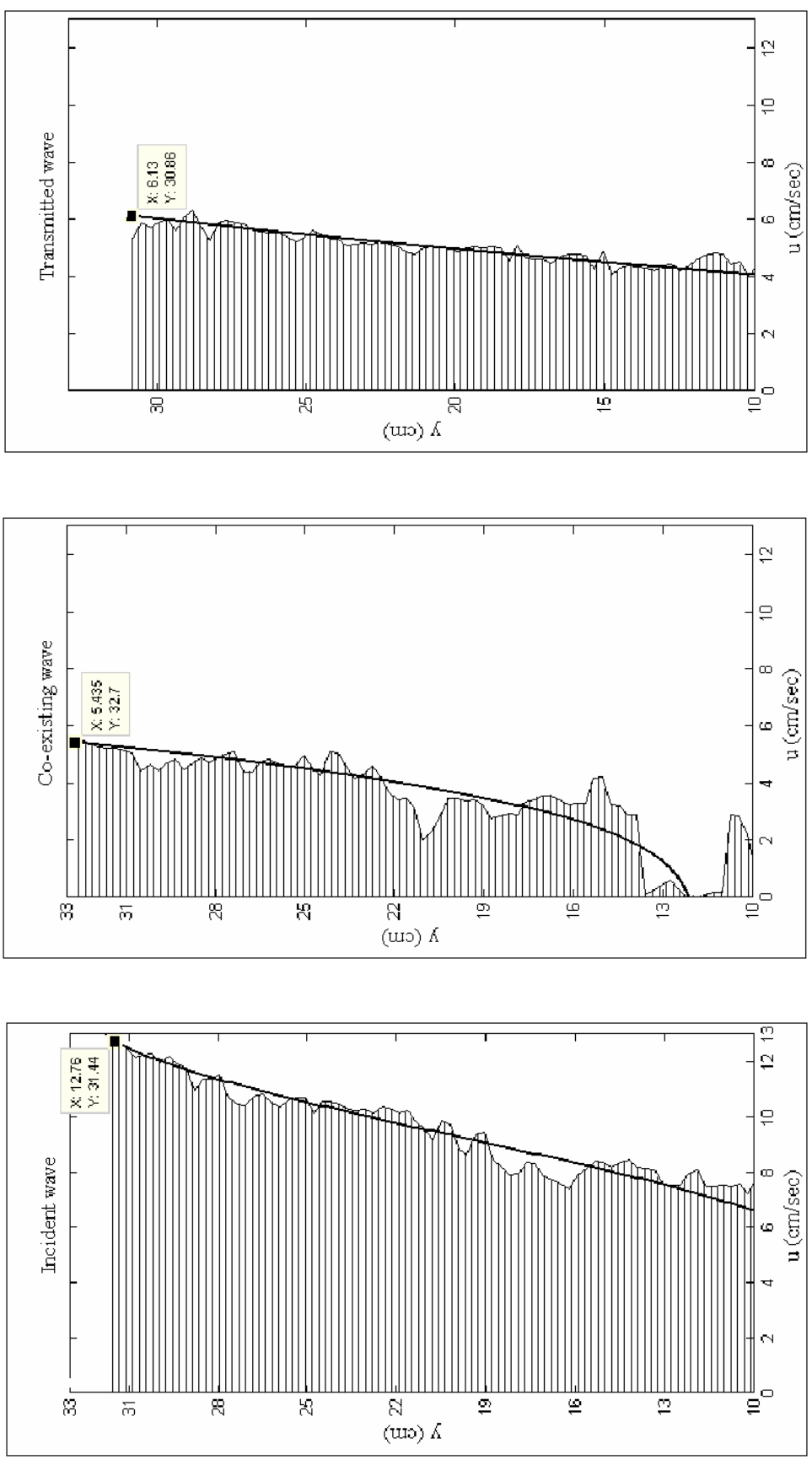

Figure 4.17: Distribution of the horizontal velocity of incident, co-existing and transmitted waves at the wave crest for the frequency of wave $F = 0.75$ Hz.

CHAPTER 5
RESULTS AND DISCUSSIONS

5.1 INTRODUCTION

In this section, the experimental and the numerical investigations are presented and discussed for the single and double vertical slotted walls with impermeable upper and lower parts, which have different draft as a proportion of the water depth. The performances of the vertical slotted wall with respect to reflection, transmission and dissipated energy are studied experimentally and theoretically. The numerical models depend on an Eigen function expansion method for regular waves including both linear and nonlinear wave theory. The experimental works were carried out by regular waves and include those for both single slotted vertical wall and double identical parallel walls with different chamber width. The porosity of the walls was constant and equal to 50 % for the permeable part. A comparison between the numerical results and the experimental results are also presented. The values of friction parameter in the numerical model are varied to find a match with the experimental results. The results of a parametric study of various parameters governing the present wave structure interaction problem are also presented. This section is divided into three main parts:

- Wave interaction with a single row of a vertical slotted wall breakwater under linear waves.
- Wave interaction with a single row of a vertical slotted wall breakwater under nonlinear waves (Stokes second-order wave theory).
- Wave interaction with double rows of identical vertical slotted wall breakwater under linear waves.

5.2 DATA ANALYSIS

The wave interaction with a vertical slotted single or double wall breakwaters are determined by its reflection, transmission and dissipation characteristics. The energy of the reflected waves from the permeable barrier is quantified in terms of reflection coefficient. The reflection coefficient (*CR*) is defined as the ratio of the reflected wave height to the incident wave height. A *CR* value of 1 corresponds to complete reflection and 0 corresponds to either complete wave transmission or complete wave absorption. The energy of the transmitted waves through the breakwater is quantified in terms of the transmission coefficient (*CT*). A *CT* value of 1 corresponds to transmission of entire energy past the permeable barrier and 0 corresponds to complete wave reflection with zero energy past the barrier which seldom is possible. The energy dissipation through the permeable part corresponds to the difference in energy between incident wave and the sum of the energy of reflected and transmitted waves. The energy dissipation coefficient (*CE*) is expressed as:

$$CE = 1 - \left(CR^{2} + CT^{2}\right) \tag{5-1}$$

The time histories of the composite wave elevations were measured by the three wave probes (WP1, WP2 and WP3) positioned in-front of the model were decomposed into incident (h_i) and reflected (h_r) wave components as per the procedure suggested by Mansard and Funke (1980). The transmitted wave height, h_t was obtained from the measured time history of the wave height from the wave probe (WP4) positioned on the lee side of the model. From the time histories of measured regular wave heights, the reflection coefficient $CR = h_r / h_i$ and the transmission coefficient, $CT = h_t / h_i$, were obtained for all the wave characteristics adopted for the study.

5.3 WAVE INTERACTION WITH A SINGLE VERTICAL SLOTTED WALL

5.3.1 General

In this section, the numerical results for a vertical slotted wall with impermeable upper and lower parts, the draft of them, which are a proportion of the water depth, are validated by comparison with previous studies. Some of them are theoretical and experimental and others are theoretical and also are validated by comparison with the experimental results of the single vertical slotted wall. The numerical model depends on Eigen function expansion method for regular waves (linear wave theory) and utilizes a boundary condition at the barrier, which accounts for energy dissipation within the barrier. The number of terms used in the Eigen function expansion is taken as $N = 50$. This is found to give accurate results over the range of values presented here. The experimental work were carried out with regular waves for various wave periods (T = 0.75 to 2 sec), wave heights (1, 2, 3, 4 cm), a fixed water depth of $d = 30$ cm and constant porosity of ε = 50 % for the permeable part. The model consists of impermeable upper and lower parts and a permeable part in the middle. The influence of both impermeable lower and upper parts and the influence of location of permeable part on the hydrodynamic characteristics of single vertical slotted wall are reported.

In addition to that, some important relations related to the friction factor, porosity and added mass coefficients are investigated. All results are presented and discussed as follows.

5.3.2 Influence of the porosity (ε), friction (f) and added mass (cm) factors on the permeability parameter (G)

The hydrodynamic coefficients of permeable barriers are affected by the permeability parameter G, which depend on the porosity ε, the friction factor f and the added mass factors cm as mentioned previously in equations (3.7, 3.8).

Figure 5.1 shows the influence of porosity, friction and added mass coefficients on permeability parameter *G*. Figure 5.1a shows the effect of the porosity ε on *G* at fixed added mass coefficient (*cm* = 0.00) and fixed friction coefficient (*F* = 2). Figure 5.1b shows the effect of the friction factor *f* on G at fixed added mass coefficient *cm* = 0.00 and various porosity ε. Figure 5.1c shows the effect of the added mass coefficient *cm* on G at fixed friction coefficient *F* = 2 and various porosity ε. It is clear that the relationship between *G* and ε is a direct proportion while the relationship between *G* and *f*, *G* and *cm* is an inverse proportion. The permeability parameter *G* increases continuously with increasing porosity ε at fixed *f* and *cm*, while *f* and *cm* are on the contrary with ε , where the permeability parameter *G* decreases with increasing the friction coefficient at fixed ε and *cm* and decreases with increasing the added mass coefficient at fixed ε and *f*. The friction coefficient has a clear influence on *G*. The rate of the decreasing is sharp and rapid for small values of *f* and high values of ε, while the rate is slow for high values of *f* and for small values of porosity at fixed *cm.* The influence of *cm* at fixed *f* is minor on *G*, so it can be neglected within this investigation.

5.3.3 Influence of the porosity (ε), friction (f) and added mass (cm) factors on CR, CT, and CE

The hydrodynamic characteristics of permeable barriers are affected by the porosity ε, the friction factor *f* and the added mass factor *cm*.

Figure 5.2 shows the influence of porosity ε at fixed *F* = 2 and *cm* = *0.00*, Figure 5.3 shows the influence of friction factor *f* at fixed ε = 0.5 and *cm* = 0.00 and Figure 5.4 shows the influence of the added mass coefficients *cm* at fixed ε = 0.5 and *F* = 2 on the hydrodynamic coefficients CR, *CT* and *CE* as a function of *kd* for h_i = 0.025 *L* and *dm* = 0.6 *d*. The Figures follow the expected trend, and correspond to the various limits indicated earlier: Thus, the reflection coefficient *CR* increases with increasing *kd, f* and *cm* and decreases with increasing porosity ε, while the transmission coefficient *CT* follows the opposite trend, and the energy dissipation coefficient *CE*

is nonzero, accounting for the energy loss across the barrier. Increasing the porosity is seen quite clearly (Figure 5.2) to reduce the reflection coefficient and increase transmission coefficient, as expected. At lower values of *kd*, an increasing of porosity is seen to reduce the energy dissipation coefficient, but for high values of *kd* an increasing porosity actually causes an increase in the energy dissipation coefficient. An increasing friction coefficient is seen quite clearly (Figure 5.3) to increase the reflection coefficient and reduce the transmission coefficient, as expected. At lower values of *kd*, an increasing friction coefficient is seen to increase the energy dissipation coefficient, but for high values of *kd* an increasing friction coefficient actually causes a decrease in the energy dissipation coefficient. These somewhat surprising results are also observed in the exact solution of Isaacson et al. (1998) for a partially submerged barrier. Increasing the added mass coefficient is seen (Figure 5.4) to cause similar trends of friction coefficient but the influence of added mass coefficient is weak and can be neglected.

From the foregoing, it is clear that both the friction coefficient f and the porosity ε have a significant influence on *G*, *CR*, *CT* and *CE* of the vertical slotted walls, while the influence of the added mass coefficient is powerless and can be neglected.

5.3.4 Comparison of the present numerical model with vertical slotted barrier

The validation of the numerical model can be done by comparing with theoretical results of Isaacson et al. (1998) for the hydrodynamic characteristics of vertical slotted barriers. The numerical model as proposed by Isaacson et al. (1998) was initially developed for studying the wave transmission through a single thin vertical slotted barrier extending from the water surface to some distance above the seabed. The comparison is carried out to investigate the hydrodynamic characteristics of a single barrier through *CR, CT* and *CE* coefficients as a function of *k*du* for various porosities ε = 5 % and 20 % , h_i/L = 0.07, f = 2 and *cm* = 0.00 as shown in Figure 5.5. It is clear from the Figure that *CR* increases, whereas *CT* decreases with an increase in *k*du*. This is due to the reason that long waves will propagate past the

barrier without being attenuated. Further, an increase in the porosity leads to an increase in the flow through the barrier leading to a decrease in *CR* and an increase in *CT*. The comparison is found to be sound thus validating the present numerical model.

5.3.5 Comparison of the present numerical model with vertical submerged and semi-submerged barriers

The validation of the numerical model can be also done by comparing with theoretical result of Abu-Azm (1993) for both hydrodynamic characteristics of a rigid thin breakwater that extend from above the water surface to some distance below and a rigid thin submerged breakwaters that extends from the seabed until below the waterline. The numerical model as proposed by Abu-Azm (1993) was initially developed for studying the wave transmission beneath or above single thin vertical barrier. The comparison is carried out to investigate the hydrodynamic characteristics of a single barrier through *CR, CT* and *CE* coefficients as a function of *kd* for a porosity $\varepsilon = 1$ for the present study, $h_i/L = 0.025$, friction f and the thickness of the wall is 0.01 d. The added mass coefficient *cm* is not taken into account.

It is clear from the Figure 5.6a that the *CR* increases, whereas *CT* decreases with an increase of *kd*. This is due to the reason that long waves propagate beneath the barrier without being attenuated. While, the transmitted wave above the barrier is very high along *kd* and the reflection coefficient is significant for lesser *kd* but insignificant for higher *kd*. Short waves are transmitted completely as shown in Figure 5.6b. In both cases the comparison is found to be excellent thus validating the present numerical model.

From the foregoing, it is clear that the numerical of the present study is validated by several of the previous studies and it helps in deducing the most important hydrodynamic characteristics of a vertical slotted single wall for various parameters and condition. It has proved its efficiency in deducing the most important hydrodynamic characteristics for several types of permeable breakwaters like a row

of single piles, pile-supported vertical walls, single slotted barriers extending from above the water surface to some distance above the seabed, and submerged rigid thin barriers extending from the seabed until below the waterline, semi-submerge rigid thin barrier extending from above the water surface to some distance below with taking into account limits of the study in each case.

5.3.6 Comparison of the present numerical model with pile-supported vertical wall

The numerical results for a single vertical slotted wall breakwater with impermeable upper and lower parts with different drafts as a proportion of the water depth are validated by comparison with theoretical and experimental results of Suh et al. (2006).

Figure 5.7 shows a comparison of the predicted results for a vertical slotted wall with the predicted and measured results for a pile-supported vertical wall. The comparison is conducted for transmission and reflection coefficients as a function of *kd* where, the lower impermeable part *dw* = 0, the permeable part has a porosity of ε = 50 % and various draft of the upper part *du = 0 d , 0.4 d* and *0.6 d*. In this study, the permeability parameter G is expressed in terms of porosity ε, friction parameter f and the added mass coefficient *cm* as suggested by Sollitt and Cross (1972) and adopted by Isaacson et al. (1998, 1999). The friction coefficient f which realizes the best fitting *is* 0.5 and added mass coefficient *cm = 0,* since the porous medium is a fixed structure here, while Suh et al. (2006) adopted the method of Mei et al. (1974). In the study of Suh et al. (2006) G was expressed by.

$$G = \frac{1}{\frac{\beta}{\omega} - il} \tag{5-2}$$

where β = energy dissipation coefficient which were given by Kim (Suh et al., 2006).

$$\beta = \frac{8\alpha}{9\pi} H\omega \frac{1}{\sqrt{(R+2)^2 + P^2}} \frac{5 + \cosh(2kd)}{2kd + \sinh(2kd)} \tag{5-3}$$

where $P = lk$; $R = \beta k / \omega$, α = head loss coefficient and given by the plate orifice formula (Mei,1983)

$$\alpha = \left(\frac{1}{\varepsilon C_c} - 1 \right)^2 \tag{5-4}$$

where C_c = empirical contraction coefficient for which Mei et al. (1974) suggested to use the formula

$$C_c = 0.6 + 0.4\varepsilon^2 \tag{5-5}$$

and l = length of the jet flowing through the gap between piles and related to the blockage coefficient as

$$l = b\left(\frac{1}{\varepsilon} - 1\right) + \frac{4B}{\pi}\left[1 - \log(4\varepsilon) + \frac{1}{3}\varepsilon^2 + \frac{281}{180}\varepsilon^4\right] \tag{5-6}$$

In general, the results demonstrate a reasonable agreement for *kd* greater than 0.8 but for *kd* less than 0.8, the numerical model of Suh et al. (2006) is found to over predict the *CR* and under predict the *CT*. This trend in the variation of *CR* and *CT* with *kd*, could be due to inability of the numerical model of Suh et al. (2006) in properly representing the permeability parameter for lower values of *kd* as stated by these investigators in their findings.

5.3.7 Comparison results of the present numerical model with the experimental results

Figure 5.8 shows a simulation for the measured results of PIV with the measured results of Ultrasonic sensor. In addition to that, a comparison of a numerical model of wave interaction with a vertical slotted wall depending on an Eigen function expansion method with the pervious experimental results of PIV and Ultrasonic sensor is conducted. To achieve the fit between the experimental and the prediction results for reflection and transmission coefficients in the present study, the values of friction and added mass coefficient could be $f = 2$, and $cm = 0$ respectively.

In general, PIV is able to measure the velocity of co-existing and transmitted waves and able to find the wave interaction of the linear wave with permeable breakwaters. The numerical model is compatible with measurements of PIV and Ultrasonic wave gauges although with the presence of some scattering.

Finally, the results of PIV are perfectly acceptable and the application of PIV is encouraging. Almost total compatibility is found between the results of PIV and Ultrasonic sensor. Very close agreement is found between the results of the numerical model and experimental results of PIV and Ultrasonic sensor.

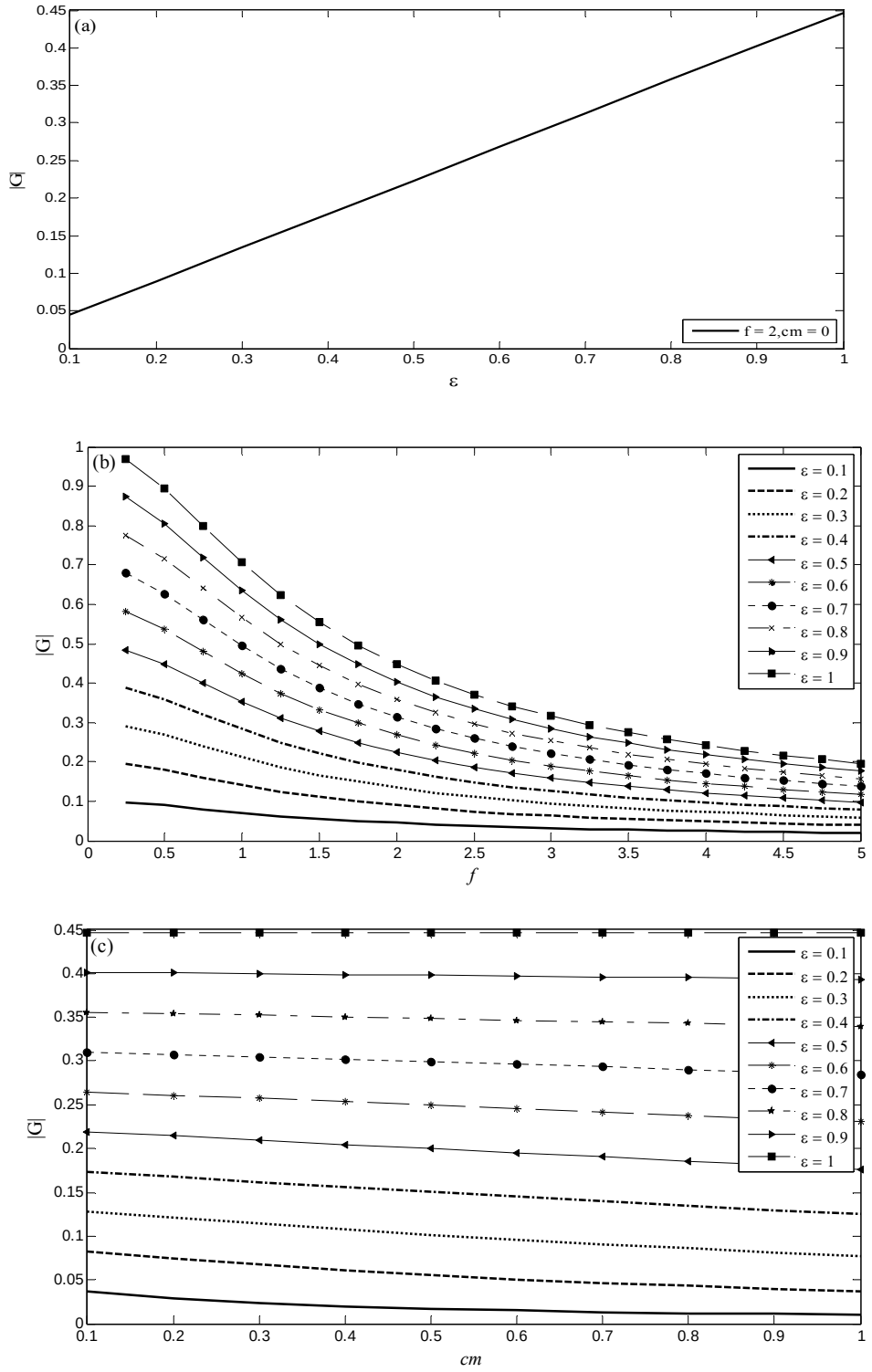

Figure 5.1: Influence of porosity ε , f and cm on the permeability parameter G.

(a) G as a function of the porosity ε for fixed f and cm,

(b) G as a function of f for various ε and fixed cm and

(c) G as a function of cm for various ε and fixed f .

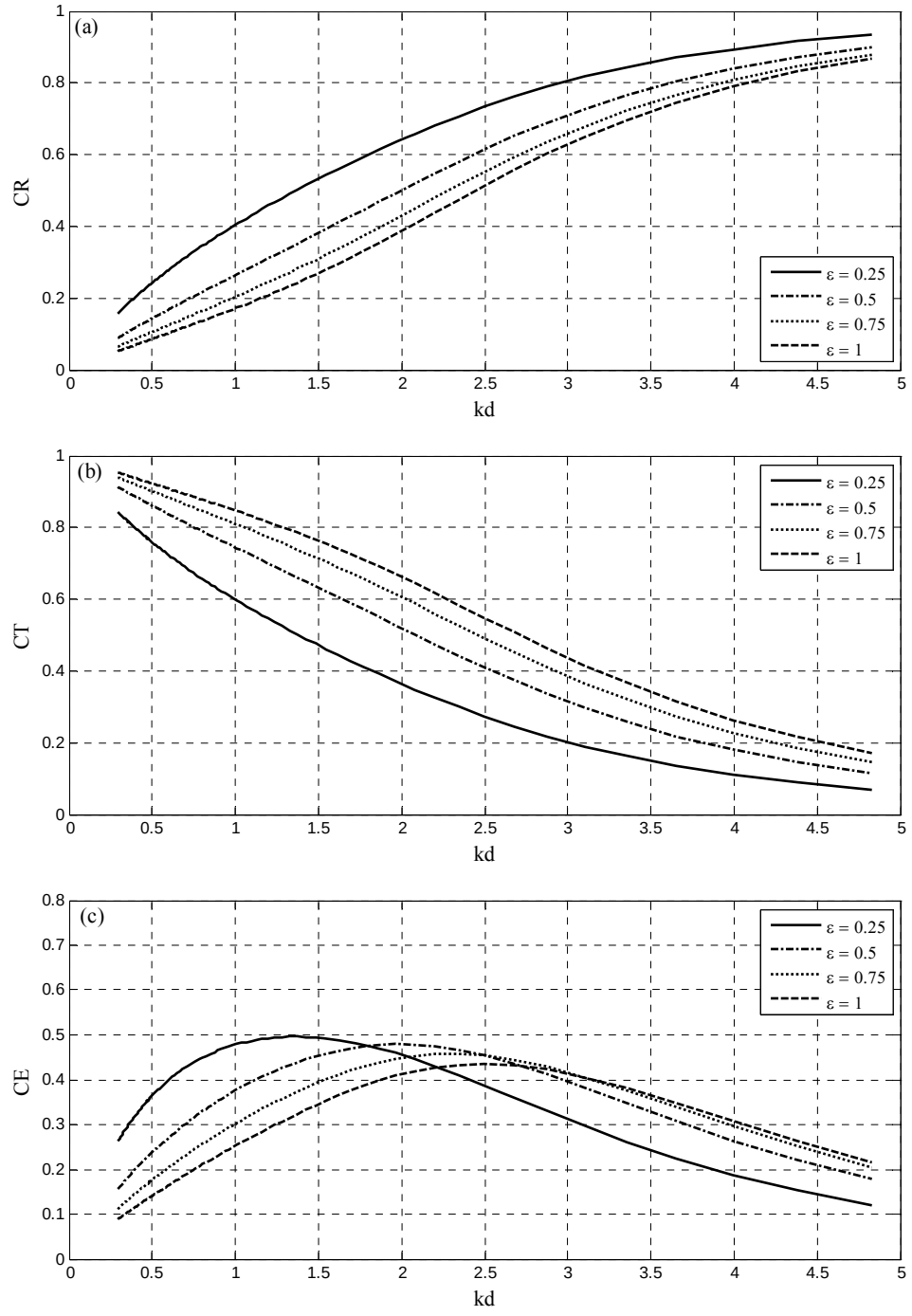

Figure 5.2: Influence of ε on hydrodynamic coefficients for a single vertical slotted wall breakwater as a function of *kd* and with $dm = 0.6\ d, f = 2$ and $cm = 0$.

(a) Reflection coefficient,

(b) Transmission coefficient and

(c) Energy dissipation coefficient, calculated values.

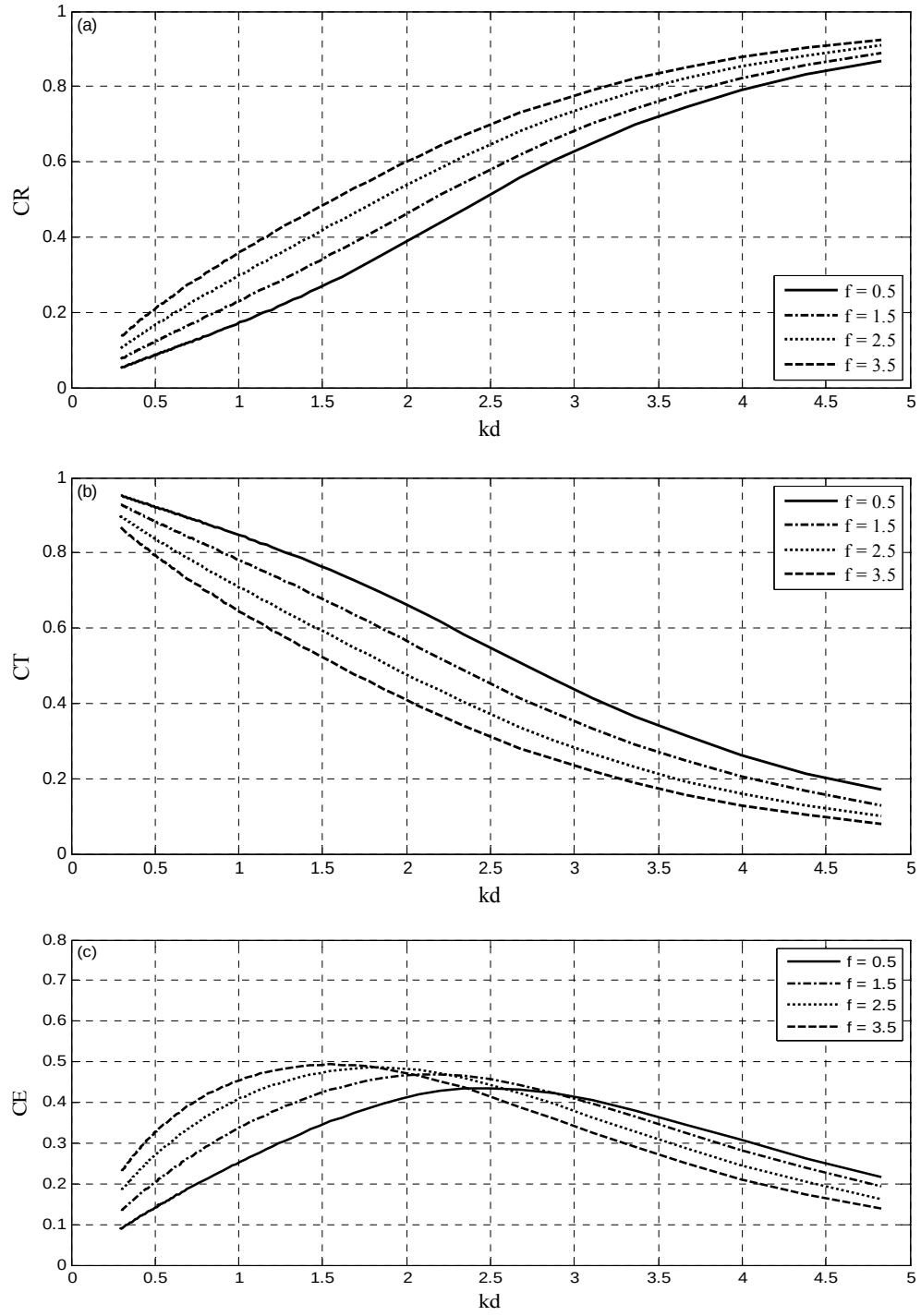

Figure 5.3: Influence of f on hydrodynamic coefficients for a single vertical slotted wall breakwater as a function of kd and with $dm = 0.6\ d$, $\varepsilon = 50\ \%$ and $cm = 0$.

(a) Reflection coefficient,

(b) Transmission coefficient and

(c) Energy dissipation coefficient, calculated values.

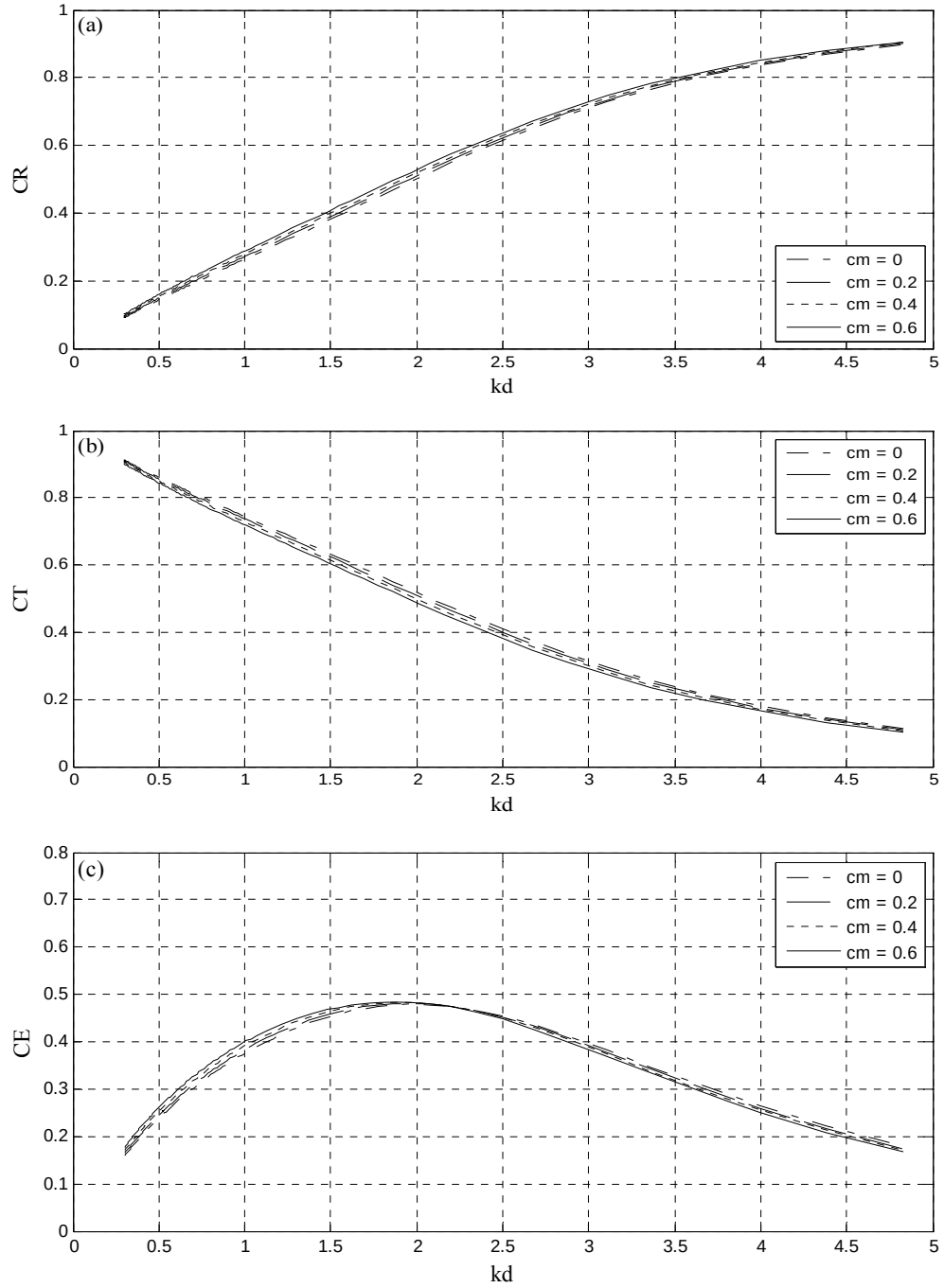

Figure 5.4: Influence of *cm* on hydrodynamic coefficient for a single vertical slotted wall breakwater as a function of *kd* and with *dm* = 0.6 *d*, ε = 50 %, and *f* = 2.

(a) Reflection coefficient,

(b) Transmission coefficient and

(c) Energy dissipation coefficient, calculated values.

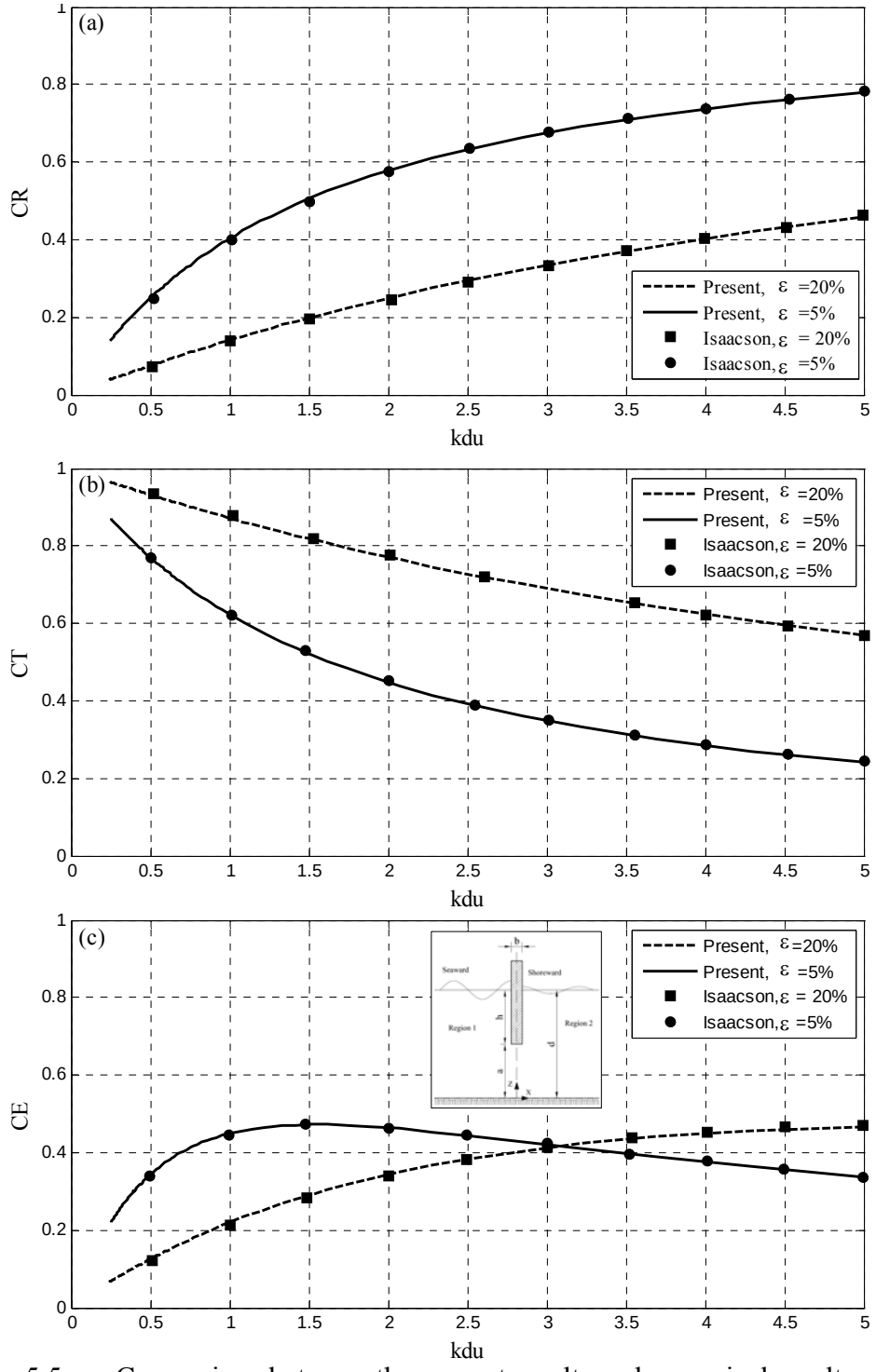

Figure 5.5: Comparison between the present results and numerical results of Isaacson et al. (1998) as a function of (k^*du) for various ε , and constant $du = 0.5d$, $h_i/L = 0.07$, $f = 2$ and $cm = 0$.

(a) Reflection coefficient,

(b) Transmission coefficient and

(c) Energy dissipation coefficient.

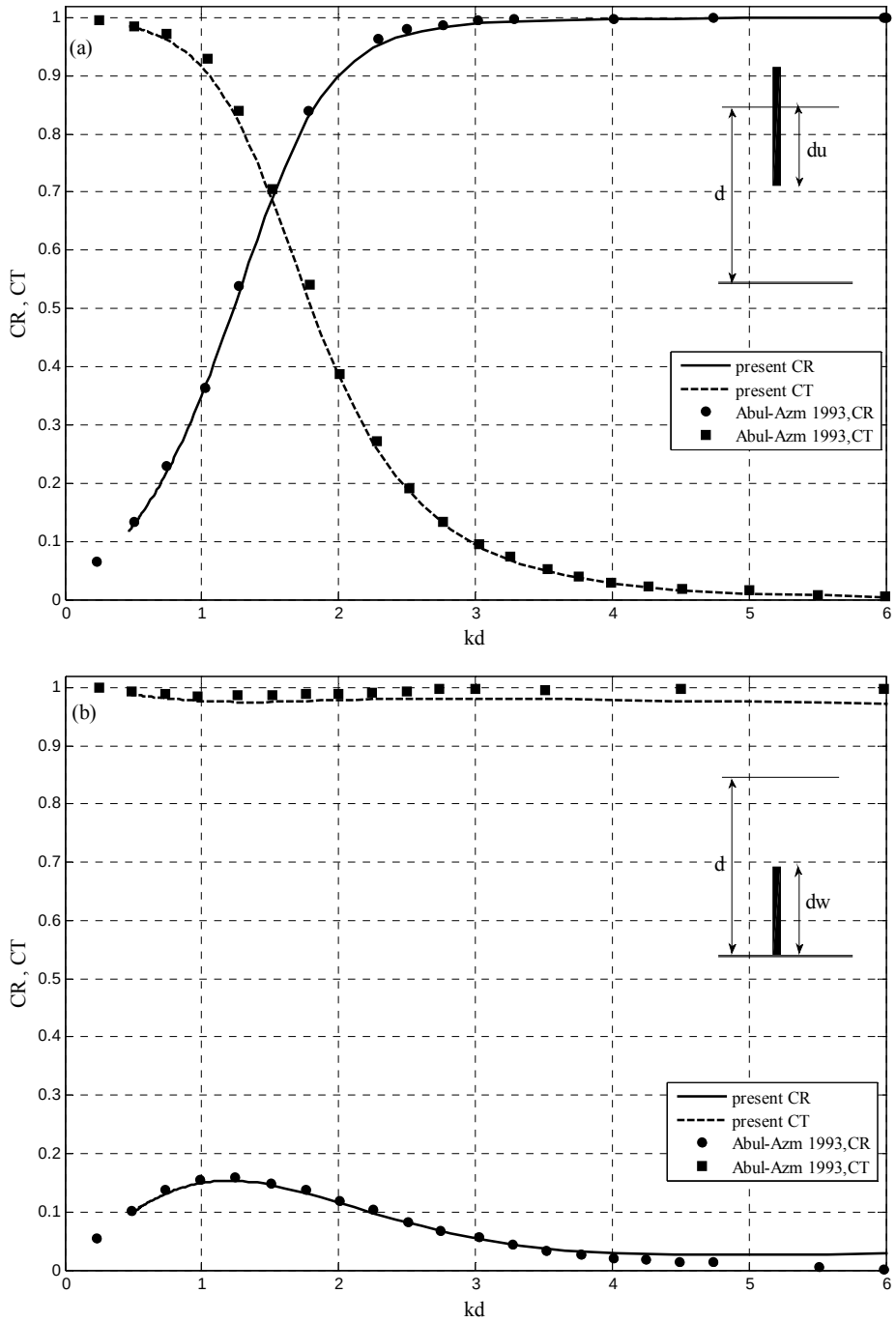

Figure 5.6: Comparison of the present results with prediction results of Abul-Azm (1993) as a function of (kd) for $h_i/L = 0.025$.

(a) A rigid thin submerged BW that extends from above the sea surface to the middle depth ($du = 0.5\ d$, $dw = 0$),

(b) A rigid thin submerged BW that extends from the seabed to the middle depth ($du = 0$, $dw = 0.5\ d$).

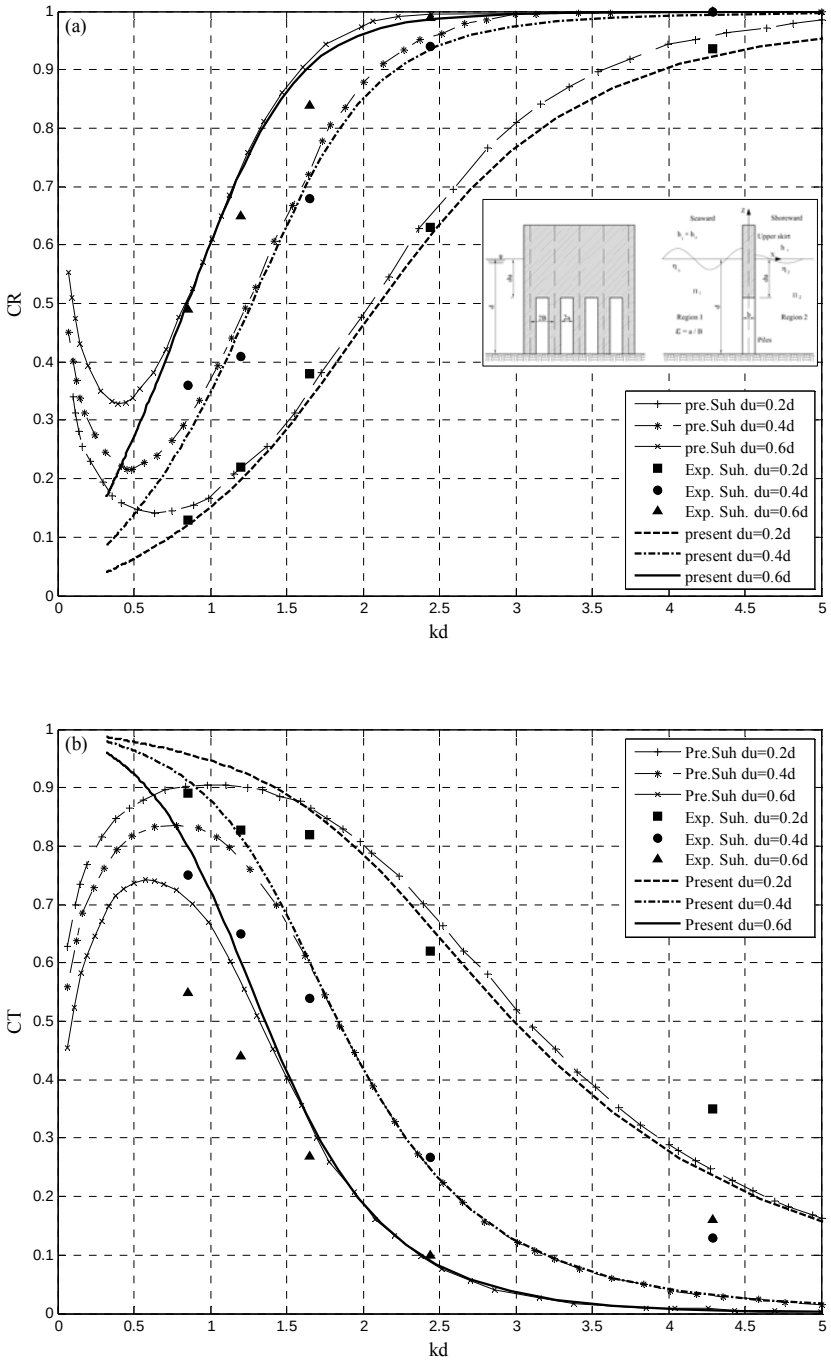

Figure 5.7: Comparison of the present results with prediction and experimental results of Suh. et al. (2006) for a pile-supported vertical wall as a function of (*kd*) for various *du* with constant $\varepsilon = 0.5, f = 0.50$ and $cm = 0$.

(a) Reflection coefficient,

(b) Transmission coefficient.

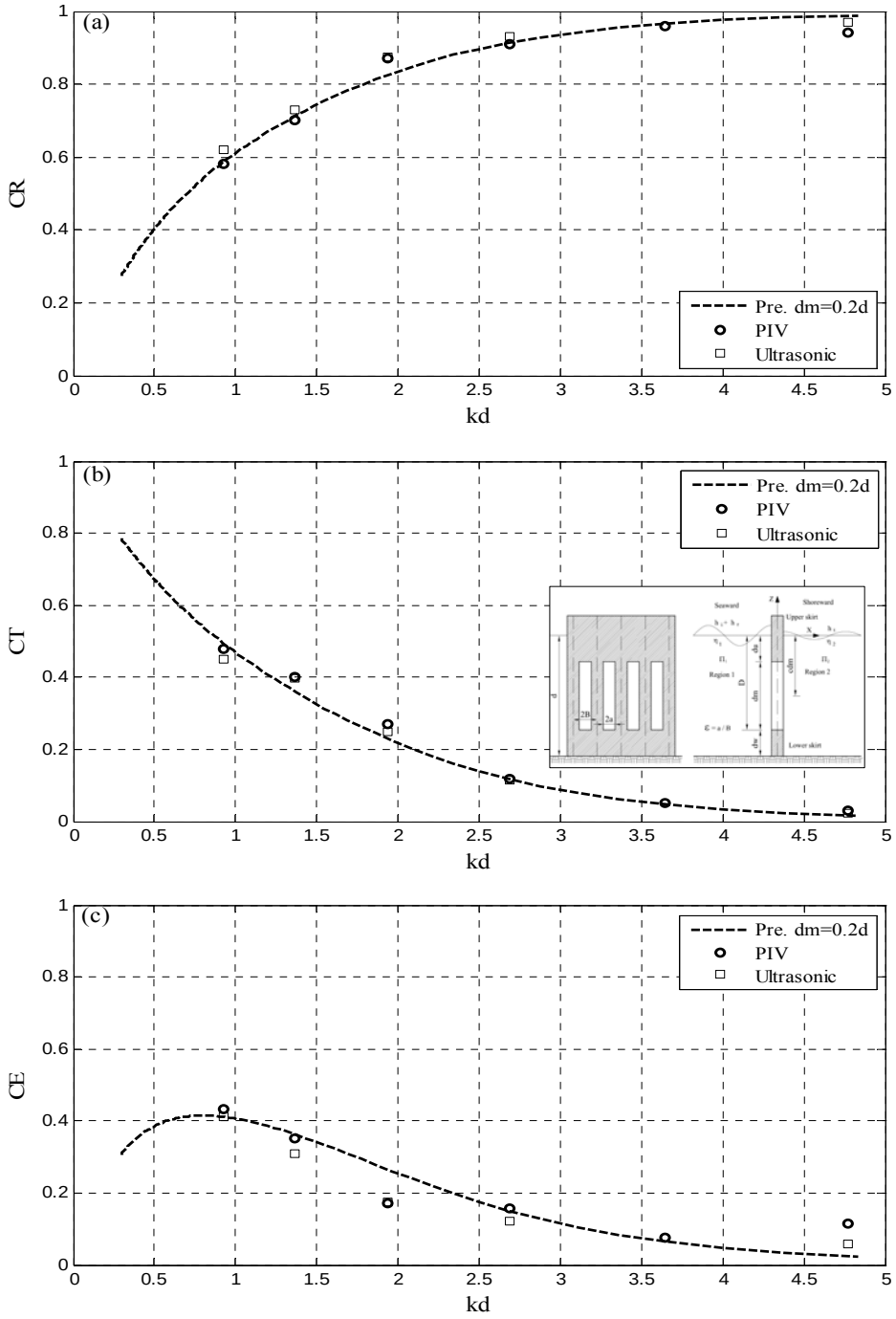

Figure 5.8: Comparison of predicted with experimental results of PIV and Ultrasonic measurements for $dm = 0.2\,d$, $\varepsilon = 0.5$, $f = 2$ and $cm = 0$.

(a) Reflection coefficient,

(b) Transmission coefficient and

(c) Energy dissipation coefficient.

5.3.8 Influence of the permeable depth

The effect of permeable depth *dm* on the hydrodynamic characteristics of permeable barriers is plotted in Figures 5.9: 5.11. The first two Figures show a comparison of the measured and predicted transmission, reflection, and energy dissipation coefficients as functions of *kd* and the third Figure shows a comparison of the measured and predicted transmission and reflection coefficients as a functions of *dm/d* for a vertical slotted wall. The middle part is permeable with a porosity ε = 50 %, the water depth d = 0.3 m, the thickness of breakwater b = 2.5 cm, h_i/L = 0.025, the upper and lower parts are impermeable and various permeability draft as a proportion of water depth *dm* = 0.8 *d,* 0.6 *d,* 0.4 *d* and 0.2 *d*, thus the draft of upper and lower part changed according to *dm*.

The permeability parameter is expressed in terms of porosity, friction and added mass coefficients as suggested by Sollitt and Cross (1972), and adopted by Isaacson et al. (1998, 1999). The friction parameter f', which describes the frictional losses, associated with the flow through the barrier, where the flow contracts and expands through the gap and assumed to be known as per Yu (1995). The added mass coefficient was taken as zero since the porous medium here is a fixed structure, resulting in the value of inertia coefficient, S = 1. The value S = 1 was used by many researchers for flow through fixed porous structures. The success of applying Eigen function expansion method to the flow through porous medium depends on the selected value of G to model the physical behavior of the porous structure. The value of G is calibrated through the adjustment of the friction parameter f to find a match with the experimental results. To achieve the fit between the experimental and the prediction results for reflection and transmission coefficients in the present study, the values of friction and added mass coefficient could be f = 2, and *cm* = *0* respectively.

In general, the numerical model is able to adequately reproduce the most important features of the experimental results although there is some scatter in the experimental result. The reflection coefficient, *CR,* increases with increasing *kd* at fixed *dm* and increases with decreasing *dm* for the fixed *kd*. The transmission coefficient, *CT*

follows the opposite trend. It is noticed that, the reflection coefficient is less for the model when *dm* = *d* (i.e. the pile case) and maximum for *dm* = 0.00, i.e. the reflection coefficient = 100 % for a wall, while the transmission coefficient for the same case is *CT* = 0. It is obvious that the reflection and transmission coefficients approx. one and zero respectively for high wave number associated short waves where the short waves reach the depth of submergence of the upper skirt with small degree. The effect of the portion of the permeability is seen for example at *kd* = 1 where the reflection and transmission coefficients vary from 20 % and 80 % to 60 % and 45 % respectively. The energy dissipation, *CE* slowly increases with increasing *kd* for lower *kd* and inversed for higher *kd*, while the energy dissipation for the pile increases continuously and the energy dissipation *CE* = 0 for the wall. The differences between the measured and predicted results are most notable in the energy loss coefficients. Note that the measured energy loss coefficient is calculated directly from the measured transmission and reflection coefficients so that the scatter in the measured values is due in part to experimental errors in measuring the transmitted and reflected waves.

Figure 5.11 (a, b) illustrates the predicted transmission, reflection coefficients as functions of relative middle permeable part *dm/d* for vertical slotted walls, where the middle part is permeable with a porosity of ε = 50 % and various draft *dm* = 0 to d, *kd* = 4.772 for Figure 5.11a and 1,363 for Figure 5.11b. In general, a choice of the opening area is particularly important. The reflection coefficient, *CR* decreases with increasing *dm/d* while the transmission coefficient, *CT* follows the opposite trend. It is noticed that, the reflection coefficient is 100 % at *dm/d* = 0 while the transmission coefficient = 0 (wall case) and the less reflection at *dm/d* = 1 while the transmission is maximum (pile case). Therefore, the efficiency of this type surpasses the efficiency of pile breakwater, which has the same porosity. The target protection can be achieved through the best choice for the permeability area.

5.3.9 Influence of the draft of the impermeable lower part

The pure influence of the impermeable lower part *dw* on the hydrodynamic characteristics of vertical slotted walls is plotted in Figures 5.12 and 5.13. The porosity ε is 50 % for the permeable part, the water depth d = 0.3 m, the thickness of breakwater b = 2.5 cm, h_i/L = 0.025 and the draft of the impermeable upper part *du* is fixed at 0.4 *d*. The lower impermeable part *dw* is various from *0* to *0.6 d*, the friction factor f = 2 and the added mass coefficient *cm* = 0.00. In general, the lower impermeable part has a high efficiency for intermediate and long waves where the reflection coefficient increases with increasing the draft of the lower impermeable part, while the transmission coefficient *CT* follows the opposite trend. It is obvious that the reflection coefficient approx. one for high wave numbers associated with short waves. The effect of the portion of the impermeability lower part is seen for example at kd = 1, where the reflection and transmission coefficients vary from 25 % to 72 % and 75 % to 32 % for *dw* = 0:0.5 *d* respectively. For short waves, it has no influence on the reflection and transmission coefficients. This is because the particle orbits is circular and the amplitude of the velocity and the displacement decreasing exponentially with the depth, until at z = *-L/2,* after this depth the energy of the wave is vanished according to the linear wave theory and the wave is totally reflected by the impermeable upper part. The particle orbits in the intermediate depth diminish in amplitude with the depth and also become flatter until the vertical component vanishes at the seabed in accordance with the seabed boundary condition. Therefore, the efficiency of this type surpasses the efficiency of pile-supported vertical wall breakwaters, which have the same porosity, and the same draft of the impermeable upper part for intermediate and long wave.

5.3.10 Influence of the draft of the impermeable upper part

The pure influence of the impermeable upper part *du* on the hydrodynamic characteristics of vertical slotted barriers is plotted in Figures 5.14 and 5.15. The porosity ε is 50 % for the permeable part, the water depth d = 0.3 m, the thickness of breakwater b = 2.5 cm, h_i/L = 0.025 and the draft of the impermeable lower part is

fixed at 0.4 *d* while the upper impermeable part is various from *0* to *0.6 d*, the friction factor f = 2 and the added mass coefficient cm = 0. In general, the upper impermeable part has significant influence for short, intermediate and long waves. The reflection *CR* coefficient is close to one for short waves when the draft of the upper is skirt higher than 0.3 *d,* while the transmission *CT* coefficient is close to zero. The effect of the portion of the impermeability upper part is seen for example at kd = 1, where the reflection and transmission coefficients vary from 20 % to 75 % and 80 % to 30 % for du = 0:0.5 *d* respectively.

Finally, the upper impermeable part has significant influence for all types of waves.

5.3.11 Influence of the location of the permeable part

The influence of the location of the permeable part *dm* on the hydrodynamic characteristics of vertical slotted walls is plotted in Figure 5.16. The porosity ε is 50 %, the water depth d = 0.3 m and the thinness of breakwater b = 2.5 cm, h_i/L = 0.025, the friction F = 2, the added mass coefficient cm = 0 and the draft of the permeable part is fixed at 0.2 *d* and have various locations "*cdm*" measured from the water surface and vary from 0.1 to 0.7 *d*. In general, the location of the permeable part has a significant influence for short and intermediate wave up to $kd \geq 0.5$ and $cdm \leq 0.5\ d$. For $kd < 0.5$ and also for $kd \geq 0.5$ and $cdm > 0.5\ d$. The location of the permeable part has insignificant influence on the hydrodynamic characteristics at $cdm \leq 0.5\ d$. It is noticed that, for cdm = 0.1 d and $kd \geq 1$ the *CR*, *CT* and *CE* seems to be constant at 50 %, 58 % and 38 % respectively.

Therefore, the hydrodynamic performance characteristics of permeable breakwaters vary according to the location of the permeable part. The degree of the target protection can be achieved through the best choice for the permeability area and its location together.

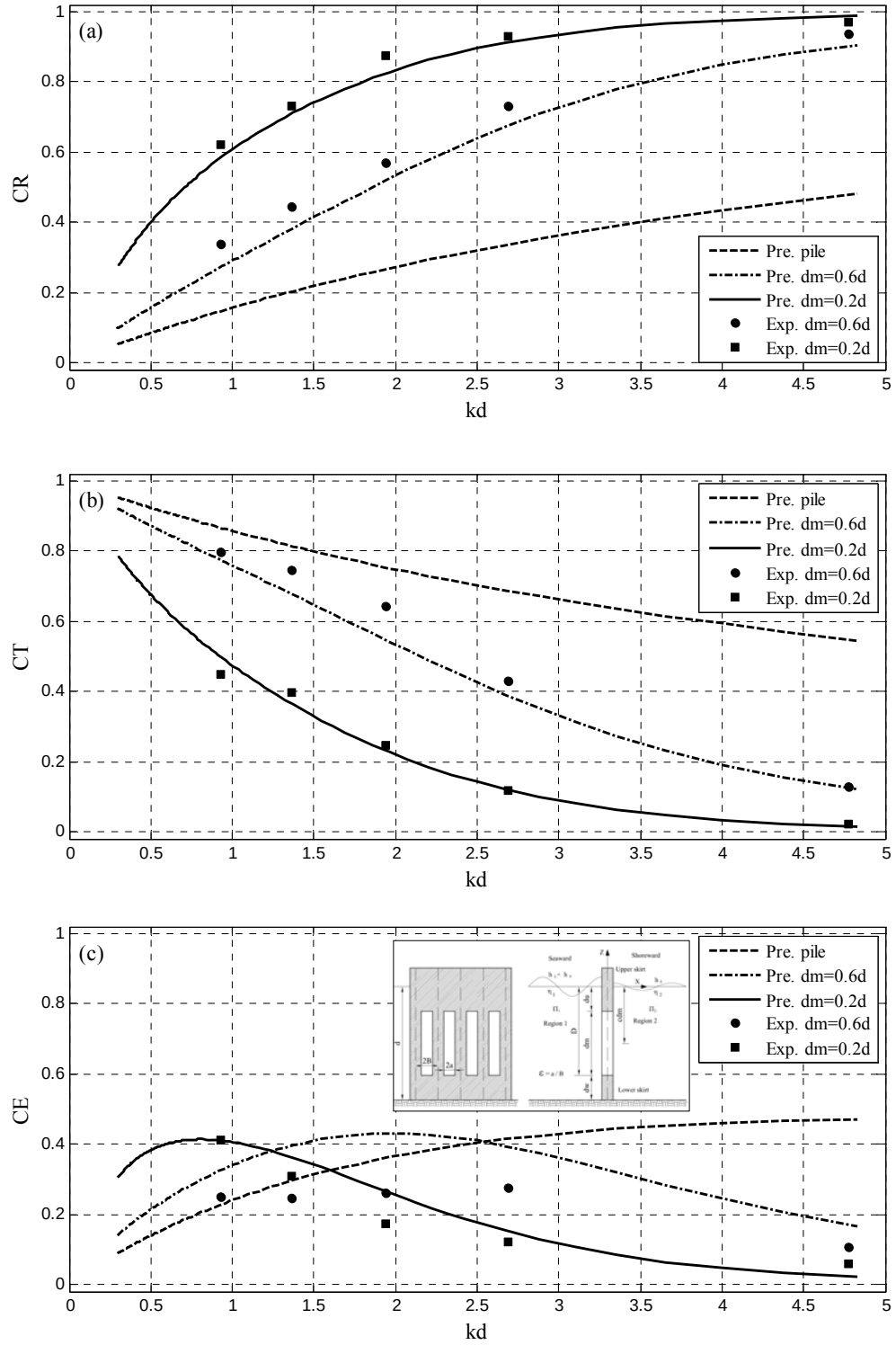

Figure 5.9: Comparison of experimental and predicted results as a function of (kd) for various middle permeable part with $\varepsilon = 0.5, f = 2$ and $cm = 0$.

(a) Reflection coefficient,

(b) Transmission coefficient and

(c) Energy dissipation coefficient.

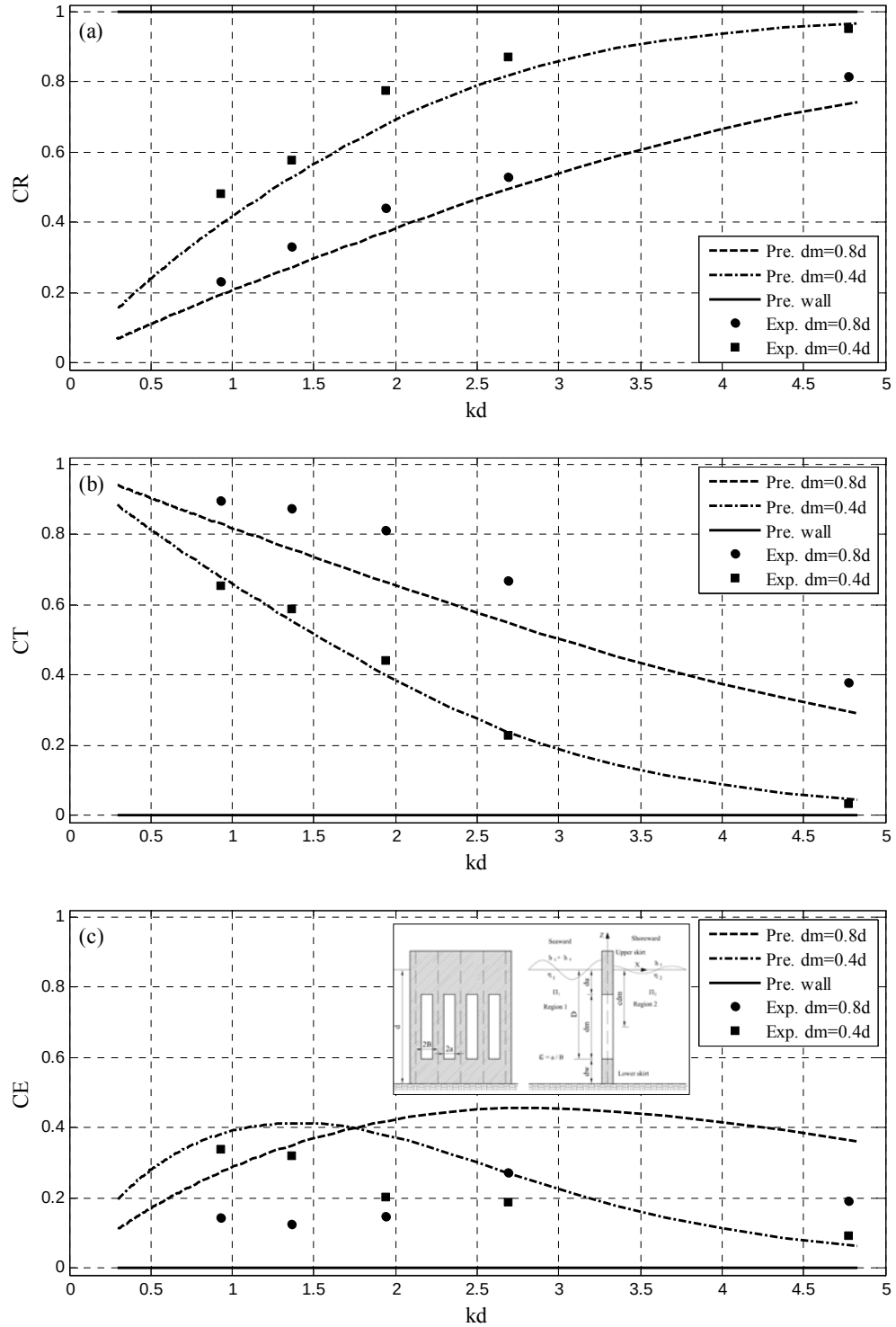

Figure 5.10: Comparison of experimental and predicted results as function of (*kd*) for various middle permeable part with $\varepsilon = 0.5$, $f = 2$ and $cm = 0$.

(a) Reflection coefficient,

(b) Transmission coefficient and

(c) Energy dissipation coefficient.

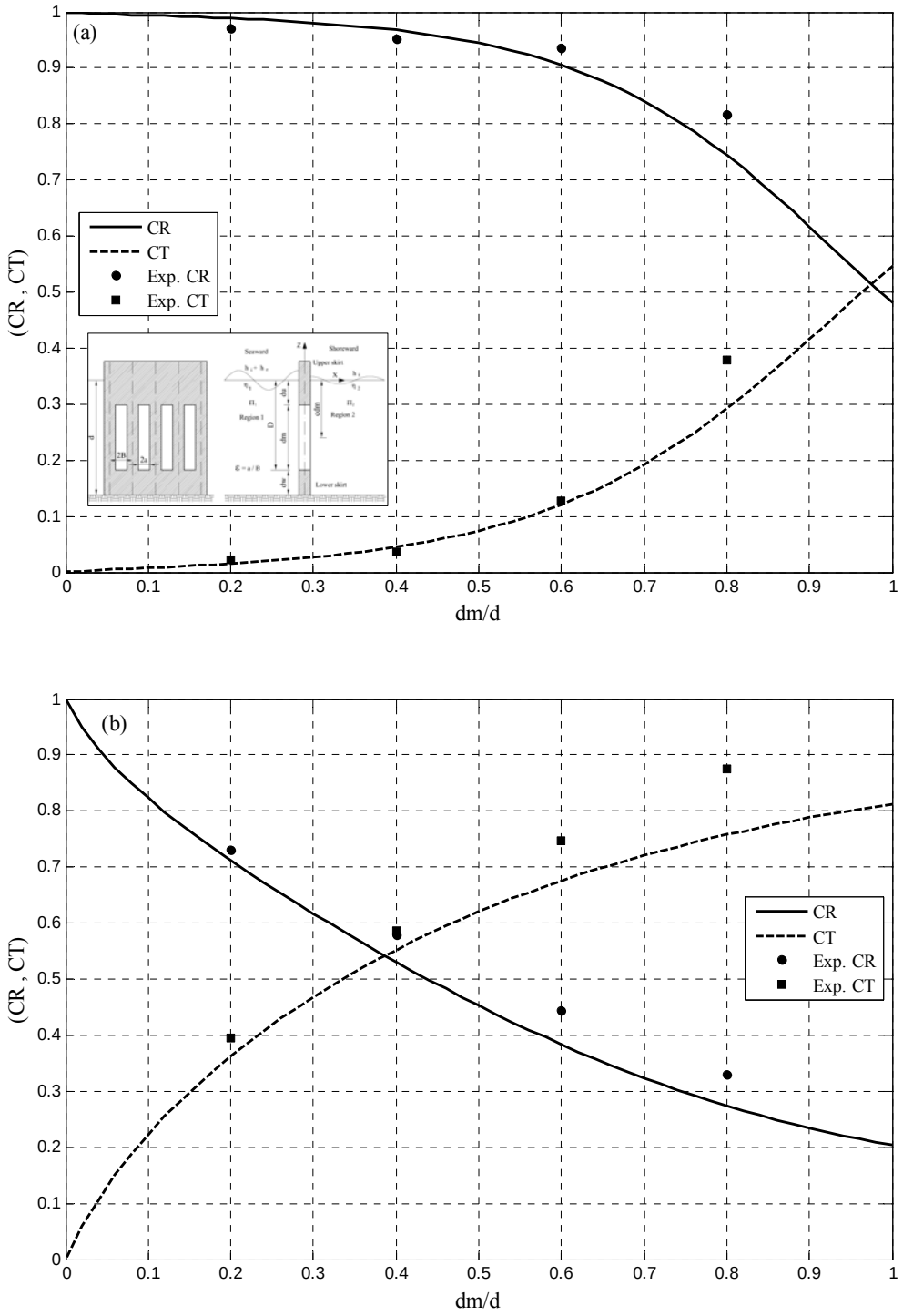

Figure 5.11: Comparison of measured and predicted reflection and transmission coefficients as a function of relative permeable middle part *dm/d* and with constant $\varepsilon = 0.5, f = 2$ and $cm = 0$.

(a) at wave period $T = 0.5$ s and $kd = 4.772$

(b) at wave period $T = 1.0$ s and $kd = 1.363$.

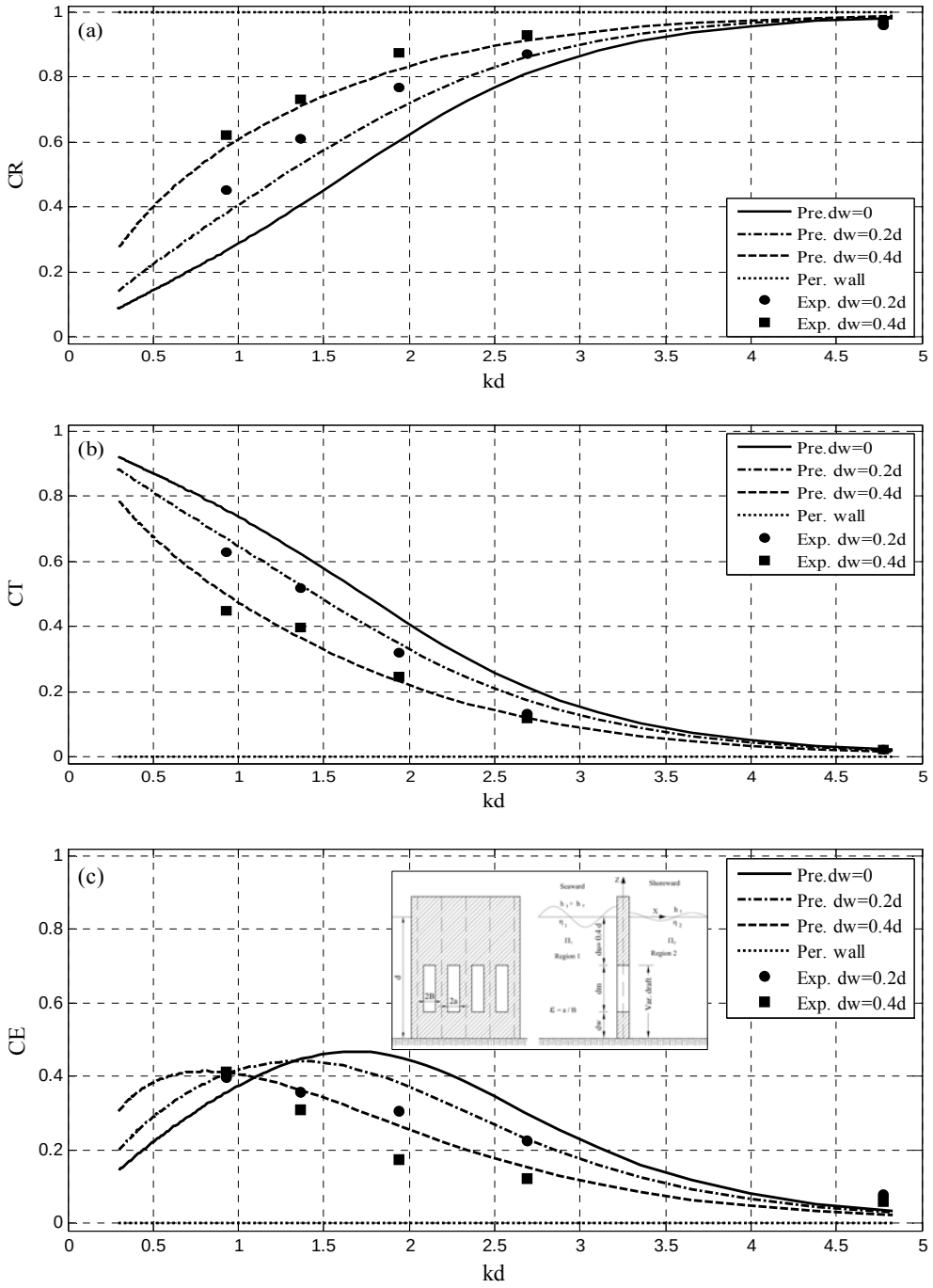

Figure 5.12: Comparison of experimental and predicted results as a function of (*kd*) for fixed upper skirt at *du* = 0.4 d and various draft of lower skirt with $\varepsilon = 0.5$, $f = 2$ and $cm = 0$.

(a) Reflection coefficient,

(b) Transmission coefficient and

(c) Energy dissipation coefficient.

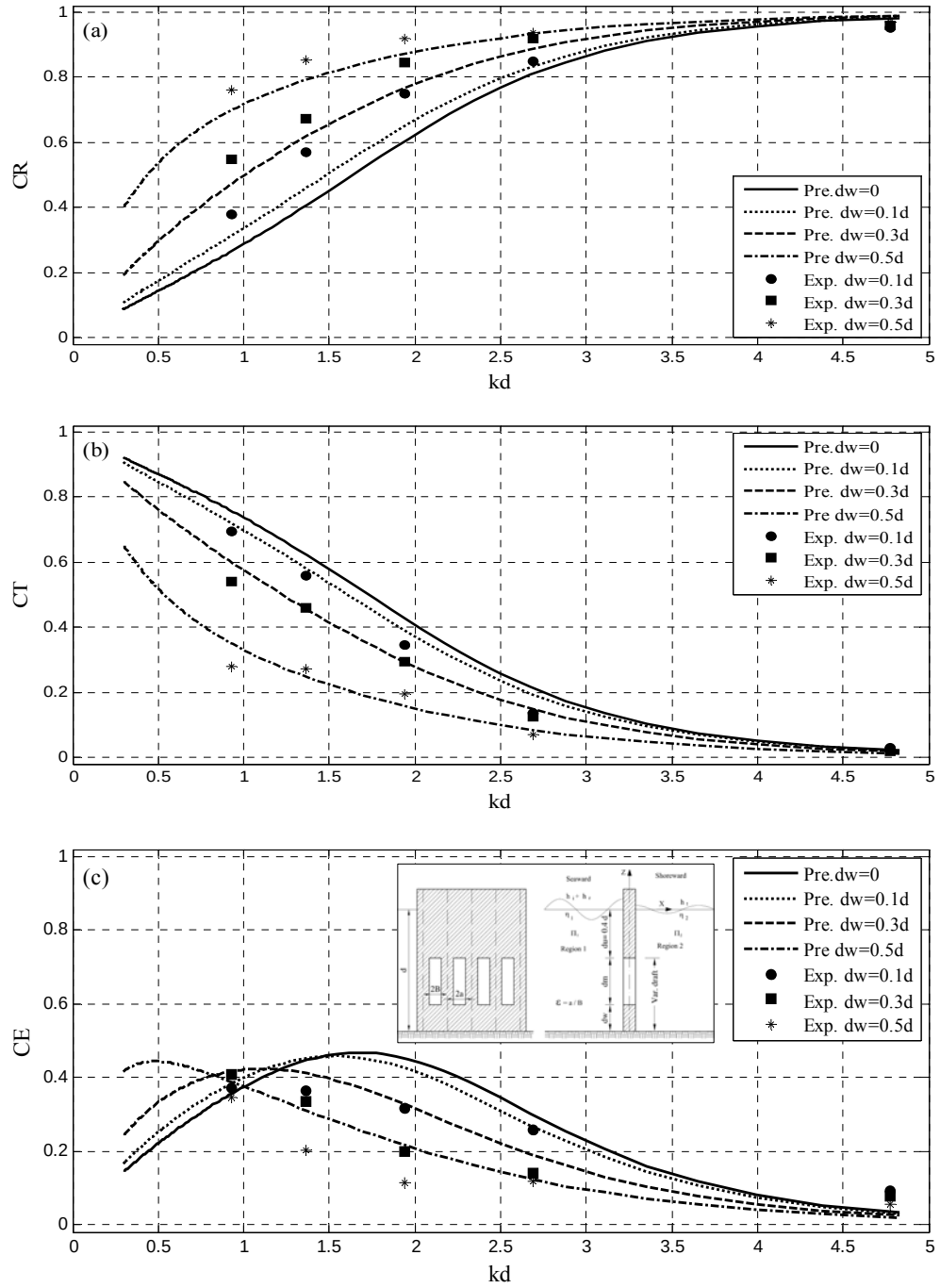

Figure 5.13: Comparison of experimental and predicted results as a function of (kd) for fixed upper skirt at du = 0.4 d and various draft of lower skirt with ε = 0.5, f = 2 and cm = 0.

(a) Reflection coefficient,

(b) Transmission coefficient and

(c) Energy dissipation coefficient.

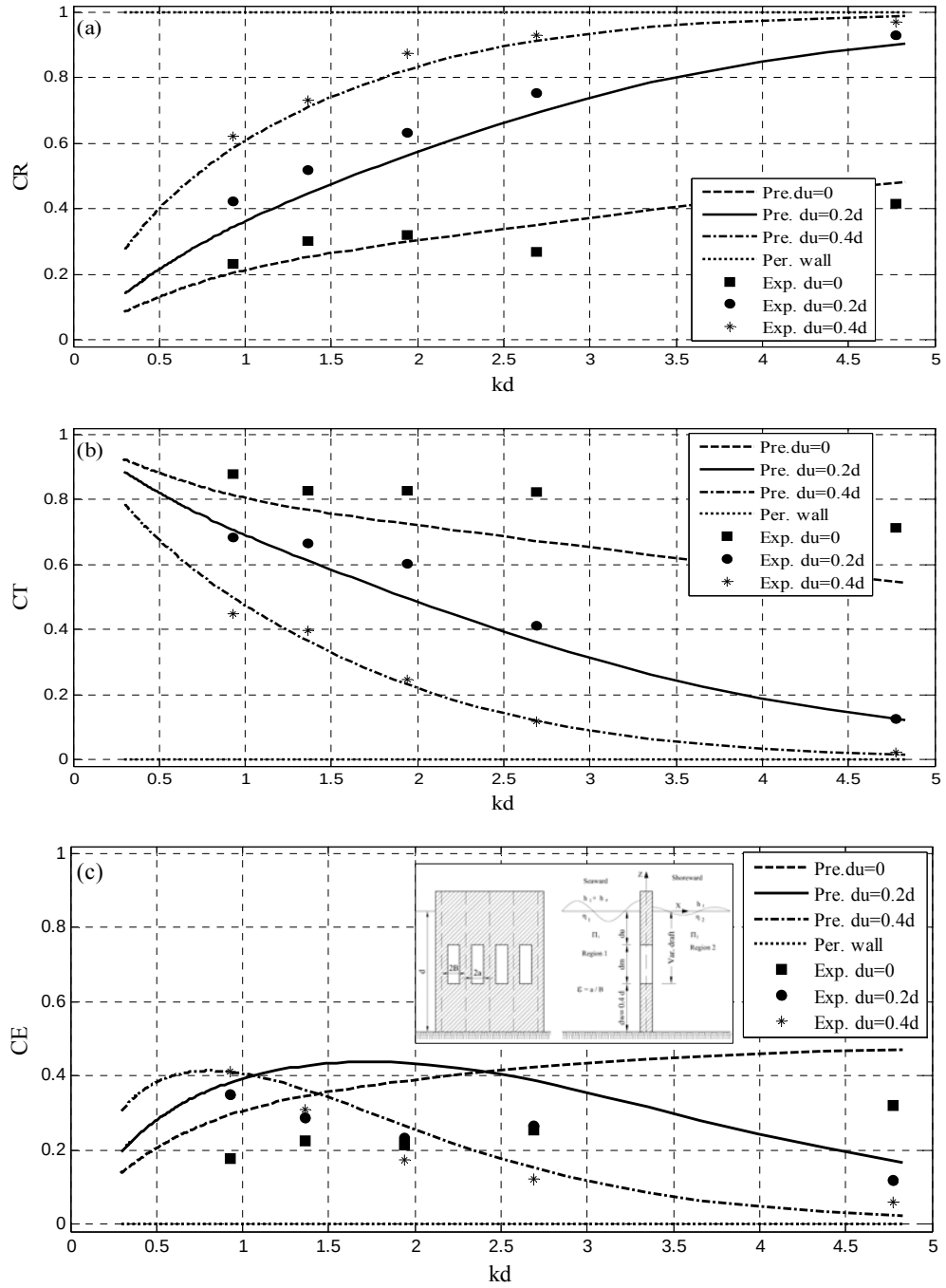

Figure 5.14: Comparison of experimental and predicted results as a function of (kd) for fixed lower skirt at dw = 0.4d and various draft of upper skirt with $\varepsilon = 0.5, f = 2$ and cm = 0.

(a) Reflection coefficient,

(b) Transmission coefficient and

(c) Energy dissipation coefficient.

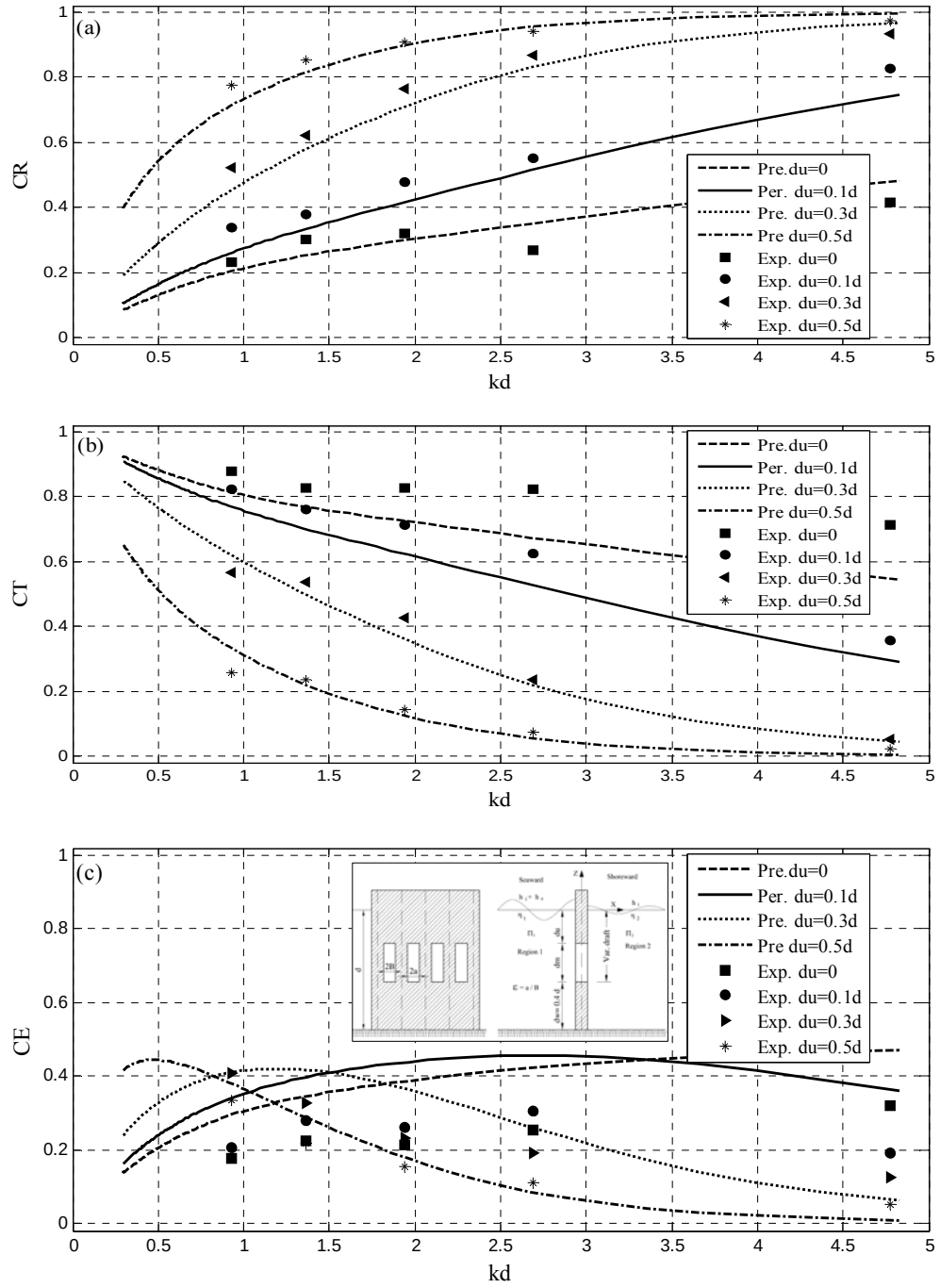

Figure 5.15: Comparison of experimental and prediction results as a function of (kd) for fixed lower skirt at dw = 0.4 d and various draft of upper skirt with $\varepsilon = 0.5, f = 2$ and $cm = 0$.

(a) Reflection coefficient,

(b) Transmission coefficient and

(c) Energy dissipation coefficient.

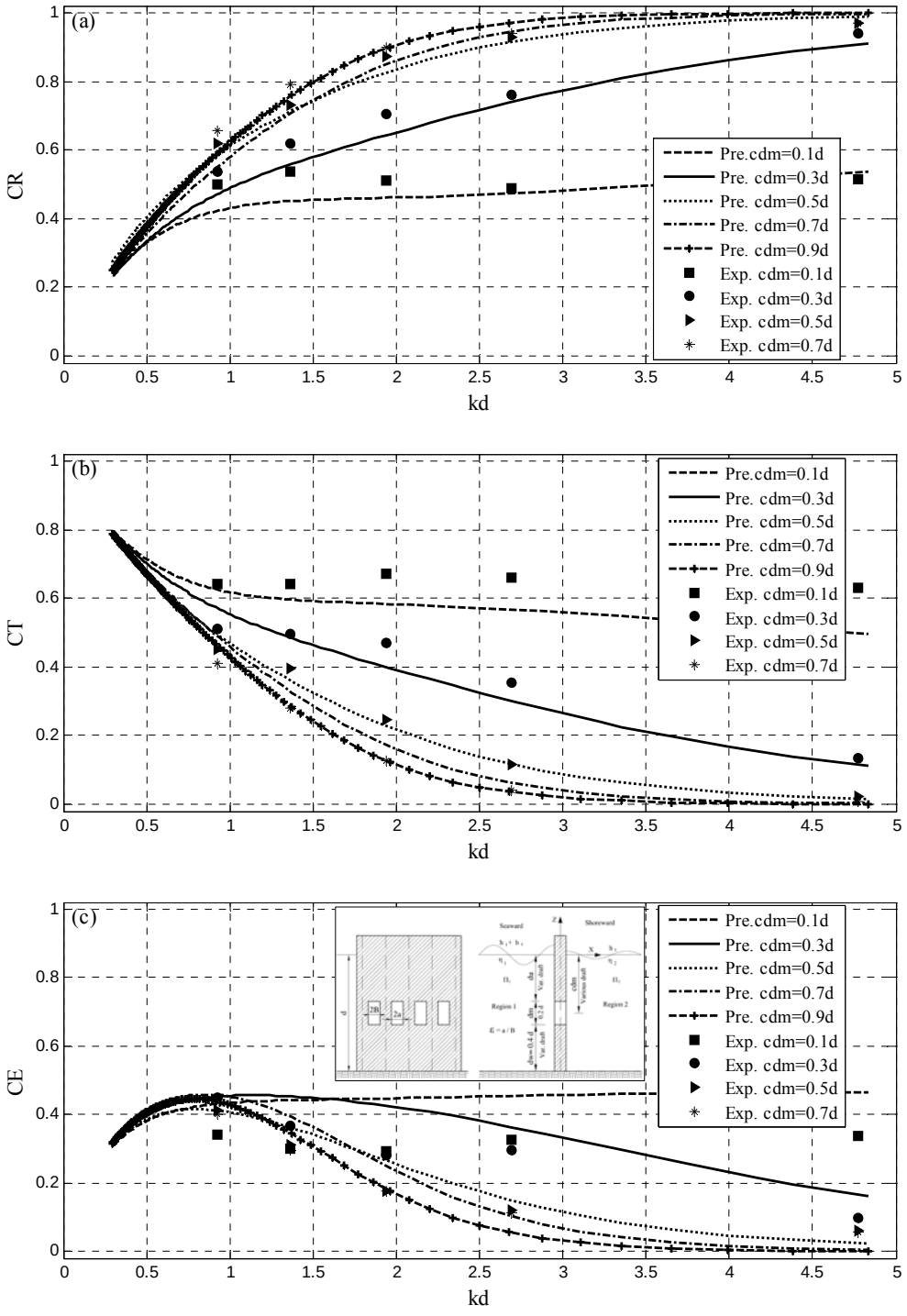

Figure 5.16: Comparison of experimental and prediction results as a function of (*kd*) for fixed middle permeable part *dm* = 0.2 *d* and different location from water surface with constant porosity ε = 0.5, *f* = 2 and *cm* = 0.
(a) Reflection coefficient,
(b) Transmission coefficient and
(c) Energy dissipation coefficient.

5.4 NON LINEAR WAVE (STOKES SECOND-ORDER WAVE) INTERACTION WITH SINGLE VERTICAL SLOTTED WALL

5.4.1 General

In this section, numerical results for a single vertical slotted wall derived by applying Stokes second-order wave theory are compared with experimental and numerical results from linear wave theory. The numerical model deepens on Eigen function expansion method for regular and non-linear waves (Stokes second-order wave theory) and utilizes a boundary condition at the barrier, which accounts for energy dissipation within the barrier. The number of terms used in the Eigen function expansion was taken as $N = 50$. This was found to give accurate results over the range of values presented here. The model of this study is the same as for linear wave interaction with a single vertical slotted wall breakwater. The hydrodynamic characteristics of single vertical slotted wall under nonlinear waves are investigated. All results are presented and discussed as follows.

5.4.2 Influence of the permeable depth

The effect of the permeable part *dm* on the hydrodynamic characteristics of permeable barriers is investigated and indicated that the behavior of hydrodynamic characteristics *CR*, *CT* and *CE* for nonlinear wave (Stokes second-order wave) is similar to the behavior of linear wave which was discussed earlier within the same limits and conditions. There is no need to mention all these results here but it is important to mention the differences between them in the next section.

5.4.3 Comparison of Stokes second-order wave with linear wave

The predicted results of Stokes second-order wave interaction is compared with experimental and predicted results of linear wave interaction for a single vertical slotted wall model. The results are plotted in Figures 5.18 and 5.19. The parameter of waves and the barrier are the same in the numerical model and the experimental work for previous Figures 5.9 and 5.10. It's clear from the Figures that the trend of

Stokes second-order waves is identical to the trend of linear waves for short and intermediate waves up to $kd \geq 1$ but the trend of Stokes second-order waves is higher than the trend of linear waves for intermediate waves at $kd < 1$ and the long waves. This may be because the profile of the second-order is a steeper crest and shallower trough than the profile of a linear wave as shown in Figure 5.17 and the energy of short wave and lower intermediate is quite reflected. But for higher intermediate and long waves, the energy of a second-order wave is reflected more than the linear wave and transmitted lesser than it. It is noted that the reflection coefficient increases with about 5 % and the transmission coefficient decreases with about 5 % than linear wave theory seen for example at $kd = 0.5$. This ratio increases with decreasing kd.

Finally, the numerical results of the present study are in convergence with the experimental results especially for $kd < 1$ and the Stokes second-order component can be neglected for short waves and may become significant for intermediate and long wave.

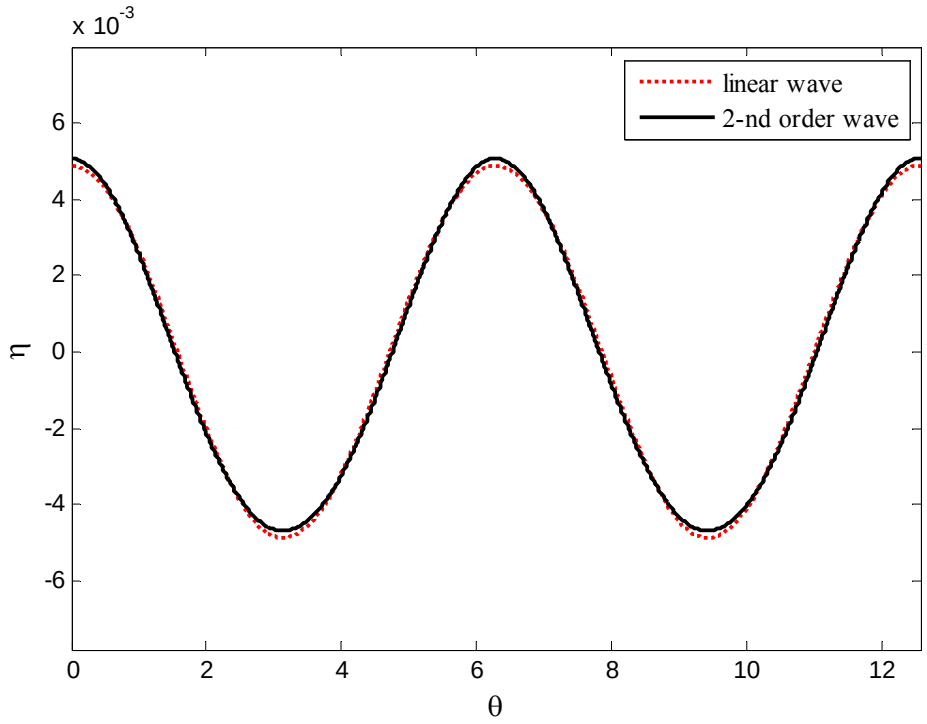

Figure 5.17: Comparison between the waves profile of linear and Stokes second-order waves at $T = 1$ s and $h_i = 0.025\ L$.

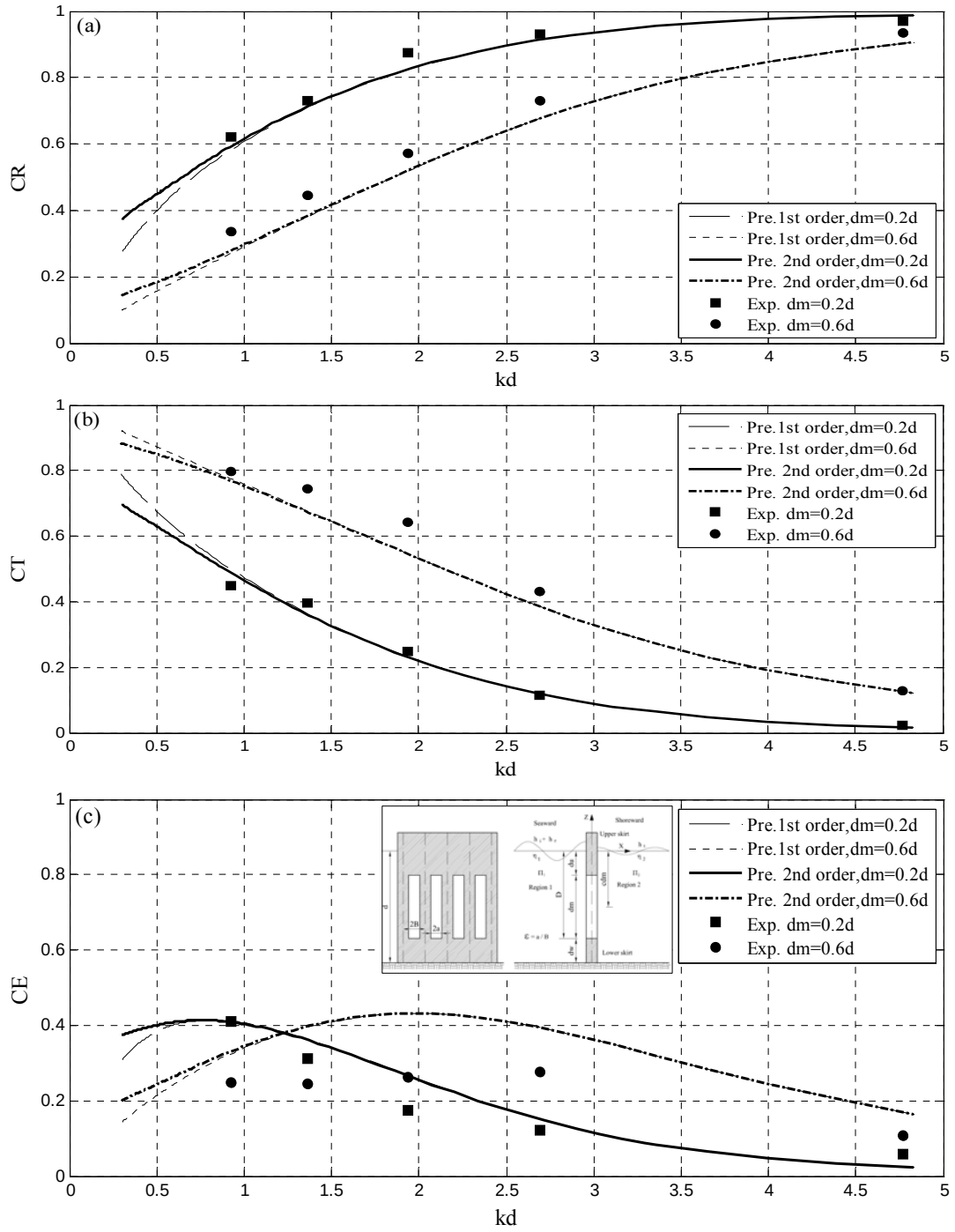

Figure 5.18: Comparison of predicted results of nonlinear waves (Stokes second-order theory) with measured and predicted results of linear waves as a function *kd* for various *dm*, and $\varepsilon = 0.5, f = 2$ and $cm = 0$.

(a) Reflection coefficient,

(b) Transmission coefficient and

(c) Energy dissipation coefficient.

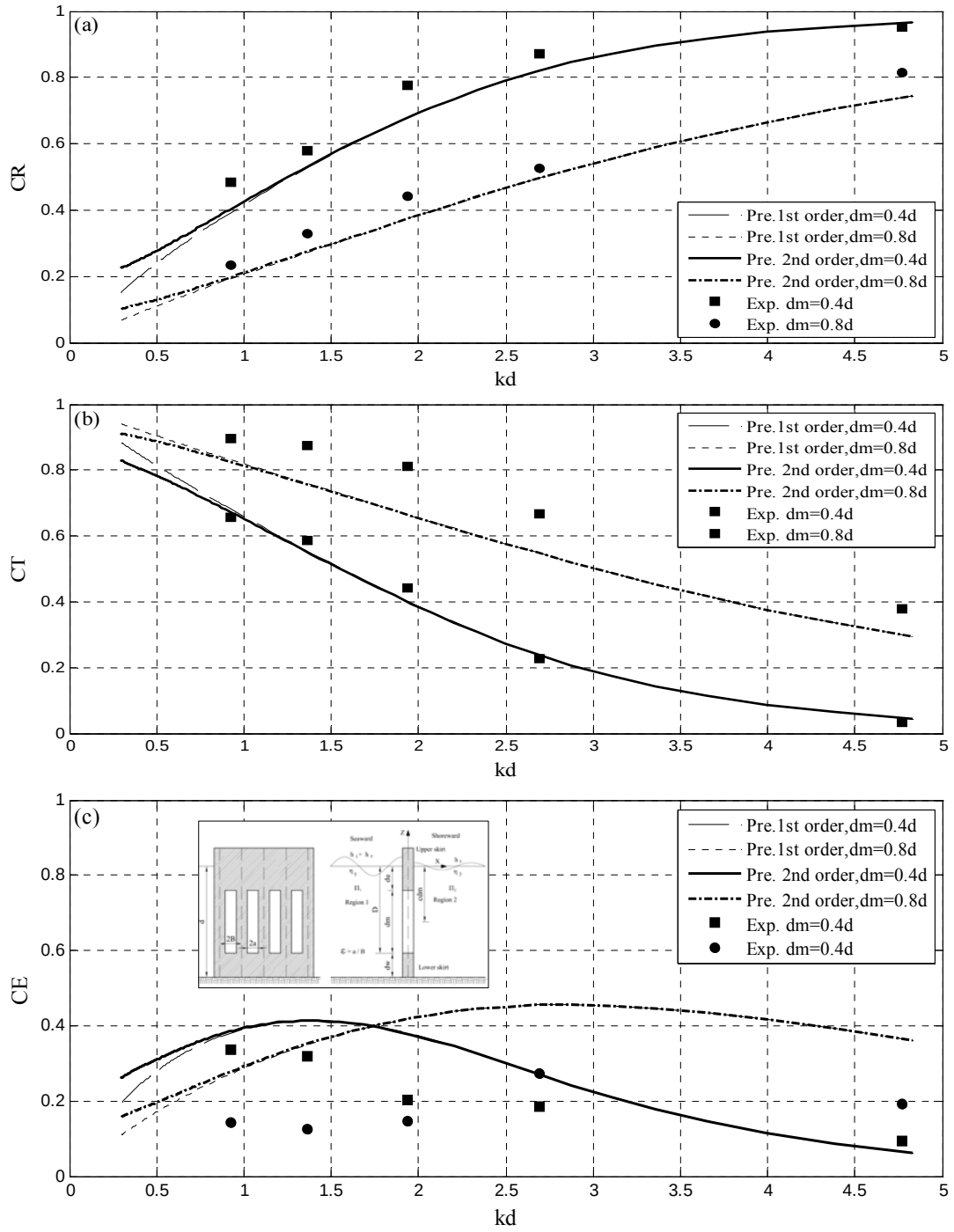

Figure 5.19: Comparison of predicted results of nonlinear waves (Stokes second-order theory) with measured and predicted results of linear waves as a function *kd* for various *dm*, and constant $\varepsilon = 0.5$, $f = 2$ and $cm = 0$.

(a) Reflection coefficient,

(b) Transmission coefficient and

(c) Energy dissipation coefficient.

5.5 LINEAR WAVE INTERACTION WITH DOUBLE VERTICAL SLOTTED WALLS BREAKWATER

5.5.1 General

In this section, numerical results for a double identical vertical slotted walls breakwater are compared with previous studies and experimental results of this study. The numerical model depends on Eigen function expansion method for regular waves (linear wave theory) and utilizes a boundary condition at the surface of the barrier which accounts for energy dissipation within the barrier. The number of terms used in the Eigen function expansion was taken as $N = 30$. This was found to give reasonable accurate results over the range of values presented here. The experimental work is carried out with regular waves for various wave periods (T = 0.5 to 2), wave heights are (1, 2, 3, 4 cm), a fixed water depth d = 30 cm, constant porosity of ε = 50 % for the permeable part. The second wall is located at different distances from the first wall. All results are presented and discussed as follows.

5.5.2 Validation of the numerical model for double vertical slotted barriers

The validation of the numerical model can be done through comparing the results with theoretical and experimental results of Isaacson et al. (1999) for hydrodynamic characteristics of double vertical slotted barriers. The numerical model as proposed by Isaacson et al. (1998) was proposed for studying the wave transmission through double thin vertical slotted barrier extending from the water surface to some distance above the seabed.

Figure 5.20 shows the comparison between the present study and the numerical and experimental study of Isaacson et al. (1998) which were carried out to investigate the hydrodynamic characteristics of two identical barrier through hydrodynamic characteristics CR, CT and CE coefficients as a function of k^*du. The porosity ε = 5 %, h_i/L = 0.07, f = 2, cm = 0.00, b = 1.3 cm, d = 0.45 cm and barrier spacing λ = 1.1 du.

The comparison is found to be good, despite some of the dispersion in *CR*, *CT* which clearly appears in *CE*, that may be related to the difference in mathematical approximation in both numerical models. It is clear from the figure that the *CR* increases, whereas *CT* decreases with an increase in *k*du*. This is due to the reason that long waves, which are lesser *k*du* will propagate past the barrier without being attenuated. It is worth mentioning that the variations of single slotted barrier are observed to be smooth as shown previously in Figure 5.6, whereas in the case of double walls, secondary peaks are observed due to the interaction between two obstructions with the propagating waves.

Generally, the numerical model of the present study is more convergent with the experimental results of Isaacson et al. (1998), thus validating the present numerical model.

5.5.3 Influence of the permeable depth

The effect of the permeable part *dm* on the hydrodynamic characteristics of identical double vertical slotted walls is plotted in Figures 5.21 to 5.44, which indicate the comparison of the measured and predicted transmission, reflection, and energy dissipation coefficients as a function of *kd* as shown in Figures 5.21 to 5.36 and as a function of *dm/d* as shown in Figures 5.37 to 5.44. The middle part is permeable with a porosity ε = 50 % , the water depth d = 0.3 m, the thickness of breakwater b =2.5 cm, h_i/L = 0.025, the upper and lower parts are impermeable, various permeability draft as a proportion of water depth *dm = d,* 0.8 *d,* 0.6 *d,* 0.4 *d* 0.2 *d and* 0.00. The draft of the upper and lower parts changed according to *dm*. The permeability parameter previously discussed in section 5.3.7, the values of the friction and the added mass coefficient are given f = 2, and *cm = 0* on the basis of a best fit between the measured and predicted values of the transmission, reflection and energy dissipation coefficients. The chamber width vary as a proportion of the water depth 2 λ = 0.5 *d*, *d*, 1.5 *d* and 2 *d* as shown in Figures 5.21 to 5.28 and 5.37 to 5.40 as well as vary as a proportion of the wave length 2 λ = 0.25 *L*, 0.5 *L*, 0.75 *L* and *L* as shown in Figures 5.29 to 5.36 and 5.41 to 5.44.

In general, the Figures 5.21 to 5.36 follow the expected trends. The reflection coefficient, *CR* increases with increasing *kd* at fixed *dm* and increases with decreasing *dm* at fixed *kd* The transmission coefficient, *CT* follows the opposite trend. It is noticed that, the reflection coefficient is less for the model when the *dm* = *d* (i.e. a pile case) and maximum for *dm* = 0.00, i.e. the reflection coefficient is 100 % for the wall, while the transmission coefficient for this case is *CT* = 0. It is obvious that the reflection and transmission coefficients approx. one and zero respectively for high wave number associated with short waves. The effect of the portion of the permeability is seen for example at *kd* = 1 where the reflection and transmission coefficients vary from 25 % and 75 % to 58 % and 30 % respectively. The energy dissipation, *CE* slowly increases with increasing *kd* for the lower *kd* and reaches more than 80 % because the second barrier causes additional vortex, which dissipate more wave energy. The differences between the measured and predicted results are most notable in the energy loss coefficients. Note that the measured energy loss coefficient is calculated directly from the measured transmission and reflection coefficients so that the scatter in the measured values is due in part to experimental errors in measuring the transmitted and reflected waves. Interestingly; the peaks in *CR*, *CT*, and *CE* are occurred. The number of peaks increases with increasing the chamber width. For larger relative spacing, peaks in the transmission and reflection coefficients occur when the relative draft $kd = n\pi /(2\lambda / d)$, corresponding to resonant excitation of partial standing waves between the barriers. This result agrees with the result of double slotted barriers (Isaacson et al. 1999).

Figures 5.29 to 5.36 illustrate the relation between the hydrodynamic characteristics and *kd* when the chamber width varies as a proportion of the wave length. In general, the Figures follow the expected trends. The reflection coefficient, *CR* increases with increasing *kd* at the fixed *dm* and increases with decreasing *dm* for the fixed *kd.* The transmission coefficient, *CT* follows the opposite trend. The energy dissipation *CE* increases with increasing *kd* for the lower *kd* and reaches more than 80 % for position 2λ = 0.25*L* and 0.75*L* while *CE* reaches 45 % for position 2λ = 0.5*L* and *L*. Thereafter, *CE* inversed for the higher *kd*, while the energy dissipation for the pile increases continuously and the energy dissipation *CE* = 0 for the wall. The effect of

the portion of the permeability is seen for example at kd = 1 where the reflection and transmission coefficients vary from 8 % and 18 % to 72 % and 74 % respectively.

The effect of the permeability part is also presented as a function of the relative middle permeable part dm/d for different chamber width as a proportion of the water depth as shown in Figures 5.37 to 5.40 and as a proportion of the wave length as shown in Figures 5.41 to 5.44. The middle part is permeable with porosity ε = 50 % and various draft dm = 0 to d, for different kd = 4.772, 2.689, 1.363 and 0.577. In general, a choice of the opening area is particularly important. The reflection coefficient, CR decreases with increasing dm/d while the transmission coefficient, CT follows the opposite trend. It is noticed that, the reflection coefficient is 100 % at dm/d = 0 while the transmission coefficient = 0 (wall case). The less reflection at dm/d = 1 while the transmission is maximum (pile case). Therefore, the efficiency of this type surpasses the efficiency of double rows of pile breakwater, which has the same porosity. The target protection can be achieved through the best choice for the permeability area.

Overall, the agreement is seen to be satisfactory when the chamber width is a proportion of both water depth and wave length, although there is some scatter between the experimental and predicted results. Therefore, the numerical model is able to adequately reproduce the most important features of the experimental results, including the energy dissipation through the double vertical slotted barrier.

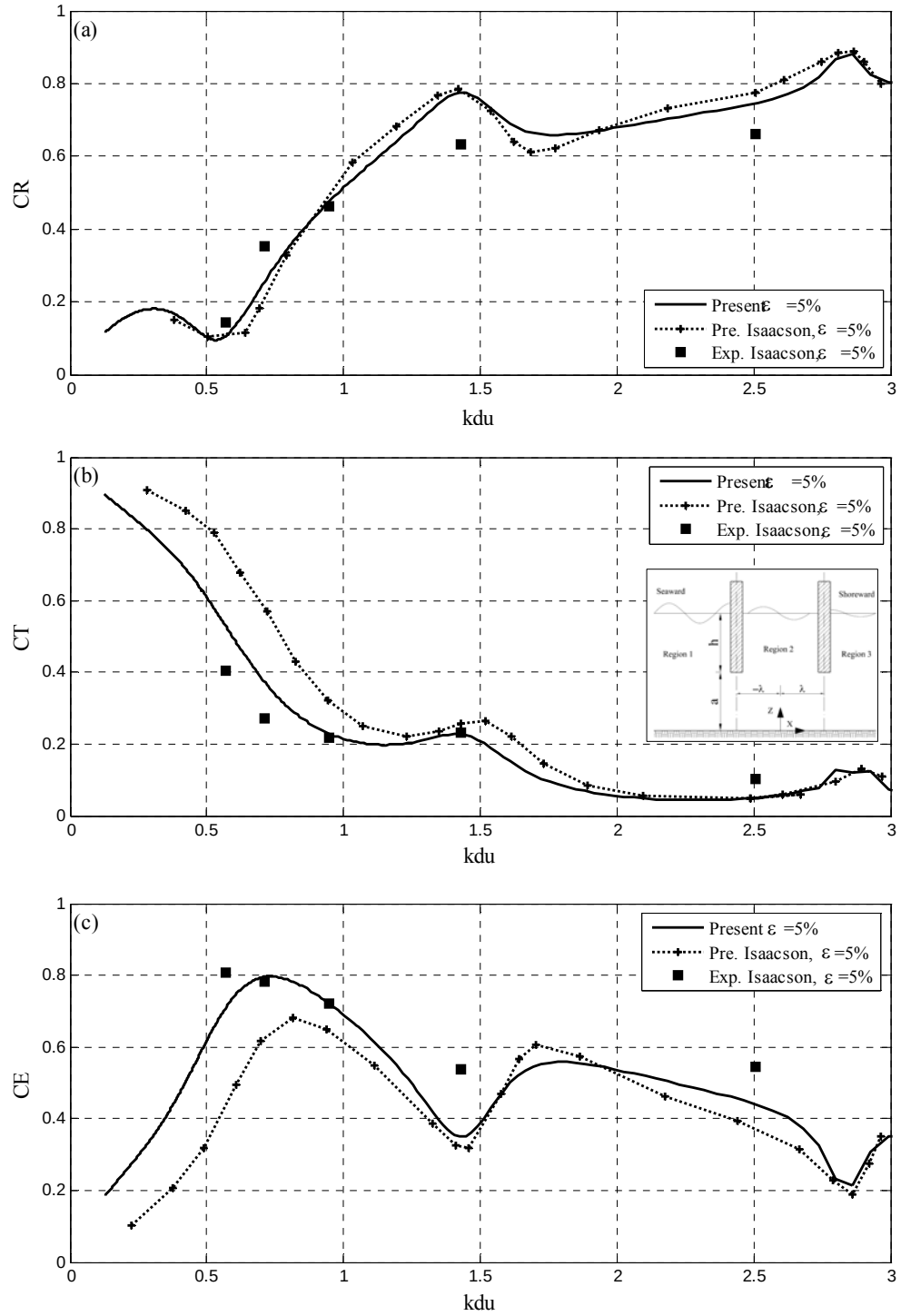

Figure 5.20: Comparison of the present results with prediction and experimental results of Isaacson et al. (1999) as a function of ($k\,du$) for ε = 5 % , du = 0.5d, h_i /L = 0.07 λ/du = 1.1, f = 2 and cm = 0.
(a) Reflection coefficient,
(b) Transmission coefficient and
(c) Energy dissipation coefficient.

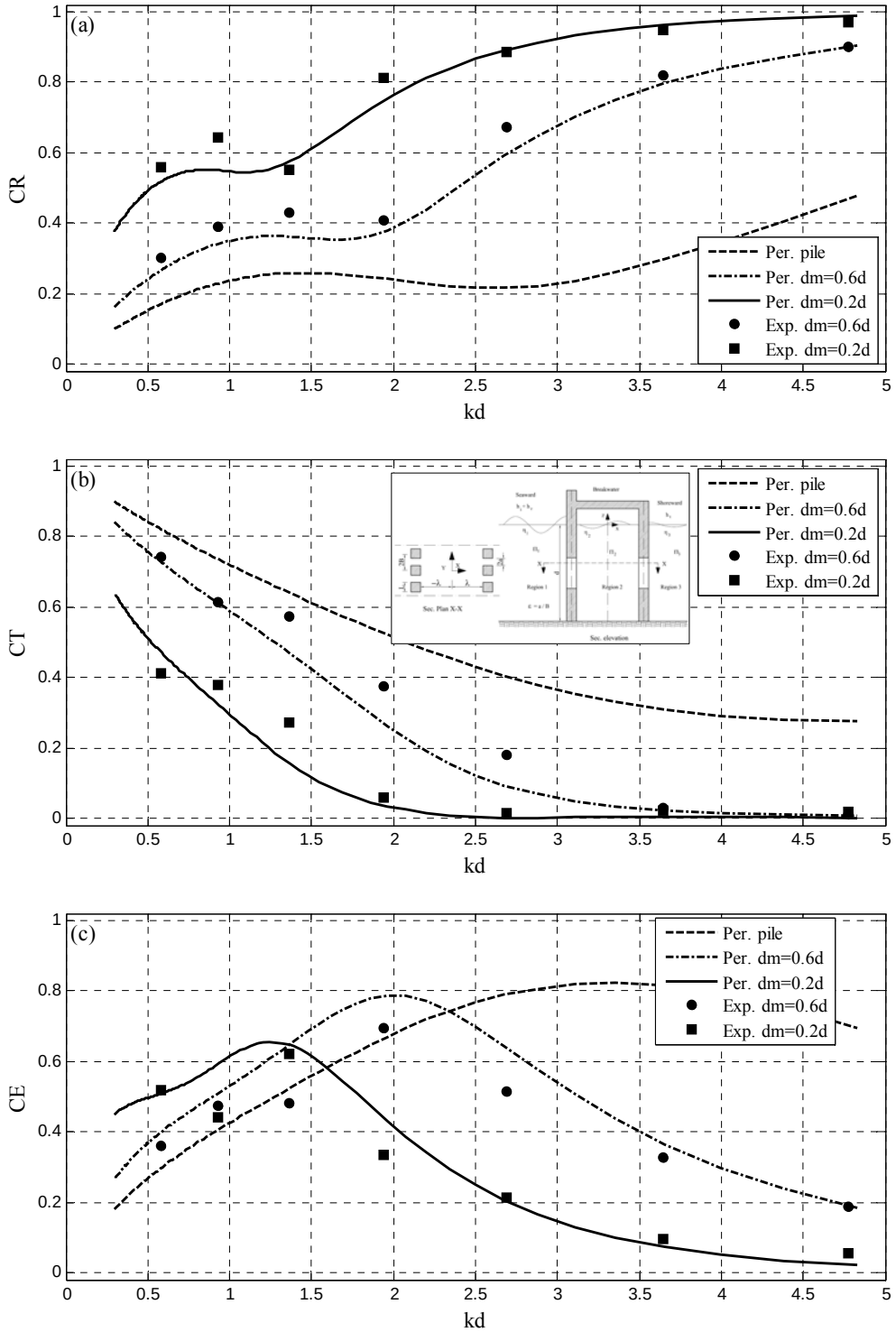

Figure 5.21: Comparison of experimental and prediction results as function of (*kd*) for various middle permeable part with $\varepsilon = 0.5$, $\lambda/d = 0.25$, $f = 2$ and $cm = 0$.

(a) Reflection coefficient,
(b) Transmission coefficient and
(c) Energy dissipation coefficient.

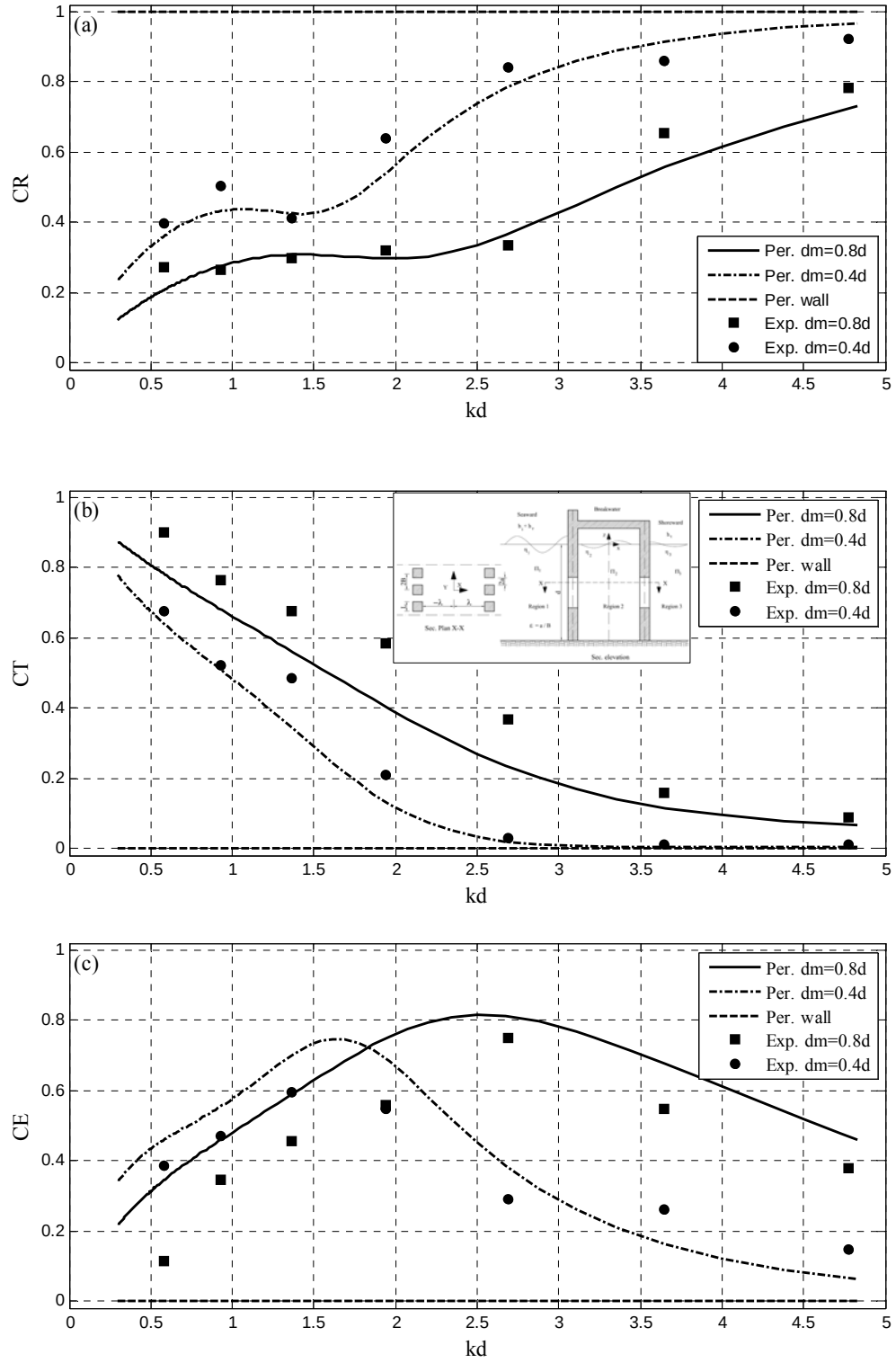

Figure 5.22: Comparison of experimental and prediction results as function of (kd) for various middle permeable part with $\varepsilon = 0.5$, $\lambda/d = 0.25$, $f = 2$ and $cm = 0$.

(a) Reflection coefficient,
(b) Transmission coefficient and
(c) Energy dissipation coefficient.

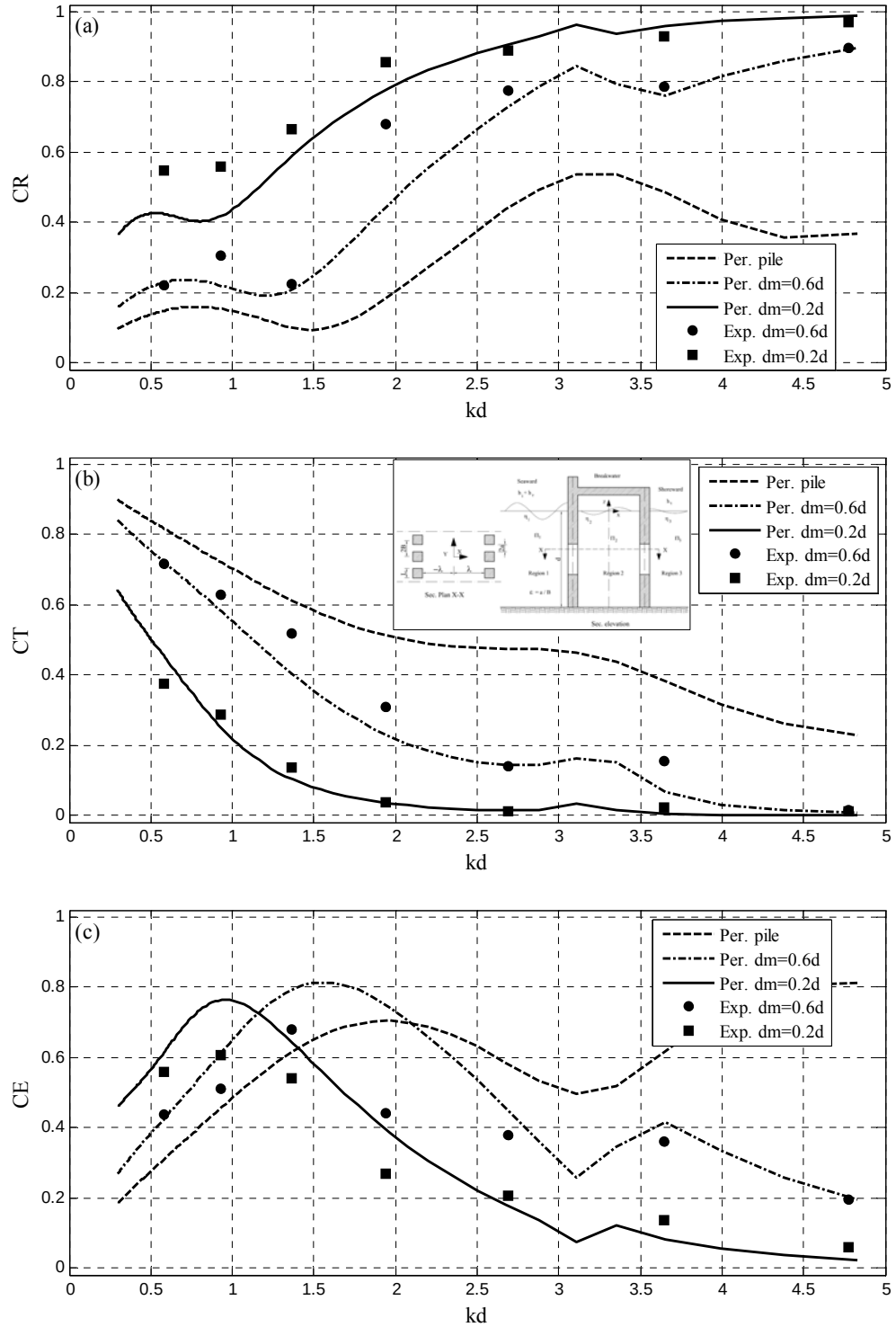

Figure 5.23: Comparison of experimental and prediction results as function of (kd) for various middle permeable part with $\varepsilon = 0.5$, $\lambda/d = 0.5$, $f = 2$ and $cm = 0$.
(a) Reflection coefficient,
(b) Transmission coefficient and
(c) Energy dissipation coefficient.

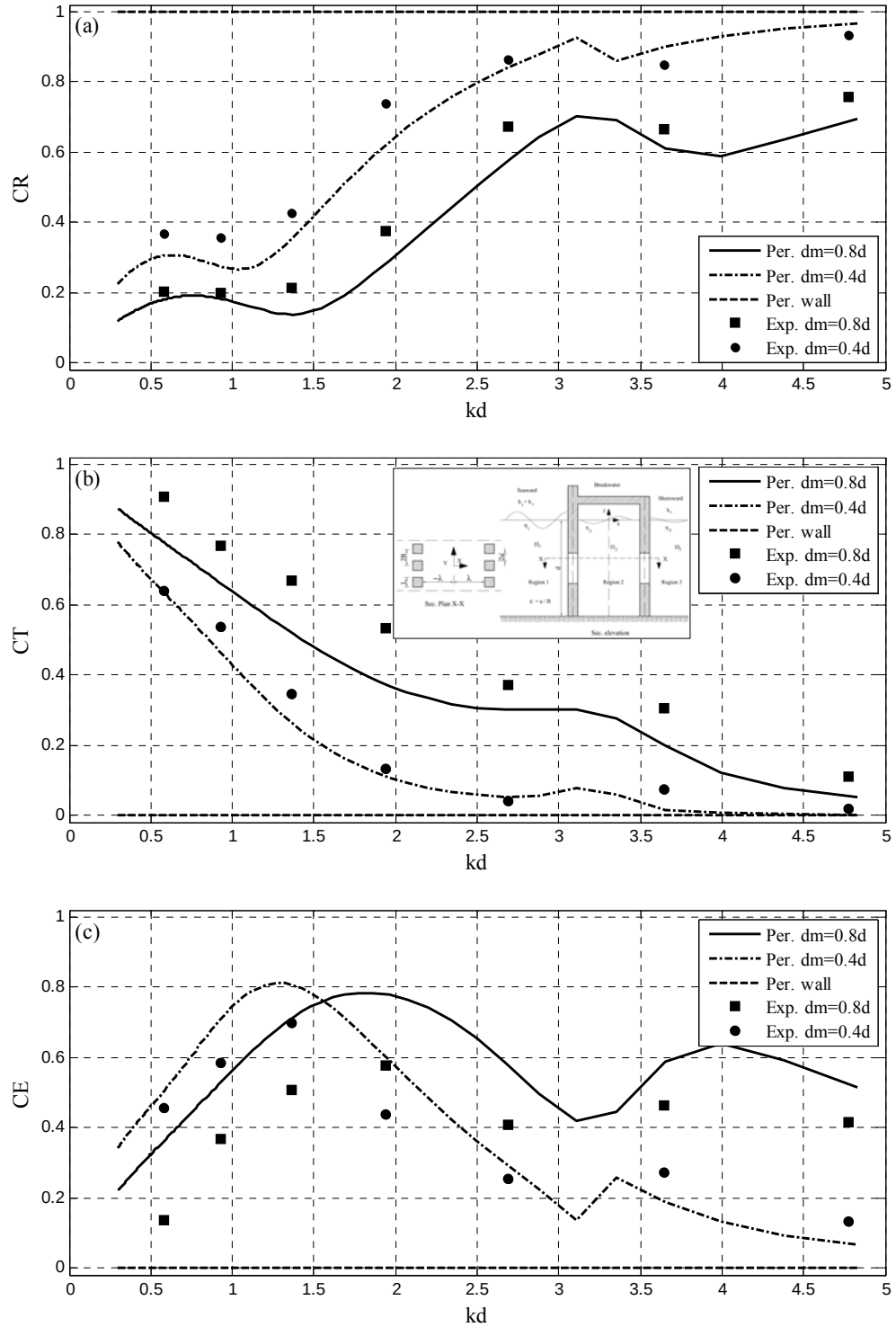

Figure 5.24: Comparison of experimental and prediction results as function of (kd) for various middle permeable part with $\varepsilon = 0.5$, $\lambda/d = 0.5$, $f = 2$ and $cm = 0$.
(a) Reflection coefficient,
(b) Transmission coefficient and
(c) Energy dissipation coefficient.

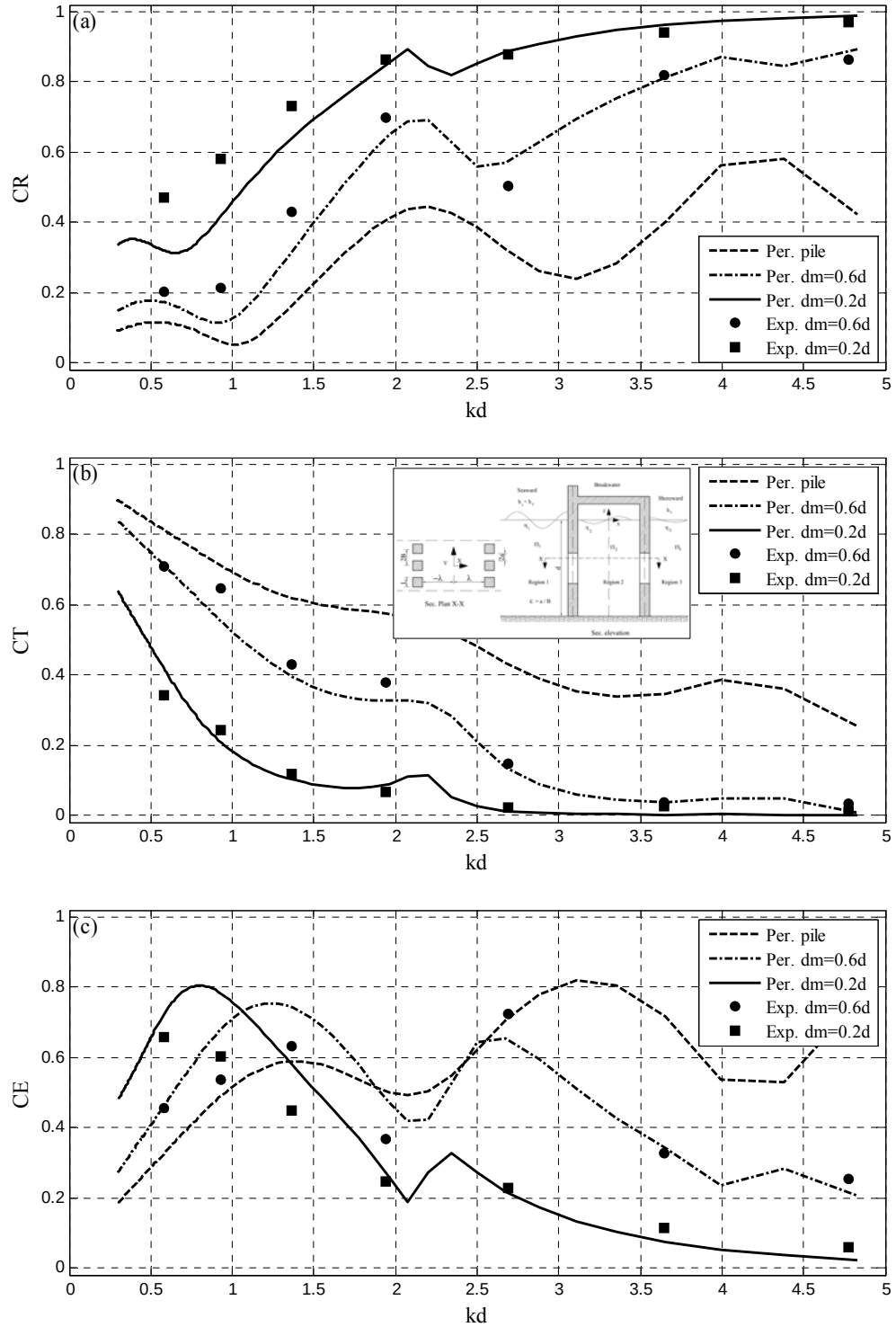

Figure 5.25: Comparison of experimental and prediction results as function of (*kd*) for various middle permeable part with $\varepsilon = 0.5$, $\lambda/d = 0.75$, $f = 2$ and $cm = 0$.
(a) Reflection coefficient,
(b) Transmission coefficient and
(c) Energy dissipation coefficient.

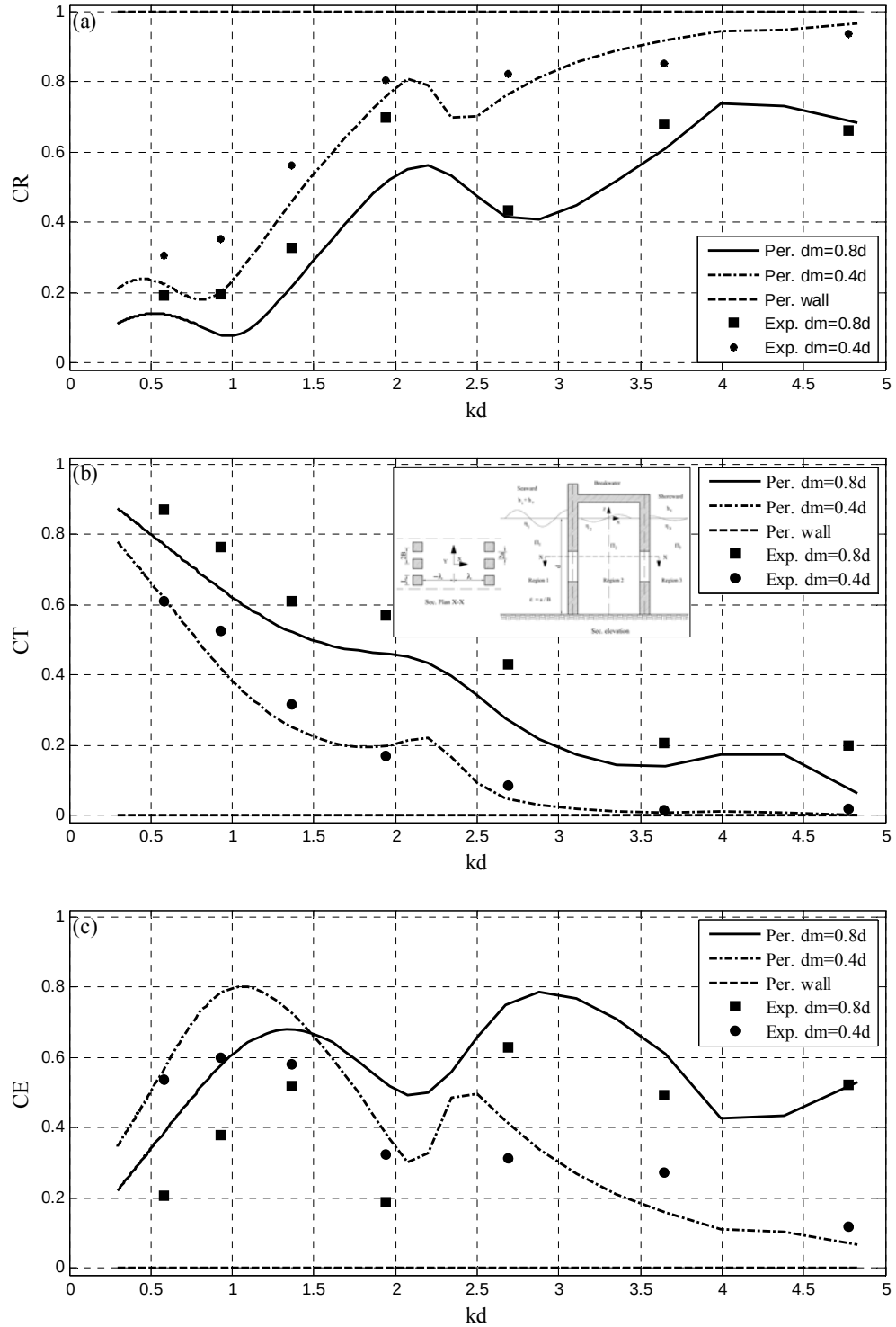

Figure 5.26: Comparison of experimental and prediction results as function of (kd) for various middle permeable part with $\varepsilon = 0.5$, $\lambda/d = 0.75$, $f = 2$ and $cm = 0$.
(a) Reflection coefficient,
(b) Transmission coefficient and
(c) Energy dissipation coefficient.

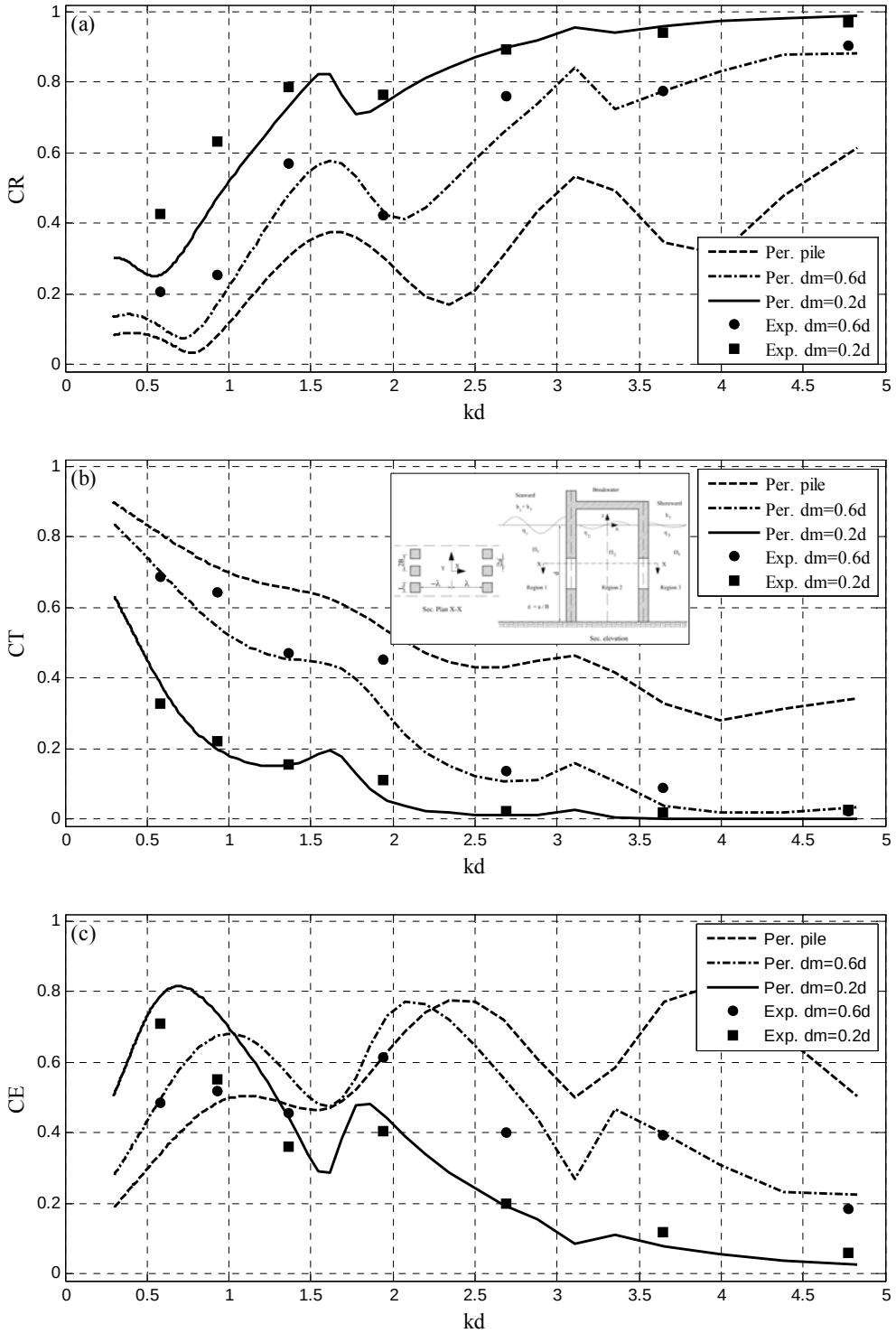

Figure 5.27: Comparison of experimental and prediction results as function of (kd) for various middle permeable part with $\varepsilon = 0.5$, $\lambda/d = 1$, $f = 2$ and $cm = 0$.
(a) Reflection coefficient,
(b) Transmission coefficient and
(c) Energy dissipation coefficient.

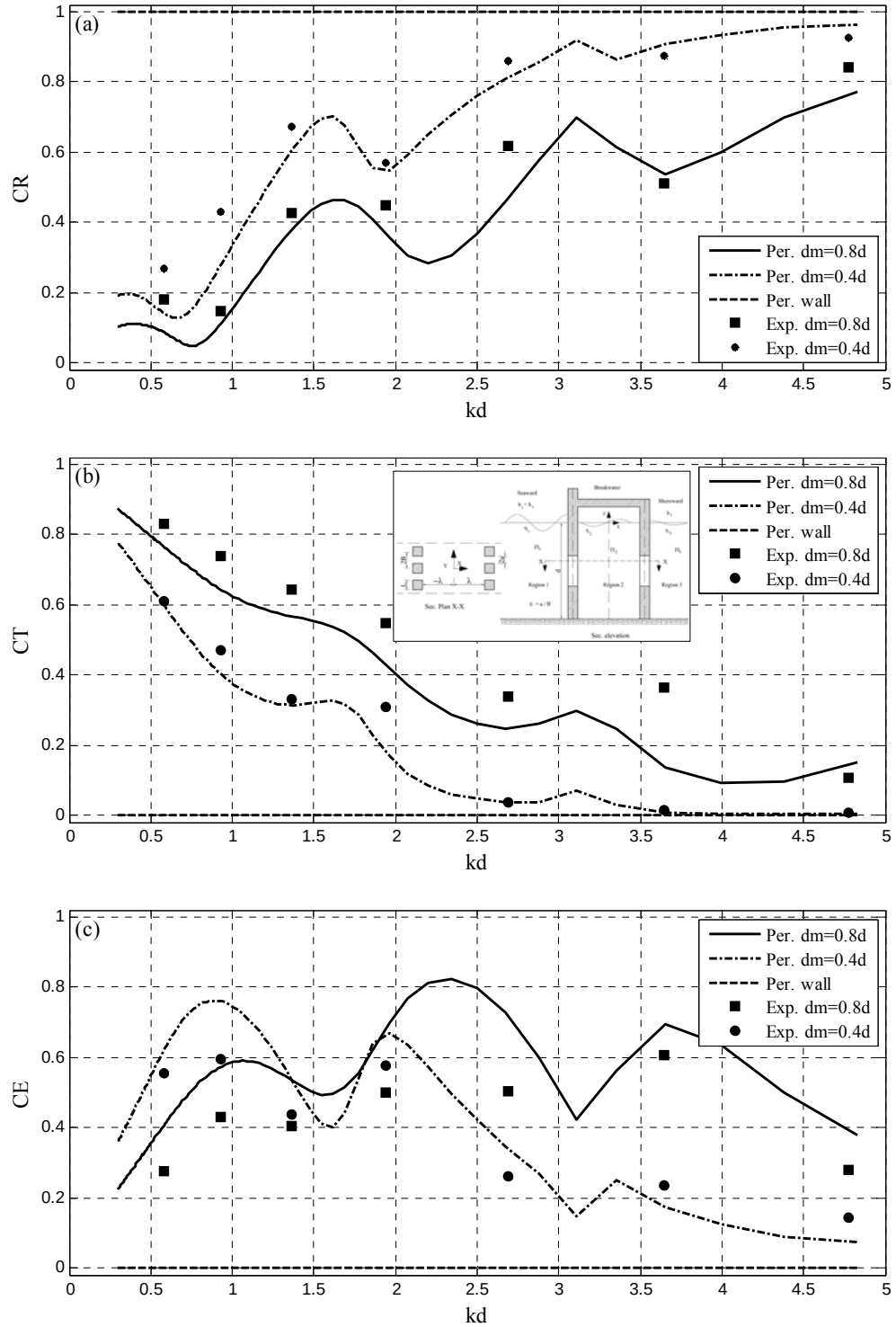

Figure 5.28: Comparison of experimental and prediction results as function of (kd) for various middle permeable part with $\varepsilon = 0.5$, $\lambda/d = 1$, $f = 2$ and $cm = 0$.
(a) Reflection coefficient,
(b) Transmission coefficient and
(c) Energy dissipation coefficient.

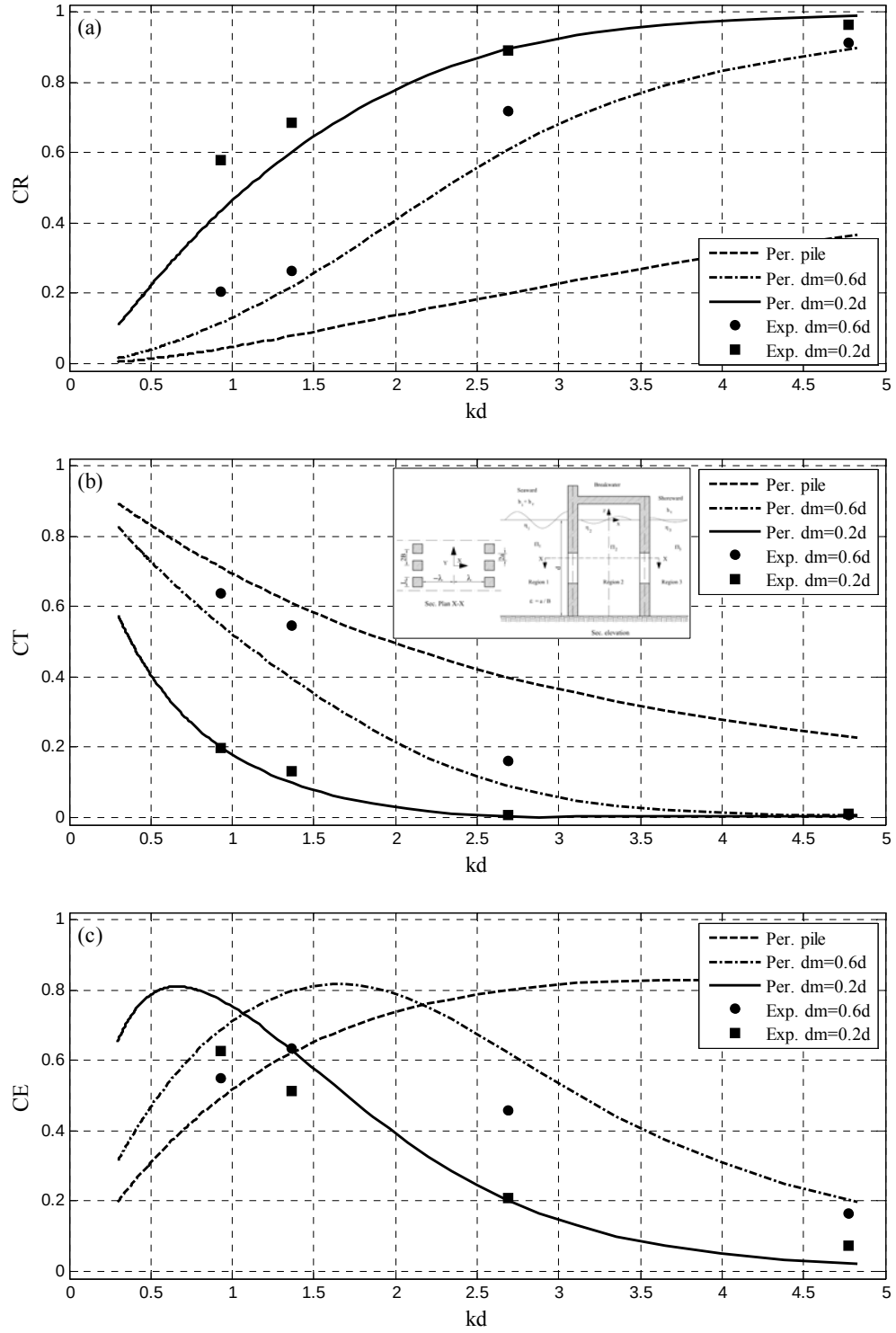

Figure 5.29: Comparison of experimental and prediction results as function of (*kd*) for various middle permeable part with $\varepsilon = 0.5$, $\lambda/L = 0.125$, $f = 2$ and $cm = 0$.

(a) Reflection coefficient,
(b) Transmission coefficient and
(c) Energy dissipation coefficient.

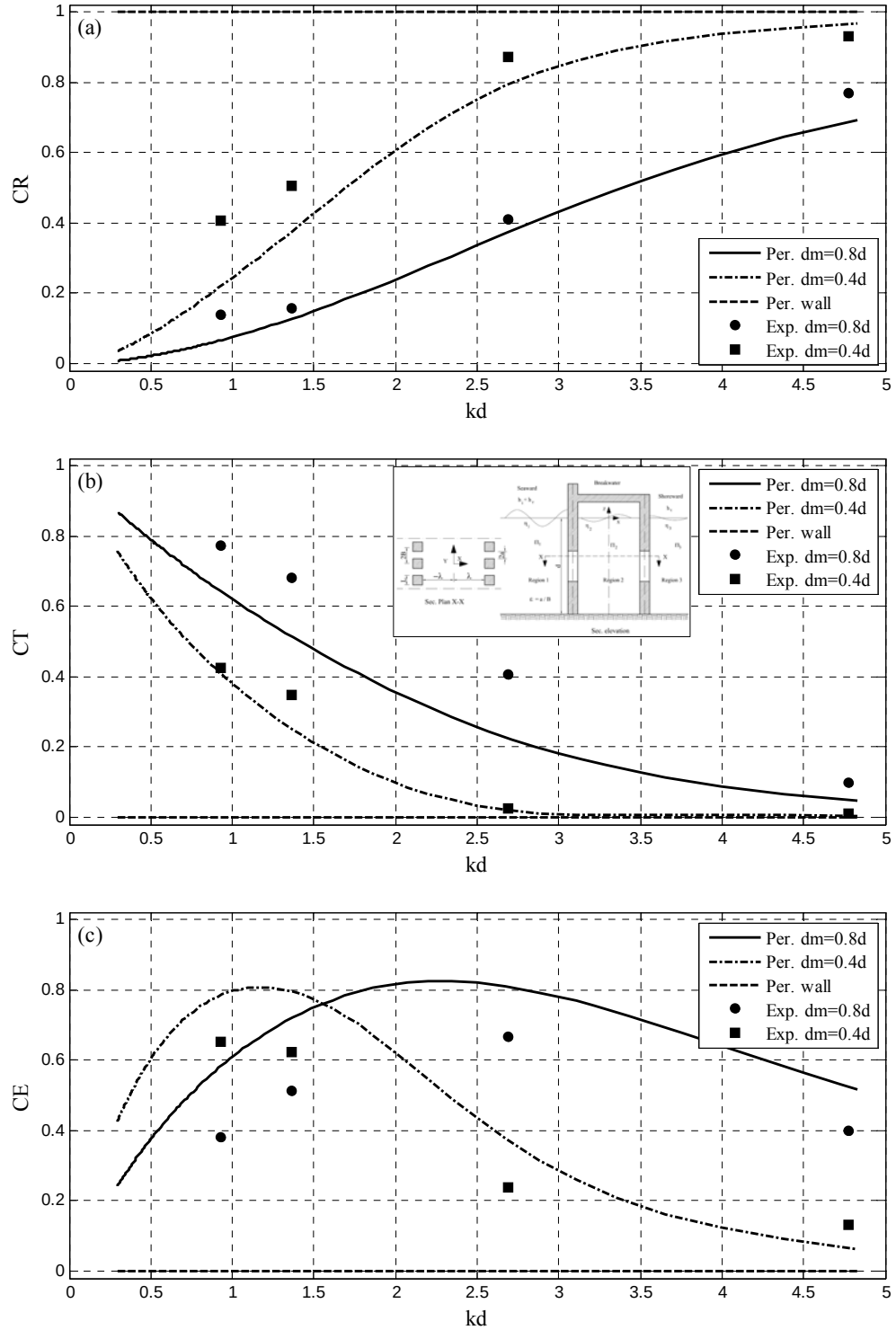

Figure 5.30: Comparison of experimental and prediction results as function of (*kd*) for various middle permeable part with $\varepsilon = 0.5$, $\lambda/L = 0.125$, $f = 2$ and $cm = 0$.

(a) Reflection coefficient,
(b) Transmission coefficient and
(c) Energy dissipation coefficient.

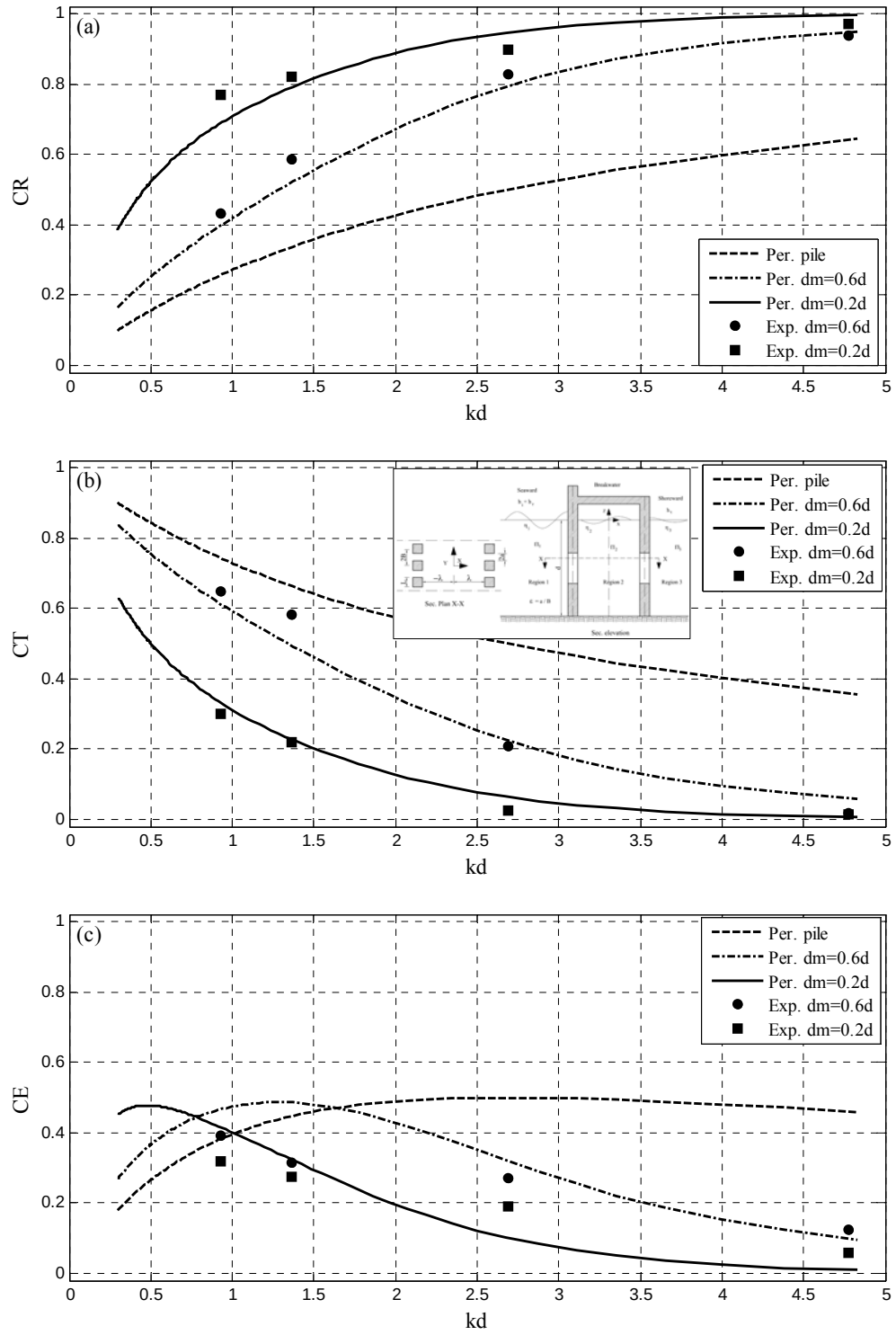

Figure 5.31: Comparison of experimental and prediction results as function of (*kd*) for various middle permeable part with $\varepsilon = 0.5$, $\lambda/L = 0.25$, $f = 2$ and $cm = 0$.

(a) Reflection coefficient,
(b) Transmission coefficient and
(c) Energy dissipation coefficient.

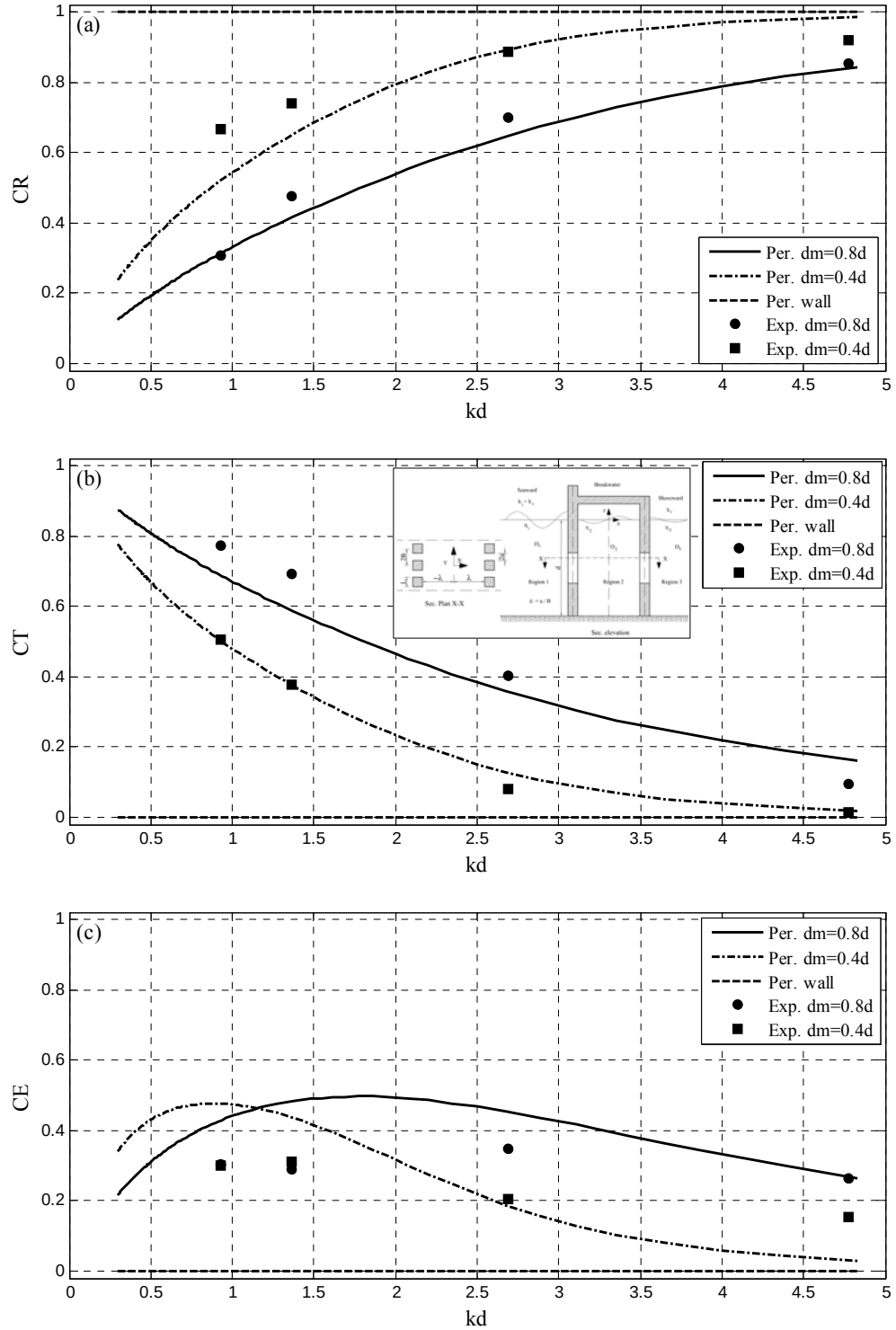

Figure 5.32: Comparison of experimental and prediction results as function of (*kd*) for various middle permeable part with $\varepsilon = 0.5$, $\lambda/L = 0.25$, $f = 2$ and $cm = 0$.

(a) Reflection coefficient,

(b) Transmission coefficient and

(c) Energy dissipation coefficient.

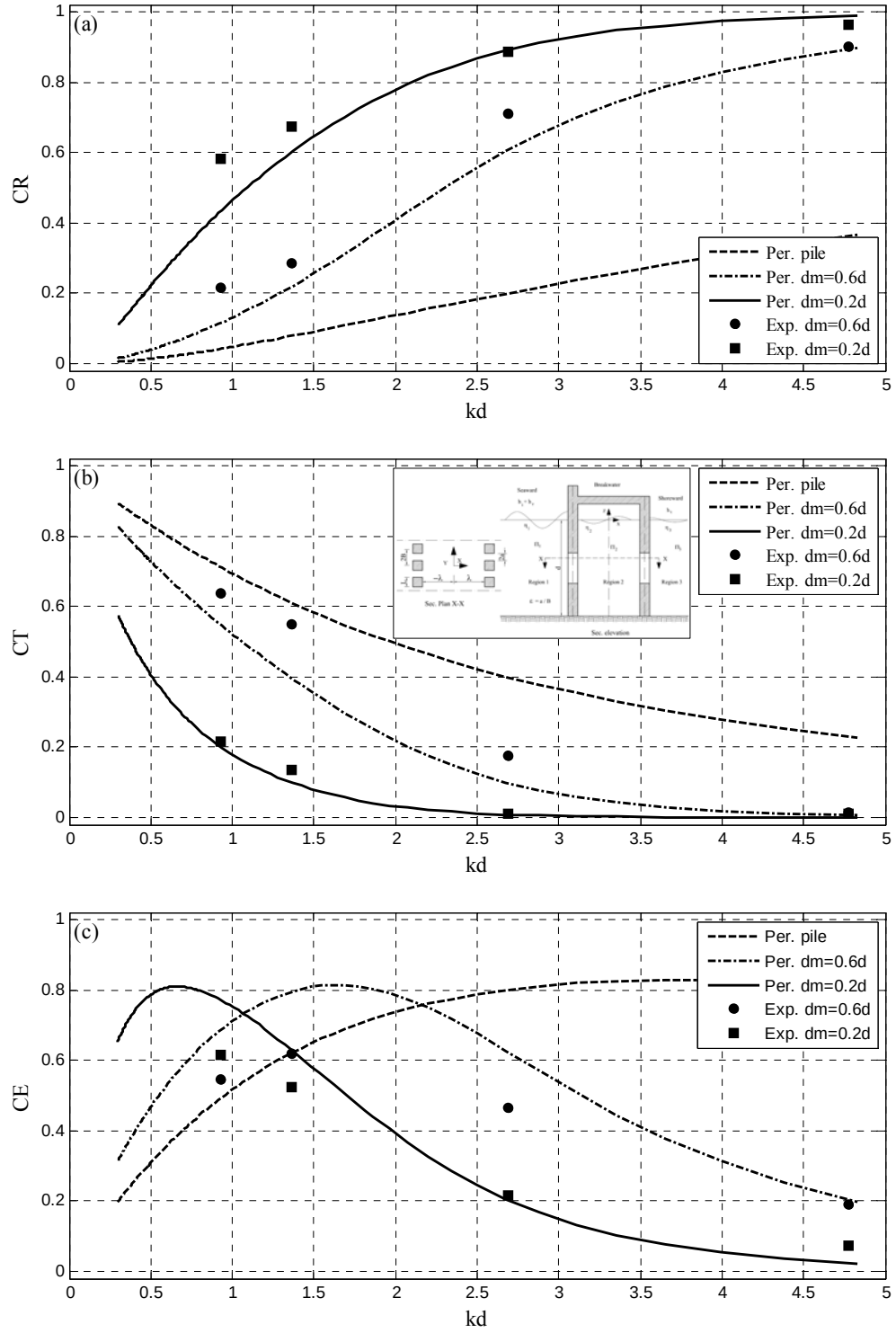

Figure 5.33: Comparison of experimental and prediction results as function of (*kd*) for various middle permeable part with $\varepsilon = 0.5$, $\lambda/L = 0.375$, $f = 2$ and $cm = 0$.

(a) Reflection coefficient,
(b) Transmission coefficient and
(c) Energy dissipation coefficient.

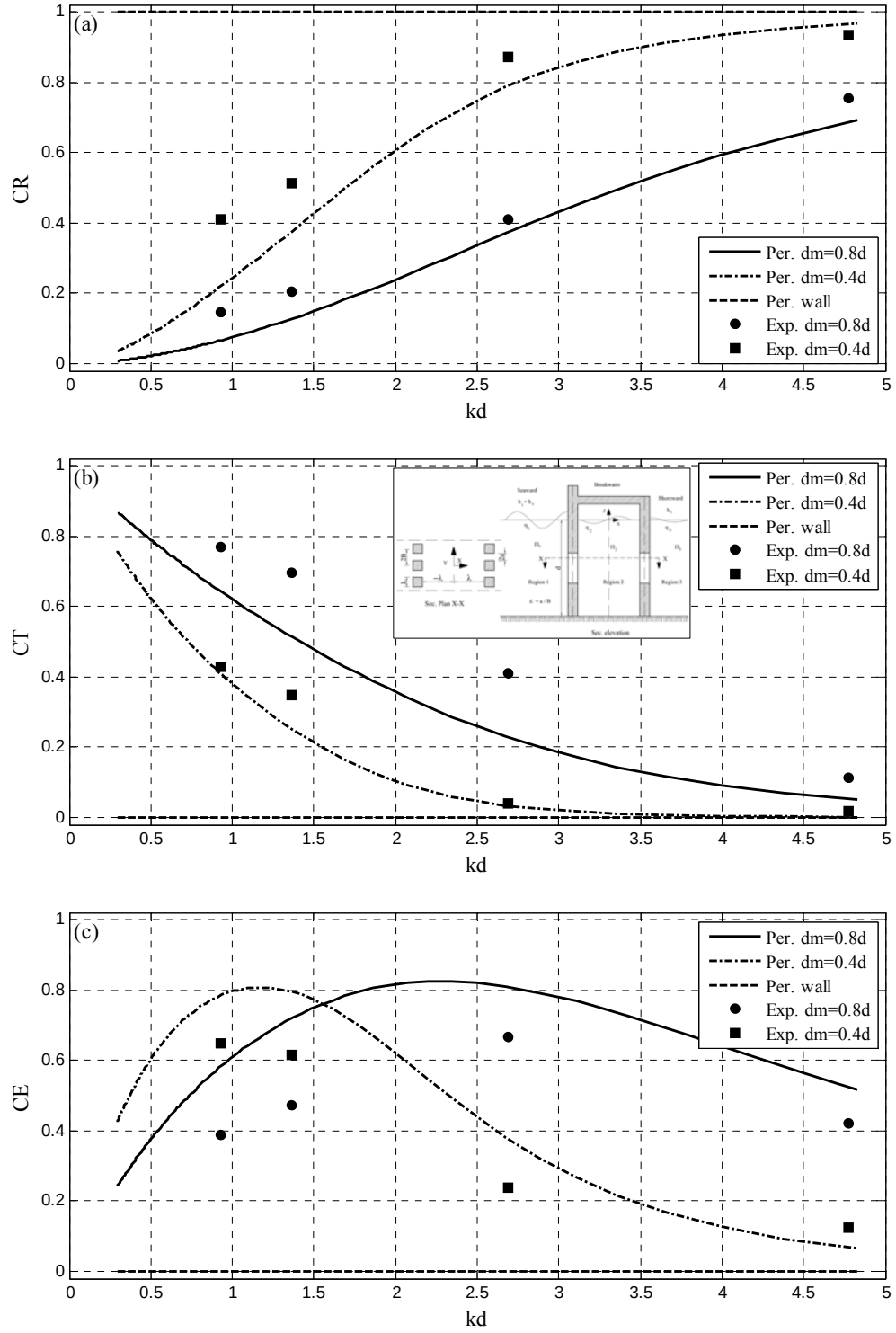

Figure 5.34: Comparison of experimental and prediction results as function of (*kd*) for various middle permeable part with $\varepsilon = 0.5$, $\lambda/L = 0.375$, $f = 2$ and $cm = 0$.

(a) Reflection coefficient,

(b) Transmission coefficient and

(c) Energy dissipation coefficient.

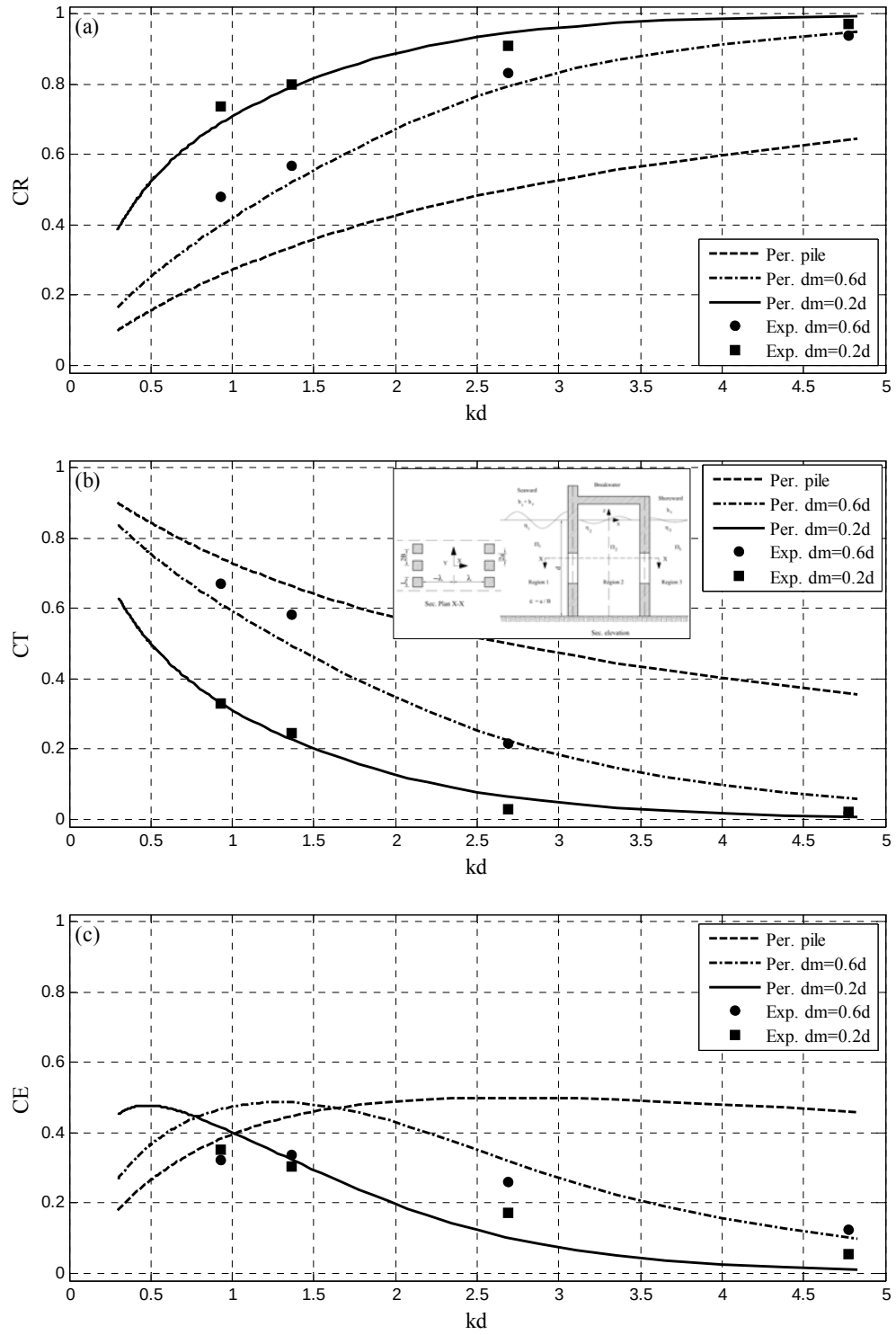

Figure 5.35: Comparison of experimental and prediction results as function of (*kd*) for various middle permeable part with constant $\varepsilon = 0.5$, $\lambda/L = 0.5$, $f = 2$ and $cm = 0$.
(a) Reflection coefficient,
(b) Transmission coefficient and
(c) Energy dissipation coefficient.

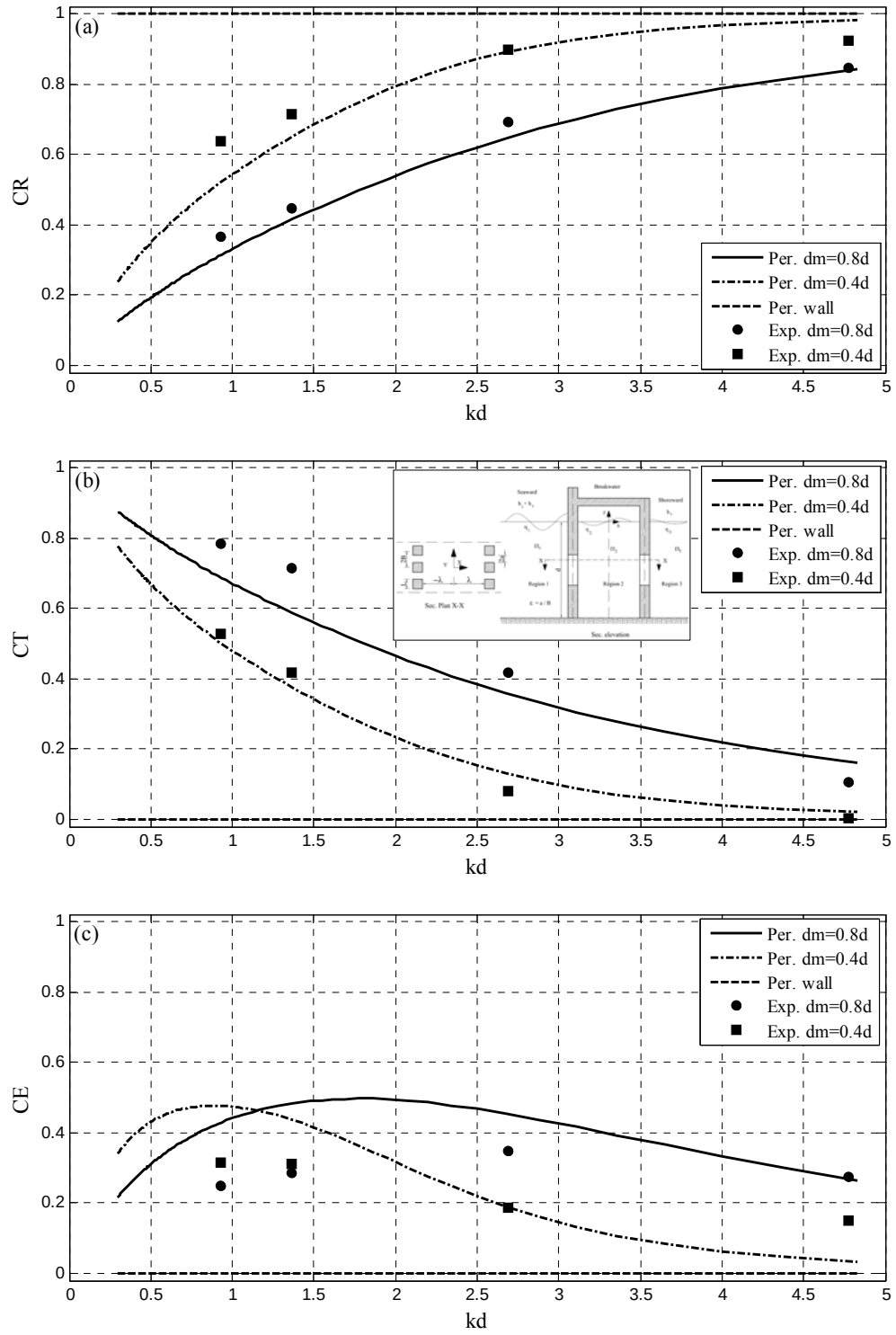

Figure 5.36: Comparison of experimental and prediction results as function of (*kd*) for various middle permeable part with $\varepsilon = 0.5$, $\lambda/L = 0.5$, $f = 2$ and $cm = 0$.

(a) Reflection coefficient,
(b) Transmission coefficient and
(c) Energy dissipation coefficient.

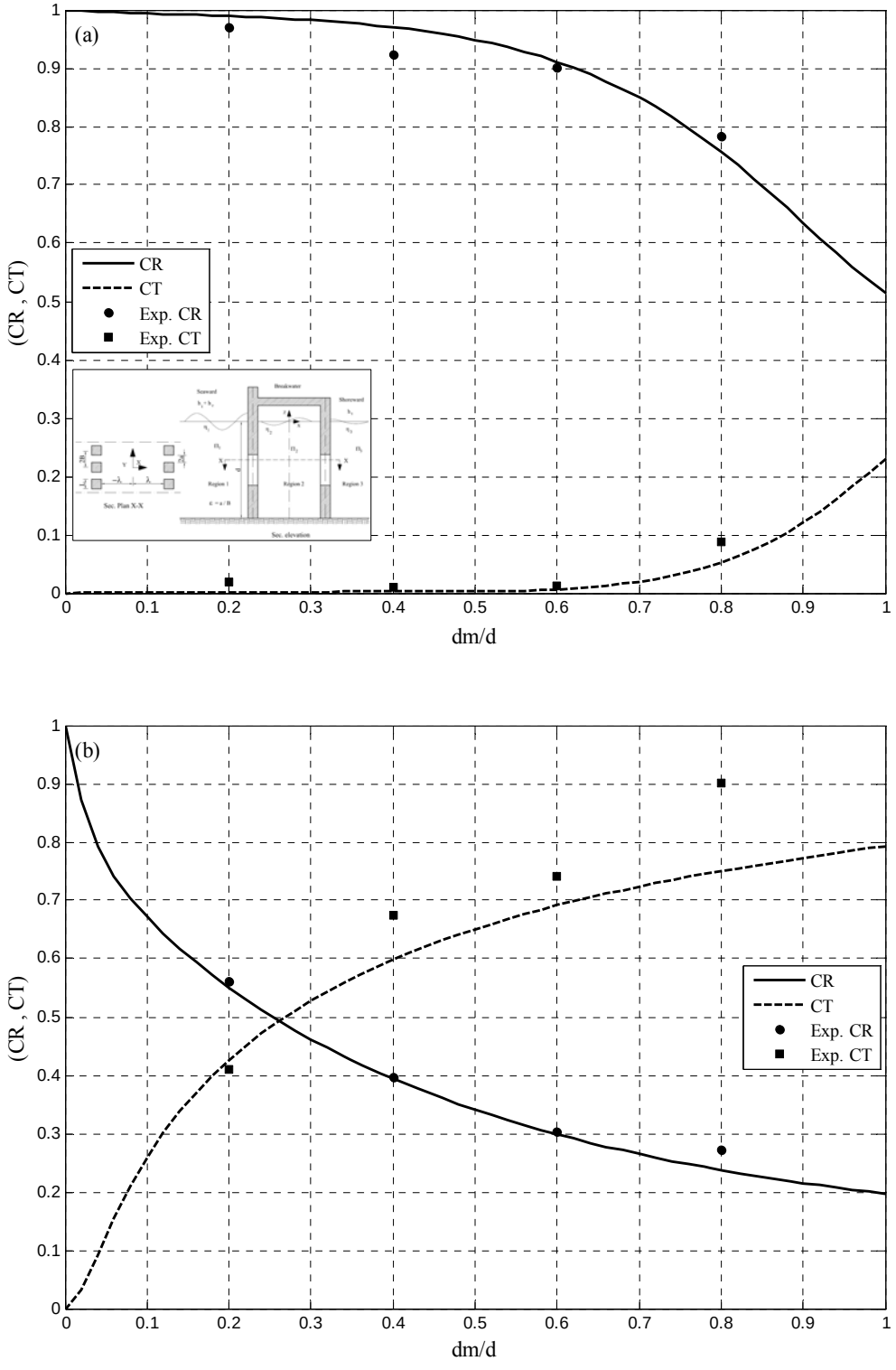

Figure 5.37: Comparison between measured and predicted reflection and transmission coefficients as a function of relative permeable middle part *dm/d* and with constant $\varepsilon = 0.5$, $\lambda/d = 0.25$, $f = 2$ and $cm = 0$.
(a) at wave period $T = 0.5$ s and
(b) at wave period $T = 2$ s.

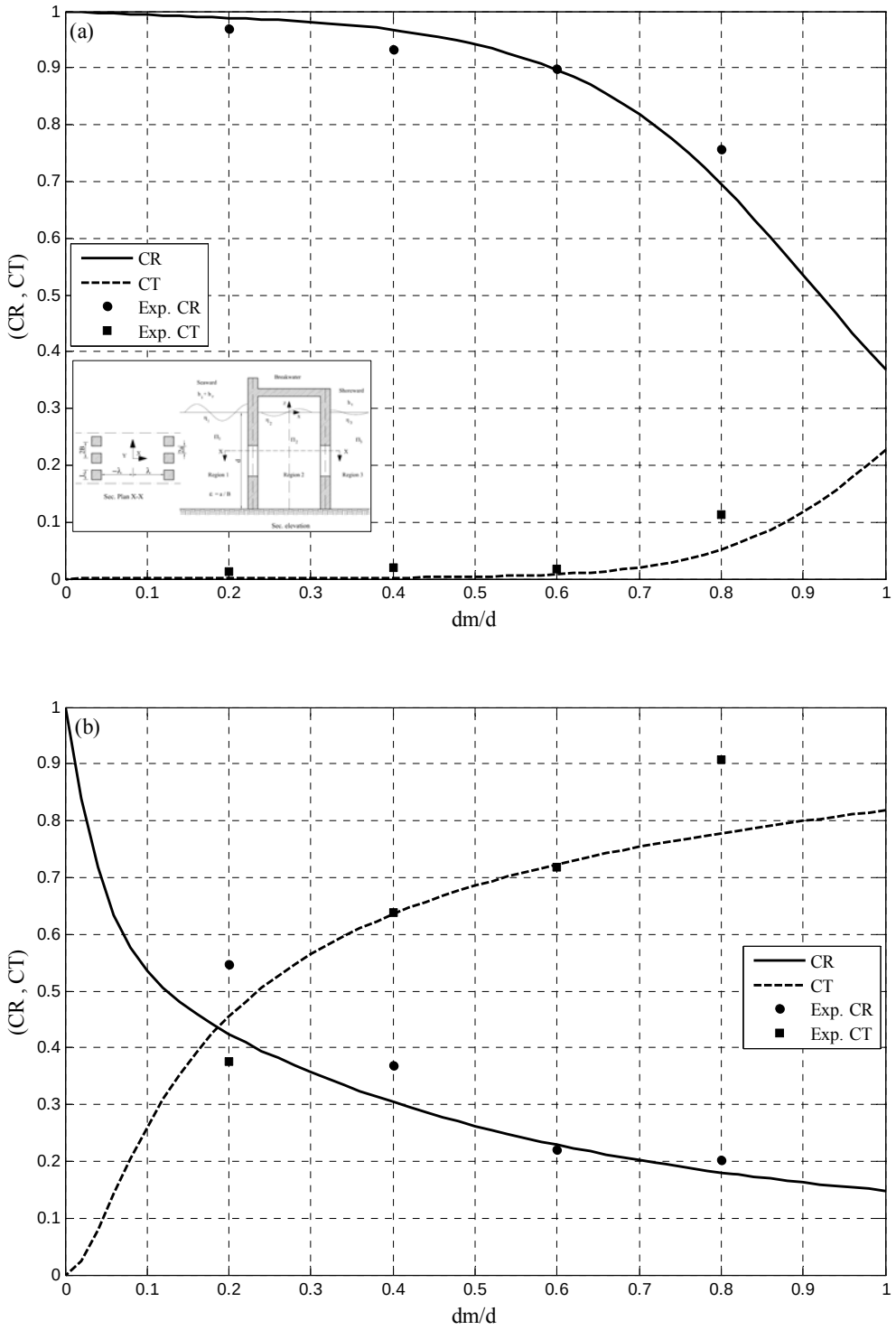

Figure 5.38: Comparison between measured and predicted reflection and transmission coefficients as a function of relative permeable middle part *dm/d* and with constant ε = 0.5, λ/d = 0.5, f = 2 and *cm* = 0.
(a) at wave period T = 0.5 s and
(b) at wave period T = 2 s.

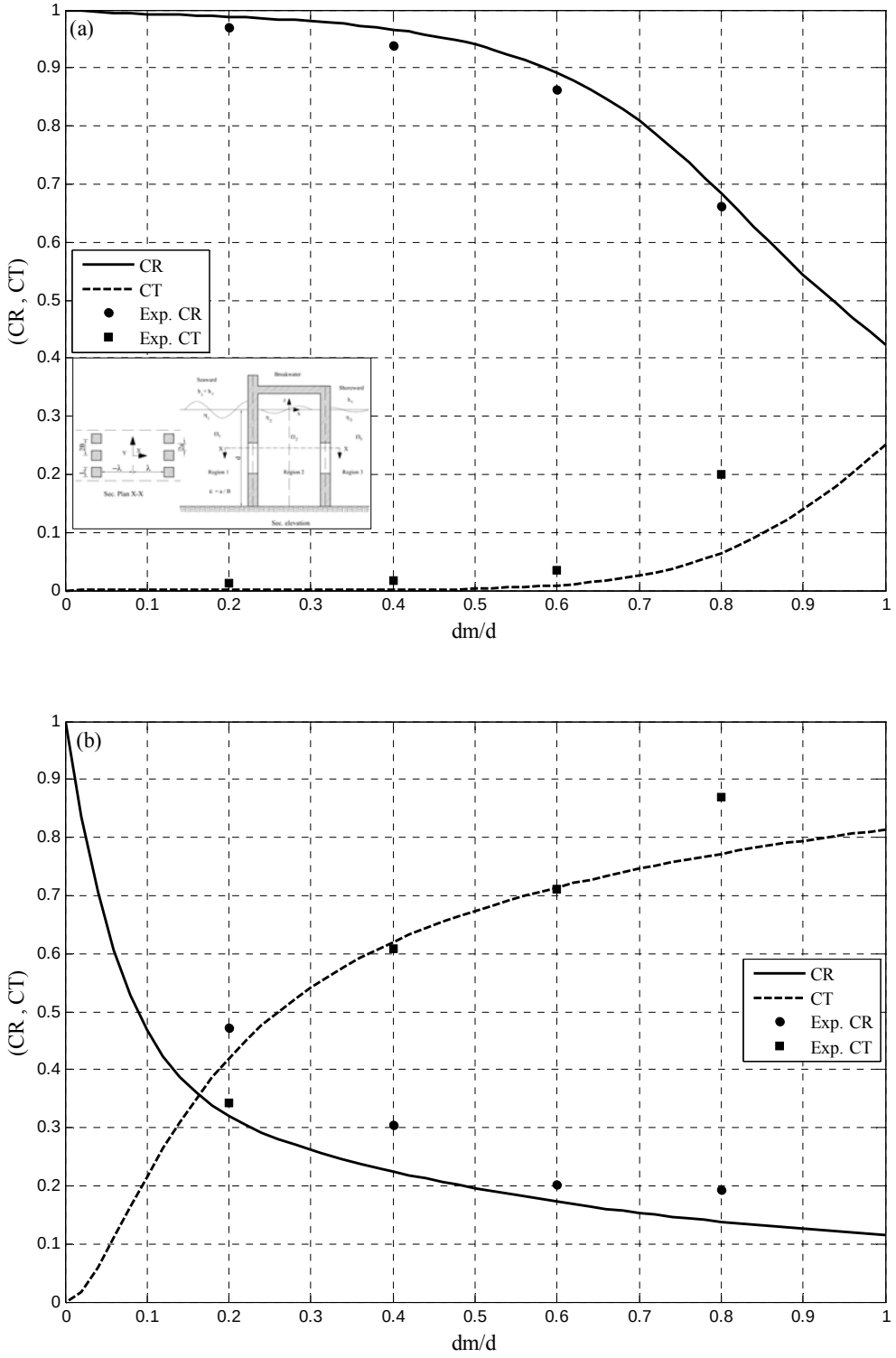

Figure 5.39: Comparison between measured and predicted reflection and transmission coefficients as a function of relative permeable middle part dm/d and $\varepsilon = 0.5$, $\lambda/d = 0.75$, $f = 2$ and $cm = 0$.
(a) at wave period $T = 0.5$ s and
(b) at wave period $T = 2$ s.

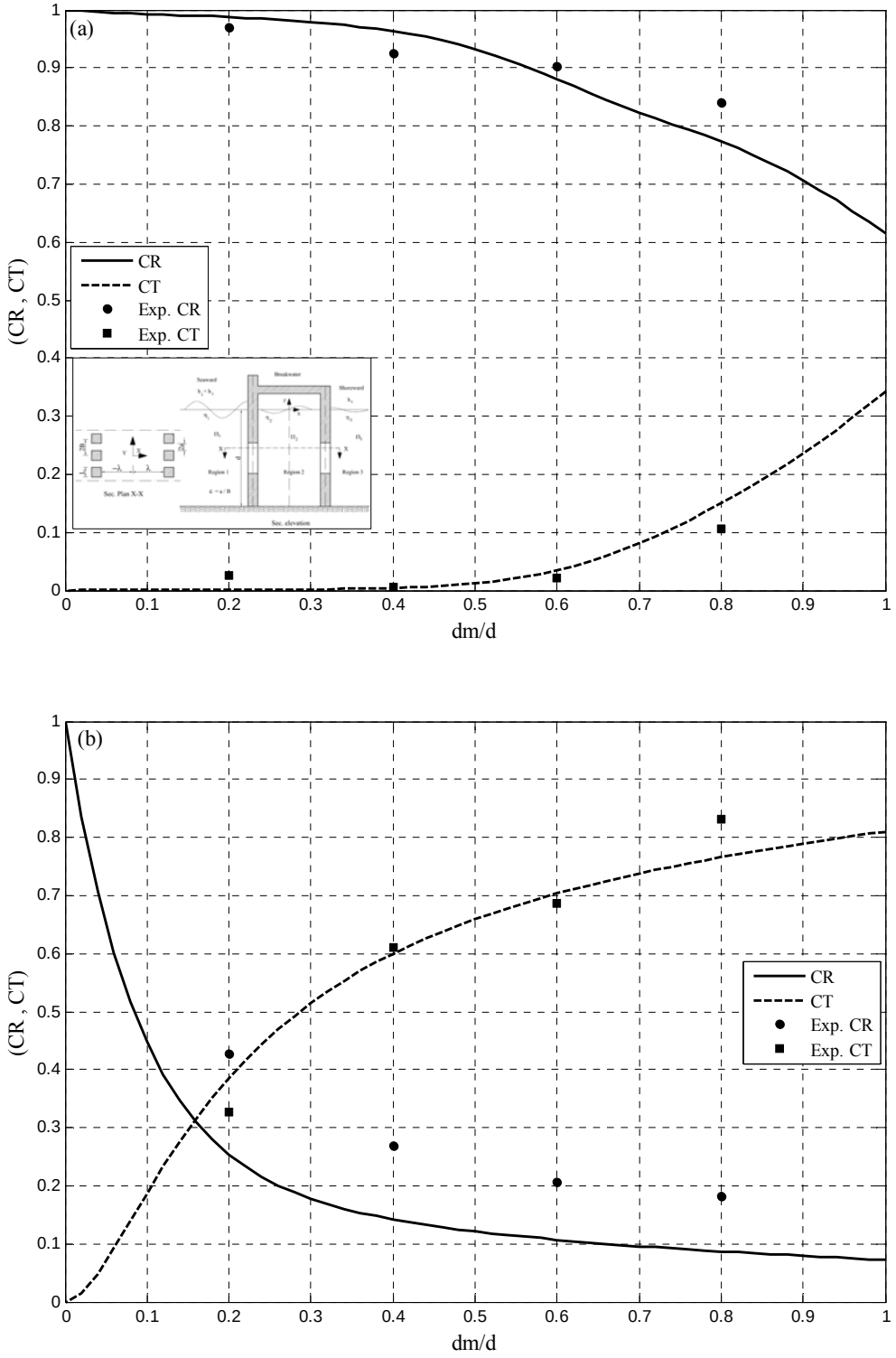

Figure 5.40: Comparison between measured and predicted reflection and transmission coefficients as a function of relative permeable middle part dm/d and $\varepsilon = 0.5$, $\lambda/d = 1$, $f = 2$ and $cm = 0$.
(a) at wave period $T = 0.5$ s and
(b) at wave period $T = 2$ s

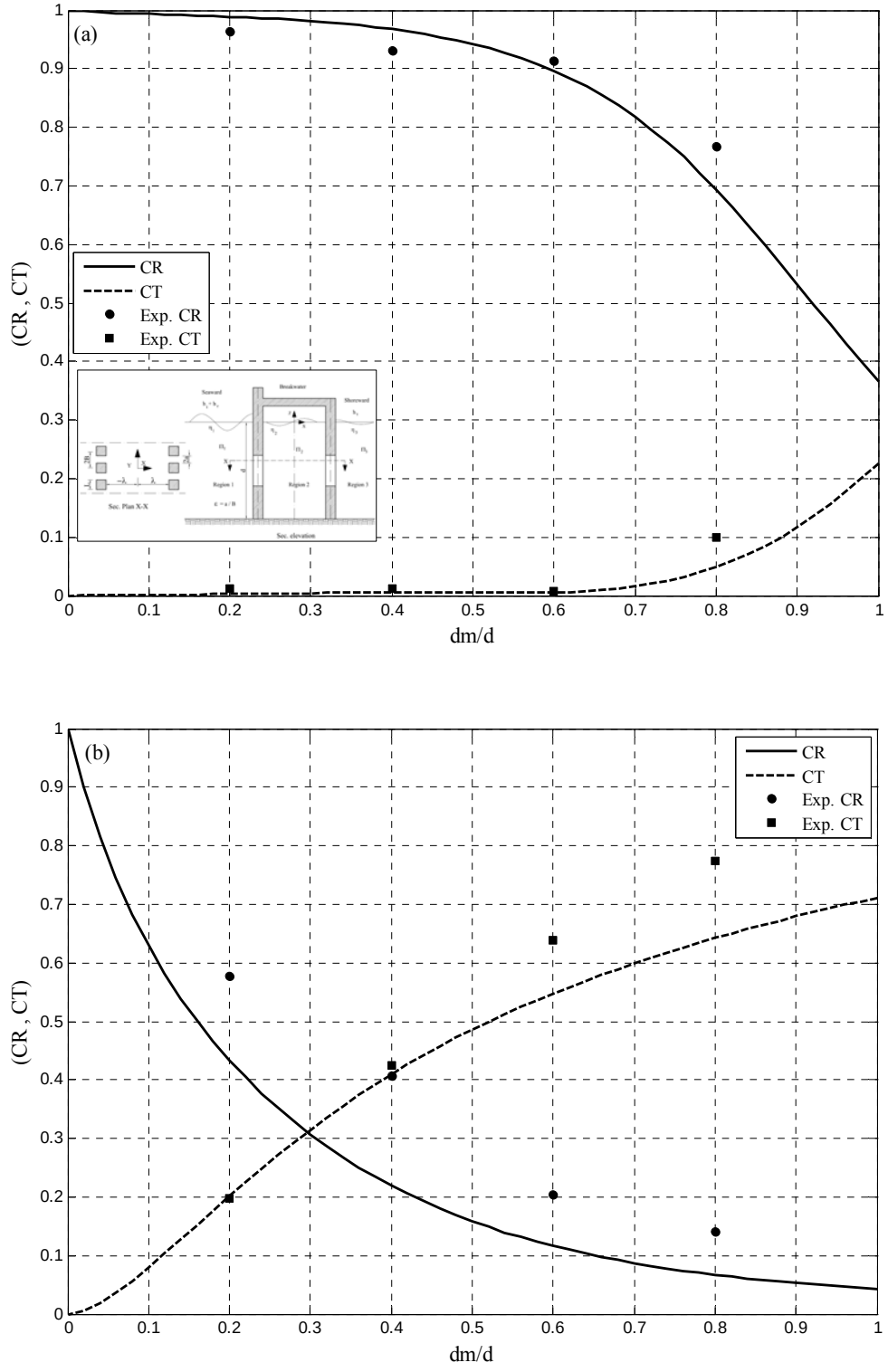

Figure 5.41: Comparison between measured and predicted reflection and transmission coefficients as a function of relative permeable middle part dm/d, $\varepsilon = 0.5$, $\lambda/L=0.125$, $f = 2$ and $cm = 0$.
(a) at wave period $T = 0.5$ s and
(b) at wave period $T = 1.333$ s.

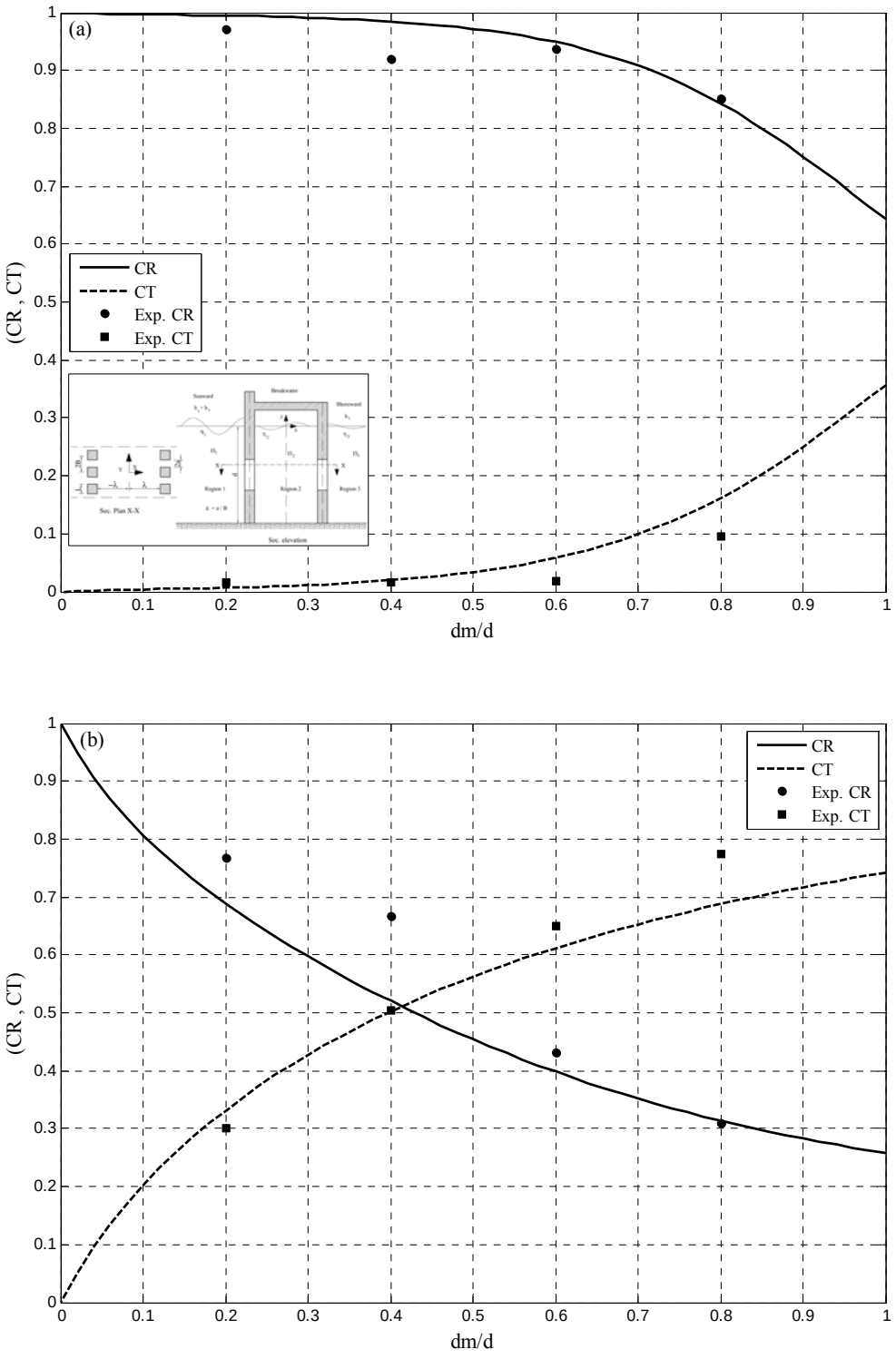

Figure 5.42: Comparison between measured and predicted reflection and transmission coefficients as a function of relative permeable middle part dm/d and $\varepsilon = 0.5$, $\lambda/L = 0.25$, $f = 2$ and $cm = 0$.
(a) at wave period $T = 0.5$ s and
(b) at wave period $T = 1.333$ s.

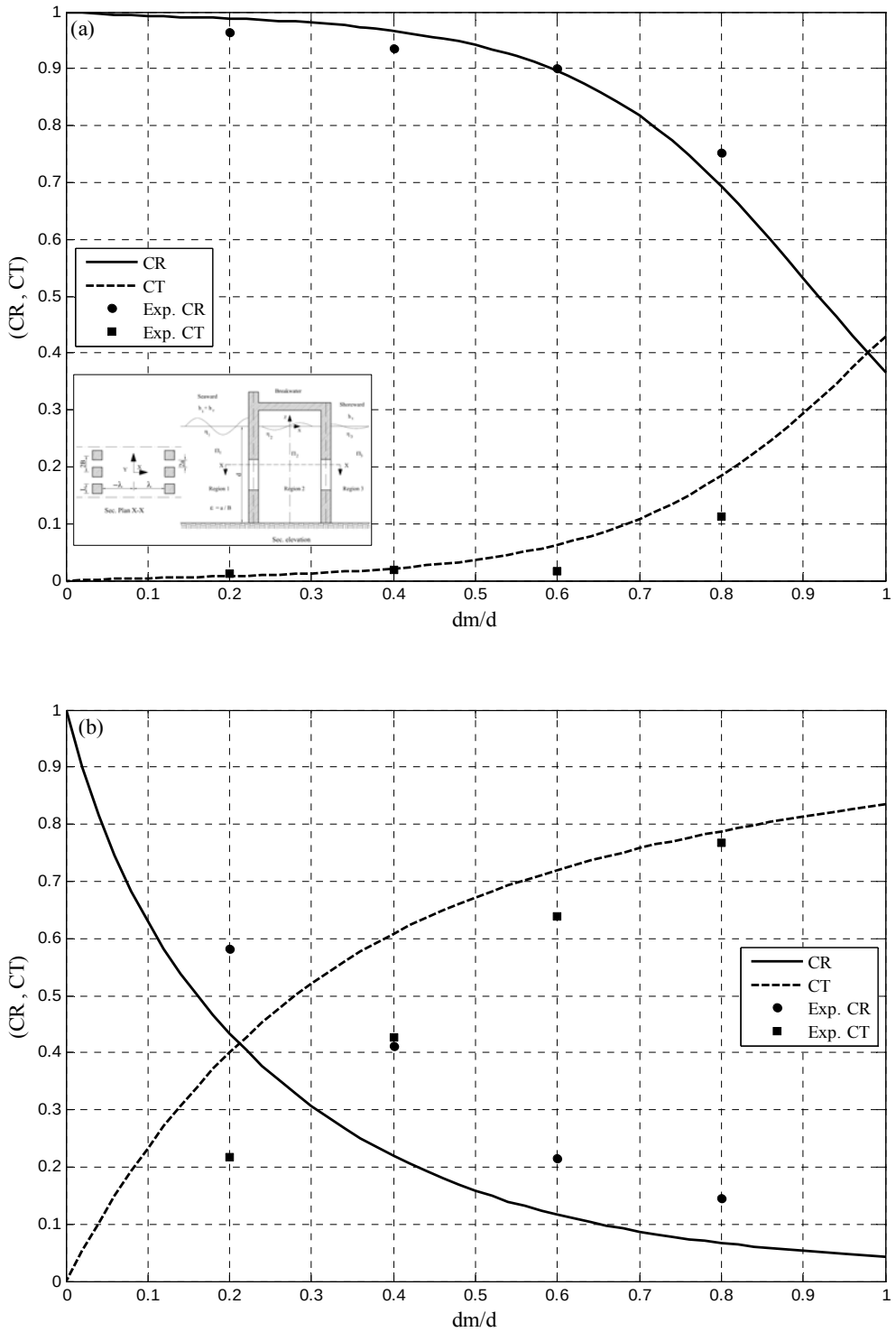

Figure 5.43: Comparison between measured and predicted reflection and transmission coefficients as a function of relative permeable middle part dm/d and $\varepsilon = 0.5$, $\lambda/L = 0.375$, $f = 2$ and $cm = 0$.
(a) at wave period $T = 0.5$ s and
(b) at wave period $T = 1.333$ s.

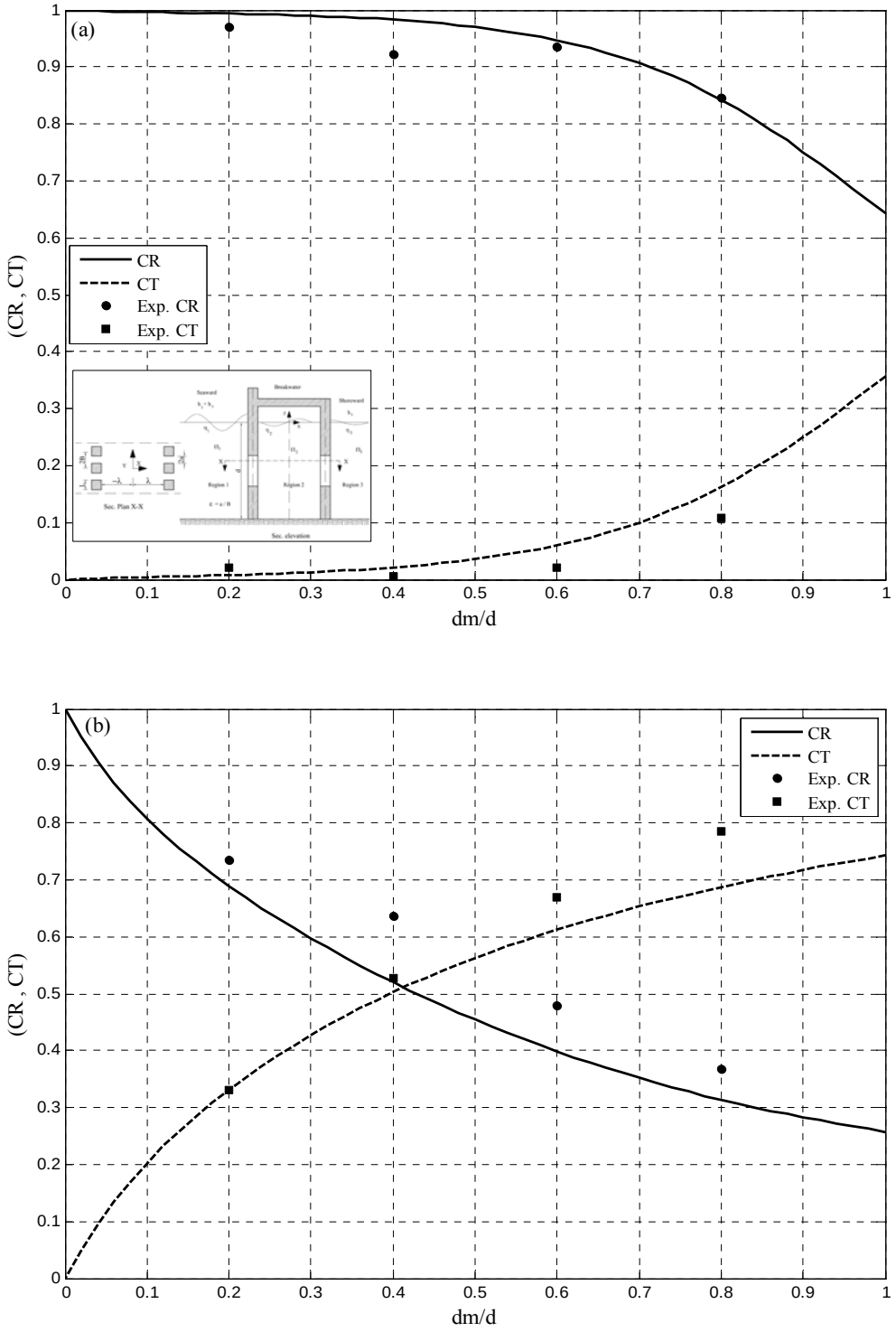

Figure 5.44: Comparison between measured and predicted reflection and transmission coefficients as a function of relative permeable middle part dm/d and $\varepsilon = 0.5$, $\lambda/L = 0.5$, $f = 2$ and $cm = 0$.
(a) at wave period $T = 0.5$ s and
(b) at wave period $T = 1.333$ s.

5.5.4 Influence of the chamber width

The effect of the chamber width 2λ on the hydrodynamic characteristics of two identical double vertical slotted walls is plotted in Figures 5.45:5.52. These Figures indicate the comparison of the measured and predicted transmission, reflection, and energy dissipation coefficients as a function of λ / d as shown in Figures 5.45 : 5.48 and as a function λ / L as shown in Figures 5.49: 5.52, where the middle part is permeable with a porosity ε = 50 % , the water depth *d* = 0.3 m, the thickness of breakwater *b* = 2.5 cm, h_i/L = 0.025, *F* = 2*, cm = 0* , various *kd* = 4.772, 2.689, 1.363 and 0.577, the upper and lower parts are impermeable, the middle part is permeable as a proportion of water depth *dm = 0.8 d, 0.6 d, 0.4 d* and *0.2 d*, and the draft of the upper and lower part changed according to *dm*. In general, the reflection coefficient, *CR* decreases with increasing *dm/d* at fixed λ / d and λ / L , while the transmission coefficient *CT* and dissipation energy coefficient *CE*, follows the opposite trend. It is amazing that the hydrodynamic characteristics *CR*, *CT* and *CE* oscillating along λ / d and λ / L in form crests and bottoms. The number of pikes is fixed along λ / L and different along λ / d where the crest occurs at 2λ = (n-0.5) *L* and (*n) L* associated to maximum value of *CR* and *CT* and minimum value of *CE* and the bottom occurs at 2λ = *(n*-0.75*) L* and *(n* -0.25*) L* associated to minimum *CR* and *CT* and maximum value of *CE*.

The influence of the chamber width can also be seen more clearly: the hydrodynamic performance of the double vertical slotted wall is insensitive to the spacing between the barriers and is influenced only by excitation of partially standing waves between the barriers. In fact, no distinct influence could be noted if the chamber width is related to the water depth but to the wave length.

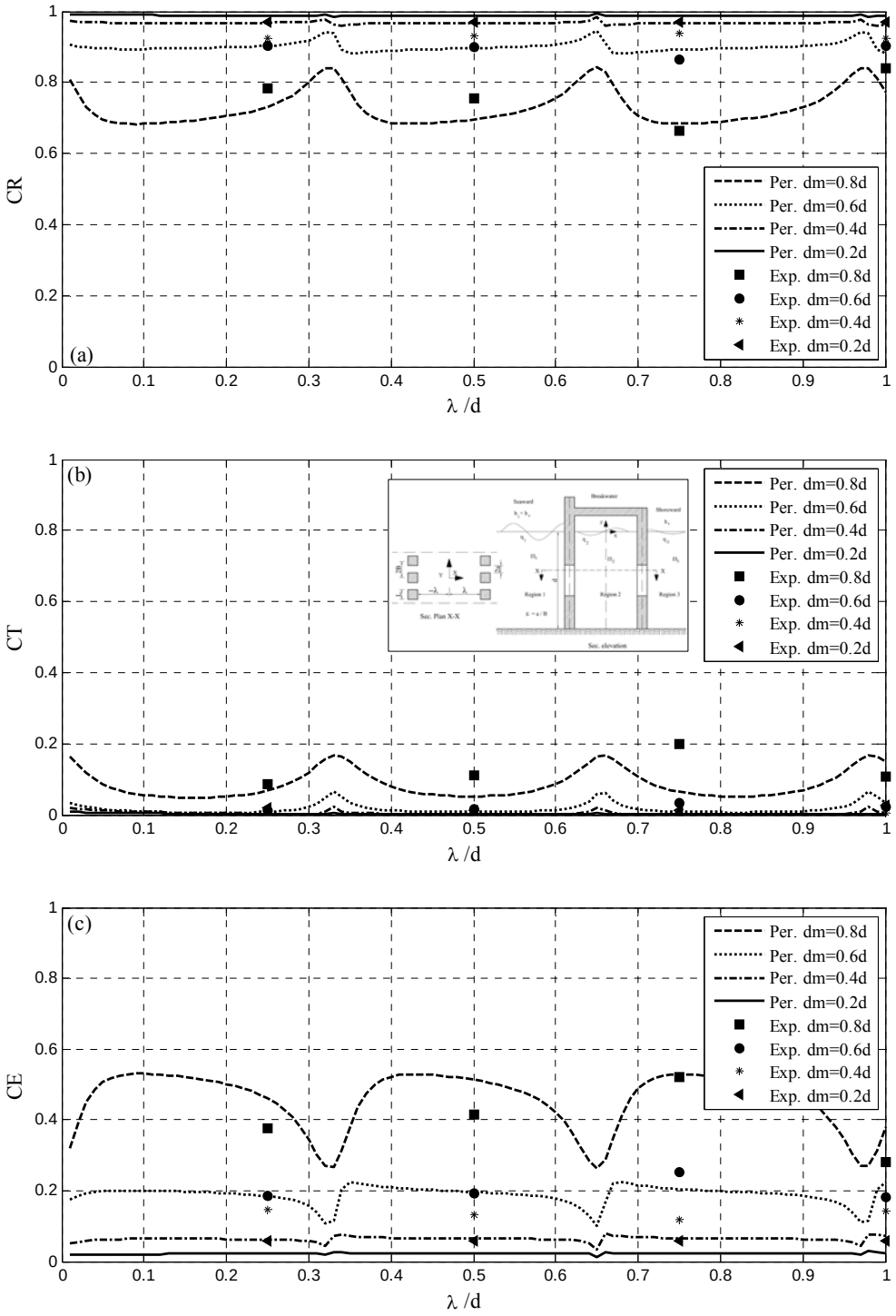

Figure 5.45: Effect of chamber width on reflection, transmission and energy dissipation coefficients for various λ/d , and with $\varepsilon = 0.5$, $kd = 4.772$, $f = 2$ and $cm = 0$.
(a) Reflection coefficient,
(b) Transmission coefficient and
(c) Energy dissipation coefficient.

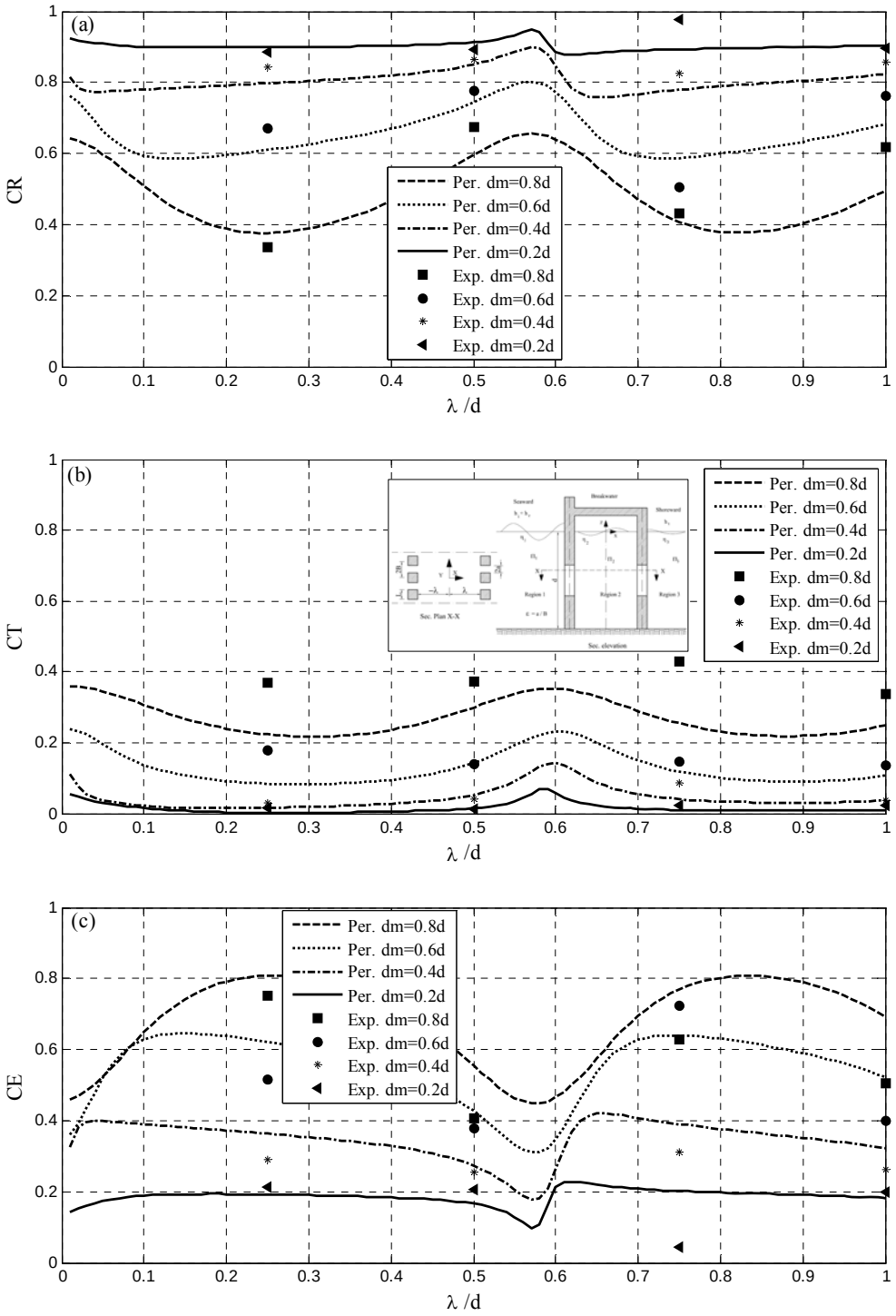

Figure 5.46: Effect of chamber width on reflection, transmission and energy dissipation coefficients for various λ/d, and with $\varepsilon = 0.5$, $kd = 0.2689$, $f = 2$ and $cm = 0$.
(a) Reflection coefficient,
(b) Transmission coefficient and
(c) Energy dissipation coefficient.

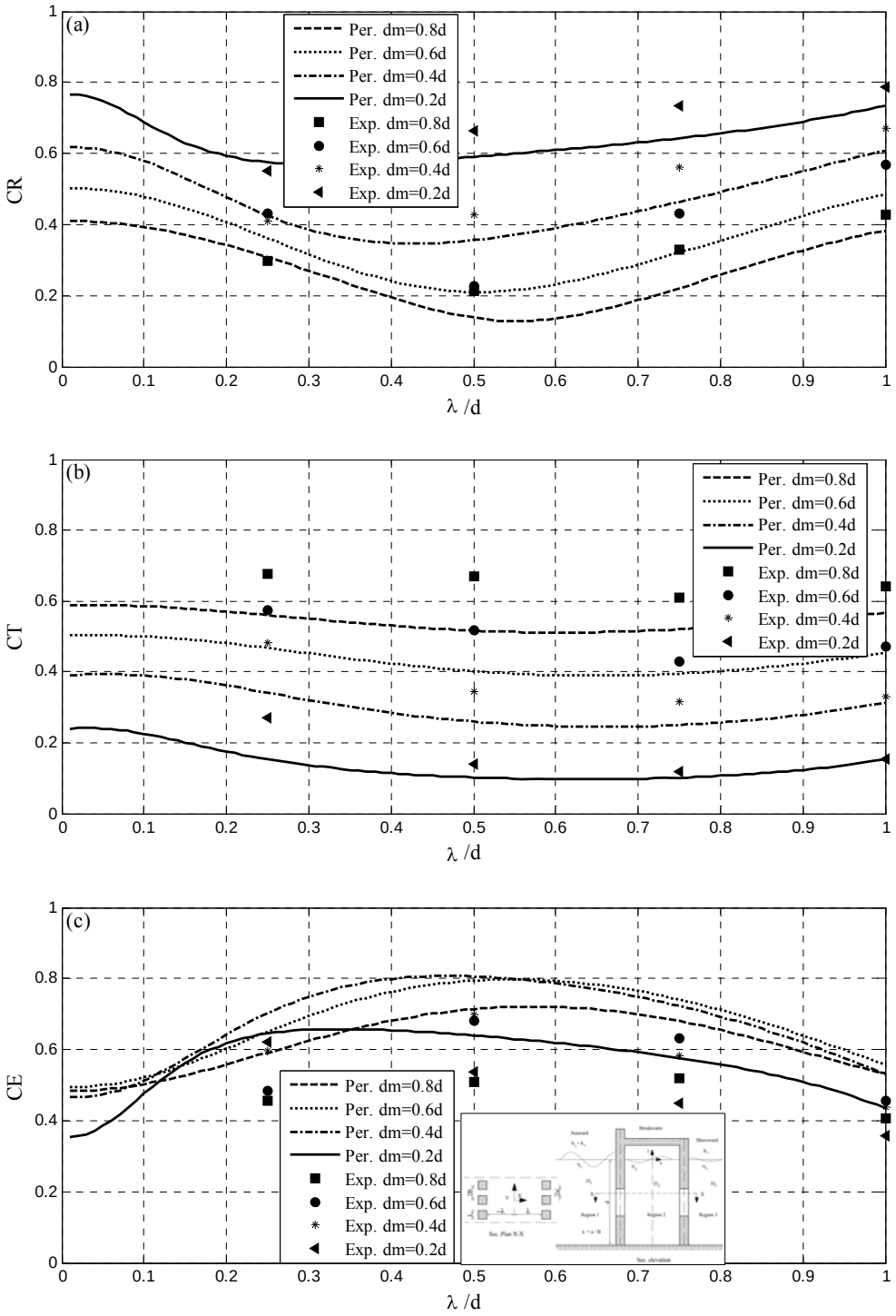

Figure 5.47: Effect of chamber width on reflection, transmission and energy dissipation coefficients for various λ/d, and with $\varepsilon = 0.5$, $kd = 1.363$, $f = 2$ and $cm = 0$.
(a) Reflection coefficient,
(b) Transmission coefficient and
(c) Energy dissipation coefficient.

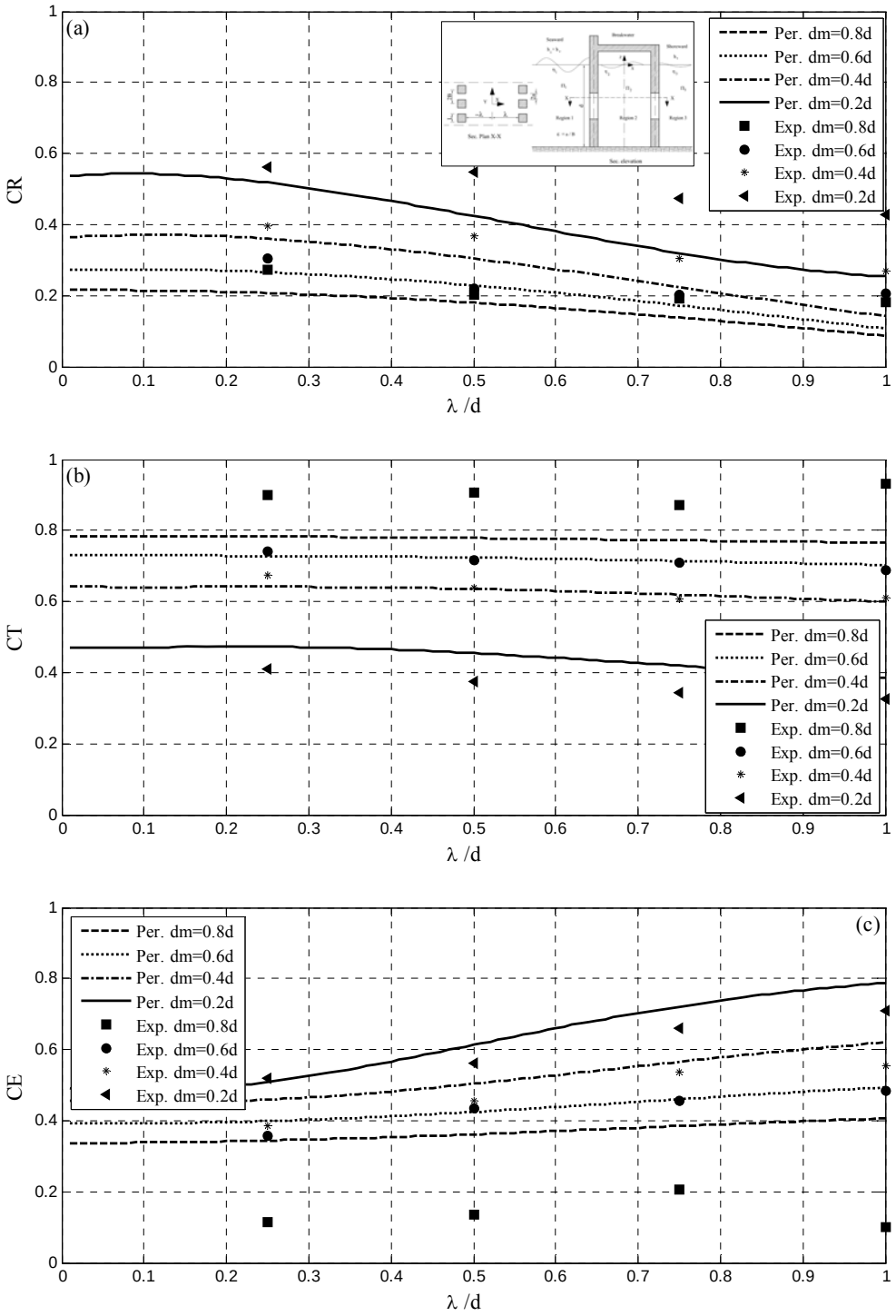

Figure 5.48: Effect of chamber width on reflection, transmission and energy dissipation coefficients for various λ/d, and with $\varepsilon = 0.5$, $kd = 0.577$, $f = 2$ and $cm = 0$.
(a) Reflection coefficient,
(b) Transmission coefficient and
(c) Energy dissipation coefficient.

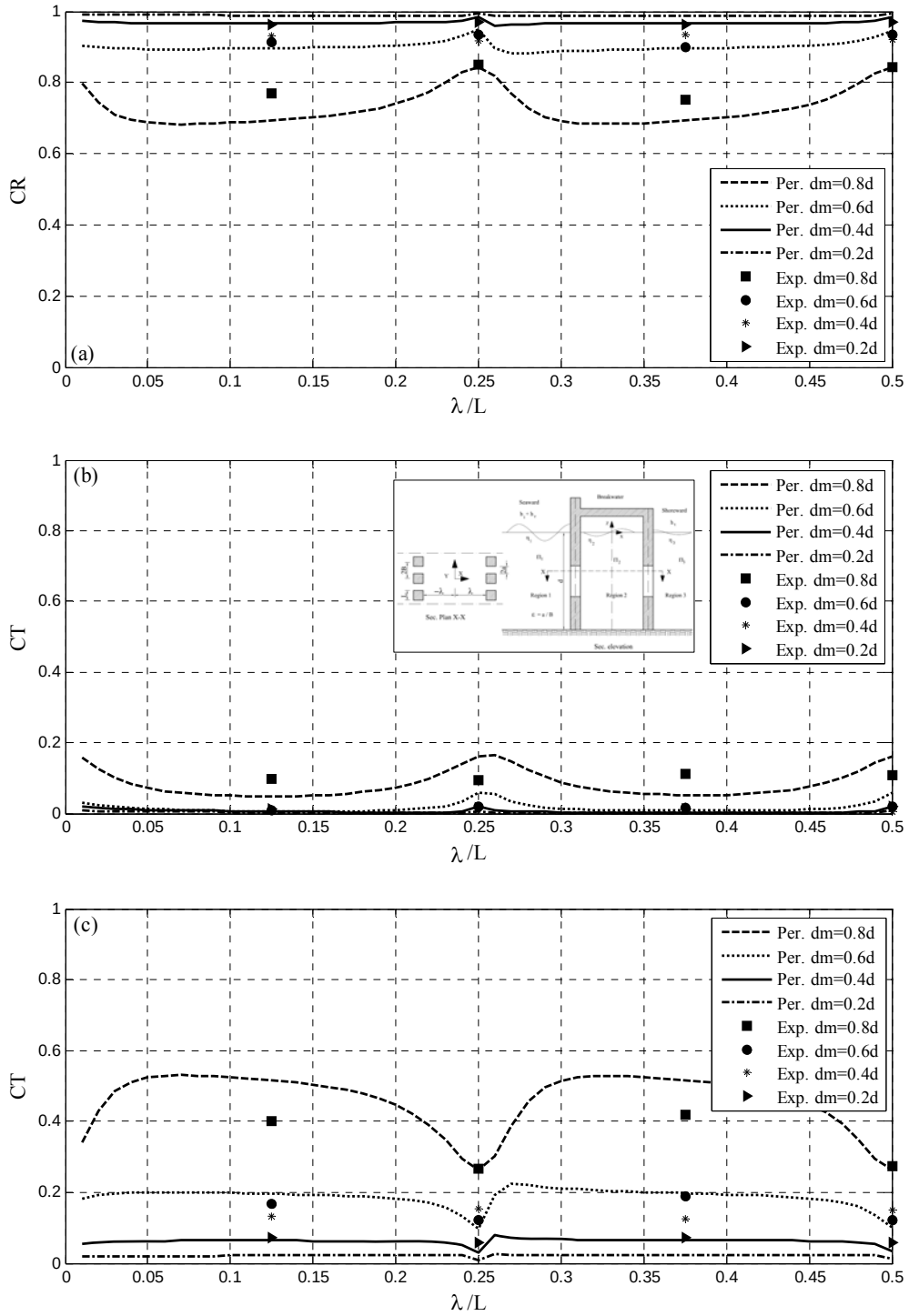

Figure 5.49: Effect of chamber width on reflection, transmission and energy dissipation coefficients for various λ/L, and with $\varepsilon = 0.5$, $kd = 4.772$, $f = 2$ and $cm = 0$.
(a) Reflection coefficient,
(b) Transmission coefficient and
(c) Energy dissipation coefficient.

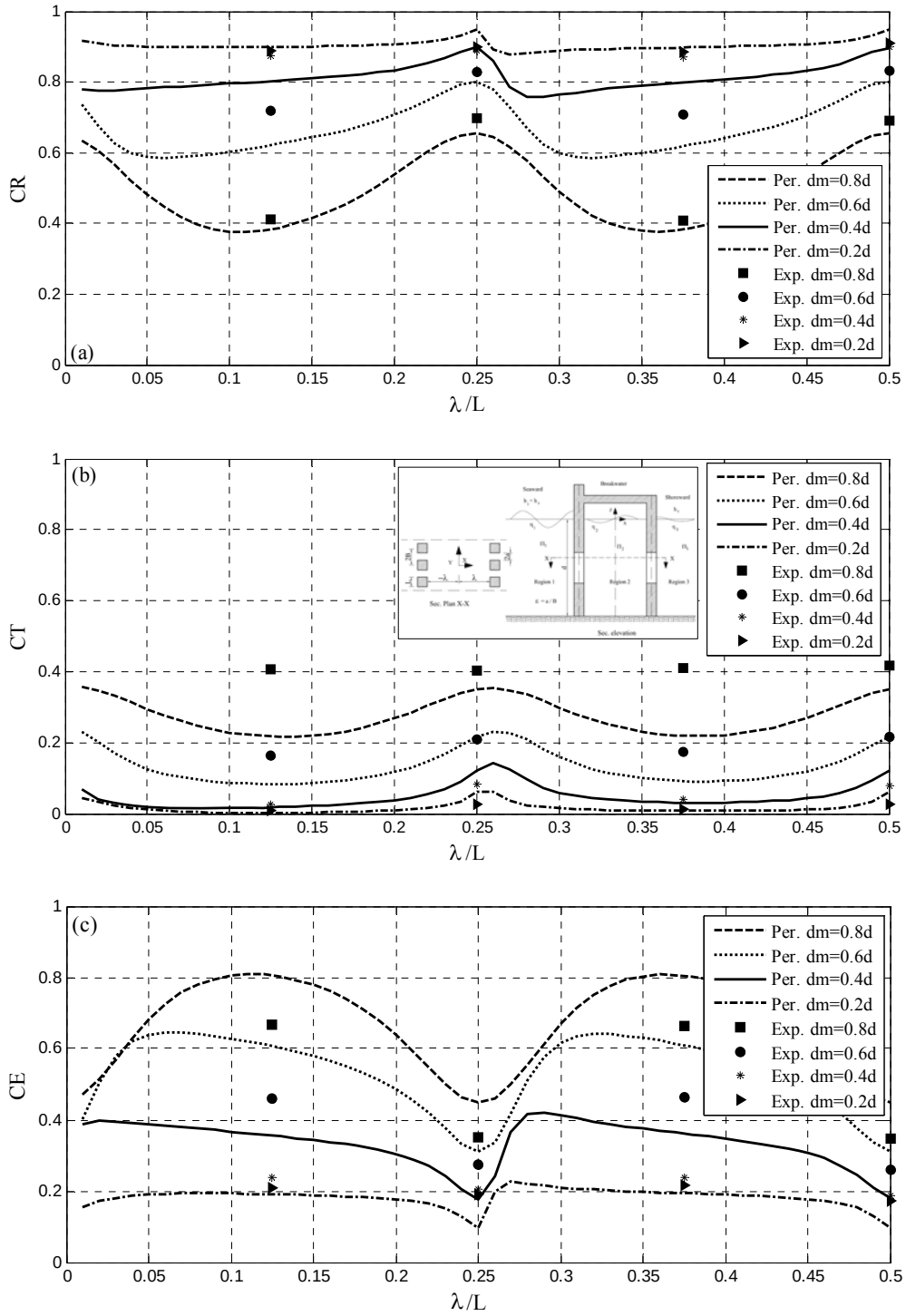

Figure 5.50: Effect of chamber width on reflection, transmission and energy dissipation coefficients for various λ/L, and with $\varepsilon = 0.5$, $kd = 2.689$, $f = 2$ and $cm = 0$.
(a) Reflection coefficient,
(b) Transmission coefficient and
(c) Energy dissipation coefficient.

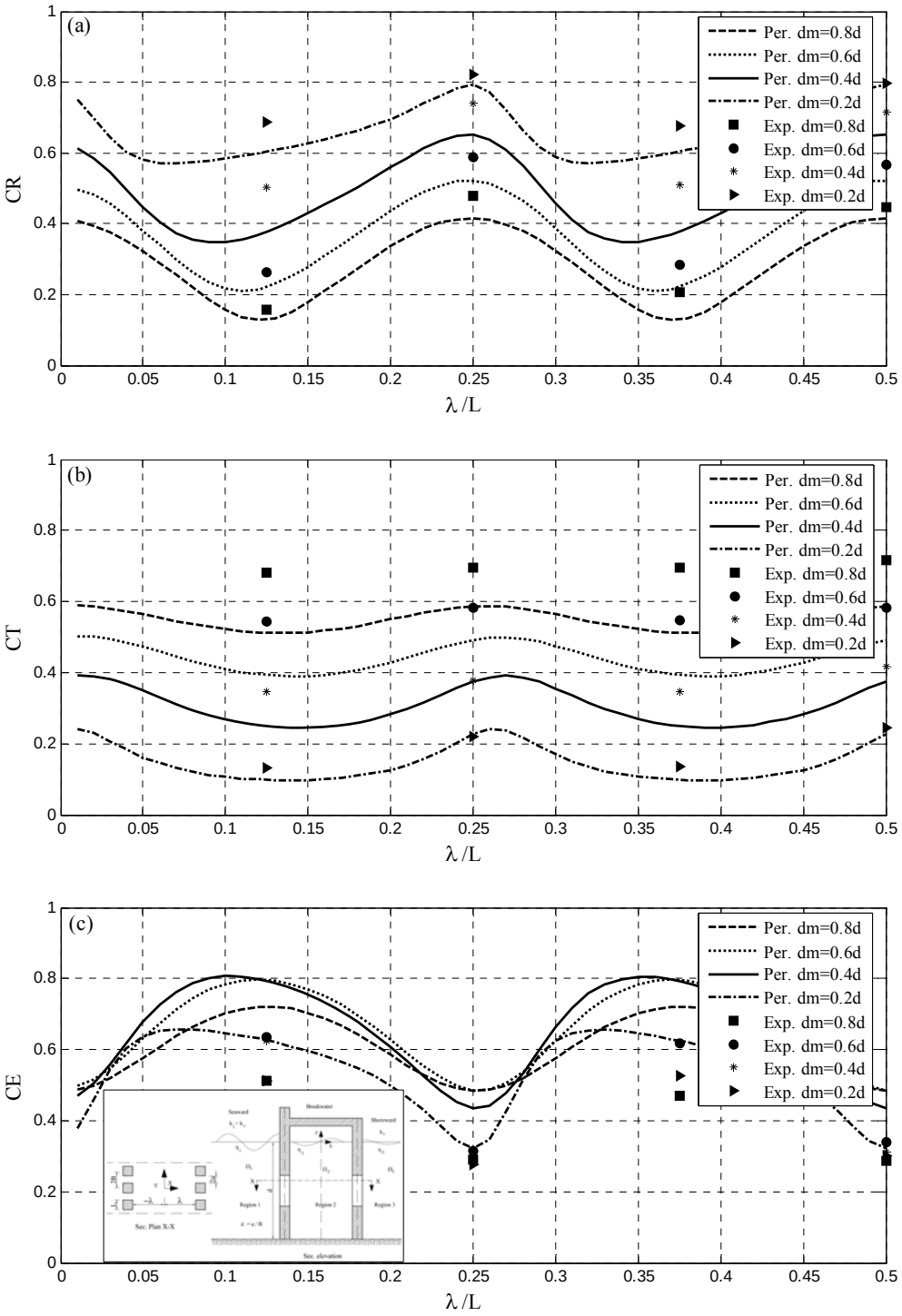

Figure 5.51: Effect of chamber width on reflection, transmission and energy dissipation coefficients for various λ/L, and with $\varepsilon = 0.5$, $kd = 1.363$, $f = 2$ and $cm = 0$.
(a) Reflection coefficient,
(b) Transmission coefficient and
(c) Energy dissipation coefficient.

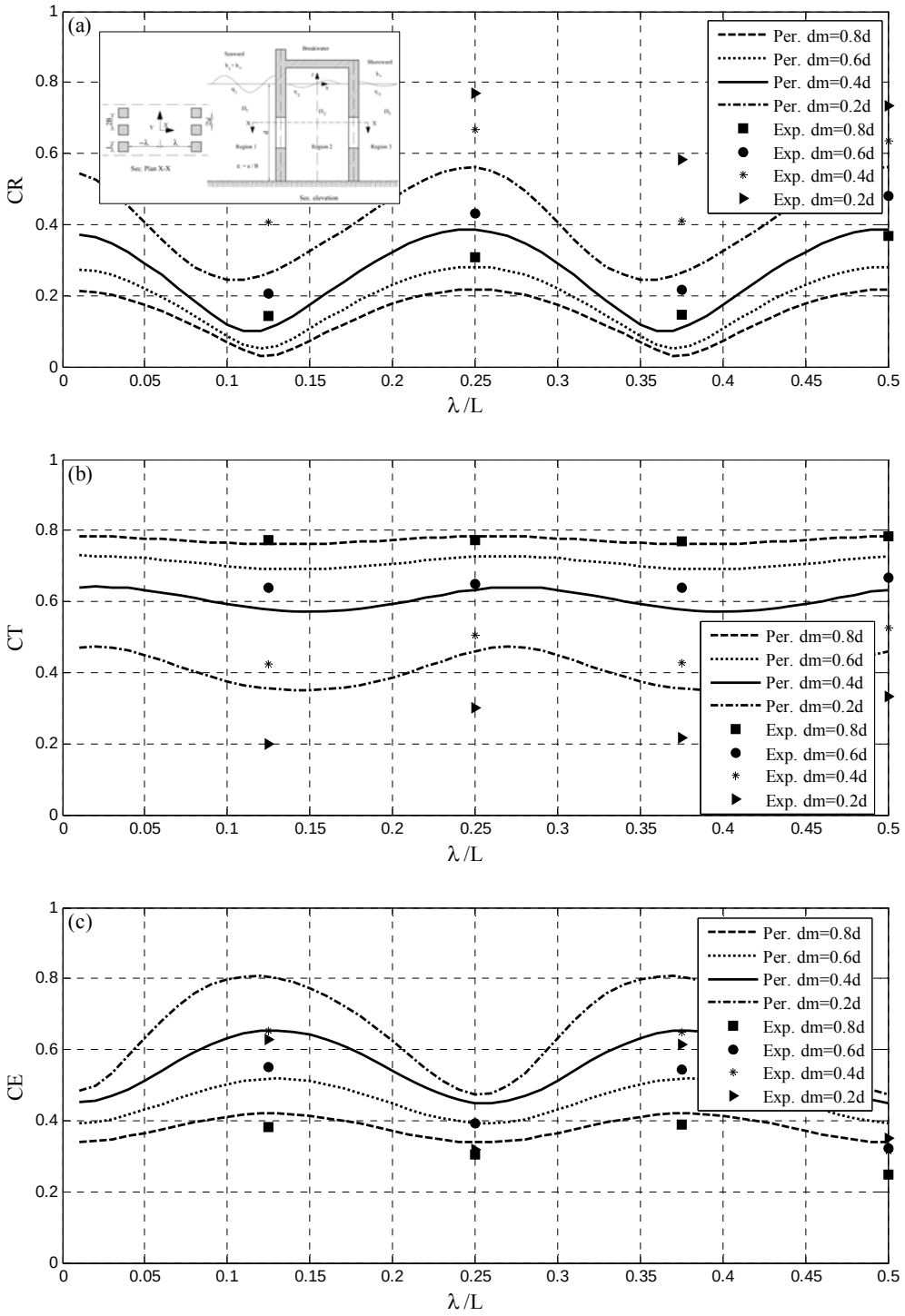

Figure 5.52: Effect of chamber width on reflection, transmission and energy dissipation coefficients for various λ/L, and with $\varepsilon = 0.5$, $kd = 0.577$, $f = 2$ and $cm = 0$.
(a) Reflection coefficient,
(b) Transmission coefficient and
(c) Energy dissipation coefficient.

5.5.5 Comparison between single and double vertical slotted walls

It is also of interest to compare the performance of double vertical slotted walls with that of a single wall. Figures 5.53 to 5.56 show a comparison of the transmission, reflection and energy dissipation coefficients of single and double vertical slotted wall as functions of *kd*, for various λ / d = 0.25, 0.5 , 0.75 and *d*, F = 2, *cm* = 0.00, ε = 50 % and *dm* = 0.2 d, 0.4 *d*, 0.6 *d* and 0.8 *d* as shown in Figures 5.53, 5.54, 5.55 and 5.56 respectively. As expected, the addition of the second barrier has no distinct influence on the reflection coefficient but has distinct influence on the transmission and energy dissipation coefficient. It is noted that there is a noticeable decrease in the transmission coefficient up to 30 % and a noticeable increase in the energy dissipation coefficient up to 40 %, because the second wall dissipate an additional part from the energy of the wave. Therefore, the reflection coefficient is not affected so much, unlike the transmission and energy dissipation coefficients.

Figures 5.57 to 5.60 show a comparison of the transmission, reflection and energy dissipation coefficients of single and double vertical slotted walls as a function of *kd*, for various λ / L = 0.125 , 0.25 , 0.375 and 0.5, F = 2, *cm* = 0.00, ε = 50 % and *dm* = 0.2 d, 0.4 *d*, 0.6 *d* and 0.8 *d* as shown in Figures 5.57, 5.58, 5.59 and 5.60 respectively. It is noted that the hydrodynamic performance in the case of the chamber width 2λ = 0.25 *L* is identical with that of 2λ = 0.75 *L*. The reflection and transmission coefficients are less than both the single wall and the case of double walls at 2λ = 0.5 *L* and *L*. The energy dissipation coefficient is greater. The energy dissipation increases up to 40 % for long waves and the energy dissipation do not change much for short waves.

This can be explained as follows: in the case of 2λ = 0.25 *L* and 0.75*L* the reflection and transmission coefficients are caused by the superposition in opposite direction. The reflected and transmitted waves from the second wall have an opposite phase with the reflected and transmitted waves from the first one. It is observed during the experimental work that the oscillating of waves in front and behind the first wall is in the opposite direction as shown in Photos 5.1 and 5.2. This leads to a decreasing of

the reflection and transmission coefficients and increasing of the dissipation of wave energy.

Similarly, the hydrodynamic performance in the case of a chamber width $2\lambda = 0.5\ L$ is identical with $2\lambda = L$, where the CR is larger than both the single wall and double walls when the chamber width $2\lambda = 0.25\ L$ and $0.75L$. The transmission coefficient *CT* is less than for a single wall and greater than for double walls in the case $2\lambda = 0.25\ L$ and $0.75\ L$. The energy dissipation coefficient is less than the double wall in the case $2\lambda = 0.25\ L$ and $0.75L$ and do not change much in the case the single wall.

This can be explained as follows: in the case of the chamber width $2\lambda = 0.5$ and L the reflection and transmission coefficient are caused by the superposition in the same direction. The reflected and transmitted waves from the second wall have the same phase of the reflected and transmitted waves from the first one. It is observed during experimental work that the oscillating of wave in front and behind the first wall is in the same direction as shown in Photos 5.3 and 5.4.

It is important to recognize that the best locations for the second wall should be constructed at distances of an uneven multiple of a quarter of the wavelength (0.25 *L*, 0.75 *L* and 1.25 *L*), (where *L* is the predominant wave length). This position can increase the dissipation of the energy up to 40 % more than a single wall and double walls when the chamber widths are 0.25 *L*, 0.75 *L*, 1.25 *L*...and so on. Furthermore, it gives the least reflection coefficient, which leads to decrease the force on the wall as well as to decrease the transmission of waves inside the harbor. Finally, the efficiency of this type surpasses the efficiency of a single vertical wall, which has the same parameter in all cases.

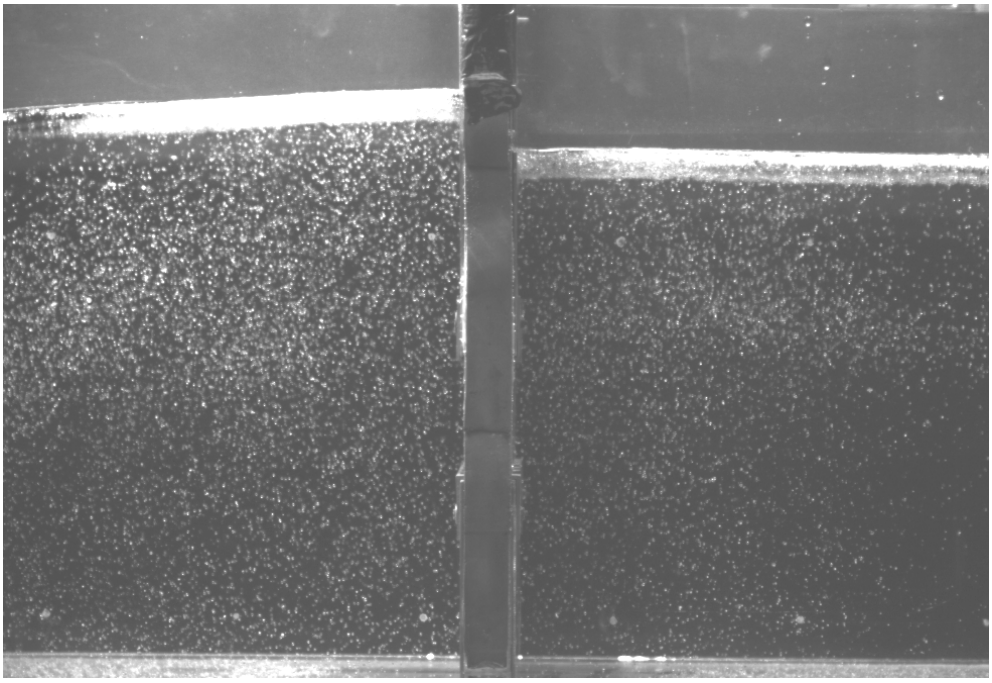

Photo 5.1: Water profile at the first wall at $\lambda / L = 0.125$ at $\theta = 90$ and $h_i = 3$ cm, $T = 1$ s, $\varepsilon = 0.5$ and $dm = 0.2\ d$.

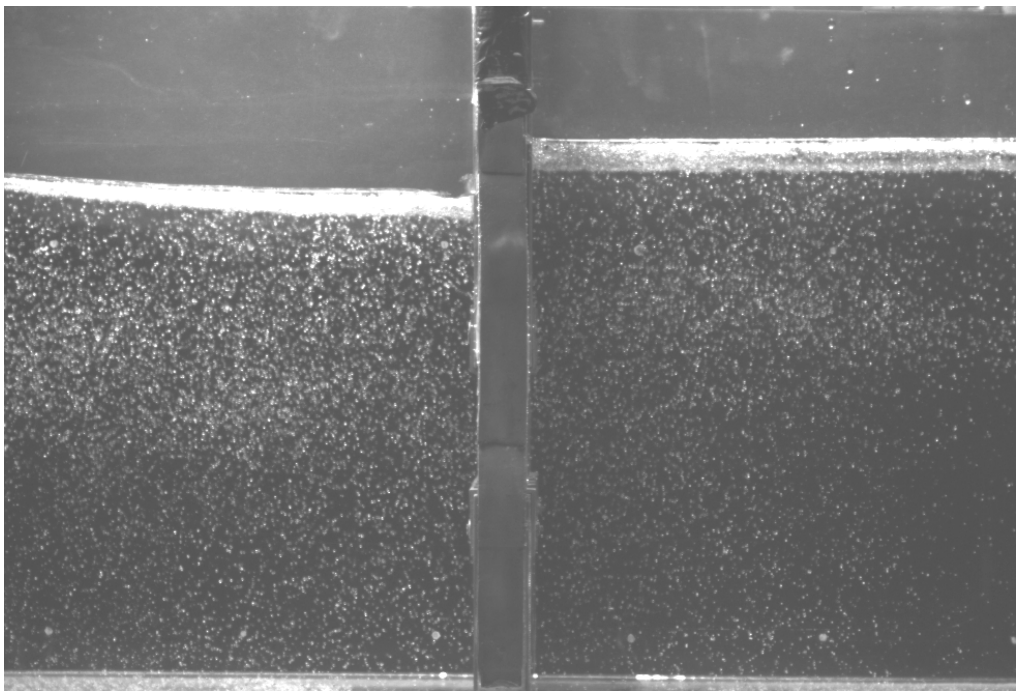

Photo 5.2: Water profile at the first wall at $\lambda / L = 0.125$ at $\theta = 270$ and $h_i = 3$ cm, $T = 1$ s, $\varepsilon = 0.5$ and $dm = 0.2\ d$.

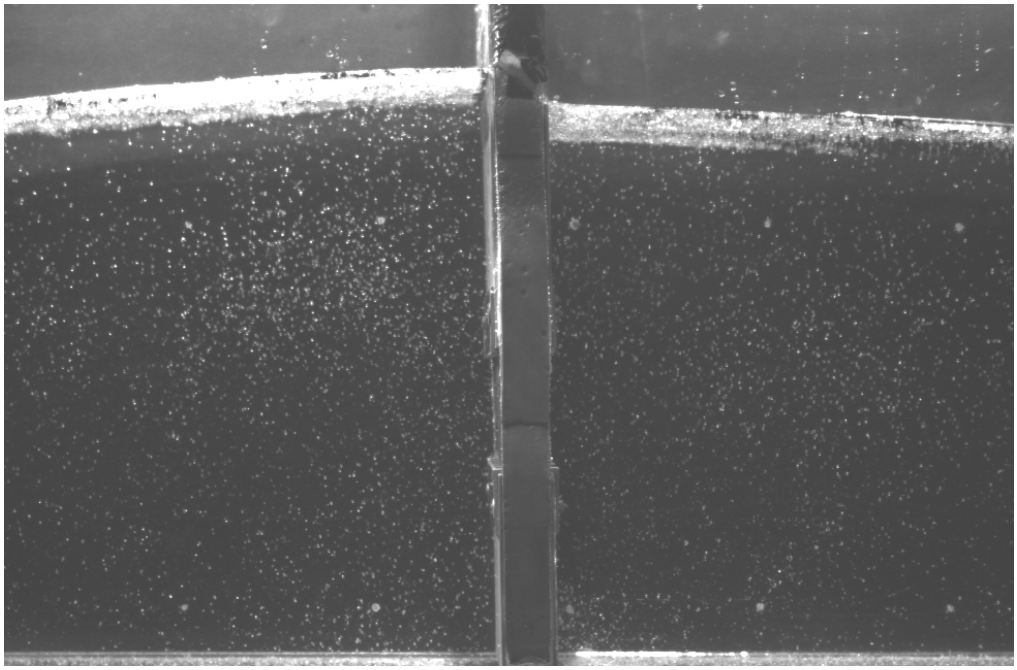

Photo 5.3: Water profile at the first wall at $\lambda / L = 0.25$ at $\theta = 90$ and $h_i = 3$ cm, $T = 1$ s, $\varepsilon = 0.5$ and $dm = 0.2\ d$.

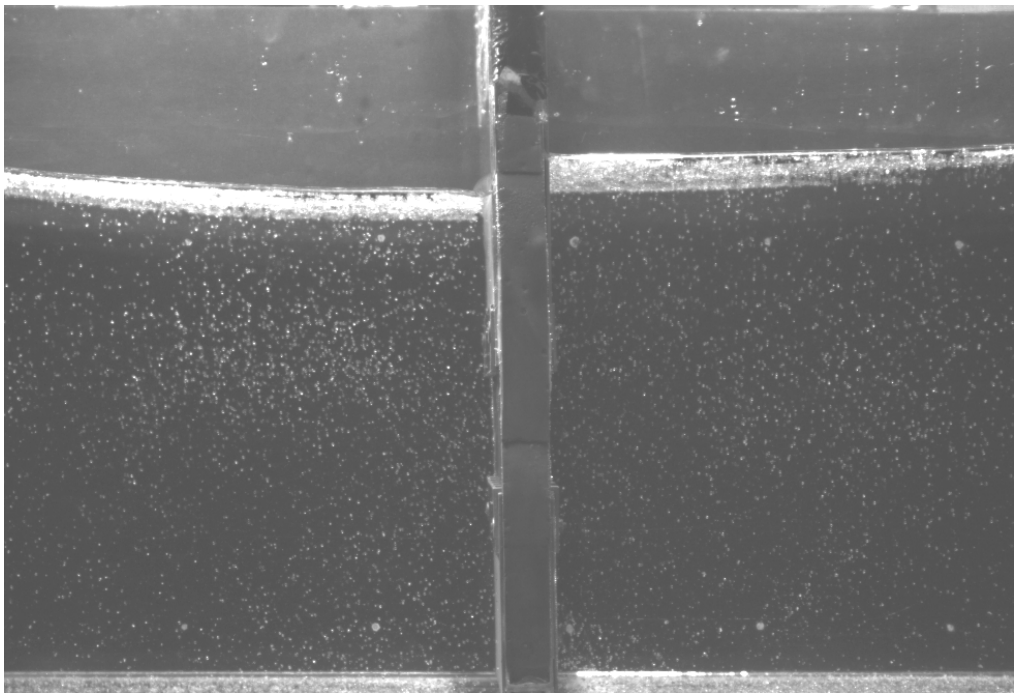

Photo 5.4: Water profile at the first wall at $\lambda / L = 0.25$ at $\theta = 270$ and $h_i = 3$ cm, $T = 1$ s, $\varepsilon = 0.5$ and $dm = 0.2\ d$.

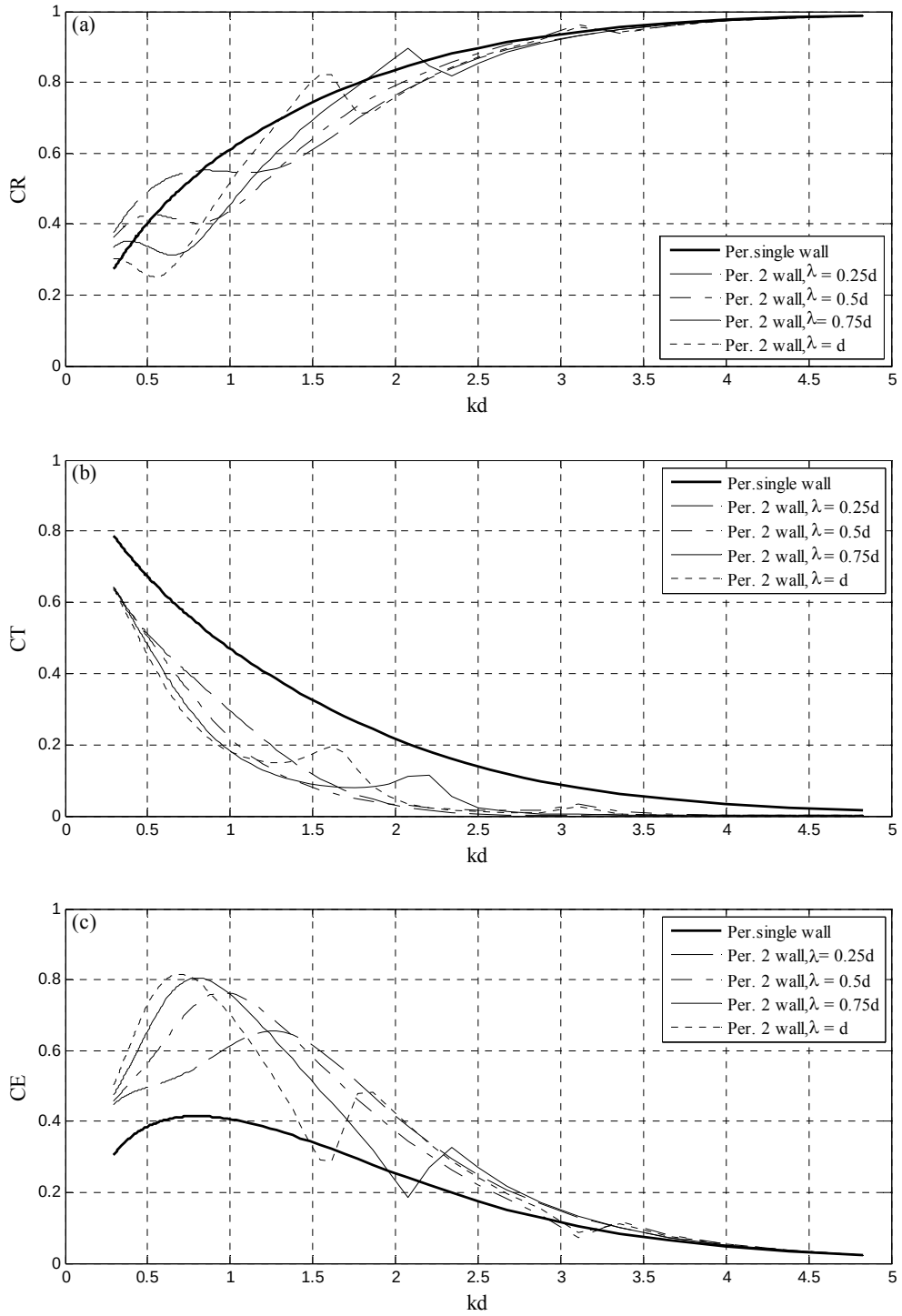

Figure 5.53: Comparison between prediction results for single and double vertical slotted wall as function of (kd) for various λ/d,and with $\varepsilon = 0.5$, $dm = 0.2$ d, $f = 2$ and $cm = 0$.
(a) Reflection coefficient,
(b) Transmission coefficient and
(c) Energy dissipation coefficient.

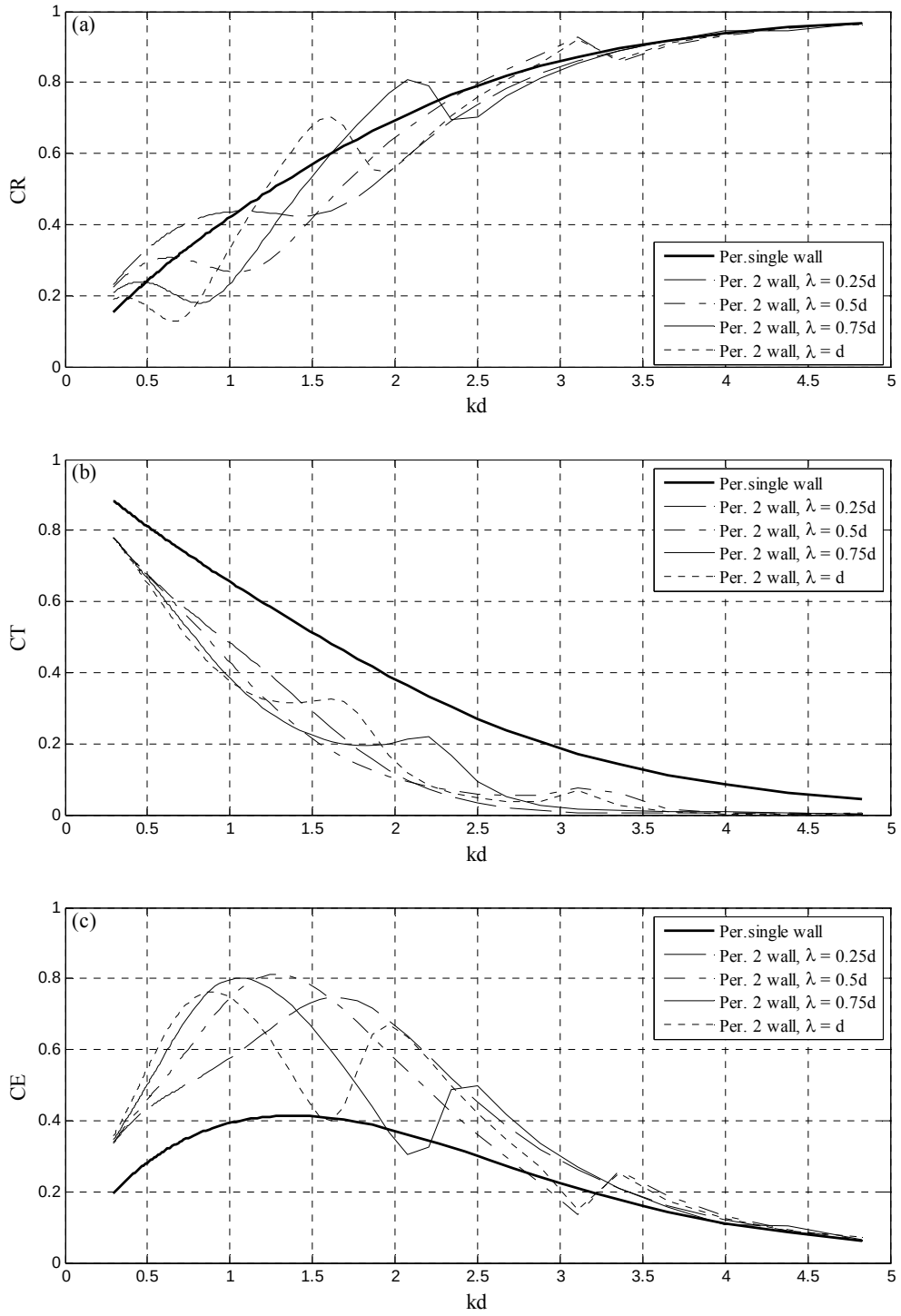

Figure 5.54: Comparison between prediction results for single and double vertical slotted wall as function of (kd) for various λ/d, and with $\varepsilon = 0.5$, $dm = 0.4\ d$, $f = 2$ and $cm = 0$.
(a) Reflection coefficient,
(b) Transmission coefficient and
(c) Energy dissipation coefficient.

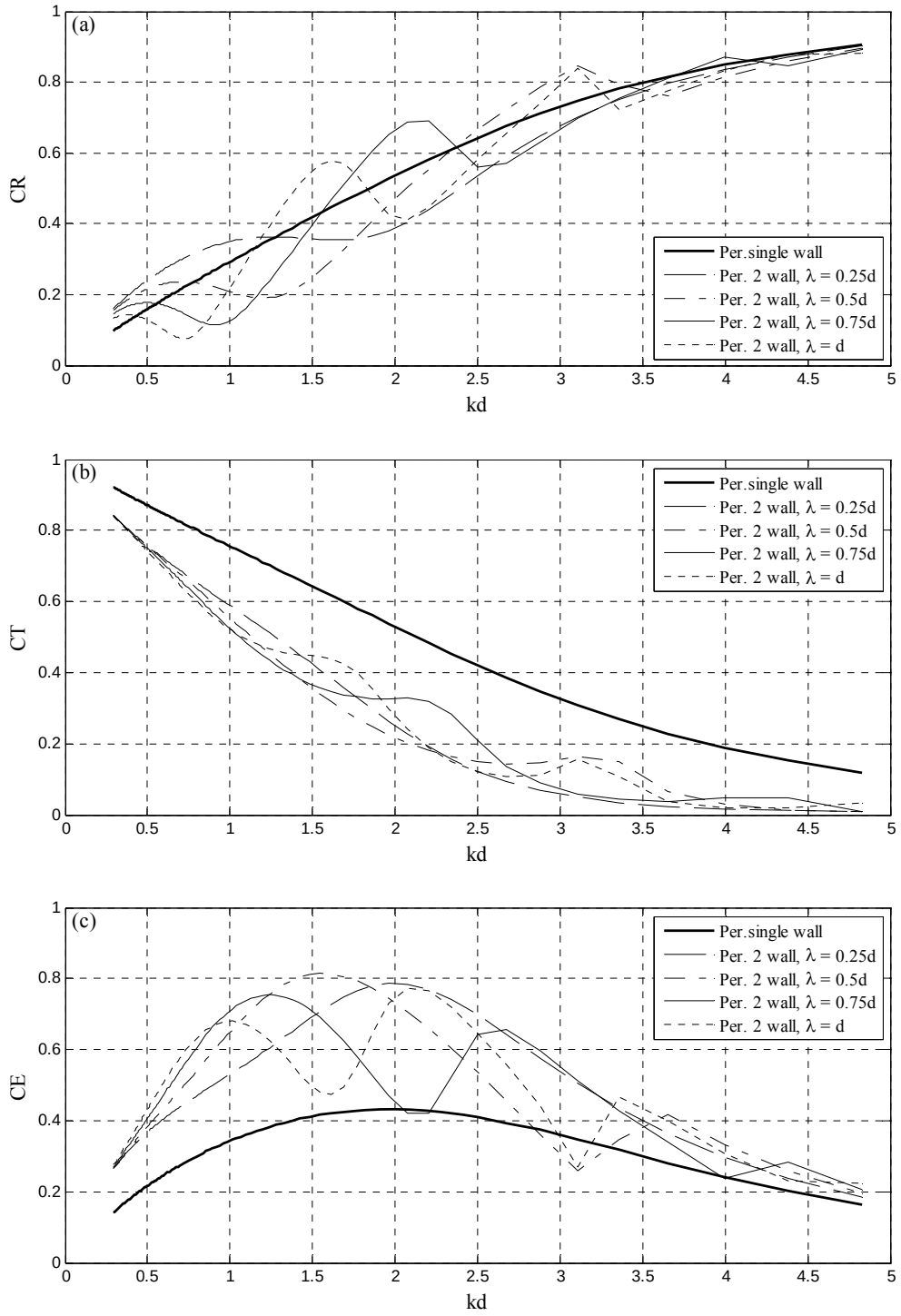

Figure 5.55: Comparison between prediction results for single and double vertical slotted wall as function of (kd) for various λ/d, and with $\varepsilon = 0.5$, $dm = 0.6$ d, $f = 2$ and $cm = 0$.
(a) Reflection coefficient,
(b) Transmission coefficient and
(c) Energy dissipation coefficient.

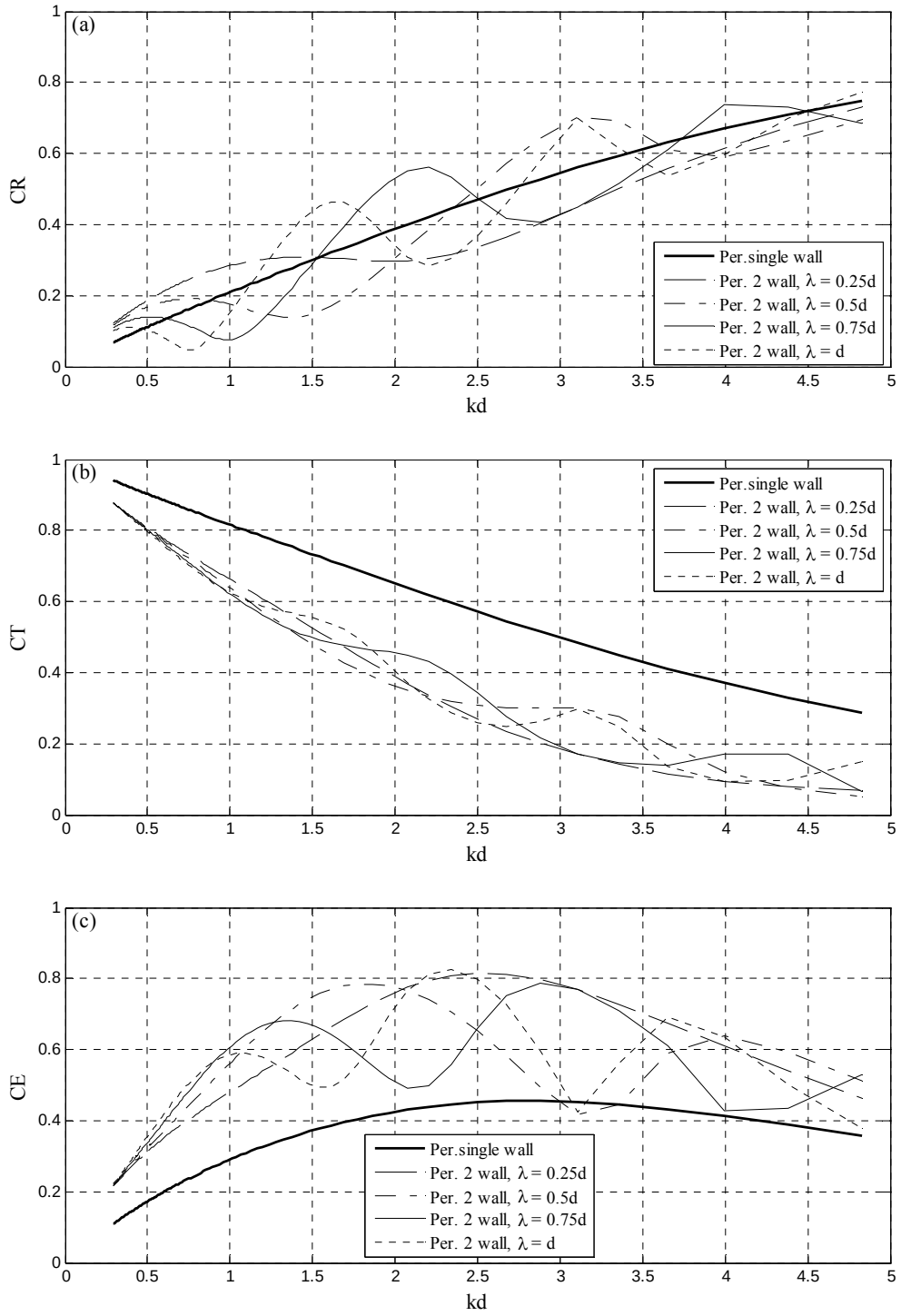

Figure 5.56: Comparison between prediction results for single and double vertical slotted wall as function of (kd) for various λ/d, and with $\varepsilon = 0.5$, $dm = 0.8\ d$, $f = 2$ and $cm = 0$.
(a) Reflection coefficient,
(b) Transmission coefficient and
(c) Energy dissipation coefficient.

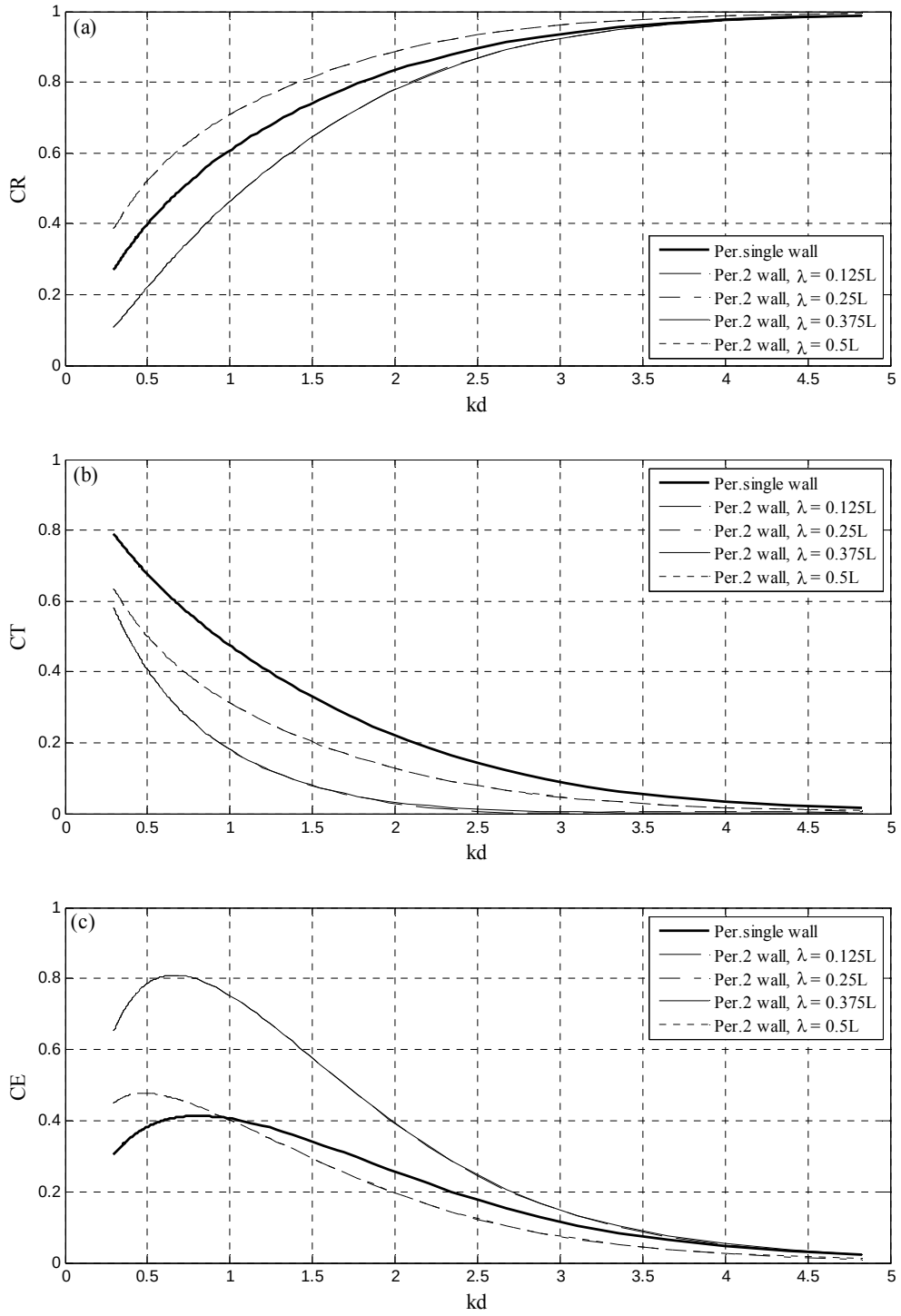

Figure 5.57: Comparison between prediction results for single and double vertical slotted wall as function of (kd) for various λ/L, and with $\varepsilon = 0.5$, $dm = 0.2\ d$, $f = 2$ and $cm = 0$.
(a) Reflection coefficient,
(b) Transmission coefficient and
(c) Energy dissipation coefficient.

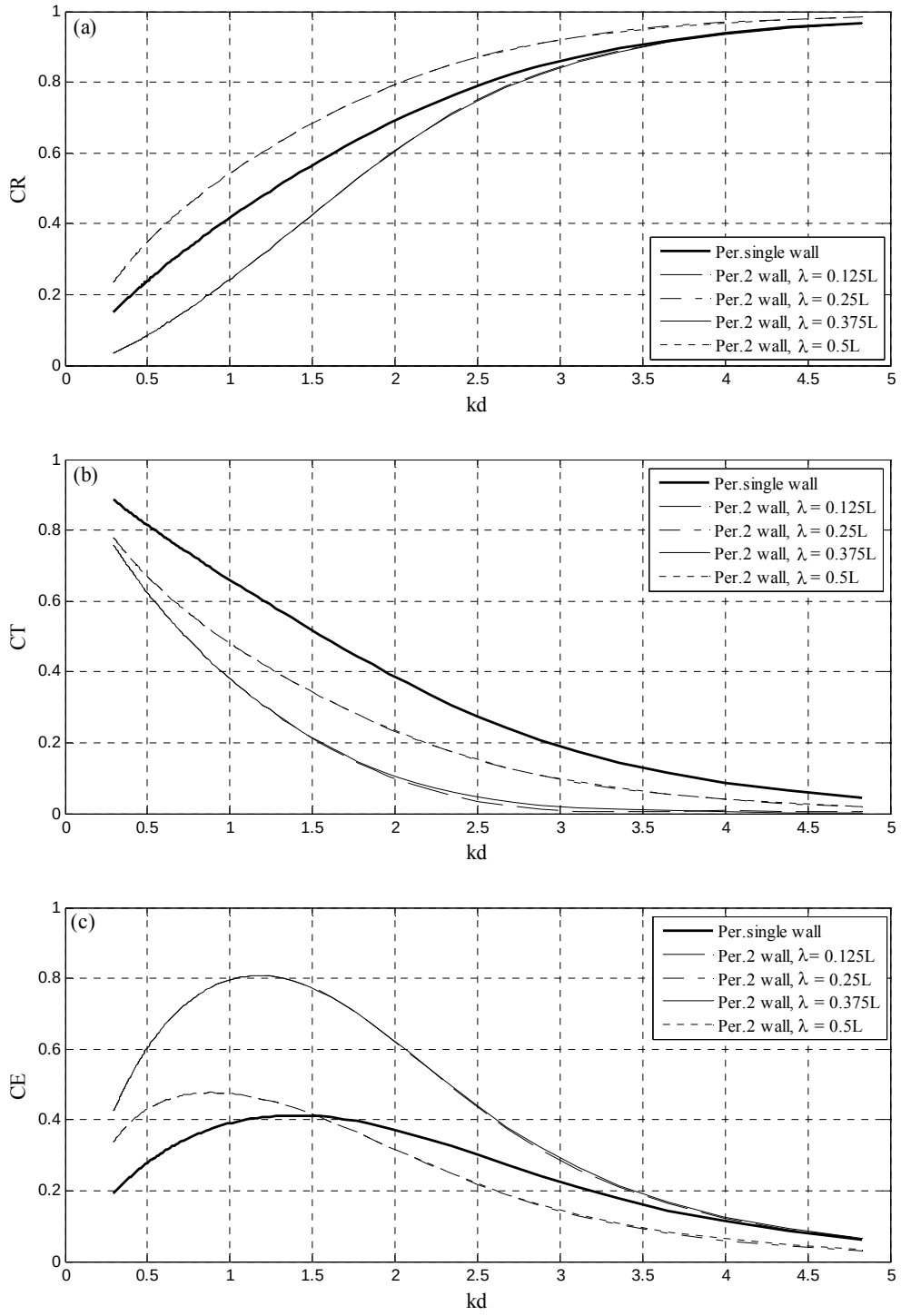

Figure 5.58: Comparison between prediction results for single and double vertical slotted wall as function of (kd) for various λ/L, and with $\varepsilon = 0.5$, $dm = 0.4\,d$, $f = 2$ and $cm = 0$.
(a) Reflection coefficient,
(b) Transmission coefficient and
(c) Energy dissipation coefficient.

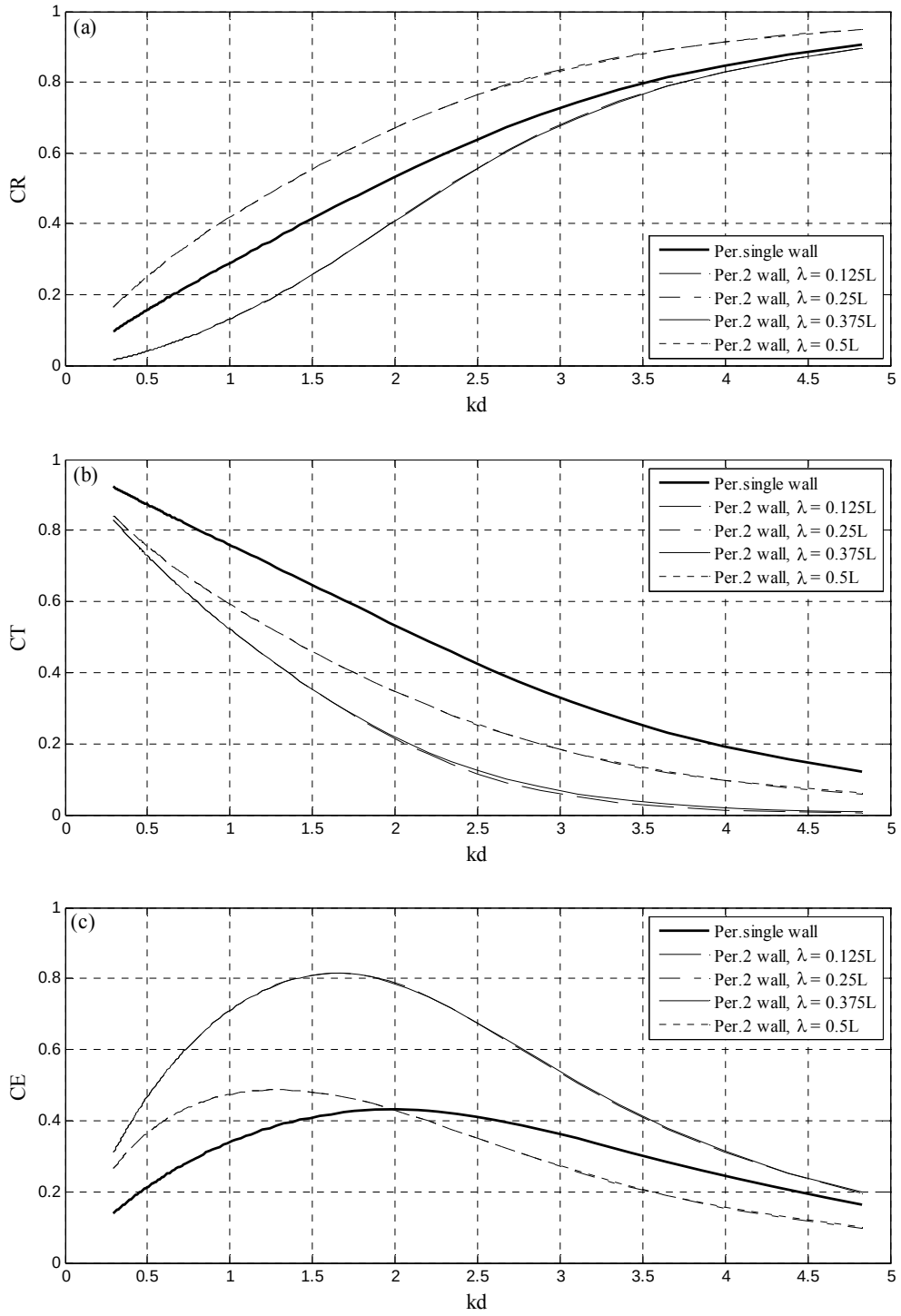

Figure 5.59: Comparison between prediction results for single and double vertical slotted wall as function of (kd) for various λ/L, and with $\varepsilon = 0.5$, dm = 0.6 d, $f = 2$ and $cm = 0$.
(a) Reflection coefficient,
(b) Transmission coefficient and
(c) Energy dissipation coefficient.

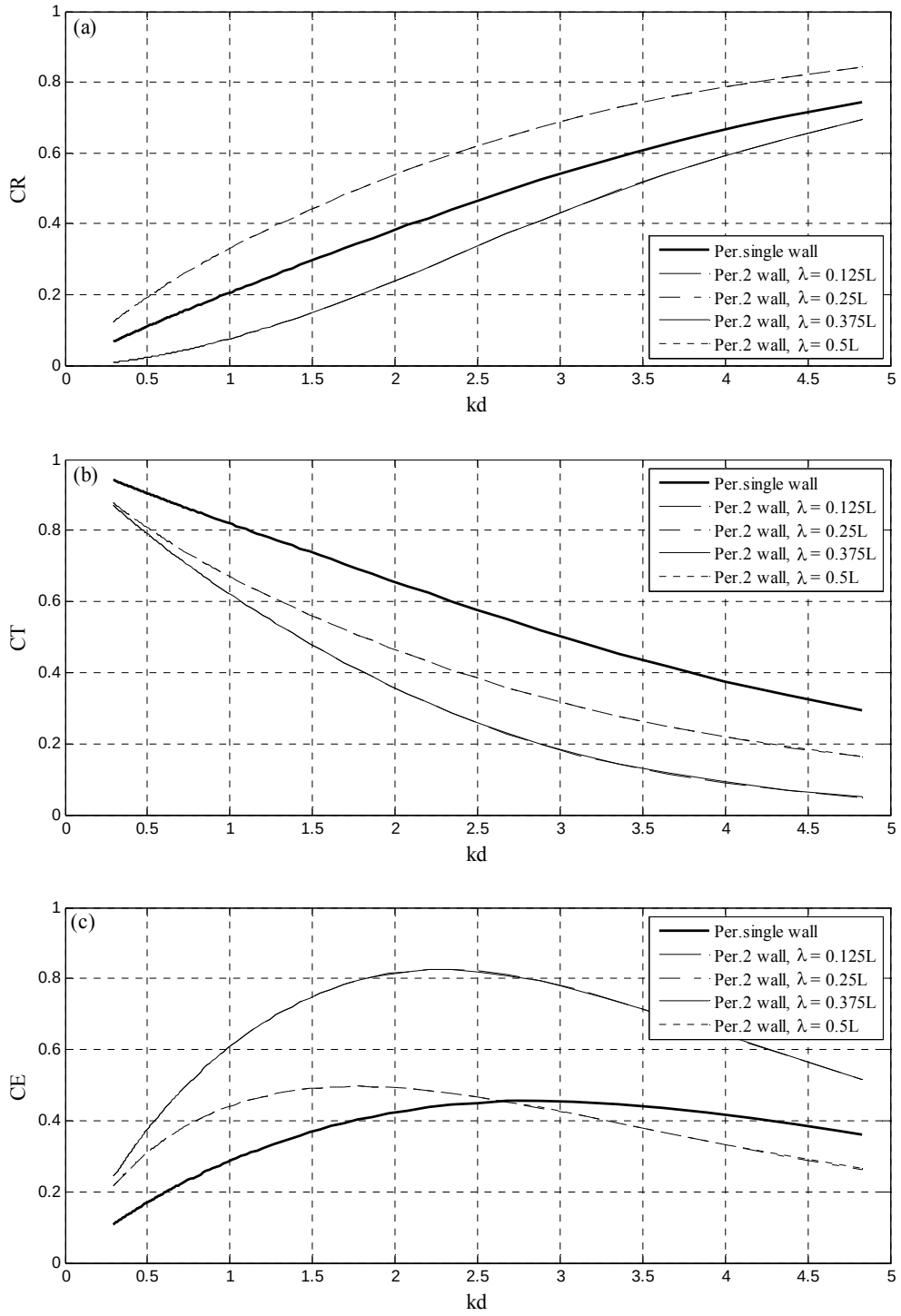

Figure 5.60: Comparison between prediction results for single and double vertical slotted wall as function of (kd) for various λ/L, and with $\varepsilon = 0.5$, $dm = 0.8\ d$, $f = 2$ and $cm = 0$.
(a) Reflection coefficient,
(b) Transmission coefficient and
(c) Energy dissipation coefficient.

CHAPTER 6
SUMMARY, CONCLUSIONS AND RECOMMENDATIONS

6.1 SUMMARY

In this study, many of the scientific results in the protection of coast and ports are accomplished. These results could be used to achieve impressive progress in the use of permeable breakwaters. This study is based on the flowing steps:

- Developing a numerical model based on the Eigen function expansion to investigate the hydrodynamic performance of a single vertical slotted wall with linear waves.
- Establishing a proposal of a numerical model based on the Eigen function expansion to investigate the hydrodynamic performance of a single vertical slotted wall with nonlinear waves (stoke second-order wave theory).
- Developing a numerical model based on the Eigen function expansion to investigate the hydrodynamic performance of double vertical slotted walls with linear waves.
- Extensive laboratory studies were conducted to validate the present numerical models and to measure the velocity field.
- Innovation a new laboratory method to deduce the wave interaction with structures via a new application of PIV.
- Comparisons of the present results with some previous studies were conducted to validate the present numerical models.

The conclusions of this study are reported as follow.

6.2 CONCLUSIONS

The following section presents the salient conclusions drawn from the present study on vertical slotted walls breakwater.

6.2.1 Linear wave interaction with a single vertical slotted wall

This study describes the numerical prediction of wave interaction with a vertical slotted wall breakwater with impermeable upper and lower parts; the draft of them is a proportion of the total depth and the middle part is permeable with porosity 50 %. For regular wave, an Eigen function expansion method has been adopted to predict various hydrodynamic characteristics (*CR, CT* and *CE*). Laboratory tests were carried out and comparisons with previous studies were conducted to validate the numerical model. The velocities and the vortices that results from the separation of flow through the slots in front and behind the single vertical slotted wall were recorded by PIV. In addition, PIV was employed to investigate the wave interaction with permeable wall through measuring the reflection, transmission and energy dissipation coefficients.

- The time increment should be taken in a range of $0.01\ T < \delta t < 0.015\ T$, such that the error of measurements will be less than $\pm$ 5 % within this study. The achievable accuracy of PIV measurement within this set-up is shown to be limited by the influence of the relative time increment $\delta t / T$.
- A comparison between the velocity measurements via PIV and the linear velocity for incident waves was carried out. The comparison clarifies that the results of PIV are perfectly acceptable for high velocities and satisfactory to some extent in the low velocities.
- The measured results of PIV were simulated by the measured results of Ultrasonic wave gauges. The agreement is generally satisfactory and indicates that PIV is able to measuring the co-existing and transmitted waves and also is able to find the wave interaction with permeable breakwaters.

- A comparison of corresponding numerical predictions with the experimental results of PIV and results of Ultrasonic wave gauges was conducted and indicated that the numerical model is compatible with measurements of PIV and Ultrasonic wave gauges despite of the presence of some scattering.
- The results of PIV are perfectly acceptable and the application of PIV is encouraging.
- Comparisons of corresponding numerical predictions with some previous studies, some of them are numerical and experimental and others are numerical with taking into account limits of the study in each case have been conducted, and close agreements were obtained.
- The friction coefficient f and the porosity ε have significant influence on G, so CR, CT and CE of the vertical slotted walls, while the influence of added mass coefficient is powerless and can be neglected. The value of f and cm are given based on the best fit between the numerical and the predicted values of the transmission, and reflection coefficients.
- Comparisons of corresponding numerical predictions with experimental results showed that the agreement is generally satisfactory and indicates that the numerical model is able to adequately reproduce most of the important features of the experimental results.
- The reflection coefficient, CR increases with increasing kd at fixed dm and increases with decreasing dm at fixed kd. The transmission coefficient, CT follows the opposite trend. The energy dissipation, CE slowly increases with increasing kd for the lower kd and inversed for the higher kd.
- The lower impermeable part has high efficiency for intermediate and long wave, where the reflection coefficient CR increases with increasing the draft of dw. The transmission coefficient, CT follows the opposite trend, but it has no influence on short waves.
- The upper impermeable part has significant influence for all types of waves.
- The location of the permeable part has a significant influence for short waves until the location of permeable part equal 0.3 d. After this draft, the influence is insignificant, while it has a significant influence for intermediate and long waves at any location.

- At the location where $du = 0$ and $dw = 0.8\ d$, the reflection and transmission coefficients seemed to be fixed at about 0.52 % and 0.59 % respectively and the energy dissipation coefficient is about 0.38 %.
- The Hydrodynamic Performance Characteristics of permeable Breakwaters vary depending on the permeability area and its location. Thus, the degree of target protection can be achieved through a combination of permeability area and its location.
- The efficiency of this type surpasses the efficiency of pile breakwaters in general and surpasses the efficiency of pile-supported vertical wall breakwaters, especially for intermediate and long waves.

6.2.2 Nonlinear wave interaction with a vertical slotted wall

This study describes the numerical prediction of nonlinear wave (Stokes second-order wave) interaction with a vertical slotted wall breakwater. For regular wave, an Eigen function expansion method has been developed to predict various hydrodynamic characteristics (*CR, CT* and *CE*). A comparison of hydrodynamic characteristic of single vertical slotted wall under linear wave with the same type under nonlinear wave has been investigated. All results are presented and discussed as follows.

- The behavior of hydrodynamic characteristics CR, CT and CE for nonlinear wave (Stokes second-order wave) is similar to the behavior of linear wave within the same limits and conditions, and thus the numerical model is able to adequately reproduce most of the important features of the experimental results.
- Comparisons of Stokes second-order wave interaction with linear wave interaction of vertical slotted wall showed that the behavior of Stokes second-order waves is identical to the behavior of linear waves for short and intermediate waves up to $kd \geq 1$ but the behavior of Stokes second-order waves is higher than linear waves theory for intermediate waves at $kd < 1$ and the long waves.

- The reflection coefficient increases with about 5 % and the transmission coefficient decreases with about 5 % than linear wave theory seen for example at $kd = 0.5$. This ratio increases with decreasing kd.
- The Stokes second-order components can be neglected for short waves and may become significant for intermediate and long waves.

6.2.3 Linear wave interaction with double vertical slotted walls

This study describes numerical predictions of linear wave interaction with double vertical slotted walls breakwater with impermeable upper and lower parts; the draft of them is a proportion of the total depth, the middle part is permeable with porosity 50 % and various chamber widths. For regular wave, an Eigen function expansion method has been developed to predict various hydrodynamic characteristics (*CR, CT* and *CE*). Laboratory tests were carried out and comparisons with previous studies were conducted to validate the numerical model. The influence of the chamber width on the reflected and transmitted waves has been investigated. A comparison between the hydraulic performance of a single and double vertical slotted walls breakwaters has been conducted.

- A comparison of corresponding numerical results of *CR*, *CT* and *CE* with numerical and experimental results of Isaacson et al. (1999) was conducted, to validate the numerical model, and a close agreement was obtained.
- Comparisons of corresponding numerical predictions of *CR*, *CT* and *CE* with experimental results showed that the agreement is generally satisfactory and indicates that the numerical model is able to adequately reproduce most of the important features of the experimental results.
- The reflection coefficient, *CR* increases with increasing *kd* at fixed *dm* and increases with decreasing *dm* at fixed *kd*. The transmission coefficient, *CT* follows the opposite trend. The energy dissipation, *CE* slowly increases with increasing *kd* for the lower *kd* and reaches more than 80 % because the second barrier causes additional vortex, which dissipate more wave energy.

- The reflection coefficient, *CR* decreases with increasing *dm/d* while the transmission coefficient, *CT* follows the opposite trend. Therefore, the efficiency of this type surpasses the efficiency of double rows of pile breakwater, which has the same porosity. The target protection can be achieved through the best choice for the permeability area.
- The peaks in *CR*, *CT*, and *CE* occurred when the chamber width related to the water depth. The number of peaks increases with increasing the chamber width. For larger relative spacing, peaks in the transmission and reflection coefficients occur when the relative draft, corresponding to resonant excitation of partial standing waves between the barriers. This result agrees with result of Isaacson et al. (1999).
- *CR, CT* and *CE* oscillating along λ / d and λ / L in form crests and bottoms. The number of pikes is fixed along λ / L and different along λ / d where the crest occurs at 2λ = (n-0.5) *L* and (n) *L* associated to maximum value of *CR* and *CT* and minimum value of *CE* and the bottom occurs at 2λ = (n-0.75) *L* and (*n* -0.25) *L* associated to minimum *CR* and *CT* and maximum value of *CE*.
- No distinct influence was noted if the chamber width related to the water depth, but distinct influence was noted if related to the wave length.
- The addition of the second barrier has no distinct influence on CR but has distinct influence on *CT* and *CE* when the chamber width is related to the water depth. A noticeable decrease in *CT* up to 30 % and a noticeable increase in the energy dissipation coefficient up to 40 %, were remarked because the second wall dissipate additional part from the energy of wave.
- The hydrodynamic performance of this type in case the chamber width 2λ = 0.25 *L* identical with 2λ = 0.75 *L*. CR and CT are less than both *CR* and *CT* of single and double walls at other chamber width, while *CE* is greater than of both types. The additional energy dissipation up to 40 % for long wave and the energy dissipation do not change much for short wave. The reflection *CR* and the transmission *CT* coefficients are caused by the superposition in opposite direction for both the reflected and the transmitted wave from the first and second walls.

- The hydrodynamic performance of this type in case the chamber width $2\lambda = 0.5\ L$ identical with $2\lambda = L$, where the CR larger than both *CR* of single and double walls, while the transmission coefficient *CT* is less than *CT* of the single wall and greater than *CT* of the double walls in case $2\lambda = 0.25\ L$ and $0.75\ L$. The reflection coefficient *CR* and the transmission coefficient *CT* are caused by the superposition in the same direction for both the reflected and the transmitted wave from the first and second wall.
- The best locations for the second wall could be constructed at a distance of an uneven multiple of a quarter of the wavelength (0.25 L, 0.75 L and 1.25 L). This position can increase the dissipation of the energy up to 40 % more than the single and double walls when the chamber widths are 0.25 *L*, 0.75 *L*, 1.25 *L* and so on. Furthermore, it gives the least reflection coefficient, which leads to decreasing the force on the walls as well as decreasing the transmission of waves inside the harbor to minimal limit.

6.3 RECOMMENDATIONS

It is recommended to use vertical slotted walls breakwater in protection procedures against waves and currents because they are an environmental means that have the less negative effects on neighboring beaches and have high significant degree of protection. The vertical slotted walls breakwaters could be used advantageously in both soft and hard soils, where, it can be used as pile-supported slotted walls or slotted walls supporting on foundations, and can be used when the water depth is intermediate and wave climate is moderate. The progressively decreasing depth of permeable part of the wall is recommended to minimize the transmission so that the dissipation of the incident wave energy will increase. For double rows of vertical slotted walls, the second wall should be constructed at a distance of an uneven multiple of a quarter of the wavelength (0.25 L, 0.75 L and 1.25 L), where L is the predominant wave length. This type of structure can be constructed advantageously in locations where tidal ranges and currents are more, which prevent the normal type of rubble mound construction. The double vertical slotted wall would be relatively

economical as the structure serves multipurpose. The vessels can be berthed on the lee side and the top surface could also be used for loading/unloading as well as for movement of men and material. Such structures could also be used as a minimum reflection structure, inside the harbors, for separating the area for sailing boats/yachts without affecting the free circulation and quality of water.

6.4 SCOPE FOR FUTURE STUDY

This subject is still very important and needs more studies to discover other types of permeable breakwaters that could be more effective and has less side effects on the environment and economy.

- Pointing out that the hydraulic performance of single or double inclined slotted walls, single or double slotted walls that have untraditional slots and combination between several types of permeable breakwaters, like horizontal plate or permeable material between double rows of pile or slotted wall, are another area of practical interest.
- Attempting to model the effect of curvature on the sea side skirt could also be taken up.
- Expanding the use of PIV in studying the wave interaction with such structures for further clarification in understanding the means dissipating the energy.
- Examining the scour beneath such these structures to discover the influence of permeability on the scour of the seabed is very important.
- Studying the efficiency of the proposed breakwaters under the action of the others types of nonlinear and random waves.
- Studying the efficiency of the proposed breakwaters when subjected to oblique incident waves.
- Studying the integration between the transmitted waves through the permeable breakwaters and diffracted waves through breakwaters opening to determine the actual height of waves within the harbors.

REFERENCES

1. Abdul Khader, M. H. & Rai, S.P., 1981. "Wave attenuation due to closely spaced circular cylinders.", Proc. of the International Association for hydraulic Research, XIX Congress, New Delhi, pp. 93-102.

2. Abul-Azm, R. G., 1993 "Wave diffraction through submerged breakwaters." J. Waterway, Port, Coastal and Ocean Eng. 1993; 119(6):587–605.

3. Allsop, N. W. H. & McBride, M. W., 1994. "Reflections from vertical wall: The potential for improvement in vessel safety and wave disturbance." Paper 4.3, 2nd MCS project Workshop MAST II, Monolithic Coastal Str., Madrid, pp. 1-27.

4. Allsop, N. W. H., 1995. "Vertical walls and breakwaters: Optimization to improve vessel safety and save disturbance by reducing wave reflections." Wave forces on inched and vertical wall Str., ASCE, New York, pp. 232-257.

5. Belorgey, M., Bas, J. Le., J., & Grandjean, A., 1986. "Application of the Laser Doppler Velocimeter to the study of the turbulence generated by the swell in the vicinity of walls or obstacles." Proc. 3rd International Conf. on Application of laser Anemometry to Fluid Mechanics, Lisbon, Portugal.

6. Bennett, G. S., McIver, P. & Smallman, J. V., 1992. "A mathematical model of a slotted wave screen breakwater." Coastal Eng. 18 (1992), pp. 231–249.

7. Bergmann, H., & Oumeraci, H., 1999. "Hydraulic performance of perforated structures." Proceedings of Vth International Conference on Coastal and Port Engineering in developing countries (COPEDEC V), Cape Town, South Africa, pp. 1340-1349.

8. Chakrabarti, S. K., 1987. “Hydrodynamics of Offshore Structures.” ISBN 0-905451-66-X computational Mechanics Publications Southampton, Page 57.

9. Chakrabarti, S. K., 1999. “Wave interaction with an upright breakwater structure.” Ocean Engineering, 26(10), pp. 1003-1021.

10. Chang, K.-A., Hsu, T-J. & Liu, P. L-F., 2001. “Vortex generation and evolution in water waves propagating over a submerged rectangular obstacle: Part I. Solitary waves.” Coastal Eng., Vol. 44, Issue 1, pp. 13-36.

11. Chang, K-A., Hsu T-J. & Liu, P. L-F., 2005. “Vortex generation and evolution in water waves propagating over a submerged rectangular obstacle: Part II: Cnoidal waves.” Coastal Engineering, Vol. 52, Issue 3, Pages 257-283.

12. Cowen E. A., Sou I. M., Liu, p. L. F. & Raubenheimer, B., 2003. “Particle Image Velocimetry measurements within a laboratory-generated Swash zone.” J. of Eng. Mech. ASCE, Vol. 129, No. 10, pp. 1119-1129.

13. Cox, R. J., Horton, P. R. & Bettington, S. H., 1998. “Double walled low reflection wave barriers.” Proc. International conference on Coastal Engineering, Copenhagen, June 22-26, pp. 2221-2234.

14. Dalrymple, R. A., Losada, M. A. & Martin, P. A., 1991. “Reflection and transmission from porous structures under oblique wave attack.” J. of Fluid Mech., 224, pp. 625-644.

15. Fugazza, M. & Natale, L., 1992. “Hydraulic design of perforated breakwaters.” J. Water w. Port Coastal Ocean Eng., Vol. 118, No. 1, pp. 1–14.

16. Gardner, J. D. & Townend, I. H., 1988. “Slotted vertical screen Breakwater.” Proc. Breakwaters 88, pp. 283-298.

17. Galal, S., 2002. “The Use of permeable breakwater for Sea defense and Shore protection” M.S. Thesis, Faculty of Eng., Suez Canal Univ., Port-Said.

18. Goda, Y. & Suzuki, Y., 1976. “Estimation of incident and reflected waves in Random wave experiments.” Proc. 15th. ICCE, ASCE, Hawaii. pp. 828-845.

19. Gray, C. & Greated, C. A., 1993. “Processing system for the analysis of particle displacement holograms.” Proc. SPIE 2005, pp. 636-647.

20. Greated, C.A., Skyner, D. J. & Bruce, T., 1992. “Particle Image Velocimetry in the coastal engineering laboratory.” Proc. 23rd Coastal Eng Conf: pp. 212-225. Venice, Italy.

21. Grüne, J. and Kohlhase, S., 1974. “Wave transmission through vertical slotted walls.” Proceedings of 14th Coastal Engineering Conference, ASCE, 3, 1906-1923.

22. Hagiwara, K., 1984. “Analysis of upright structure for wave dissipation using integral equation.” Proc., 19th Int. Conf. on Coastal Engineering (ICCE), ASCE, Reston, Va., 2810–2826.

23. Hall, K., 2000. “Wave Transmission Through Multi-layer Wave Screens.” M.Sc. thesis at Queen's University, Kingston, Ontario, Canada.

24. Hall, K., and Thomson, G., 2001. “Prediction of Wave Transmission Through Single and Multiple Wave Screens.” Proceedings of International Conference on Breakwaters, coastal structures and coastlines, ICE, Thomas Telford Publishers, London, pp. 421-432.

25. Hayashi, T., & Kano, T., 1966. “Hydraulic research on the closely space Pile breakwater.” 10th Coastal Eng. Conf., ASCE, New York, Vol. 11, Chapter 50.

26. Hayashi, T., Hattori, M. & Shirai, M., 1968. “Closely spaced Pile breakwater as protection structure against beach erosion.” Proc. 11th Intl. conf. on Coastal Eng., 39, pp. 606-621.

27. Herbich, J. B., 1989. “Wave transmission through a double-row Pile breakwater.” Proc. 21st Int. Conf. on Coastal Eng., ASCE, Chapter 165, Torremolinos, Spain.

28. Hinsch, K. D., 1995. “Three-dimensional particle velocimetry.” Meas. Sci. Technol. Vol. 6, No. 6. pp. 742-753.

29. Hsu, H-H. & Wu, Y-C., 1999. “Numerical solution for the second-order wave interaction with porous structures.” International Journal for Numerical Methods in Fluids, Vol. 29 Issue 3, pp. 265-288.

30. Huang, Z. & Ghidaoui, M. S., 2007. “A model for the scattering of long waves by slotted breakwaters in the presence of currents.” J., Acta Mechanica Sinica, Vol. 23, No. 1, pp. 1-9.

31. Huang, Z., 2007. “Wave Interaction with one or two rows of closely spaced rectangular cylinders.” Journal of Waterway, Port, Ocean Engineering, Vol. 34, Issues 11-12, pp. 1584-1591.

32. Huang, Z., 2006. “A method to study interactions between narrow-banded random waves and multi-chamber perforated structures.” Journal, Acta Mechanica Sinica,. Vol.22, pages 285–292.

33. Hutchinson, P. S. & Raudkivi, A. J., 1984. "Case history of a spaced Pile breakwater at half moon bay marina." Auckland, New Zealand, Proceedings of19th Intl. Conf. on Coastal Eng., pp. 2530-2535.

34. Isaacson, M., Premasiro, S. & Yang, G., 1998. "Wave interaction with vertical slotted barrier." Journal Waterway, Port, Coastal and Ocean Eng., Vol. 124, No. 3, pp. 118-126.

35. Isaacson, M., Baldwim, J., Premasiro, S. & Yang, G., 1999. "Wave interaction with double slotted barriers." Journal Applied Ocean Research, Vol. 21, No. 2, pp. 81-91.

36. Kriebel, D. L., 1992. "Vertical wave barriers: Wave transmission and wave forces." 23rd Int. Conf. on Coastal Eng., ASCE, Vol.2. pp. 1313-1326.

37. Kakuno, S. & Liu, P. L. F., 1993. "Scattering of water waves by vertical cylinders" J. Waterway, Port, Coastal and Ocean Eng., ASCE, Vol.119, No. 3.

38. Kakuno, S. & Nakata, Y., 1997. "Scattering of water waves by rows of cylinders with/without a back wall." Applied Ocean Research, Vol. 20, Issue 4, Pages 191-198.

39. Koraim, A. S., 2005. "Suggested model for the protection of shores and marina." Ph.D. thesis in Civil Eng., Zagazig University, Zagazig, Egypt.

40. Laju, K., Sundar, V. & Sundaravadivelu, R., 2007. "Studies on Pile supported double skirt breakwater models." Journal of Ocean Technology, Vol. 2, No. 1. pp.

41. Lengricht, J., 1995. "Design of semi-submerged sea walls to increase dissipation." Hydra 2000, Proc. *XXVIth IAHR* Congress. London, Vol.3 , pp. 239-244.

42. Lengricht, J. & Graw, K-U., 1995. “Flow field analysis beneath gravity waves.” In: “Flow Visualization and Image Proc. of Multiphase Systems”. New York: ASME, FED-209: pp.57-64.

43. Lengricht, J., Graw, K-U. & Kronewetter, H., 2000. “Stereoscopic PIV adapted to gravity wave analysis.” Proc. 10th Int. Symp. Appl. of Laser Tech. to Fluid Mech., Paper 14.4. Lisbon, Portugal.

44. Liu, Y., Li, Y. & Teng, B., 2007. “Wave interaction with a new type perforated breakwater.” J. Acta Mechanica Sinica, Vol. 23, No. 4, pp. 351-358.

45. Losada, I. J., Losada, M. A., & Baquerizo, A., 1993. “An analytical method to evaluate the efficiency of porous screens as wave dampers.” Applied Ocean Research, 15, 207-215.

46. Mani, J. S., 1989. “Wave damping characteristics of Pile breakwaters.” Proc. Third Nat. Conference on Dock and Harbour Eng., Dept. , of Appl. Mech. , KREC, India , pp181-187.

47. Mani, J. S., & Jayakumar, S., 1995. “Wave transmission by suspended pipe breakwater.” J. of Waterway, Port, Coastal Eng., Vol. 121, No 6. ASCE, 121(6), 335-338.

48. Mani, J. S., 1998. “Wave forces on partially submerged pipe breakwater.” Proc. of Conference on Ocean Wave Kinematics, Dynamics and Loads on Structures. pp. 502-512

49. Mani, J. S., 2009. “Experimental and numerical investigations on zigzag porous screen breakwater” Journal, Natural hazards, Springer Netherlands, Vol. 49, No. 2 , pp. 401-409.

50. Mansard, E .P. D. & Funke, E. R., 1980. “The measurement of incident and reflected spectra using a least squares method.” In Proc. 17th Coastal Eng. Conf., Sydney, Australia, pp. 159-174.

51. Mei, C. C., Liu, P. L.-F., & Ippen, A. T., 1974. “Quadratic loss and scattering of long waves.” J. of waterways, Port, Coastal and Ocean Engineering. ASCE, 100(3), pp. 217–239.

52. Mei, C. C., 1983. “The applied dynamics of ocean surface waves.” Advanced Series on Ocean Engineering, V. 1, Wiley, New York.

53. Meinhart, C. D., Wereley, S. T. & Gray, M. H. B., 2000. “Volume illumination for two-dimensional Particle Image Velocimetry.” Measurement Science and Technology Vol. 11, No. 6, pp. 809–814. UK.

54. Nakamura, T., Kohno, T., Makimotto, K., & Kamikawa, H., 1999. “Enhancement of wave energy dissipation by a double curtain-walled breakwater with different drafts.” Proc. of Coastal Structures 99, Rotterdam, pp. 533-540.

55. Nakamura, T., Kohno, T., Morita, Y. & Morishita, S., 2001. “Development of a Pile-supported breakwater with dissipative front walls.” Proc. of International Conf. on Breakwaters, coastal structures and coastlines, ICE, Thomas Telford Publishers, London, pp. 409-419.

56. Neelamani, S. & Rajendran, R., 2002. “Wave interaction with ‘T’-type breakwaters.” Ocean Engineering, Vol. 29, No. 2, pp. 151-175.

57. Neelamani, S. & Rajendran, R., 2002. “Wave interaction with the ‘⊥’ –type breakwaters.” Ocean Engineering, Vol. 29, No. 5, pp. 561-589.

58. Neelamani, S. & Vedagiri, M., 2002. “Wave interaction with partially immersed twin vertical barriers.” Ocean Engineering, Vol. 29 No. 2, pp. 215–238.

59. Okamoto, K., Hassan, Y. A. & Schmidl, W. D., 1995. “Simple calibration technique using image cross-correlation for three dimensional PIV flow visualization and Image processing of Multiphase systems.” Ed: W. J. Yang et al (New York: ASME), pp. 99–106.

60. Oertel M. “MatPIV_GUI based on Sveen's MatPIV 1.6.1.” University of Wuppertal, Germany.

61. Park, W. S., Kim, B., Suh, K. & Lee, K., 2000. “Irregular wave scattering by cylinder breakwaters.” Korea-China Conf. on Port and Coastal Eng., Seoul, Korea.

62. Patarapanich, M. & Khader, M. H. A., 1985. “Wave force on a skirt breakwater.” Australian conf. on coastal and Ocean Eng., New Zealand, Vol. 2, pp.325-333.

63. Rageh, O. S. & Koraim, A. S., 2009. “The use of vertical walls with horizontal slots breakwaters.” 30th international water technology conf., IWTC 13, Hurghada, Egypt.

64. Requejo, S., Vidal, C. & Losada, I. J., 2002. “Modeling of wave loads and hydraulic performance of vertical permeable structures.” Coastal Engineering Vol. 46, Issue 4, pp. 249-276.

65. Sarpkaya, T. & Isaacson, M., 1981. “Mechanics of wave forces on offshore structures”, ISBN 0-442-25402-4 Van Nostrand Reinhold Company, pp. 174.

66. Sahoo, T., Lee, M. M. & Chwang, A.T., 2000. “Trapping and generation of waves by vertical porous structures.” Journal of Engineering Mechanics, 126, 10, 1074-1082.

67. She, K., Created, C. A. & Easson, W. J., 1997. “Experimental study of three-dimensional breaking wave kinematics.” Applied Ocean Research Vol. 19, Iss. 5-6, pp. 329-343.

68. Sollitt, C. K. & Cross, R.H., 1972. “Wave transmission through permeable breakwaters.” Proceedings of the 13th Coastal Eng. Conf., ASCE, Vancouver, pp. 1827-1846.

69. Subba, R., Rao, N. B. S. and Sathyanarayana, V. S., 1999. “Laboratory investigation on wave transmission through two rows of perforated hollow Piles.” Ocean Engineering, 26 (7), pp. 675-699.

70. Suh, K. D. & Park, W. S., 1995. “Wave reflection from perforated-wall caisson breakwaters.” J. of Waterways, Port, Coastal Eng., Vol. 26, Issues 3-4, December 1995, Pages 177-193.

71. Suh, K. D., Shin, S. & Cox, D. T., 2006. “Hydrodynamic characteristics of Pile-Supported vertical wall breakwaters.” J. of Waterways, Port, Coastal and Ocean Engineering, Vol.132, No.2, pp.83-96.

72. Suh, K. D., Jung, H. Y. & Pyun C. K., 2007. “Wave reflection and transmission by Curtain wall-Pile breakwaters using circular piles.” J. of waterways, Port, Coastal and Ocean Eng., Vol.34, Issues 14-15, pp. 2100-2106.

73. Sundar, V. & Subbarao, B. V. V., 2003. “Hydrodynamic performance characteristics of quadrant front face pile supported breakwater.” J. Waterways, Port, Coastal and Ocean Engineering, vol.129, no.1, pp.22-33.

74. Sveen, J. K., 2004. “An introduction to MatPIV v. 1.6.1.” Department of Math. Mechanics and applied Mathematics, No. 2, University of Oslo, Norwegian.

75. Tao, L., Song, H. & Chakrabarti, S., 2009. “Wave interaction with a perforated circular breakwater of non-uniform porosity.” J. Eng. Math, Vol. 65, No. 3, pp. 257–271.

76. Thornton, E. B. & Calhoun, R. J., 1972. “Spectral resolution of breakwater reflected waves.” J. of the Waterways, Harbour and Coastal Eng. Div., ASCE, Vol. 98, No. WW4, pp. 443-460.

77. Truit, C. L. & Herbich, J. B., 1987. “Transmission of Random waves through Pile breakwaters.” Proc. 20th Coastal Engineering Conf., pp. 2303-2313.

78. Tsinker, G., 1995. “Marine structures engineering: Specialized applications.” Chapman and Hall, NY 10119, New York. ISBN. 0-1412-98571-3.

79. U. S. Army, 1984. “Shore Protection Manual.” Coast. Eng. Res. Ctr., 2, Government Printing Office, Washing, D. C.

80. Wiegel, R. L., 1960. “Transmission of wave past a rigid vertical thin barrier” J. Waterway, Port, Coastal and Ocean Eng., ASCE, Vol. 86, No.1.

81. Willert, C. E. & Gharib, M., 1992. “Three-dimensional particle imaging with a single camera.” Exp. in Fluids 12, pp. 353–358

82. Williams, A. N., Mansour, A. M. & Lee, H. S., 2000. “Simplified analytical solutions for wave interaction with absorbing–type caisson breakwaters.” Ocean Eng., 27, pp.1231-1248.

83. Yu, X. & Chwang, A. T., 1994. “Wave induced oscillation in harbor with porous breakwaters”, J. of Waterway, Port, Coastal and Ocean Eng., Vol. 120, No. 2, pp. 125-144.

84. Yu, X., 1995. “Diffraction of water waves by porous breakwater.”, J. of Waterway, Port, Coastal and Ocean Engineering, Vol. 121, No. 6, pp. 275-282.

85. Zhu, S. & Chwang, A. T., 2001. “Investigations on the reflection behavior of a slotted seawall.” Coastal Engineering, Vol. 43 (2), pp. 93-104.

ELECTRONIC REFERENCES

86. http://www.panoramio.com/user/4739534/tags/Denmark.

87. http://www.generalacoustics.com/products/index_ultralabuls80D.html

PUBLICATIONS BASED ON THE RESEARCH WORK

88. Ahmed, H. & Schlenkhoff, A., 2010. " Wave interaction with vertical slotted wall." Proc. of CZM of River Deltas and Low land Coastline, Alexandria – Egypt. pp. 643-658.

89. Ahmed, H. & Schlenkhoff, A. and Bung D. B., 2011. " Hydrodynamic characteristics of vertical slotted wall breakwaters." 34th IAHR World Congress, Brisbane – Australia.

90. Ahmed, H. G., Schlenkhoff, A. and Oertel, M., 2011. "Stokes second-order wave interaction with vertical slotted wall breakwater." Coastal structures conference. Yokohama, Japan, 2011.

Curriculum Vitae

Name	Hany Gomaa Ibrahim Ahmed
1977	Born in Dakahlia, Egypt.
1983-1990	Al-Azhar Preparatory Institute, Egypt.
1990-1995	Al-Azhar Secondary Institute, Egypt
1995-2000	Civil Engineering Department, Faculty of Engineering, Al-Azhar University
2001-2005	Demonstrator at Civil Engineering Department, Faculty of Engineering, Al-Azhar University.
2005-2007	Assistant lecturer at Civil Engineering Department, Faculty of Engineering, Al-Azhar University.
2007-2011	PhD. Student at Institute for Geo-technic, Waste Management and Hydro Sciences (IGAW), University of Wuppertal, Germany.